THE UNIVERSITY *of* EDINBURGH

A Numerical Framework for Solving PDE-Constrained Optimization Problems from Multiscale Particle Dynamics

Mildred Aduamoah

Doctor of Philosophy
University of Edinburgh
2022

Declaration

I declare that this thesis was composed by myself and that the work contained therein is my own, except where explicitly stated otherwise in the text.

(*Mildred Aduamoah*)

To my parents,
Alex and Felicia.

Acknowledgement

First and foremost, I would like to thank my supervisors Benjamin Goddard and John Pearson. Thank you both for your continuous feedback and support, your experienced suggestions and advice, and for so many invaluable lessons. I owe the quality of my work to your rigorousness and expertise. I am very grateful for being able to have you as my advisors and mentors for my PhD.

I would like to thank the School of Mathematics of the University of Edinburgh for funding my PhD studies. I am very grateful to Iain Gordon and Isabelle Hanlon who were always very helpful whenever I encountered any issue. I am also very grateful to the organizers of the Autumn School on Optimal Control and Optimization with PDEs for their financial support that helped me to develop my research and BAMC, EMS, and LMS for holding regular seminars where I exchanged ideas with like-minded academics. .

I am grateful to many friends and colleagues at the School of Mathematics, in particular within the Applied and Computational Mathematics and the Optimization and Operational Research groups, for creating such a stimulating environment. A special thanks goes also to John, Finlay, Jonna, Santolo, and Stefania, with whom I was able to ease into my life as a PhD student.

I believe that a separate place should be given to all my closest friends and to my family. For all the laughs, the jokes, the good times, and the encouraging words, I would like to thank all my friends Emmanuel, Kingsley, Evans. Despite the (long) time away from one another and despite the distance between us, it has always seemed as if we never departed from one another. Here, I would like to thank also my parents, my siblings and relatives, whose support has helped me in completing my PhD studies. Their words and their love have always been pushing me towards my goals. I would not be here without them.

Lay Summary

The modelling of natural phenomena with mathematical equations has been widely applied in all spheres of the natural and social sciences. In particular, partial differential equations (PDEs) have been utilized to model systems from biology, physics, chemistry, and social science. Since computer algorithms have been developed to solve a range of complex partial differential equations, many industrial applications in engineering, medical sciences, and chemical systems have been able to predict quantities of interest via numerical solutions of PDE models.

The PDEs of interest in this thesis primarily describe a system of interacting 'particles'. Such a formulation is able to describe several systems including swarming and flocking of animals, opinions of individuals in a population, yeast fermentation during brewing of beer, growth of cancer cells, and interactions of electrons. These interacting PDEs are generally non-linear and non-local and present several numerical challenges.

The concept of optimization comes from the pragmatic standpoint that there are almost never infinite resources at our disposal to accomplish a task. To accomplish a desired result, limited resources must be managed effectively. Aerodynamics, geosciences, chemical process industry, environment, infrastructure, manufacturing, and medicine are just a few of the domains where optimization theory and techniques have found widespread application. PDE-constrained optimization falls under the broad class of optimal control problems, and arises in a huge variety of industrial, technological, economic, medical, and environmental applications. A simple example of a PDE-constrained optimization problem is the control of temperature in a yeast fermentation vessel during beer production. The optimal fermenting temperatures of yeast varies considerably. This is because exothermic processes like fermentation produce their own heat. Having the ability to cool the fermentation once it starts to take off is an imperative. Some ale yeasts, for example, do not perform well below 18C. Therefore we can formulate an optimization problem that finds the optimal temperature for yeast fermentation given a control factor of the cost to heat or cool the vessel, and constrained by a PDE such as the heat equation, or a more complicated PDE model.

The design of fast, robust, and effective computer algorithms to solve optimization problems has been a focus in the field of numerical analysis. For a state-of-the-art-framework to solve PDE-constrained optimization problems, it is critical to combine innovative optimization techniques with new algorithmic and numerical approaches. The successful implementation of optimization methodologies, however, requires more than just the quick solution of an optimization problem. Optimization algorithms should also deliver accurate approximations of the solution, and be able to handle PDE models of growing size and complexity.

In this thesis, we consider a class of optimization problems constrained by non-linear generalizations of the heat equation, opinion dynamics models, and swarming models. The main difficulty in solving the optimal control problems discussed in this thesis comes from the addition of a non-linear, non-local term arising from interaction of particles. We develop a highly modular numerical framework for treating PDE-constrained optimal control systems for general DDFTs.

Abstract

In this thesis, we develop accurate and efficient numerical methods for solving partial differential equation (PDE) constrained optimization problems arising from multiscale particle dynamics, with the aim of producing a desired time-dependent state at the minimal cost. A PDE-constrained optimization problem seeks to move one or more state variables towards a desired state under the influence of one or more control variables, and a set of constraints that are described by PDEs governing the behaviour of the variables. In particular, we consider problems constrained by one-dimensional and two-dimensional advection–diffusion problems with a non-local integral term, such as the associated mean-field limit Fokker–Planck equation of the noisy Hegselmann–Krause opinion dynamics model. We include additional bound constraints on the control variable for the opinion dynamics problem. Lastly, we consider constraints described by a two-dimensional robot swarming model made up of a system of advection–diffusion equations with additional linear and integral terms. We derive continuous Lagrangian first-order optimality conditions for these problems and solve the resulting systems numerically for the optimized state and control variables. Each of these problems, combined with Dirichlet, no-flux, or periodic boundary conditions, present unique challenges that require versatility of the numerical methods devised.

Our numerical framework is based on a novel combination of four main components: (i) a discretization scheme, in both space and time, with the choice of pseudospectral or finite difference methods; (ii) a forward problem solver that is implemented via a differential–algebraic equation solver; (iii) an optimization problem solver that is a choice between a fixed-point solver, with or without Armijo–Wolfe line search conditions, a Newton–Krylov algorithm, or a multiple shooting scheme, and; (iv) a primal-dual active set strategy to tackle additional bound constraints on the control variable.

Pseudospectral methods efficiently produce highly accurate solutions by exploiting smoothness in the solutions, and are designed to perform very well with dense, small matrix systems. For a number of problems, we take advantage of the exponential convergence of pseudospectral methods by discretising in this way not only in space, but also in time. The alternative finite difference method performs comparatively well when non-smooth bound constraints are added to the optimization problem. A differential–algebraic equation solver works out the discretized PDE on the interior of the domain, and applies the boundary conditions as algebraic equations. This ensures generalizability of the numerical method, as one does not need to explicitly adapt the numerical method for different boundary conditions, only to specify different algebraic constraints that correspond to the boundary conditions.

A general fixed-point or sweeping method solves the system of equations iteratively, and does not require the analytic computation of the Jacobian. We improve the computational speed of the fixed-point solver by including an adaptive Armijo–Wolfe type line search algorithm for fixed-point problems. This combination is applicable to problems with additional bound constraints as well as to other systems for which the regularity of the solution is not sufficient to be exploited by the spectral-in-space-and-time nature of the Newton–Krylov approach. The recently devised Newton–Krylov scheme is a higher-order, more efficient optimization solver which efficiently describes the PDEs and the associated Jacobian on the discrete level, as well as solving the resulting Newton system efficiently via a bespoke preconditioner. However, it requires the computation of the Jacobian, and could potentially be more challenging to adapt to more general problems. Multiple shooting solves an initial-value problem on sections of the time interval and imposes matching conditions to form a solution on the whole interval. The primal-dual active set strategy is used for solving our non-linear and non-local optimization problems

obtained from opinion dynamics problems, with pointwise non-equality constraints. This thesis provides a numerical framework that is versatile and generalizable for solving complex PDE-constrained optimization problems from multiscale particle dynamics.

Contents

Chapter 1

Introduction

Over centuries, interest in mathematical modelling of natural phenomena has vastly increased. All spheres of the natural sciences: physics, biology, chemistry, and even social sciences have adopted principles of mathematical modelling to study and predict the behaviour of systems. When the systems in question depend on more than one variable or quantity, partial differential equations are preferred to construct the models.

The study of partial differential equations, and consequently their numerical solutions have been applied in several areas of mathematical modelling. The aim is usually to predict the behaviour of some quantity of interest or estimate unknown parameters present in the partial differential equation.

Many PDEs of interest, and particularly those considered in this thesis, describe a system of interacting 'particles'. Such a formulation is rather generic, and able to describe dynamics as diverse as particles suspended in a bath, animal flocking and swarming, or opinions of individuals in a population. The key advantage of using such PDE models is their computational complexity. Typical applications have very large numbers of particles, and the associated numerical methods for simulating each individual particle tend to scale poorly with the number of particles. This prevents the direct numerical study of such systems, for example, via Langevin dynamics. The associated PDE models are derived through dimensionality reduction approaches, and have a fixed dimension (typically that of the underlying 'space'), regardless of the number of particles. However, these PDEs are generally complicated, often being non-local and non-linear, leading to other numerical challenges.

Optimization, on the other hand, is a concept that is used across disciplines. It stems from the realistic point of view that there are almost never unlimited resources available to achieve a goal. Therefore, the limited resources have to be managed appropriately to achieve the set goal. Mathematical optimization, in the simplest case, involves maximizing or minimizing some objective function. The case where the optimal solution is subject to additional criteria, is called constrained optimization, while unconstrained optimization has no such additional criteria. Optimization problems arise in many quantitative disciplines including computer science and engineering, operations research, and economics. The generalization of optimization theory and techniques constitutes a large area of applied mathematics, and has gained popularity in fields as varied as aerodynamics, atmospheric and geosciences, chemical process industry, environment, homeland security, infrastructure, manufacturing, and medicine. A relevant aspect of mathematical optimization that has, and continues to be, actively been studied is the development of computer algorithms to solve optimization problems. The focus of such studies has been to design fast, robust, and effective algorithms that can be applied to a plethora of numerically challenging systems.

PDE-constrained optimization falls under the broad class of constrained optimization, and is characterized by constraints specified as a PDE equation or system. It arises in a huge variety of industrial, technological, economic, medical, and environmental applications. The questions that appear in this field originate from a plethora of optimal control problems. The work of researchers in PDE-constrained optimization is not only driven by challenging mathematical problems, but also fascinating future applications. Recent applications of PDE-constrained optimization include optimal treatment planning in radiotherapy [21], stabilization of gas transportation networks [75], optimization of particle synthesis in the chemical indus-

try [106], optimal control of self-consistent classical and quantum particle systems in the design of semiconductor devices [45], and real time PDE-constrained optimal control of multicomponent separation process [25].

For a state-of-the-art-framework to solve PDE-constrained optimization problems, it is critical to combine innovative optimization techniques with new algorithmic and numerical approaches. Significant optimization issues are frequently presented by the scale and complexity of PDE simulations. PDE solvers, optimization techniques, and computational power have all made steady improvement in recent years. The successful implementation of optimization methodologies, however, requires more than just the quick solution of an optimization problem. Optimization algorithms should also deliver accurate approximations of the solution. Depending on the application, the reliability and efficiency of the optimization algorithms are essential. They must scale to large problem sizes, be robust, and cope with the ill-posedness of the problems. Applications that need or want real-time optimizations are growing in both quantity and complexity. As a result, it is necessary for optimization methods to be able to handle PDE models of growing size and complexity.

There are two schools of thoughts on how to solve PDE-constrained optimization problems: the *discretize-then-optimize*, and the *optimize-then-discretize* approaches. Both approaches involve applying discretization schemes, and solving a system of optimality conditions that the optimal solutions satisfy. The difference lies in which order discretization is applied. Solutions to optimization problems using both approaches do not usually coincide, hence the choice of approach is dependent on the objectives of the research. Since we seek accurate solutions to the continuous optimization problem, we follow the *optimize-then-discretize* approach. Hence our framework begins with obtaining a continuous optimality system, then discretizing with a suitable scheme and finally utilizing a numerical algorithm to solve the discretized system.

In this thesis, we develop a highly modular numerical framework to solve PDE-constrained optimization problems from multiscale particle dynamics constrained by non-linear Dynamical Density Functional Theory (DDFT) models, opinion dynamics models, and swarming models. In the current literature, algorithms to solve PDE-constrained optimization problems from multiscale particle dynamics have largely employed the *optimize-then-discretize* approach. However, in general, these methods do not include the non-linear, non-local interaction terms that provide the main challenges in our work. Therefore, standard results, and numerical implementations in optimal control theory cannot readily be applied, and new approaches have to be developed to address theoretical and numerical challenges. The novelties in our framework include combining pseudospectral discretization with a fixed-point iterative solver, and an active-set strategy to solve opinion dynamics and DDFT optimization problems with box constraints, and combining the pseudospectral discretization and Newton–Krylov iterative solver to solve 2D opinion dynamics and robot swarming optimization problems. The modular nature of our framework also allows change of the discretization scheme or iterative solver, which we demonstrate by substituting the pseudospectral discretization with a finite difference method in an opinion dynamics problem with box constraints.

This thesis is structured as follows. In Chapter 2, we focus on multiscale particle problems from Dynamical Density Function Theory (DDFT). We provide some background on the derivation of DDFT problems from their equilibrium counterpart Density Function Theory (DFT). We then detail generalizations of the standard DDFT model, specifically the problems considered in this thesis, and conclude with a history of numerical methods developed to solve DDFT problems.

In Chapter 3, we introduce PDE-constrained optimization problems, and discuss the *discretize-then-optimize* and *optimize-then-discretize* methods. We mention the advantages and disadvantages of each approach including why we choose the *optimize-then-discretize* method. We then demonstrate the *optimize* step on an optimal control problem constrained by the diffusion (or heat) equation, where we obtain continuous Lagrangian optimality conditions that result in a coupled system of partial differential equations. We then introduce additional bound constraints into the diffusion equation optimization problem and detail how an active-set strategy can be used to tackle the additional constraints. The inclusion of bound constraints is motivated by real-life applications, for example, in opinion dynamics where the quantities of interest refer to the density of a human population, and hence require non-negativity constraints. The diffusion equation is a suitable example to demonstrate the workings for bound constraints, as it is a

simplified form of the PDEs we are interested in. We conclude the chapter by providing various applications of PDE-constrained optimization.

Chapter 4 details the numerical framework we developed to solve the continuous optimality conditions we obtain from an optimization problem. We discuss the *discretize* step of the *optimize-then-discretize* approach, describing the pseudospectral discretization and explaining how we compute the convolution matrices that apply the convolution in the non-local non-linear integral term in our examples. We then introduce the iterative solvers we employ to solve the discretized optimality conditions, namely a fixed-point solver combined with an Armijo-Wolfe-like rule and a Newton–Krylov algorithm. We also mention a multiple shooting solver that is simple, but too computationally inefficient for the problems we solve in this thesis.

Chapter 5 focusses on a class of optimization problems we are interested in, and their numerical solutions. We construct two examples of DDFT optimization problems constrained by the advection-diffusion equation including a non-local and non-linear integral term and a control that is applied as a source term or a flow vector. We obtain continuous first-order Lagrangian optimality conditions for examples with Dirichlet and Robin type boundary conditions applied. We then obtain their numerical solutions using a fixed-point with Armijo-Wolfe-like algorithm together with the pseudospectral discretization. We perform the experiments for one-dimensional and two-dimensional examples and provide validation results for the numerical methods employed. The fixed-point framework for optimization within a pseudospectral method is new, as is the specific DDFT–PDE-constrained optimization framework we consider. In addition, we utilize an original software framework that enables the construction of grids, differential operators, convolution integrals, and boundary conditions, along with optimization solvers. This forms part of a publication [2], along with some material relating to the Newton–Krylov method described in Chapters 4 and 7.

In Chapter 6, we present PDE-constrained optimization problems arising from opinion dynamics. We begin with the derivation of the bounded confidence interval model, and construct the associated optimization problem. We obtain continuous first-order Lagrangian optimality conditions, and apply an Active Set strategy to tackle additional non-negativity constraints on the solutions. We then present numerical experiments for one-dimensional examples showing the dynamics when bound constraints are added or not added to the optimization problem. These PDE-constrained optimization problems for opinion dynamics are a novelty of this thesis, as is the combination of Active Set and fixed-point solvers in the way we tackle them.

In Chapter 7, we present optimization problems from another real-world application in robotic swarming. This time, we employ a Newton–Krylov algorithm together with the pseudospectral discretization to first solve an opinion dynamics optimization problem in two dimensions, then a robot swarming optimization problem constrained by a system of advection-diffusion equations. We detail the Newton–Krylov algorithm and provide numerical results. The Newton–Krylov approach we devise is new for these problems.

Finally, in Chapter 8, we summarize the work in this thesis and provide an outlook of future work that may follow from the results obtained.

Chapter 2

Background on Dynamic Density Functional Theory

Dynamic Density Functional Theory (DDFT) is the dynamical counterpart of the static Density Functional Theory (DFT), a statistical-mechanical theory for the equilibrium state of a classical many-body system. The DFT model centres around a free energy functional that requires an expression for practical applications, and DDFT focusses on a connection between microscopic particle dynamics and macroscopic physics which dates back to the famous Boltzmann equation [39]. DDFT is now used in many areas of physics, as well as in related subjects such as biology [4, 85, 239], chemistry [18, 153, 267], materials science [82, 137, 159], engineering [7], mathematics [87, 142], and philosophy [238]. This diversity arises, since the problem of finding a useful and accurate description of the collective dynamics in many-particle systems is of importance in a large number of areas in and beyond physics (see [241] for a historical review).

2.1 An Introduction to Density Functional Theory

Classical static DFT is a statistical-mechanical theory for the equilibrium state of a classical many-body system. We present the standard DFT model following [241]. Let $\mathbf{x}_i$ and $\mathbf{p}_i$ be the position and momentum of particle i in an N-particle system, respectively. The function $\Psi(\mathbf{x}_i, \mathbf{p}_i)$ describes the phase-space distribution of the individual particles. A grand-canonical free energy functional $\Omega(T, \mu, \Psi)$ is introduced that depends on the temperature T, chemical potentials μ which are treated as fixed parameters, and the distribution Ψ.

The trace of an arbitrary function G on phase space, in the grand-canonical case, on a 3D system is given by

$$\mathrm{Tr}(G) = \sum_{N=0}^{\infty} \frac{1}{N! h^{3N}} \int d^3x_1 \int d^3p_1 \ldots \int d^3x_N \int d^3p_N G,$$

where h is the Planck constant, and is Ψ normalized as $\mathrm{Tr}(\Psi) = 1$. The grand-canonical free energy functional is then given by

$$\Omega(T, \mu, \Psi) = \mathrm{Tr}(\Psi(H_N - \mu N + k_B T \ln(\Psi))), \tag{2.1}$$

where k_B is the Boltzmann constant and H_N is the N-particle Hamiltonian describing the total energy of the system given by

$$H_N = K + V_{\mathrm{ext}} + U,$$

where K is the kinetic energy, V_{ext} is the external potential (potential energy from the external field) and U is the inter-particle interaction energy. This complicated many-particle equation (2.1) is not separable into simpler single-particle equations because of the interaction term U. Now, Ω is minimized and equal to the actual equilibrium grand-canonical free energy, denoted

by Ω_{eq}, when evaluated at the equilibrium distributed Ψ_{eq} given by

$$\Psi_{eq} = \frac{1}{\Xi} e^{-\beta(H_N - \mu N)}, \tag{2.2}$$

where $\beta = 1/(k_B T)$, and the grand-canonical partition function $\Xi = \mathrm{Tr}(e^{-\beta(H_N-\mu N)})$. The equilibrium distribution Ψ_{eq} is completely determined by the external potential $V_{\mathrm{ext}}(\mathbf{x})$ if we fix the particle interactions.

The function Ψ can be very complicated as it depends on position and momentum, and in a three-dimensional space is defined on a $6N$-dimensional phase space, which makes it virtually impossible to efficiently apply this methodology to larger, more complex systems. Here, DFT provides an appealing alternative, being much more versatile, as it systematically maps the many-particles problem onto a problem with the one-body density $\rho(\mathbf{x})$ that gives the probability of finding a particle at position $\mathbf{x}$, and is given by

$$\rho(\mathbf{x}) = \left\langle \sum_{i=1}^{N} \delta(\mathbf{x} - \mathbf{x}_i) \right\rangle,$$

where $\langle \cdot \rangle$ denote an ensemble average and $\delta(\mathbf{x})$ is the Dirac delta distribution. It is shown in [172], that the external potential $V_{ext}(\mathbf{x})$ for Ψ_{eq} in equation (2.2) is uniquely determined once the one-body distribution at equilibrium denoted by ρ_{eq} is known, so that Ψ_{eq} is a functional of ρ_{eq}. Furthermore, the mapping $\rho \to V$ can be shown to exist under very general conditions [57]. Hence we can introduce a well-defined ("intrinsic free energy") functional

$$\mathcal{F}_{in}(T, \rho) = \mathrm{Tr}(\Psi_{eq}(\rho)(K + U + k_B \ln(\Psi_{eq}(\rho)))),$$

that is independent of the external potential. Another functional given by

$$\Omega(T, \mu, \rho) = \mathcal{F}_{in}(T, \rho) + \int d^3x\, \rho(\mathbf{x}) V_{ext}(\mathbf{x}) - \mu \int d^3x\, \rho(\mathbf{x})$$

becomes minimized and equal to the equilibrium grand-canonical free energy Ω_{eq} when evaluated at equilibrium density ρ_{eq}. These considerations lead to the central *variational principle of DFT*

$$\left. \frac{\delta \Omega(T, \mu, \rho)}{\delta \rho(\mathbf{x})} \right|_{\rho = \rho_{eq}} = 0,$$

and $\Omega(T, \mu, \rho_{eq})$ gives the grand-canonical free energy of the system [157]. In [81], the grand-canonical free energy is related to the Helmholtz free energy functional $\mathcal{F}(T, \rho)$, through a Legendre transformation, given by

$$\Omega(T, \mu, \rho) = \mathcal{F}(T, \rho) - \mu \int d^3x \rho(\mathbf{x}).$$

The free energy is often split into three parts:

$$\mathcal{F}(T, \rho) = \mathcal{F}_{id}(T, \rho) + \mathcal{F}_{exc}(T, \rho) + \mathcal{F}_{\mathrm{ext}}(\rho).$$

where $\mathcal{F}_{id} = k_B T \int \rho(\mathbf{x})(\ln(\Lambda^3 \rho(\mathbf{x})) - 1)\, d^3x$ is the exact expression for the free energy of an ideal gas with the thermal de Broglie wavelength Λ, $\mathcal{F}_{exc}$, known as *excess free energy* is the contribution from the particle interactions, and $\mathcal{F}_{\mathrm{ext}} = \int \rho(\mathbf{x}) V(\mathbf{x})\, d^3x$ takes into account the external potential. In general, the particle interaction energy cannot be calculated exactly, hence the excess free energy $\mathcal{F}_{exc}$ needs to be approximated. This approximation is also required in DDFT, as it is in most cases based on a free energy functional from DFT. An exception is when treating systems with a finite, and in particular small, fixed number of particles in the grand-canonical ensemble [101, 260]. The choice of which approximation gives good results depends on the system under consideration. The *mean-field approximation* has been used in the case of ultrasoft particles [79], active particles [262], and social interactions [239]. For particles with hard-core interactions, such as hard spheres, *fundamental measure theory* [215–217] is a very

successful approach.

2.2 An Introduction to Dynamic Density Functional Theory

In DFT, only equilibrium situations are considered where the density $\rho(\mathbf{x})$ is constant with respect to time and minimizes the grand-canonical free energy. The main idea of DDFT is to extend this principle to nonequilibrium situations. DDFT describes the time evolution of the one-body density, $\rho(\mathbf{x}, t)$, measured over space and time using a continuity equation that results in an equation of motion that describes the relaxation towards the equilibrium (in the case where we use the DFT free energy functional). Since the mass of $\rho(\mathbf{x}, t)$, $\int \rho(\mathbf{x}, t)\, dx$ is a conserved quantity, the rate of change, $\partial_t \rho(\mathbf{x}, t)$ will be proportional to the gradient of a flux. These lead to the central equation of *deterministic DDFT* [241]:

$$\partial_t \rho(\mathbf{x}, t) = \Gamma \nabla \cdot \left(\rho(\mathbf{x}, t) \nabla \frac{\delta \mathcal{F}(\rho)}{\delta \rho(\mathbf{x}, t)} \right), \tag{2.3}$$

with the mobility Γ and free energy $\mathcal{F}$. One typically uses free energy functionals from DFT, which are grand-canonical in order to inform the choice of the free energy $\mathcal{F}$. The general result (2.3) can be derived in a number of ways. The deterministic form of DDFT was derived microscopically for colloidal fluids by Marconi and Tarazona [166] as well as Archer and Evans [14], and for simple fluids by Archer [12]. For simplicity, we follow the derivation in [211], and for a more detailed approach, see [99]. We start with the stochastic Langevin equation describing a system of N spherical colloidal particles with mass m in a bath of many more smaller solvent molecules [55, 73, 143, 223]. The colloidal particles undergo Brownian motion due to thermal collisions with the solvent molecules. This erratic motion can be described using Newton's equations of motion, where a force takes into account the Brownian motion of the colloidal particles,

$$m \frac{d^2 \mathbf{x}_i}{dt^2} = -\gamma m \sum_{j=1}^{N} \Gamma_{ij} \frac{d\mathbf{x}_j}{dt} + V_i(\mathbf{x}^N, t) + \sum_{j}^{N} A_{ij} dW_j, \tag{2.4}$$

where $\mathbf{x}^N = (\mathbf{x}_1, \mathbf{x}_2, \ldots, \mathbf{x}_N)$ and $A = \sqrt{2\gamma m k_B T \Gamma}$. The interaction of the ith Brownian particle with the solvent is made up of two parts. Firstly, it contains a friction force due to systematic collisions with the solvent molecules as the particle attains a velocity $d\mathbf{x}_i/dt$. For not too large velocities, that friction force is directly proportional to the velocity of the Brownian particle, with γ being the constant of proportionality for a single isolated particle, and $\Gamma_{ij} \in \mathbb{R}^{3\times 3}$, $\Gamma = (\Gamma_{ij}) \in \mathbb{R}^{3N\times 3N}$, defining the friction tensor, which is positive definite and thus has a square root. Secondly, the interaction includes a rapidly varying force as the result of the random collisions of solvent molecules and the Brownian particle. The force is known to have a Gaussian probability distribution and can be expressed as

$$\sum_{j}^{N} \sqrt{2\gamma m k_B T \Gamma} d\mathbf{W}_j$$

where $d\mathbf{W}_j$ have mean zero, uncorrelated stochastic white noise terms and satisfy

$$\langle d\mathbf{W}_j(t), d\mathbf{W}_k(t') \rangle = \delta_{jk} \delta(t - t').$$

The friction tensor Γ is related to the strength of the stochastic white noise terms via a generalized fluctuation-dissipation theorem. The term $V_i(\mathbf{x}^N, t)$ accounts for the total potential energy of the particle i at time t, which includes interactions with other Brownian particles and external potentials. If we use the definition of velocity, $d\mathbf{x}_i = \dfrac{\mathbf{p}_i}{m} dt$, where $\mathbf{p}_i$ is the momentum

coordinates of the ith particle, then (2.4) can be rewritten as the system of equations:

$$\begin{aligned} d\mathbf{x}_i &= \frac{\mathbf{p}_i}{m} dt, \\ d\mathbf{p}_i &= \left[-\gamma \sum_{j=1}^{N} \Gamma_{ij} \mathbf{p}_j + \nabla_{\mathbf{x}_i} V(\mathbf{x}^N, t) \right] dt + \sum_{j=1}^{N} A_{ij} d\mathbf{W}_j, \end{aligned} \tag{2.5}$$

with A as described above. Using Itô's Lemma [93] from stochastic calculus, (2.5) can be written for the N-body distribution function, $f^{(N)}(\mathbf{x}_1, \mathbf{x}_2, \ldots, \mathbf{x}_N, \mathbf{p}_1, \mathbf{p}_2, \ldots, \mathbf{p}_N, t)$ as

$$\begin{aligned} &\partial_t f^{(N)} + \frac{1}{m} \sum_{i=1}^{N} \mathbf{p}_i \cdot \nabla_{\mathbf{x}_i} f^{(N)} - \sum_{i=1}^{N} \nabla_{\mathbf{x}_i} V(\mathbf{x}^N, t) \cdot \nabla_{\mathbf{p}_i} f^{(N)} \\ &\qquad = \gamma \sum_{i,j=1}^{N} \nabla_{\mathbf{p}_i} \cdot \left[\Gamma_{ij}(\mathbf{x}^N)(\mathbf{p}_j + \nabla_{\mathbf{p}_j}) f^{(N)} \right]. \end{aligned} \tag{2.6}$$

The equation above is precisely the N-body Kramers equation and $f^{(N)}$ is the probability of finding each particle i at position $\mathbf{x}_i$, with momentum $\mathbf{p}_i$ at time t. It is clear that $f^{(N)}$ contains information about all N particles, making it numerically highly challenging to compute. This motivates the need to reduce the dimensionality of $f^{(N)}$. If we consider the case when $\gamma \gg 1$, then we have an overdamped system and can assume that the time derivative of the momentum goes quickly to zero [243]. Hence we can have a explicit expression for $\mathbf{p}^N$ and rewrite equation (2.6) in terms of only the position variable $\mathbf{x}^N$ for the probability density function $\rho^{(N)}(\mathbf{x}^N, t)$ as

$$\partial_t \rho^{(N)}(\mathbf{x}^N, t) = \Gamma \sum_{i=1}^{N} \nabla_{\mathbf{x}_i} \cdot \left(\left[k_B T \nabla_{\mathbf{x}_i} + \nabla_{\mathbf{x}_i} V(\mathbf{x}^N, t) \right] \rho^{(N)}(\mathbf{x}^N, t) \right), \tag{2.7}$$

which is referred to as the Smoluchowski equation. See [99] for the heuristic derivation of Equation (2.7). To obtain a closed equation, it is necessary to make some assumptions. First, we assume that the potential $V(\mathbf{x}^N, t)$ and friction tensor Γ only contain at most two-body interactions, such that $V(\mathbf{x}^N, t)$ reads as

$$V(\mathbf{x}^N, t) = \sum_{i=1}^{N} V_{\text{ext}}(\mathbf{x}_i, t) + \frac{1}{2} \sum_{i=1}^{N} \sum_{j \neq i} V_2(\mathbf{x}_i, \mathbf{x}_j),$$

where $V_{\text{ext}}(\mathbf{x}, t)$ is the one-body time-dependent external potential acting on each particle and $V_2(\mathbf{x}_i, \mathbf{x}_j)$ is the pair interaction potential, which is assumed to be time independent.

Since we are interested in the distribution of the average values of the positions and momenta, the reduced n-body probability densities are introduced as integrals over the probability density [14] given by

$$\rho^{(n)}(\mathbf{x}^n, t) := \frac{N!}{(N-n)!} \int d\mathbf{x}^{N-n} \rho^{(N)}(\mathbf{x}^N, t), \tag{2.8}$$

where $d\mathbf{x}^{N-n} = d\mathbf{x}_{n+1} d\mathbf{x}_{n+2} \ldots, d\mathbf{x}_N$. Hence, multiplying (2.7) by N and integrating over $d\mathbf{x}^{N-1}$ (all but one particle), gives the evolution of the one-body density, since all terms in the sums with $i \neq 1$ vanish [99], and is given by

$$\partial_t \rho(\mathbf{x}, t) = \Gamma \nabla \cdot \left[k_B T \nabla_{\mathbf{x}} \rho(\mathbf{x}, t) + \rho(\mathbf{x}, t) \nabla V_{ext}(\mathbf{x}, t) + \int d\mathbf{x}' \rho^{(2)}(\mathbf{x}, \mathbf{x}', t) \nabla_{\mathbf{x}} V_2(\mathbf{x}, \mathbf{x}') \right]. \tag{2.9}$$

where $\rho^{(2)}(\mathbf{x}, \mathbf{x}', t)$ is the time-dependent two-body density. We ignore hydrodynamics interactions here for ease of presentation, and as it will not be considered further in this thesis. We make the Enskog approximation, in particular assuming that $\rho^{(2)}(\mathbf{x}, \mathbf{x}', t) = \rho^{(2)}(\mathbf{x}, t) \rho^{(2)}(\mathbf{x}', t) g(\mathbf{x}, \mathbf{x}')$, where the pair-distribution function g is assumed to be independent of ρ, and further simplified by the mean field approximation ($g \equiv 1$) [99]. For an equilibrium fluid, we can relate the

inter-particle forces to the direct one-body correlation function $c^{(1)}(\mathbf{x})$ as [167]:

$$-k_B T\rho(\mathbf{x})\nabla c^{(1)}(\mathbf{x}) = \int d\mathbf{x}'\rho(\mathbf{x})\rho(\mathbf{x}')\nabla_{\mathbf{x}} V_2(\mathbf{x},\mathbf{x}'),$$

and $c^{(1)}$ to the excess free energy $\mathcal{F}_{exc}$ as

$$k_B T c^{(1)}(\mathbf{x}) = \frac{\partial \mathcal{F}_{exc}(\rho)}{\partial \rho(\mathbf{x})}.$$

Making the approximation that these relations also hold out of equilibrium, therefore replacing the nonequilibrium correlations in (2.9) with their equilibrium counterparts leads us to the standard DDFT

$$\partial_t \rho(\mathbf{x},t) = \Gamma\nabla\cdot\left(\rho(\mathbf{x},t)\nabla\frac{\delta\mathcal{F}(\rho)]}{\delta\rho(\mathbf{x},t)}\right).$$

Some authors add a noise term to the standard DDFT (2.3) to make a stochastic DDFT equation that is concerned either with the exact microscopic or with a coarse-grained density [15]. In this thesis, we are confine ourselves to the deterministic DDFT in equation (2.3).

The Brownian particles modelled in (2.4) are assumed to be spherical and the standard DDFT describes spherical particles. This assumption is made for the interaction potential and not for the physical particles. For example, the effective interaction between polymers is often assumed to have a Gaussian form even though the polymers are not spherical [13, 156]. The same form has been used for a DDFT model of humans [239]. A Gaussian interaction potential has spherical symmetry, but this does not mean that polymers or humans are spheres.

DDFT has been very successful in theory, however, it has some limitations as a result of the approximations and assumptions involved in its derivation. One limitation arises from DDFT having the form of a continuity equation which conserves the total number of particles. The canonical free energy functional $\mathcal{F}$ should be used, however since this is not known, the grand-canonical functionals Ω from DFT are used instead. This could lead to wrong predictions for systems with few particles or large density gradients [69] and result in unphysical self-interactions [207]. Canonical approaches to DDFT have been developed to address this [69]. Another assumption which is a limitation is the fact that DDFT is a closed equation of motion. We arrived at a closed equation by making an approximation that the relaxation of the system is very slow, such that it can be assumed that the pair correlation is always given by that of the corresponding equilibrium system. This is not exactly true, such that predictions for DDFT for non-equilibrium pair correlations are not correct [89, 140]. In particular, flow fields can induce distortions of the correlation function that DDFT does not capture [220]. Another disadvantage is the density being the only variable in standard DDFT. Apart from the obvious reason that properties of the system cannot be captured by the density alone, for example temperature gradients, it assumes that other variables characterizing the system relax very quickly compared to the density, which is a strong approximation [113].

2.3 Generalizations of the Standard Dynamic Density Functional Theory Model

DDFT has been extended in a vast number of directions, making the theory applicable to systems with non-uniform temperature [261], hydrodynamic interactions [210], or superadiabatic forces [222], and to particles with inertia [167], non-spherical shape [212], or self propulsion [257]. A many-body particle interaction potential is also discussed in [97].

DDFT has a significant number of applications in the derivation of phase field crystal (PFC) models [251], phase separation [14], and solidification [131], cancer growth [56], or quantum hydrodynamics [74]. It has also been extended to a wider class of nonlinear, nonlocal partial differential equations, used in the continuum modelling of many natural phenomena consisting of complex, many body, multi-agent inter-particle effects including: pattern formation [46], the flocking of birds, cell proliferation, the self organising of morphogenetic and bacterial species [49], nonlocal reaction-diffusion equations [4], and even consensus modelling in opinion dynamics [58].

There are many extensions of the standard DDFT model (2.3), and for this section, we focus on the addition of source, sink, and potential flow terms as they appear in the PDEs targeted in this thesis.

2.3.1 Source and Sink Terms

If the system of particles is not closed, the number of particles is not necessarily conserved and particle inflow and outflow is possible. This introduces sources and sinks into the standard DDFT. This was discussed by Löwen and Heinen [158] for the case of particles being injected into a confined system at position $\mathbf{x}$ with rate $q_{in}(t)$. In this case, a point source $q_{in}(t)(\delta\mathbf{x}) = r(\mathbf{x}, t)$ has to be added to the DDFT (2.3). If (2.3) is linearized (assuming small density variations), an analytical solution of this problem is possible using Green's functions. In [152], source terms are employed to describe diffusion of chemicals around a point source. Other cases in which source terms have to be added to the conserved DDFT equation include evaporating thin films [214], surface charge densities [258, 259], biological dynamics [4, 56], chemical reactions [153, 161, 162], and epidemic spreading [239, 240].

2.3.2 Potential Flow Terms

Generally, the solvent in which the colloids are immersed cannot be assumed to be at rest. Hence, a natural generalization of DDFT is to allow for solvent flow with a velocity. Early models studied effects, such as colloids being dragged through a polymer solution, by shifting to a frame that is co-moving with a velocity and did not consider perturbations of the flow [146]. Essentially, this corresponds to assuming that the solvent simply flows through the colloid [203]. However, as discussed in [6, 203], the colloids also influence the solvent. A DDFT for colloidal particles advected by a flow field was derived by Rauscher et al. [203], who did not take hydrodynamic interactions between solvent and colloidal particles into account. The starting point are the overdamped Langevin equations for the motion of the ith particle in the presence of a flow field $\mathbf{w}(\mathbf{x}, t)$, given by

$$\frac{\mathbf{x}_i(t)}{dt} = \mathbf{w}(\mathbf{x}, t) - \Gamma\nabla_{\mathbf{x}_i}\left(V_{\text{ext}}(\mathbf{x}_i) + \sum_{j=1, j\neq i}^{N} V_2(\|\mathbf{x}_i - \mathbf{x}_j\|)\right) + \Psi_i(t)$$

For these Langevin equations, one can obtain a corresponding Fokker-Planck equation from which the evolution of the averaged density ρ is computed. If we have a potential flow, which is always the case when detailed balance holds, we can write

$$\mathbf{w}(\mathbf{x}) = -\Gamma\nabla V_{\text{vel}}(\mathbf{x})$$

and define a modified external potential $V^*(\mathbf{x}) = V_{\text{ext}}(\mathbf{x}) + V_{\text{vel}}(\mathbf{x})$ with the velocity potential V_{vel}. This allows to approximate the interaction term in the usual way. The resulting advected DDFT reads

$$\frac{\partial\rho}{\partial t} + \nabla\cdot(\mathbf{w}(\mathbf{x}, t)\rho(\mathbf{x}, t)) = \Gamma\nabla\cdot\left(\rho(\mathbf{x}, t)\nabla\frac{\delta F(\rho)}{\delta\rho(\mathbf{x}, t)}\right). \tag{2.10}$$

This corresponds to a standard DDFT equation with V_{ext} replaced by V^*. Advected DDFT is applied to colloids in a DNA solution in [110], microrheology [6, 208], flow of interacting particles around a fixed probe particle [124, 125], and hydrodynamic lift forces [86].

2.4 Numerical Methods for Dynamic Density Functional Theory Models

Generally, it is impossible to solve DDFT equations analytically as they are are nonlinear partial differential equations. Hence, it is important to have numerical methods available that can be used to solve them.

DDFT has computational advantages compared to Brownian dynamics (BD) simulations used for stochastic differential equations, since the computational cost does not depend on

the number of particles [164]. The computational cost of a BD simulation increases with the number of particles N, whereas the computational cost of a DDFT calculation increases with the desired resolution. As a consequence, for systems with a large number of particles, continuum simulations based on numerically solving a DDFT equation are typically much more efficient than BD simulations.

A significant amount of work has carried out on the numerical analysis of the solution of partial differential equations of the gradient-dynamics type, which DDFT belongs to. A variety of numerical strategies for DFT that may be useful for DDFT are discussed in [90], including real-space numerics, fast Fourier transformations, parallelization, preconditioning, and pseudo-arc-length continuation. A variety of authors have discussed the discretization and integration of DDFT, focusing on a variety of specific problems. A simple finite-difference integration scheme for deterministic DDFT can be found in [54]. Specialized explicit Runge-Kutta methods are employed in [209] to tackle difficulties due to the large dimensionality and nonlinearity of the problem. A discussion of the finite-element discretization of DDFT, and the relation to the physics of coarse graining, can be found in [68].

Nonlocal terms resulting from the excess free energy are particularly difficult to treat numerically. Convolution terms on Cartesian grids can be evaluated efficiently using fast Fourier transformation methods. However, these are difficult to apply on general meshes [208]. A spectral method for both DFT and DDFT is presented in [266]. It involves choosing a discretization scheme where the mesh is dense close to walls, where larger density variations are expected and a Clenshaw–Curtis quadrature is used to evaluate the DFT convolution integrals. In [182], a pseudospectral method is developed for the evaluation of the nonlocal integral terms. This scheme is discussed in a variety of contexts in DFT and fundamental measure theory and also applied to DDFT where it is checked for mass conservation. We adopt this pseudospectral method for the DDFT models in this thesis due to its exponential accuracy, while using a significantly lower number of points than most other reported methods. A Hermite spectral method which is applicable to Fokker-Planck equations with and without a gradient structure is also used in [100], and provides a possible alternative to pseudospectral methods.

Considering the diverse applications of DDFT and the numerical methods developed to solve it, it is logical to start looking at optimization problems involving these models and numerical methods to solve the optimization problems. In the next chapter, we present background information on a class of optimization problems called PDE-constrained optimization problems that can be constructed with DDFT models.

Chapter 3

An Introduction to PDE-Constrained Optimization

In this chapter, we provide background on the type of optimization problems considered in the rest of this thesis. In Section 3.1, we present a basic overview of PDE-constrained optimization problems, discussing distributed control problems, and problems with additional bound constraints. In Section 3.2, we discuss the two schools of thoughts on how to solve PDE-constrained optimization problems: the discretize-then-optimize strategy, and the optimize-then-discretize approach. We present the merits and disadvantages of each approach, and provide reasons why the optimize-then-discretize approach is the more appropriate choice for the problems considered in this thesis. In Sections 3.3 and 3.4, we illustrate a methodology for obtaining the continuous first-order optimality conditions for the PDE-constrained optimization problems of interest in this thesis, via the method of Lagrange multipliers, using an example involving the heat equation with Dirichlet and Neumann boundary conditions. Section 3.5 provides some background on additional bound constraints and describes the Active Set strategy applied to a heat equation optimization problem. Finally, in Section 3.6, we give a review of some applications of PDE-constrained optimization problems in science and industry.

3.1 The General Form of a PDE-Constrained Optimization Problem

PDE-constrained optimization problems consist of a cost functional subject to some given PDE constraints. These problems are of the form [121, Chapter 1]

$$\begin{aligned} \min_{\rho\in X, w\in Y} \quad & \mathcal{J}(\rho, w) \\ \text{s.t.} \quad & \mathcal{D}(\rho, w) = 0 \quad \text{in } X \times Y, \\ & \mathcal{B}(\rho, w) = 0 \quad \text{on } \partial X \times \partial Y, \\ & (\rho, w) \in K. \end{aligned} \tag{3.1}$$

The *objective function* $\mathcal{J} : (X \times Y) \to Z$ in problem (3.1) is the *cost functional* one wishes to minimize, while the remaining equations in problem (3.1) constitute the constraints subject to which the cost functional is to be minimized. For PDE-constrained optimization problems, the constraints consist of a PDE or a system of PDEs together with accompanying boundary conditions, and (optional) additional constraints. Here, ρ is the variable for which the PDE needs to be solved, also called the *state variable*, and w is the *control variable* that will be applied in some optimal way. The *differential operator* $\mathcal{D} : (X \times Y) \to Z$ describes the PDE on the interior of the domain, while $\mathcal{B} : (\partial X \times \partial Y) \to \partial Z$ describe the PDE on the boundary of the domain. Finally, $\mathcal{K} \subset (X \times Y)$ is a closed convex set that defines, for example, additional bound constraints that the state and control variables are subject to. Here, X, Y, and Z are real Banach spaces with boundaries ∂X, ∂Y, and ∂Z respectively, and $\rho \in X$ and $w \in Y$.

In this thesis, we wish to consider the solution of PDE-constrained optimization problems

arising from multiscale particle dynamics, with and without additional bound constraints. We motivate the class of problems we are interested in, by stating an example of a PDE-constrained optimization problem of *distributed control* form. We first define the following spaces for this problem [213, Chapter 5]:

$$
\begin{aligned}
L^2(\Omega) &= \left\{ f : \|f\|_{L^2} = \int_\Omega |f(x)|^2 dx < \infty \right\}, \\
H^1(\Omega) &= \{ f \in L^2(\Omega) : \partial_{x_i} f \in L^2(\Omega), 1 \leq i \leq d \}, \\
H_0^1(\Omega) &= \{ f \in H^1(\Omega) : f|_{\partial\Omega} = 0 \},
\end{aligned}
$$

where $\mathbf{x} = (x_1, \ldots, x_d)^T$ is the coordinate system in Ω. (For instance $d = 2$ reduces $\mathbf{x}$ to $\mathbf{x} = (x_1, x_2)^T$). Here, $\Omega \subset \mathbb{R}^d$, $d \in \{1, 2, 3\}$ and $\partial\Omega$ is the boundary of Ω.

As a motivating example, we now state the PDE-constrained optimization problem subject to constraints prescribed by Poisson's equation [204]:

$$
\begin{aligned}
\min_{\rho, w} \quad & \frac{1}{2}\|\rho - \widehat{\rho}\|^2_{L^2(\Omega)} + \frac{\beta}{2}\|w\|^2_{L^2(\Omega)}, \\
\text{s.t.} \quad & -\nabla^2 \rho = w \quad \text{in } \Omega, \\
& \rho = 0 \quad \text{on } \partial\Omega.
\end{aligned}
\tag{3.2}
$$

The variable $\widehat{\rho}$ denotes some *desired state* or *target variable*, and the value $\beta > 0$ is a *regularization parameter*. Related *time-dependent problems* would usually be solved on a domain $Q = \Omega \times (0, T)$ where $(0, T)$ is some time interval. We look for a control $w \in L^2(\Omega)$ and state $\rho \in H_0^1(\Omega)$ that solves the optimization problem, with $\widehat{\rho}$ typically assumed to be in $L^2(\Omega)$.

The squared L^2 norm in the cost functional of problem (3.2) measures how "close" the state variable is to the desired state, as well as the "size" of the control variable. It is possible to use other norms, however the choice of a Hilbert space norm is convenient when finding the continuous optimality conditions of the optimization problem.

The motivation of a problem of this type would be to attempt to drive the state variable "as close as possible" to a desired state while penalizing the input of large control into the system. The PDE describes the constraints subject to which such an optimization problem is solved. In a physical system, the control variable w can be thought of as the energy inputted into the system, which is often directly connected to the cost of running the system. For instance, consider an industrial vessel that is used to store raw materials for a manufacturing company, or a data centre with dedicated server rooms which store clusters of computer web servers. The vessel or server room is usually required to maintain certain "ideal" atmospheric conditions in order to best preserve the raw materials or prevent overheating of the computers. However, setting up a controlled environment to achieve these "ideal" conditions can be financially expensive. Hence, the two things to consider in this situation are: i) achieving ideal conditions and ii) minimizing the cost of setting up the controlled environment to achieve the ideal conditions. This problem could potentially be set up as a PDE-constrained optimization problem. The state variable in this case may be given by temperature, humidity, or a combination of these states. The desired state corresponds to the ideal set of atmospheric conditions, and the control variable could be the energy put into the system to achieve these conditions. The heat equation or another PDE of similar structure can be used to describe the constraints, and the goal of the PDE-constrained optimization problem will be to find a set of atmospheric conditions close to the "ideal" conditions, while penalizing to some extent the energy required to create these conditions.

The regularization parameter β, also known as the *penalty parameter*, therefore plays an important role, as it decides how much we care about the two objectives: i) driving the state variable as close as possible to the desired state and ii) reducing the input of control into the system. A large β means we are more interested in heavily penalizing the input of control, and less so about reaching the desired state, while a small β means the state can get closer to the desired state, and the input of control is not heavily penalized. Therefore in the above physical examples, a large β means we are more concerned with minimizing the energy used, while a small β means we are prioritizing achieving ideal atmospheric conditions.

At the core of such a PDE-constrained optimization problem is finding the optimal profile of

a control variable which ensures a state variable is close to some desired or target state. These problems are a key category of *optimal control problems*. Problem (3.2) is indeed referred to as a distributed control problem because the control variable is applied over the entire domain.

It is natural to consider time-dependent variants of the problem (3.2), as most real-world problems have a time-dependent element. In this thesis, we wish to solve distributed control PDE-constrained optimization problems, constrained by time-dependent PDEs from multiscale particle dynamics, for instance advection-diffusion equations with additional interaction terms. Existence and uniqueness of solutions to PDE-constrained problems constrained by linear, semi-linear, and nonlinear elliptic PDEs such as the Poisson's equation and parabolic PDEs, for instance the heat equation are discussed in [121].

In the next section, we introduce the two key approaches developed to solve PDE-constrained optimization problems, their advantages and disadvantages, and the preferred approach for the class of problems considered in this thesis.

3.2 Two Approaches for Solving PDE-Constrained Optimization Problems

PDE-constrained optimization problems are typically transformed into optimality conditions (a system of equations which must be satisfied by an optimal solution) which typically have no closed-form solutions, and hence are solved numerically via computational algorithms. The use of computational algorithms requires a discretization scheme to transition from the continuous spaces to a discrete space which leads to equations that are solvable on a computer (some problems are defined straight away on discrete spaces). The order in which discretization and deriving optimality conditions are carried out results in two approaches: i) *discretize-then-optimize* and ii) *optimize-then-discretize*.

The choice of approach is crucial as both approaches can produce different solutions to the optimization problem, and there are ongoing studies on how their solutions can coincide. See [61] for instance, for a simple advection-diffusion example, for which the solutions obtained using the two approaches differ.

3.2.1 Discretize-then-optimize

In the *discretize-then-optimize* approach, discretization is performed first. The PDE constraints with associated boundary conditions are discretized with a scheme of choice, for instance the finite element method, pseudospectral method or finite difference method. The finite element method for example discretizes the weak formulation of the PDE using finite element basis functions, and for example assumes that the discretized state and control variables are in $H^1(\Omega)$ and $L^2(\Omega)$, respectively. The cost functional is then discretized using the same basis functions used for the PDE constraints. This results in a finite-dimensional optimization problem where the cost functional and PDE constraints are discretized. The next step is to find the necessary optimality conditions for the discretized optimization problem using, for instance, the method of Lagrange multipliers (that is explained in further detail in the next section). The optimality conditions obtained, namely the *state*, *adjoint*, and *gradient* equations (defined in Section 3.4.1), are therefore individually in the form of linear equations and together combined have the form:

$$A\mathbf{x} = \mathbf{b}, \tag{3.3}$$

where $\mathbf{x}$ contains the discretized state, control, and adjoint variables and $\mathbf{b}$ contains the vectors that enforce the boundary conditions for the state and adjoint variables. The matrix A is often symmetric and can have a sparse structure by its construction using the finite element method. This makes the *discretize-then-optimize* approach more preferable in the linear algebra community, where a variety of solvers have been developed for symmetric matrix systems (as the *optimize-then-discretize* approach does not guarantee symmetry in the resulting linear system after discretization). However, this approach does not always reflect the continuous optimization problem and hence can produce less accurate solutions. Furthermore, for the problems that we consider, A may not be symmetric, and definitely not sparse due to a non-local term in the PDE.

There are two classes of widely researched linear algebra solvers to solve the system (3.3): *direct methods* which use techniques including Gaussian elimination to decompose the matrix such that the solution of the system becomes much simpler (see [78] for a summary of such methods), and *iterative solvers* (or indirect methods) that start with an initial guess of the solution, and repeatedly improve the guess to be close to the true solution of the system via some numerical algorithm. Appropriate iterative methods together with preconditioners can be very effective and converge fast for solving PDE-constrained optimization problems of very high dimension such as a recently developed Newton–Krylov method (see [112]) which will be extended in Chapter 7. It is known that the solution $\mathbf{x}$ to (3.3) can be written as

$$\mathbf{x} = A^{-1}\mathbf{b}. \tag{3.4}$$

If A is invertible, A^{-1} can be highly expensive to evaluate computationally when A is of high dimension. The idea of preconditioning is to create a matrix (or operator) $\mathcal{P}$ and seek to solve, instead of (3.4), the system

$$\mathcal{P}^{-1}A\mathbf{x} = \mathcal{P}^{-1}\mathbf{b}, \tag{3.5}$$

which has more "convenient" properties in the sense that it is cheaper to invert computationally. We note that symmetry of the matrix A is very important for the effectiveness of some preconditioners. There are many works concerning block iterative solvers of (3.3) in [83, 170, 171]. Recently, a number of authors studied all-at-once preconditioning of linear elliptic control problems including those with additional control bound constraints in [204–206, 235]. Iterative solvers for PDE-constrained optimization problems involving linear parabolic constraints such as the heat equation are covered in [171, 235]. Non-linear control problems are however much harder to solve. Studies in [189, 191, 233] develops fast iterative solvers for non-linear problems from chemical reactions and pattern formation.

3.2.2 Optimize-then-discretize

The alternative *optimize-then-discretize* approach first obtains the necessary optimality conditions in the continuous space the problem is defined in, then solves the continuous optimality system computationally via discretization, followed by the use of a direct or iterative solver. The advantage of this approach is that it most accurately reflects the continuous optimization problem, hence generally produces more accurate solutions on the infinite-dimensional level.

The continuous optimality conditions similarly consist of state, adjoint, and gradient equations. Hence, the *discretize-then-optimize* and *optimize-then-discretize* approaches, could lead to discretized optimality conditions with similar, but not necessarily the same, linear system.

For time-dependent problems, one obtains a state equation that is an initial value problem (with an initial time condition), and an adjoint equation that is a final-time problem (with a final time condition). The gradient equation couples the state and adjoint variables. Such a system can be solved using gradient-descent methods or Newton methods, for example, that iteratively solve the state equation forward in time, and the adjoint equation backward in time (see [121, Chpater 2]). We adopt one such iterative solver which follows the theory of fixed-point methods for one-dimensional and two-dimensional problems in Chapters 5 and 6. An alternative way is to solve both state and adjoint equations at once as systems of coupled elliptic equations in space and time. The transformation of the optimality system into an elliptic PDE for linear parabolic optimal control problems with pointwise control constraints have been considered in [178, 179]. This method is also known as the *one-shot* or *all-at-once* approach and treats the coupled optimality system in the whole space–time cylinder, where the time variable is interpreted as an additional space variable. We consider one such newly developed Newton–Krylov solver acting in space and time variables, that employs a preconditioner for fast convergence, as an alternative to the fixed-point solver for two-dimensional problems in Chapter 7.

In summary, the *discretize-then-optimize* approach often leads to symmetric matrix systems that can be solved with efficient linear algebra solvers, but compromises on the accuracy of the solutions to the continuous optimization problem. Alternatively, the solutions from the *optimize-then-discretize* approach most accurately obey the continuous optimization problem,

but produce linear systems that can be harder to solve, for example because of lack of symmetry.

In this thesis, we wish to solve PDE-constrained problems involving time-dependent, non-linear, and non-local PDEs from particle dynamics such as an advection-diffusion equation that contains additional integral terms. The discretization of such problems lead to denser and unstructured matrix systems that become difficult to solve with the iterative methods and preconditioners developed for symmetric systems. Since symmetry is not achievable for the problems we consider, it is natural to choose the *optimize-then-discretize* approach, so we can obtain solutions that more accurately reflect the continuous optimization problem. The discretization step is tackled second, also making it easier to apply different discretization schemes and optimization solvers to find solutions to the continuous optimality system. In fact, we explore this versatility in Chapters 4, 5 and 6, where we develop a comprehensive numerical framework which is a novel combination of pseudospectral or finite difference discretization methods, and fixed-point or Newton–Krylov solvers. The appearance of dense matrices in our problems of interest, greatly motivates the use of the pseudospectral discretization as it works very well for dense matrix systems on simple domains, instead of, for instance, finite element methods that works better with local operators (leading to sparse matrices) on complex domains.

In Sections 3.3, 3.4, and 3.5, we provide an introduction to the *optimize* step of the *optimize-then-discretize* approach. We show how to obtain continuous first-order optimality conditions using the method of Lagrange multipliers. We present the example of an optimization problem involving the linear heat equation, as a precursor to the problems involving non-linear and non-local advection-diffusion equations tackled later in Chapters 5, 6 and 7.

3.3 Preliminaries

The general approach we follow in this thesis for the analytical treatment of the general PDE-constrained optimization problem (3.1) is based on the theory of *Lagrange multipliers* [17, 37, 121, 128, 231, 246]. The following definitions and theorems are useful for implementing this theory. We denote the divergence of a vector field $\vec{F}$ by $\nabla \cdot \vec{F}$, and the gradient of a scalar field G by ∇G.

Definition 3.3.1. (Directional Derivative [24]) Let X, Y be Banach spaces, then the directional derivative of $f : X \to Y$ at $x \in U \subseteq X$ in the direction $h \in X$, denoted by the symbol $f'(x; h)$, is defined as

$$f'(x; h) = \lim_{t \to 0} \frac{f(x + th) - f(x)}{t}$$

whenever the limit on the right exists.

Definition 3.3.2. (Fréchet Derivative [24]) Let f be a function from an open subset U of a Banach space X into the Banach space Y. We say f is Fréchet differentiable at $x \in U$ if there is a bounded linear operator $D : X \to Y$ such that

$$\lim_{\|h\|_U \to 0} \frac{\|f(x + th) - f(x) - Df(x)h\|_Y}{\|h\|_U} = 0$$

is uniform for every $h \in S_X$, and $t > 0$ sufficiently small so that $x + th \in U$. The set S_X is the set of all subspaces of X. The operator D is called the Fréchet derivative of f at x. In addition, if the directional derivative exists for each $h \in U$, then the map

$$\begin{aligned} f'(x; \cdot) &: U \to Y \\ h &\rightarrowtail f'(x; h) \end{aligned}$$

is called the first variation of f at x. If this is a bounded linear operator, then it is the Fréchet derivative of f at x.

Theorem 3.3.1. (Divergence Theorem [192]) Let Ω be a bounded open subset of $\mathbb{R}^d$ with smooth or piecewise smooth boundary $\partial\Omega$. Let $\mathbf{F} = (F_1, \ldots, F_d)$ be a smooth vector field defined in $\mathbb{R}^d$, or at least in $\Omega \cup \partial\Omega$. Let $\mathbf{n}$ be the unit outward-pointing normal of $\partial\Omega$. Then

the Divergence Theorem states that

$$\int_\Omega \nabla \cdot \mathbf{F}\, dV = \int_{\partial\Omega} \mathbf{F} \cdot \mathbf{n}\, dA,$$

where

$$\nabla \cdot \mathbf{F} = \frac{\partial F_1}{\partial x_1} + \frac{\partial F_2}{\partial x_2} + \cdots + \frac{\partial F_d}{\partial x_d},$$

with dV the element of volume in $\mathbb{R}^d$ and dA is the element of surface area on $\partial\Omega$. We note that if $\mathbf{F}$ can be written as ∇H, then $\mathbf{F} \cdot \mathbf{n} = \nabla H \cdot \mathbf{n}$ can be written as $\dfrac{\partial H}{\partial n}$ for a scalar function H.

We use the following vector calculus identity together with the Divergence Theorem. Let G be a scalar field and $\mathbf{F}$ be a smooth vector field defined in $\mathbb{R}$ and $\mathbb{R}^d$ respectively. Then

$$\nabla \cdot (G\mathbf{F}) = G\nabla \cdot \mathbf{F} + \nabla G \cdot \mathbf{F}. \tag{3.6}$$

Theorem 3.3.2. (Fundamental Lemma of Calculus of Variations [130]) If a continuous function f on an open interval (a, b) satisfies the equality

$$\int_a^b f(x)h(x)dx = 0$$

for all compactly supported smooth functions h on (a, b), then f is identically zero.

Definition 3.3.3. (Variational Inequality Problem [10]) Given a Banach space X, a subset U of X, and a functional $\mathcal{F} : U \to X^*$ from U to the dual space X^* of X, the variational inequality problem is the problem of solving for the variable $x \in U$ the following inequality:

$$\langle \mathcal{F}(x), y - x\rangle \geq 0 \quad \forall y \in U, \tag{3.7}$$

where $\langle\cdot,\cdot\rangle : X^* \times X \to \mathbb{R}$ is the duality pairing.

A standard example in [10] is the problem of finding the minimal value of a differentiable function f over a closed interval $I = [a, b]$. Let x^* be a point in I where the minimum occurs. Three cases can occur:

$$\begin{aligned} f'(x^*) &= 0 \quad \text{if } a < x^* < b,\\ f'(x^*) &\geq 0 \quad \text{if } x^* = a,\\ f'(x^*) &\leq 0 \quad \text{if } x^* = b. \end{aligned}$$

These necessary conditions can be summarized as the problem of finding $x^* \in I$ such that

$$f'(x^*)(y - x^*) \geq 0 \quad \forall y \in I.$$

3.3.1 Theory of Lagrange Multipliers

We recall the PDE-constrained optimization problem (3.1) in Section 3.1:

$$\begin{aligned} \min_{\rho\in X, w\in Y} \quad & \mathcal{J}(\rho, w)\\ \text{s.t.} \quad & \mathcal{D}(\rho, w) = 0 \quad \text{in } X \times Y,\\ & \mathcal{B}(\rho, w) = 0 \quad \text{on } \partial X \times \partial Y,\\ & (\rho, w) \in K. \end{aligned}$$

We suppose X, Y, and Z are Hilbert spaces, with the functional $\mathcal{J}$, operators $\mathcal{D}$ and $\mathcal{B}$, convex set K on the state variable ρ, and control variable w as defined in Section 3.1. We first discuss the case where the additional constraint is $w \in K \subset Y$. We assume $\mathcal{J}$, $\mathcal{D}$ and $\mathcal{B}$ have continuous first derivatives, and denote by $D_\rho\mathcal{J}$, $D_w\mathcal{J}$ the Fréchet derivatives of $\mathcal{J}$ with respect to ρ and

w, respectively. Let Z^* be the dual space of Z and the duality product be denoted by $\langle\cdot,\cdot\rangle_{Z^*,Z}$. We form the Lagrange functional

$$\mathcal{L}(\rho, w, q) = \mathcal{J}(\rho, w) - \langle \mathcal{D}(\rho, w) + \mathcal{B}(\rho, w), q\rangle_{Z^*,Z}, \tag{3.8}$$

where $q \in Z^*$ is the Lagrange multiplier associated with the equality constraint (in our case the PDE) $\mathcal{D}(\rho, w) = 0$ with boundary condition $\mathcal{B}(\rho, w) = 0$. We note that, in other literature (see [190, 232, 234]), the minus sign in (3.8) is replaced with addition. The choice of signs does not affect the solution to the optimization problem, one only has to be consistent throughout the working. For clarity in the working, the Lagrange multiplier q is typically split into two multipliers q_1 and q_2, where q_1 is associated with the PDE in the interior of the domain, $\mathcal{D}(\rho, w) = 0$, while q_2 is associated with the boundary condition $\mathcal{B}(\rho, w) = 0$. It is shown in [128, Section 1], that a minimizing pair $(\bar{\rho}, \bar{w})$ satisfies the necessary conditions:

$$D_\rho \mathcal{L}(\bar{\rho}, \bar{w}, q) = D_\rho \mathcal{J}(\bar{\rho}, \bar{w}) - \langle D_\rho \mathcal{D}(\bar{\rho}, \bar{w}), q_1\rangle - \langle D_\rho \mathcal{B}(\bar{\rho}, \bar{w}), q_2\rangle = 0, \tag{3.9}$$

$$\langle D_w \mathcal{J}(\bar{\rho}, \bar{w}) - D_w \mathcal{D}(\bar{\rho}, \bar{w}) q_1 - D_w \mathcal{B}(\bar{\rho}, \bar{w}) q_2 \,,\, w - \bar{w}\rangle_{Z^*,Z} \geq 0 \quad \forall w \in K, \tag{3.10}$$

$$\mathcal{D}(\bar{\rho}, \bar{w}) = 0, \quad \mathcal{B}(\bar{\rho}, \bar{w}) = 0, \text{ and } \bar{w} \in K. \tag{3.11}$$

Equations (3.9), (3.10) and (3.11) are known as the *Karush–Kuhn–Tucker* (KKT) conditions [121, Chapter 1], and are referred to as *first-order optimality conditions*. In the case $K = Z$, the inequality (3.10) results in the equality

$$D_\rho \mathcal{J}(\bar{\rho}, \bar{w}) - \langle D_w \mathcal{D}(\bar{\rho}, \bar{w}), q_1\rangle_{Z^*,Z} - \langle D_w \mathcal{B}(\bar{\rho}, \bar{w}), q_2\rangle_{\partial Z^*,\partial Z} = 0. \tag{3.12}$$

In optimal control theory, the multiplier q consisting of q_1 and q_2 is called the *adjoint* variable. Equation (3.11) is known as the *state equation* or *forward equation*, equation (3.9) is referred to as the *adjoint equation* or *backward equation*, and equation (3.10) as the *variational inequality*, with its equality version (3.12) the *gradient equation*. The terminology is motivated by time-dependent problems, where (3.9) is a final-time problem with a final time condition and (3.11) is an initial value problem with initial time condition. We note that the *state equation* is derived from the Fréchet derivative of the Lagrangian operator with respect to the state variable equated to zero, $D_q \mathcal{L}(\rho, w, q) = 0$, recovering the PDE constraint.

3.4 Continuous First-Order Optimality Conditions

We now illustrate how to obtain first-order optimality conditions for the time-dependent distributed control problems we are interested in, by showing the working for an introductory example involving the heat equation, with either Dirichlet or Neumann boundary conditions. We define the following spaces for the PDEs that appear in this section. We denote $Q = \Omega \times (0, T)$ to be the space–time domain on which the PDE is modelled. Here, $\Omega \subseteq \mathbb{R}^d$, with $d \in \{1, 2, 3\}$ is some given spatial domain with boundary $\partial\Omega$, and $[0, T]$ is the time interval with a prescribed *final time*, T. The boundary ∂Q, of Q, therefore refers to $\partial\Omega \times (0, T)$. Also, a function

$$h \in C_0^\infty(Q) \implies h \in C_0^\infty(0, T; \Omega),$$

where $C_0^\infty(Q)$ is the space of all continuous functions on Q which are equal to zero on the boundary ∂Q.

3.4.1 Dirichlet Boundary Conditions

First, let us consider the following distributed control optimization problem constrained by the heat equation with Dirichlet boundary conditions:

$$\begin{aligned} \min_{\rho, w} \quad & \frac{1}{2}\int_0^T \int_\Omega (\rho - \widehat{\rho})^2 \, dx dt + \frac{\beta}{2}\int_0^T \int_\Omega w^2 \, dx dt \\ \text{s.t} \quad & \partial_t \rho - \nabla \cdot (\nabla \rho) = w \quad \text{in } Q, \\ & \rho = \rho_0 \quad \text{at } t = 0, \end{aligned} \tag{3.13}$$

$$\rho = 0 \quad \text{on } \partial Q.$$

For a problem of this type, we emphasize again that ρ is the state variable, $\widehat{\rho}$ is the target or desired state, w is the control variable, $\beta > 0$ is the regularization parameter, and Q is as defined above.

We use the method of Lagrange multipliers, discussed in Section 3.3.1, to obtain the optimality system for the problem in (3.13). We introduce two Lagrange multipliers q_1 and q_2 arising from the *adjoint* variable q, which we assume to have appropriate smoothness. The variable q_1 is related to the interior of the domain Q and q_2 to its boundary, ∂Q. The solution of (3.13) leads to the continuous Lagrangian operator:

$$\begin{aligned}\mathcal{L}(\rho, w, q_1, q_2) = \frac{1}{2}\int_0^T \int_\Omega (\rho - \widehat{\rho})^2 \, dxdt + \frac{\beta}{2}\int_0^T \int_\Omega w^2 \, dxdt \\ - \int_0^T \int_\Omega (\partial_t \rho - \nabla \cdot (\nabla \rho) - w)\, q_1 \, dxdt - \int_0^T \int_{\partial\Omega} q_2 \rho \, dsdt.\end{aligned}$$

We seek the stationary point of $\mathcal{L}$ to obtain the optimal state $\bar{\rho}$ and optimal control $\bar{w}$. We follow standard working for time-dependent PDE-constrained optimization problems, (see [246, Chapter 3] for example), and find the Fréchet derivative of the Lagrangian operator with respect to the state, adjoint, and control variables, and equate these derivatives to zero.

First, we consider the Fréchet derivative with respect to the adjoint variables q_1 and q_2 in the direction h equated to zero.

$$D_{q_1}\mathcal{L}(\bar{\rho}, \bar{w}, q_1, q_2)h = -\int_0^T \int_\Omega (\partial_t \bar{\rho} - \nabla \cdot (\nabla \bar{\rho}) - \bar{w})\, h \, dxdt = 0,$$

and

$$D_{q_2}\mathcal{L}(\bar{\rho}, \bar{w}, q_1, q_2)h = -\int_0^T \int_{\partial\Omega} \bar{\rho} h \, dsdt = 0.$$

For all $h \in C_0^\infty(Q)$, the Fundamental Lemma of Calculus of Variations implies that for $D_{q_1}\mathcal{L}(\bar{\rho}, \bar{w}, q_1, q_2)h$,

$$-(\partial_t \bar{\rho} - \nabla \cdot (\nabla \bar{\rho}) - \bar{w}) = 0, \qquad \text{in } Q,$$

and for $D_{q_2}\mathcal{L}(\bar{\rho}, \bar{w}, q_1, q_2)h$,

$$\bar{\rho} = 0 \quad \text{on } \partial Q$$

This working returns the PDE constraint in the problem (3.13) which we refer to as the *forward problem*, or the *state equation*:

$$\begin{aligned}\partial_t \bar{\rho} - \nabla \cdot (\nabla \bar{\rho}) &= \bar{w} \quad \text{in } Q \\ \bar{\rho} &= \rho_0 \quad \text{at } t = 0, \\ \bar{\rho} &= 0 \quad \text{on } \partial Q.\end{aligned} \tag{3.14}$$

Next, we consider the Fréchet derivative with respect to the state variable ρ in the direction h:

$$\begin{aligned}D_\rho \mathcal{L}(\bar{\rho}, \bar{w}, q_1, q_2)h = \int_0^T \int_\Omega (\bar{\rho} - \widehat{\rho}) h \, dxdt - \int_0^T \int_\Omega (\partial_t h - \nabla \cdot (\nabla h))\, q_1 \, dxdt \\ - \int_0^T \int_{\partial\Omega} q_2 h \, dsdt.\end{aligned}$$

We seek to make h the subject of the derivative $D_\rho \mathcal{L}(\bar{\rho}, \bar{w}, q_1, q_2)h$. From the vector calculus identity (3.6) and the Divergence Theorem,

$$\int_\Omega q_1 \nabla \cdot (\nabla h) \, dx = \int_\Omega \nabla \cdot (q_1 \nabla h) \, dx - \int_\Omega \nabla q_1 \cdot \nabla h \, dx,$$

$$= \int_{\partial\Omega} q_1 \frac{\partial h}{\partial n}\, ds - \int_\Omega \nabla q_1 \cdot \nabla h\, dx, \tag{3.15}$$

$$\begin{aligned}\int_\Omega h\nabla\cdot(\nabla q_1)\, dx &= \int_\Omega \nabla\cdot(h\nabla q_1)\, dx - \int_\Omega \nabla h\cdot\nabla q_1\, dx \\ &= \int_{\partial\Omega} h\frac{\partial q_1}{\partial n}\, ds - \int_\Omega \nabla q_1\cdot\nabla h\, dx. \end{aligned}\tag{3.16}$$

Combining (3.15)−(3.16) gives

$$\int_\Omega q_1\nabla\cdot(\nabla h)\, dx = \int_\Omega h\nabla\cdot(\nabla q_1) + \int_{\partial\Omega}\left(q_1\frac{\partial h}{\partial n} - h\frac{\partial q_1}{\partial n}\right) ds.$$

Further, using the product rule and integration by parts on the time derivative gives

$$\begin{aligned} \partial_t(q_1 h) &= h\partial_t q_1 + q_1\partial_t h, \\ \implies \int_0^T q_1\partial_t h\, dt &= \int_0^T \partial_t(q_1 h)\, dt - \int_0^T h\partial_t q_1\, dt \\ &= q_1 h|_0^T - \int_0^T h\partial_t q_1\, dt. \end{aligned}$$

Hence, the Fréchet derivative with respect to the state variable ρ in the direction h may be rewritten as:

$$\begin{aligned} D_\rho\mathcal{L}(\bar\rho,\bar w,q_1,q_2)h = &\int_0^T\int_\Omega(\bar\rho-\widehat\rho)h\, dxdt - \int_0^T\int_\Omega\left(-\partial_t q_1 - \nabla\cdot(\nabla q_1)\right)h\, dxdt \\ &- \int_\Omega q_1 h|_0^T\, dx + \int_{\partial\Omega}\left(q_1\frac{\partial h}{\partial n} - h\frac{\partial q_1}{\partial n}\right) dsdt - \int_0^T\int_{\partial\Omega} q_2 h\, dsdt. \end{aligned}$$

For a stationary point, the optimal control $\bar w$ and state $\bar\rho$ must satisfy

$$D_\rho\mathcal{L}(\bar\rho,\bar w,q_1,q_2)h = 0 \quad \forall h\in L^2(0,T;H^1(\Omega)).$$

In particular if we choose $h\in C_0^\infty(Q)$ where $h|_{\partial Q} = 0 = \dfrac{\partial h}{\partial n}|_{\partial Q}$, and $h(x,0) = h(x,T) = 0$,, we have that

$$\int_0^T\int_\Omega(\bar\rho-\widehat\rho)h\, dxdt - \int_0^T\int_\Omega\left(-\partial_t q_1 - \nabla\cdot(\nabla q_1)\right)h\, dxdt = 0,$$

which by the Fundamental Lemma of Calculus of Variations implies that

$$\bar\rho - \widehat\rho + \partial_t q_1 + \nabla\cdot(\nabla q_1) = 0 \quad \text{ on } Q.$$

Next, if we drop the condition that $h(x,T) = 0$, and combine with the PDE just derived, we obtain the equation

$$\int_\Omega q_1(\mathbf{x},T)h(\mathbf{x},T)\, dx = 0.$$

Hence by the Fundamental Lemma of Calculus of Variations, we obtain the final time condition, $q_1(\mathbf{x},T) = 0$. If we next consider $h\in H_0^1(Q)$ so that only $h|_{\partial Q} = 0$, then we have that

$$\int_0^T\int_{\partial\Omega} q_1\frac{\partial h}{\partial n}\, dsdt = 0,$$

from which we obtain the spatial boundary condition $q_1 = 0$ on ∂Q. If we then consider all remaining $h\in L^2(0,T;H^1(\Omega))$, we obtain an equation that links q_1 and q_2, that is

$$q_2 = -\frac{\partial q_1}{\partial n} \quad \text{ on } \partial\Omega.$$

After relabelling q_1 as q, we obtain the PDE

$$\begin{aligned} -\partial_t q - \nabla \cdot (\nabla q) &= \bar{\rho} - \widehat{\rho} \quad \text{in } Q, \\ q &= 0 \quad \text{at } t = T, \\ q &= 0 \quad \text{on } \partial Q. \end{aligned} \tag{3.17}$$

which we refer to as the *adjoint equation*.

Finally, we wish to find the *gradient equation* which is derived from the Fréchet derivative of the Lagrangian operator $\mathcal{L}$ with respect to the control variable, w. Once again for a stationary point, the optimal control and state must satisfy

$$D_w \mathcal{L}(\bar{\rho}, \bar{w}, q_1, q_2)h = 0 \quad \forall h \in L^2(0, T; H^1(\Omega)).$$

This gives that

$$\int_0^T \int_\Omega (\beta \bar{w} + q_1) h \, dx dt = 0 \quad \forall h \in L^2(0, T; H^1(\Omega)).$$

Hence by the Fundamental Lemma of Calculus of Variations, and after relabelling q_1 as q, we obtain

$$\beta \bar{w} + q = 0 \quad \text{a.e. in } Q. \tag{3.18}$$

We note that there are no equations on the boundary of Q involving the control variable w in this particular example. Some examples from particle dynamics have the control variable present in the boundary conditions. In fact, there is a class of PDE-constrained optimization problems referred to as *boundary control problems* [121, Chapter 1], where the control variable is only measured within $\mathcal{J}$ through the boundary, but these are not studied in this thesis.

We have now obtained the continuous first-order optimality system for problem (3.13), consisting of the *state equation* (3.14), *adjoint equation* (3.17), and *gradient equation* (3.18):

$$\begin{aligned} \partial_t \bar{\rho} - \nabla \cdot (\nabla \bar{\rho}) &= \bar{w} \quad \text{in } Q, \\ \bar{\rho} &= \rho_0 \quad \text{at } t = 0, \\ \bar{\rho} &= 0 \quad \text{on } \partial Q. \end{aligned}$$

$$\begin{aligned} -\partial_t q - \nabla \cdot (\nabla q) &= \bar{\rho} - \widehat{\rho} \quad \text{in } Q, \\ q &= 0 \quad \text{at } t = T, \\ q &= 0 \quad \text{on } \partial Q. \end{aligned}$$

$$\beta \bar{w} + q = 0 \quad \text{in } Q.$$

We can also make $\bar{w}$ the subject of the *gradient equation* to obtain $\bar{w} = -\frac{1}{\beta} q$, and substitute it into the *state equation* to obtain:

$$\begin{aligned} \partial_t \bar{\rho} - \nabla \cdot (\nabla \bar{\rho}) &= -\frac{1}{\beta} q \quad \text{in } Q, \\ \bar{\rho} &= \rho_0 \quad \text{at } t = 0, \\ \bar{\rho} &= 0 \quad \text{on } \partial Q. \\ -\partial_t q - \nabla \cdot (\nabla q) &= \bar{\rho} - \widehat{\rho} \quad \text{in } Q, \\ q &= 0 \quad \text{at } t = T, \\ q &= 0 \quad \text{on } \partial Q. \end{aligned}$$

3.4.2 Neumann Boundary Conditions

We now consider the same optimization problem constrained by the heat equation as before, but this time with Neumann boundary conditions:

$$\begin{aligned} \min_{\rho,w} \quad & \frac{1}{2}\int_0^T \int_\Omega (\rho - \widehat{\rho})^2 \, dxdt + \frac{\beta}{2}\int_0^T \int_\Omega w^2 \, dxdt \\ \text{s.t} \quad & \partial_t \rho - \nabla \cdot (\nabla \rho) = w \quad \text{in } Q, \\ & \rho = \rho_0 \quad \text{at } t = 0, \\ & \frac{\partial \rho}{\partial n} = 0 \quad \text{on } \partial Q. \end{aligned} \tag{3.19}$$

We also use the method of Lagrange multipliers to obtain the optimality system for the problem in (3.19). We again introduce the two Lagrange multipliers q_1 and q_2 (assumed to have appropriate smoothness) arising from the *adjoint* variable q, and relating to the interior and boundary of the domain respectively. We now consider the Lagrangian:

$$\begin{aligned} \mathcal{L}(\rho, w, q_1, q_2) = & \frac{1}{2}\int_0^T \int_\Omega (\rho - \widehat{\rho})^2 \, dxdt + \frac{\beta}{2}\int_0^T \int_\Omega w^2 \, dxdt \\ & - \int_0^T \int_\Omega \left(\partial_t \rho - \nabla \cdot (\nabla \rho) - w\right) q_1 \, dxdt - \int_0^T \int_{\partial\Omega} q_2 \frac{\partial \rho}{\partial n} \, dsdt. \end{aligned}$$

We note that the difference in this Lagrangian compared to that of the previous example is the change in boundary conditions. Hence our procedure remains the same, except on the boundary and this leads to the optimality system consisting of the *state equation*, *adjoint equation* and *gradient equation*:

$$\begin{aligned} \partial_t \bar{\rho} - \nabla \cdot (\nabla \bar{\rho}) &= \bar{w} \quad \text{in } Q, \\ \bar{\rho} &= \rho_0 \quad \text{at } t = 0, \\ \frac{\partial \bar{\rho}}{\partial n} &= 0 \quad \text{on } \partial Q. \end{aligned}$$

$$\begin{aligned} -\partial_t q - \nabla \cdot (\nabla q) &= \bar{\rho} - \widehat{\rho} \quad \text{in } Q, \\ q &= 0 \quad \text{at } t = T, \\ \frac{\partial q}{\partial n} &= 0 \quad \text{on } \partial Q. \end{aligned}$$

$$\beta \bar{w} + q = 0 \quad \text{in } Q.$$

Here, we can also rewrite the *gradient equation* as $\bar{w} = -\frac{1}{\beta} q$ and substitute this into the *state equation* to obtain:

$$\begin{aligned} \partial_t \bar{\rho} - \nabla \cdot (\nabla \bar{\rho}) &= -\frac{1}{\beta} q \quad \text{in } Q, \\ \bar{\rho} &= \rho_0 \quad \text{at } t = 0, \\ \frac{\partial \bar{\rho}}{\partial n} &= 0 \quad \text{on } \partial Q. \end{aligned}$$

$$\begin{aligned} -\partial_t q - \nabla \cdot (\nabla q) &= \bar{\rho} - \widehat{\rho} \quad \text{in } Q, \\ q &= 0 \quad \text{at } t = T, \\ \frac{\partial q}{\partial n} &= 0 \quad \text{on } \partial Q. \end{aligned}$$

3.5 Additional Control Constraints

3.5.1 Background

As mentioned in Section 3.1, in particular Section 3.3.1, the convex set K in the general PDE-constrained optimization problem (3.1) can be used to impose additional inequality constraints on either the state or control variable. These constraints could be of great practical use, for instance, in the example described earlier concerning storing raw materials, or cooling server rooms, an additional state constraint would involve rigidly specifying the atmospheric conditions which may occur, and an additional control constraint would put fixed limits on the amount of energy allowed to be expended on the physical system.

A variety of methods have been developed to tackle PDE-constrained with pointwise state and control constraints, for example *box constraints* [234]. State constraints typically require careful consideration of regularity requirements, compared to control constraints [31]. A few of these methods that have been shown to work on distributed control optimization problems with Dirichlet, Neumann, or periodic type boundary conditions are: Interior Point Methods (IPMs) [173, 250], Lagrangian and Augmented Lagrangian methods [33], the Moreau–Yosida Regularization [9, 190], Semi-smooth Newton methods (SSN) [127, 165, 232, 247], the Primal-Dual Active Set strategy [32, 70, 126, 147], and the Alternating Direction Method of Multipliers (ADMM) [94, 230].

Interior point methods are often considered for the *discretize-then-optimize* approach, and have been used to solve problems involving semilinear elliptic equations subject to control and state inequality constraints (see [173] for example). In [30, 33], Lagrangian and augmented Lagrangian methods are applied to optimal control problems with additional state and control constraints. The Lagrangian formulation is utilized for decoupling the state equation, and also for problems where other methods may lead to high number of iterations to converge. The Moreau–Yosida regularization and SSN methods have been used very successfully in both the *discretize-then-optimize* and *optimize-then-discretize* approaches. Comparison of the effectiveness of the Moreau–Yosida regularization against interior point methods for the *discretize-then-optimize* approach can be found in [31]. SSN methods provide state-of-the-art algorithms for solving optimal control problems constrained by any class of linear PDEs with additional box constraints. We refer to [127,165,232,247] which introduce the hybrid semismooth quasi-Newton methods for optimal control problems with the additional non-smooth pointwise state and control constraints. The Primal-Dual Active Set Strategy arose as a special case of the generalized Moreau–Yosida regularization, and is based on an active set strategy involving primal as well as dual variables (see [32, 70, 126]). The Primal-Dual Active Set strategy has been shown to converge for a general class of infinite dimensional optimal control problems with linear PDE constraints (see [147]). Previously, ADMM was used as the first step, in a two-phased approach, to find a good initial guess for the Primal-Dual Active Set strategy to solve elliptic optimal control problems with pointwise box constraints on the control variable (see [230]). However, recent studies in [230] and [94] extends ADMM to solve a range of optimal control problems constrained by linear parabolic equations, hyperbolic equations, advection-diffusion equations and fractional parabolic equations.

In Chapters 6 and 7, we will consider PDE-constrained optimization problems arising from opinion dynamics, a research area that deals with human populations. In this regard, the control variable is a section of the human population, and it becomes practical to enforce positivity of the control population resulting in inequality bounds on the control variable. We note that convergence of all the above mentioned methods for problems involving non-linear and non-local PDEs such as the type considered in this thesis are yet to be shown, and would be a valuable avenue of future work. However, we adopt the Primal-Dual Active Set strategy as the most likely method to tackle the additional bound constraints for problems in this thesis, because of its general success with similar problems constrained by non-linear parabolic PDEs (see [104]). In this section, we illustrate the theory of this strategy, by applying the Primal-Dual Active Set strategy to a version of the distributed control example involving the heat equation stated in Section 3.4 with additional control constraints.

3.5.2 Primal-Dual Active Set Strategy

First introduced in [67], the Primal-Dual Active Set strategy is a numerical method to solve problems with additional bound constraints. It is shown in [119] to be equivalent to a semismooth Newton method, which is important as superlinear convergence is therefore guaranteed under suitable conditions [36].

Let us consider the distributed control optimization problem constrained by the heat equation with Dirichlet boundary conditions which involve additional control constraints:

$$\begin{aligned} \min_{\rho,w} \quad & \frac{1}{2}\int_0^T\int_\Omega (\rho-\widehat{\rho})^2\,dxdt + \frac{\beta}{2}\int_0^T\int_\Omega w^2\,dxdt \\ \text{s.t} \quad & \partial_t\rho - \nabla\cdot(\nabla\rho) = w \quad \text{in } Q, \\ & \rho = \rho_0 \quad \text{at } t=0, \\ & \rho = 0 \quad \text{on } \partial Q, \\ & w_a \le w \le w_b \quad a.e. \text{ in } Q. \end{aligned} \tag{3.20}$$

Here, w_a and w_b are either constants or functions in terms of the spatial coordinate, and provide lower and upper bounds that the control variable w is required to satisfy. We define $W_{ad} = \{w : w_a \le w \le w_b \quad a.e. \text{ in } Q\}$ as the set of all admissible functions for the control variable. We base our methodology for solving problem (3.20) following the derivation in [234].

We note that in the corresponding problem (3.13) with no additional control constraints, we obtain the optimality system consisting of the state, adjoint and gradient equation as:

$$\begin{aligned} \partial_t\bar{\rho} - \nabla\cdot(\nabla\bar{\rho}) &= \bar{w} \quad \text{in } Q, \\ \bar{\rho} &= \rho_0 \quad \text{at } t=0, \\ \bar{\rho} &= 0 \quad \text{on } \partial Q, \end{aligned}$$

$$\begin{aligned} -\partial_t q - \nabla\cdot(\nabla q) &= \bar{\rho} - \widehat{\rho} \quad \text{in } Q, \\ q &= 0 \quad \text{at } t=T, \\ q &= 0 \quad \text{on } \partial Q, \end{aligned}$$

$$\beta\bar{w} + q = 0 \quad \text{in } Q,$$

respectively, with the gradient equation being the result of the optimality condition:

$$D_w\mathcal{L}(\bar{\rho},\bar{w},q_1,q_2)h = 0, \quad \forall h \in L^2(0,T;H^1(\Omega)). \tag{3.21}$$

From the theory of Lagrange multipliers discussed in Section 3.3.1, the additional box constraints on the control w in problem (3.20), results in the *variational inequality*:

$$(w-\bar{w})D_w\mathcal{L}(\bar{\rho},\bar{w},q_1,q_2)h \ge 0, \quad \forall h \in L^2(0,T;H^1(\Omega)), \quad \forall w \in W_{ad}, \tag{3.22}$$

which follows from the variational inequality problem defined in (3.7), and written here as:

$$\mathcal{F}'(\bar{w})(w-\bar{w}) \ge 0 \quad \forall w \in W_{ad}.$$

The functional $\mathcal{F}(w)$ is obtained by making ρ the subject of the state equation and substituting it into the objective function. From the condition (3.22), we now have the inequality:

$$(w-\bar{w})(\beta\bar{w}+q) \ge 0 \quad \forall w \in W_{ad}, \tag{3.23}$$

for problem (3.20). We note that in the absence of box constraints, (3.23) would reduce to the gradient equation, $\beta\bar{w} + q = 0$.

With W_{ad} as defined above, we obtain the expression of $\bar{w}$ from (3.23) as:

$$\bar{w} = \begin{cases} = w_b & \beta\bar{w} + q < 0, \\ \in W_{ad} & \beta\bar{w} + q = 0, \\ = w_a & \beta\bar{w} + q > 0. \end{cases} \tag{3.24}$$

Generally, we are able to introduce additional Lagrange multipliers to transform inequality constraints to equality constraints, referred to as the *complementary slackness condition* [197, Chapter 22]. The approach in [234] introduces two new Lagrange multipliers μ_a and μ_b, cleverly defined (using relation (3.24)) as $\mu_a := (\beta\bar{w} + q)_-$ and $\mu_b := (\beta\bar{w} + q)_+$, where

$$(\beta\bar{w} + q)_- = \begin{cases} \beta\bar{w} + q & \beta\bar{w} + q \geq 0, \\ 0 & \text{otherwise}, \end{cases}$$

and

$$(\beta\bar{w} + q)_+ = \begin{cases} |\beta\bar{w} + q| & \beta\bar{w} + q \leq 0, \\ 0 & \text{otherwise}. \end{cases}$$

The *complementary slackness condition* is written as:

$$\begin{aligned} &(w_a - \bar{w})\mu_a = 0, \quad \mu_a \geq 0, \quad w_a - \bar{w} \leq 0, \\ &(\bar{w} - w_b)\mu_b = 0, \quad \mu_b \geq 0, \quad \bar{w} - w_b \leq 0, \end{aligned}$$

For convenience, we introduce a new Lagrange multiplier

$$\mu := \mu_a - \mu_b = \beta\bar{w} + q,$$

and we have for the optimal control

$$\bar{w} = \begin{cases} = w_b & \mu < 0, \\ \in W_{ad} & \mu = 0, \\ = w_a & \mu > 0. \end{cases}$$

Now, let us define the *active sets* for this problem, on the discretized space domain with $N+1$ points as

$$\begin{aligned} A_+ &= \{i \in \{0, 1, \ldots, N\} : (w - \mu)_i > (w_b)_i\}, \\ A_- &= \{i \in \{0, 1, \ldots, N\} : (w - \mu)_i < (w_a)_i\}, \\ A_I &= \{0, 1, \ldots, N\} \backslash (A_+ \cup A_-), \end{aligned} \tag{3.25}$$

where $(w-\mu)_i$, $(w_a)_i$ and $(w_b)_i$ denote the values of $w - \mu$, w_a and w_b, respectively, at the i-th node. These sets correspond to the nodes at which the control constraints are achieved (A_I), or violated (A_- and A_+). In [234], an Active Set method, presented in Algorithm 1, is used to compute $\rho^{(k)}$, $q^{(k)}$ and $w^{(k)}$, which are successive approximations to the optimal solutions $\bar{\rho}$, q and $\bar{w}$. The following conditions have to hold in each step of the iterative procedure:

$$\begin{aligned} \partial_t\bar{\rho}^{(k)} - \nabla \cdot (\nabla\bar{\rho}^{(k)}) &= \bar{w}^{(k)} \quad \text{in } Q, \\ \bar{\rho}^{(k)} &= \rho_0 \quad \text{at } t = 0, \\ \bar{\rho}^{(k)} &= 0 \quad \text{on } \partial Q, \end{aligned} \tag{3.26}$$

$$\begin{aligned} -\partial_t q^{(k)} - \nabla \cdot (\nabla q^{(k)}) &= \bar{\rho}^{(k)} - \widehat{\rho} \quad \text{in } Q, \\ q^{(k)} &= 0 \quad \text{at } t = T, \\ q^{(k)} &= 0 \quad \text{on } \partial Q, \end{aligned} \tag{3.27}$$

$$\begin{aligned} \beta\bar{w}^{(k)} + q^{(k)} - \mu^{(k)} &= 0 \quad \text{in } Q, \\ \bar{w}^{(k)} &= w_a \text{ on } A_-^{(k)}, \\ \bar{w}^{(k)} &= w_b \text{ on } A_+^{(k)}, \end{aligned} \tag{3.28}$$

$$\mu^{(k)} = 0 \text{ on } A_I^{(k)}.$$

Algorithm 1 Active Set algorithm for control constrained optimal control problems

Choose $w^{(0)}, \mu^{(0)}$
Define active sets $A_-^{(0)}, A_+^{(0)}, A_I^{(0)}$ using definitions (3.25) and $u^{(0)}, \mu^{(0)}$
for $k = 1, 2, \ldots$ **do**
  Solve (3.26), (3.27), (3.28) on the free variables from previous iteration (on $\mathcal{A}_I^{(k-1)}$)
  Update $\mu^{(k)}$ via $\mu^{(k)} = \beta w^{(k)} + q^{(k)}$
  Define new active sets $A_-^{(k)}, A_+^{(k)}, A_I^{(k)}$ using $u^{(k)}, \mu^{(k)}$
  if $A_-^{(k)} = A_-^{(k-1)}$, $A_+^k = A_+^{(k-1)}$, and $A_I^k = A_I^{(k-1)}$ **then**
    Stop. Algorithm converged
  end if
end for

The procedure is terminated at the iteration where the active sets remain unchanged from the previous iteration. We note that the optimality system (3.26), (3.27), and (3.28) has to be solved at each iteration of the Active Set method. The algorithm therefore stops at an optimal (is a stationary point of the objective function, and satisfies the PDE constraints) and feasible (obeys the additional bound constraints) point.

The Active Set strategy gives a first look into the comprehensive numerical framework developed in this thesis, to solve PDE-constrained optimization problems from multiscale particle dynamics. Later, in Chapters 5, 6 and 7, we discuss the class of problems we wish to solve, and extensively detail the numerical methods employed to solve their continuous first-order optimality systems in Chapter 4.

3.6 Applications of PDE-Constrained Optimization Problems

Partial differential equations can mathematically model a multitude of natural phenomena, hence there are unlimited possibilities to formulate optimization problems in scientific applications as PDE-constrained optimization problems. To provide an illustration, we now present some applications of PDE-constrained optimization problems in industry.

One example of an optimal control problem is the Monge–Kantorovich mass transfer problem, where one wishes to find a mapping from one bounded density function to another that is optimal in a suitable sense, by minimizing the *Kantorovich distance* (least action needed) between the two functions (see [8, 27, 28]). A practical application is the mass transport of construction materials from one site to another. Optimal control is also applied to chemical processes (involving reaction-diffusion equations), where state variables relate to concentrations of reactants (with one possibly denoting a temperature), and the control relating to the rate at which a chemical is fed into the reaction mechanism or a boundary condition, with the aim of minimizing the "cost" of carrying out the reaction. See [22, 103–105] for examples of these boundary control problems governed by a system of semilinear parabolic PDEs with additional pointwise control constraints. Other applications of optimal control problems appear through the optimization of fluid flow, also called *flow control*, for example modelled by advection-diffusion equations [109,150], and in electronics, where second-order methods are proposed to solve an optimal semiconductor design problem based on the standard drift diffusion model [120].

Parameter estimation in PDE-constrained optimization typically arise from *inverse problems* (in some sense, the counterpart of *forward problems*). In forward problems, the PDE parameters (initial conditions, boundary and domain sources, material coefficients, and the domain geometry) are known, and the state of the system is determined by solving the PDE. The inverse problem reverses the process: some components of the state are observed, while some subset of PDE parameters are unknown. Parameter estimation of the unknown parameters of the PDE then involves formulating an objective function that minimizes the differences between the observed states and those predicted by the PDE. The solution to this typically

ill-conditioned and strongly nonlinear optimization problem yields components of the unknown parameters. Applications arise in medical imaging and tomography [16, 51, 59, 129, 135], a field where low-energy visible or near infra-red light is used to probe highly scattering media, in order to derive qualitative or quantitative images of the optical properties of these media. In optical tomography, light is guided by fibre optics to the surface of the subject, and detecting fibres are used to measure the transilluminated light. Thus the inverse problem is one of the recovery of coefficients in a domain from data on its boundary. Other applications appear in electromagnetic inverse problems [3, 114, 115], in which the goal is to determine coefficients of the material parameter field of a heterogeneous medium, given a source and waveform observations at receiver locations on its boundary. Inverse problems of this type arise in seismic exploration, earthquake modeling, ocean acoustics and obstacle detection.

Shape optimization involves the optimal design of the geometry of an object of interest. It is indispensable for designing and constructing industrial components and therefore appears in many applications in the engineering sector. For instance, in aerodynamics, it is used in finding the optimal shape of an *airfoil*. An *airfoil* is the cross-sectional shape of an object whose motion through a gas is capable of generating significant lift, such as a wing, a sail, or the blades of propeller, rotor, or turbine. In [183, 228], the airfoil design problem is formulated as a PDE-constrained optimization problem in which flow variables and design variables are viewed as independent, and the coupling steady-state Euler equation is used as a constraint, along with geometric and other constraints. The all-at-once approach is implemented to solve for an optimum airfoil design. Another application in biology is the optimal design of prosthetic bypasses or grafts. Prosthetic grafts are required for coronary artery bypass grafting (CAPG). A coronary artery bypass graft is a surgical procedure used to treat coronary heart disease. The procedure diverts blood around narrowed or clogged parts of the major arteries to improve blood flow and oxygen supply to the heart. Prosthetic bypasses act as alternative conduits for blood during CABG. In [201], the theory of optimal control, using Navier–Stokes equations, is applied in order to optimize the shape of Aorto–Coronaric bypass anastomoses configurations. The aim is to design prosthetic devices that minimize the mechanical loading on blood particles, for instance to avoid damage of red blood cells. This is one of many examples that combine flow control problems in fluid dynamics and shape optimization.

This section provides only a handful of useful PDE-constrained optimization problems; there are many more examples in the literature. In the next chapter, we present the first class of optimization problems tackled in this thesis, which are constructed with DDFT PDEs.

Chapter 4

Numerical Algorithms for PDE-Constrained Optimization Problems from Multiscale Particle Dynamics

In this chapter, we highlight our novel contributions to the study of numerical algorithms to solve PDE-constrained optimization problems that feature a non-linear and non-local integral operator in the forward PDE. Standard numerical implementations cannot be readily applied to these problems, hence necessitating the development of new approaches to address the numerical challenges.

We employ a novel combination of pseudospectral discretization with a first-order fixed-point iterative solver and an Armijo–Wolfe-like line search strategy, or a second-order Newton–Krylov solver to tackle the numerical challenges of solving a system of non-local PDEs. The fixed-point framework for optimization within a pseudospectral method is new for problems of this form, as is as the use of the Newton–Krylov solver for non-linear and non-local PDE-constrained optimization problems. To benchmark the performance of the fixed-point solver, we use a multiple-shooting algorithm to allow for comparisons.

The methods discussed here are implemented in our new 2DChebClass PDECO software [1] and are readily available to be used. The principal novelties added to the software concern the computation of convolution integrals and the implementation of spatial boundary conditions. We also contribute implementations of pseudospectral and finite difference discretization on periodic geometries.

The chapter is organized as follows. In Section 4.1, we detail the pseudospectral discretization and its suitability for the problems we are interested in. Next, we discuss our choice of solver for the forward PDE and present our choice of rewriting the backward adjoint equation as a forward PDE to take advantage of the forward PDE solver in Section 4.2. We then present a multiple shooting solver in Section 4.3 to solve the system of forward PDEs and state its limitations. In Section 4.4, we detail the fixed-point algorithm we employ to solve the system of PDEs from the continuous optimality conditions and present the Armijo–Wolfe step we combine to the fixed–point algorithm to increase the speed of convergence. We then conclude in Section 4.5, by introducing the Newton–Krylov algorithm which we later detail in Chapter 7 to solve 2D PDE-constrained problems.

4.1 Pseudospectral Discretization

The resulting non-linear and non-local systems of PDEs that arise from the first-order optimality conditions in Chapter 5 are highly stiff and non-linear, and pose significant numerical challenges. One particular challenge arises from the convolution terms that describe particle interactions. Most commonly, the convolutions in these integral equations are solved by using fast Fourier transforms (FFT) [107, 136, 219] (see [219] for a comparison of computations on a variety of

geometries in different dimensions). One disadvantage of FFT-based techniques is that they are limited to using periodic boundary conditions. Therefore, non-periodic scenarios must be run in large periodic domains that imitate non-periodicity.

Another option is the real-space quadrature based on the non-uniform pseudospectral discretization [182], which can also be applied for unbounded physical domains, and allows the accurate discretization of density profiles with a small number of collocation points. The pseudospectral method is particularly well-suited to problems on finite, non-periodic domains in which the interaction term involves a convolution on a region with finite support. Such applications arise in diverse fields such as hard-sphere DDFT using Fundamental Measure Theory [95, 96, 98, 182, 216, 241], and opinion dynamics [155], and others on the more popularly studied periodic domains [149]. It is highly accurate, efficient, and fast, and hence our preferred choice of discretization in our numerical framework.

Though the pseudospectral discretization is very suitable for the non-local integral equations we solve, the introduction of non-smooth piecewise bound constraints into the optimization problem presents a challenge. We alternatively employ a finite difference scheme, which requires more points to reach the same accuracy as the pseudospectral method, but is simple to implement and is not as sensitive to smoothness of solutions [225, 254, 268]. Implementing two discretization schemes in our numerical framework emphasize its modularity, and allows for other types of discretization schemes, e.g. Hermite spectral methods [100], and spectral element methods [187], to implemented, if they are suitable for the problems of interest.

In our work, we focus on domains such as intervals and boxes, however the methodology readily extends to other 2D geometries.

4.1.1 Grid Points, Differentiation and Integration Matrices

The starting point is the basic question: given a set of grid points x_j and corresponding function values $u(x_j)$, how do we approximate the derivative of u? Finite difference formulas approximate the derivative of u by utilizing truncated Taylor series expansions of u. It is clear that using higher order terms in the Taylor series leads to denser differentiation matrices that demand more computational resources to evaluate. The idea behind spectral methods is to take this process to the limit, at least in principle, and work with a differentiation formula of infinite order and infinite bandwidth, i.e. a dense matrix. For a finite grid, here is the design principle for spectral collocation methods [245]:

- Let p be a single function (independent of j) such that $p(x_j) = u_j$ for all j.
- Set $w_j = p'(x_j)$.

We are free to choose p to fit the problem at hand. For a periodic domain, where u is a 2π-periodic function, we can choose a trigonometric polynomial on an equispaced grid of points

$$x_j = \frac{2\pi j}{N}, \quad j = 0, 1, \ldots, N.$$

The interpolating polynomial can be defined by the fast Fourier transform to give dense differentiation matrices that require $\mathcal{O}(N \log N)$ operations to be evaluated. For non-periodic domains, a pseudospectral method [41] that uses algebraic polynomials on irregular grids (in our case Chebyshev points) can be used. The *Chebyshev points* are defined as

$$x_j = \cos(j\pi/N), \quad j = 0, 1, \ldots, N,$$

and can be visualized as the projections onto $[-1, 1]$ of equispaced points on the upper half of the unit circle as shown in Figure 4.1.1. They are also called the Chebyshev–Lobatto points or alternatively the Gauss–Chebyshev–Lobatto points. The effect of using these clustered points on the accuracy of the polynomial interpolant is dramatic. The Chebyshev points are used to construct Chebyshev differentiation matrices that are used to solve some boundary value problems.

Construction of the differentiation and integration matrices for periodic and non-periodic domains is detailed in [245], hence we only give an overview of the methods applied here. On

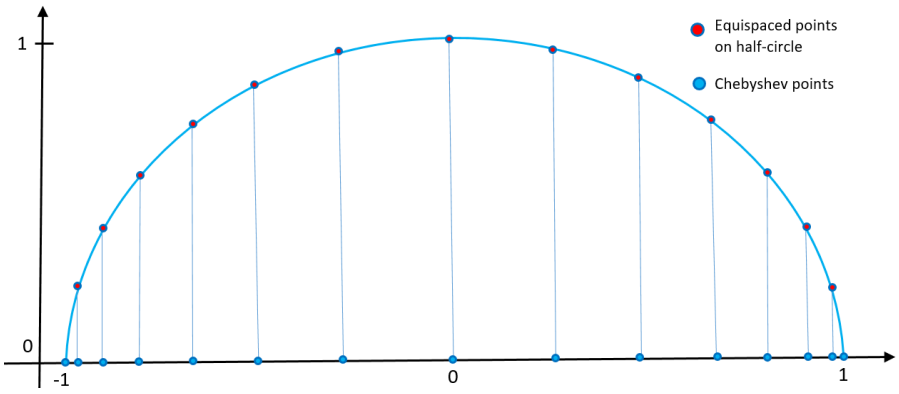

Figure 4.1: Chebyshev nodes on $[-1, 1]$ and their correspondence to a projection of equally–spaced points on a circle.

periodic domains, the inverse Discrete Fourier Transform is applied to approximate the derivatives of a periodic function on a periodic grid, while on non-periodic domains, the differentiation matrices are constructed directly on a Chebyshev grid. A periodic trapezoidal rule approximates the integral of a periodic function while integration on non-periodic domains is achieved via Clenshaw-Curtis quadrature rule [60].

4.1.2 Discretization in Two Dimensions

We naturally set up a two-dimensional rectangular grid as a tensor product grid of two one-dimensional grids in each direction via Kronecker products. The Kronecker product of two matrices A and B is computed in MATLAB by the command `kron(A,B)`. If A and B are of dimensions $p \times q$ and $r \times s$ respectively, then $A \otimes B$ is the matrix of dimension $pr \times qs$ with $p \times q$ block form, where the i, j block is $a_{ij}B$. This matrix, though not always dense, is certainly not as sparse as one typically gets with a discretization using finite differences or finite elements. Fortunately, because of spectral accuracy, we may hope to obtain satisfactory results with dimensions in the hundreds rather than the thousands or tens of thousands. Figure 4.2 shows tensor product grid of Chebyshev points on the box $[-1, 10] \times [2, 9]$.

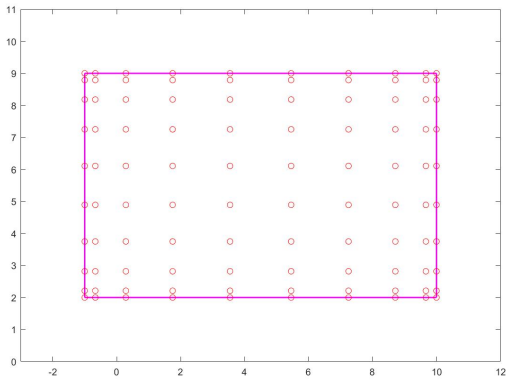

Figure 4.2: Chebyshev nodes on a box.

4.1.3 Convolution

Following the discretization scheme in [182], the convolution integrals are computed in real space, in contrast to many implementations in which they are computed via Fourier transforms. The principal advantage of Fourier methods is that they are computationally cheap, requiring only fast Fourier transforms and multiplication of functions. The main disadvantage

in non-periodic domains is that one needs to pad the domain, which both increases computational cost for no accuracy gain and introduces difficulties when applying boundary conditions. Convolution integrals in the spatial domain can be implemented by a single matrix–vector multiplication, with the matrix precomputed for all time steps. Use of the physical domain allows efficient implementation of the boundary conditions. It is highly important to numerically approximate convolutions for our class of optimization problems, as they contain non-local integral operators that are essential to the dynamics.

For a 1D domain, Ω, if we have the $1 \times (N+1)$ integration vector `Int`, and the $(N+1) \times 1$ state vector $\boldsymbol{\rho}$, and discretized space domain points $y_0, y_1, \ldots, y_N$, we compute the convolution $\mathcal{I}(\boldsymbol{\rho}) = \int_\Omega K(r-r')\rho(r)\rho(r')\,dr'$ via a $N \times N$ matrix, $\mathcal{M}(\boldsymbol{\rho})$ such that $\mathcal{M}(\boldsymbol{\rho})\boldsymbol{\rho}$ approximates $\mathcal{I}(\boldsymbol{\rho})$. We present an algorithm to construct $\mathcal{M}(\boldsymbol{\rho})$ in Algorithm 2.

Algorithm 2 Convolution Matrix

1: **for** $i = 0, 1, \ldots, N$ **do**
2: $K_i = K(x_i - r') = ((N+1) \times 1 \text{ vector})$, $r' = (x_0, x_1, \ldots, x_N)$.
3: $\mathcal{M}_i = \texttt{Int} \times (K_i)^T$ $(1 \times (N+1)$ vector$)$
4: **end for**
5: $\mathcal{M} = \begin{pmatrix} \mathcal{M}_1 \\ \vdots \\ \mathcal{M}_N \end{pmatrix}$
6: $\mathcal{M}(\boldsymbol{\rho}) = \mathcal{M}\boldsymbol{\rho}$

We can also compute the convolution integral on a sub-interval instead of over the whole domain. The integral we want to compute is $\mathcal{I}(\rho) = \int_D K(r-r')\rho(r)\rho(r')\,dr'$, where $D = \|r - r'\| \leq R \subset \Omega$ and R is a positive real number. The process for computing the convolution matrix is similar except for each point r', we create the line $D = \|r - r'\| \leq R$ with a chosen number of space points and then interpolate from the whole domain Ω onto D with an interpolation matrix `IP`. The integration matrix `Int` is obtained on D. We now construct the convolution matrix by multiplying the integration weights on the subdomain with the kernel evaluations, and in this case, also with the interpolation matrix. Hence

$$\mathcal{M}_i = \texttt{Int} \cdot (Ki)^T \cdot \texttt{IP}_i \quad (1 \times (N+1) \text{ vector})$$

For a 2D domain, we compute the convolution matrix in the same exact way except our domain Ω is now a rectangular box instead of a line. Convolution on a sub-domain also follows the same process, however we now have the choice of a box or disc for the sub-domain. We note that this can be generalized to other 2D sub-shapes.

4.2 Forward Partial Differential Equation Solver

After discretization, we are left with a system of ODEs that can be solved on the interior of the domain using standard time-stepping solvers. The challenge lies in imposing the correct spatial boundary conditions. One approach is to modify the differentiation matrix on the right-hand side of the ODE so that the boundary conditions are automatically satisfied. This is known as "boundary bordering" [41] and becomes a highly non-trivial approach when considering the non-local convolution integral. Another approach is to restrict the computation to interpolants (solutions) which satisfy the boundary conditions; we do not discuss this here as it is highly non-trivial for the non-linear, non-local problems that we are interested in. A more generalisable approach is the imposition of spatial boundary conditions, which can be seen as extending the discretized system of ODEs to a system of differential–algebraic equations (DAE), where the discretized PDE is solved on the interior of the domain, and the boundary conditions correspond to algebraic equations. We now further discuss the algebraic equations approach.

4.2.1 Algebraic Equations Approach

There are various numerical methods for solving a system of differential–algebraic equations, see e.g., [227] for a Runge–Kutta scheme with algebraic constraints, or [112] for a Newton–

Krylov scheme which allows the inclusion of algebraic constraints alongside the PDE. The main advantage here is that the numerical method does not have to be explicitly adapted when the boundary conditions change. One simply has to specify different algebraic constraints that correspond to the boundary conditions. In fact, the 2DChebClass code [1] automatically identifies the boundary of various geometries, allowing a simple implementation of this approach.

4.2.2 Implementation of the Forward PDE Solver

We use MATLAB's DAE solver `ode15s`, a variable-step, variable-order solver based on the numerical differentiation formulas of orders 1 to 5 (see [226] for details). It integrates the DAE from a start time to an end time when provided with an initial condition. It solves the DAE with a singular mass matrix, $M(\rho,t)\rho' = f(\rho,t)$, where $M$is a diagonal matrix which has 1 for entries corresponding to the interior of domain, and 0 for those corresponding to the boundary. The corresponding algebraic equation for the boundary condition which, for example, is written as $\nabla\rho\cdot\mathbf{n}=0$ for Neumann boundary condition, where $\mathbf{n}$ is the normal vector to the boundary (for example 1 or -1 for a 1D domain) is added to the ODE system. The straightforward construction of the forward problem solver is showed in this example snippet of code:

```
% Construction of RHS of PDE

function drhodt = rhs(rho)

% Defining flux
flux    = -D*rho + w.*[rho;rho] - kappa*[rho;rho].*(D*(Conv*rho));
% Defining RHS of PDE
drhodt = -D*flux;

% Applying no-flux boundary conditions
drhodt(bound) = normal*flux;

end
```

It is possible to solve the some of the examples in Chapter 5 (particularly when Dirichlet boundary conditions are imposed and the non-local interaction term is turned off) using MATLAB's inbuilt DAE boundary value problem solver `bvp4c` that uses the Lobatto III method. However, the negative Laplacian operator in the resulting ODE system after discretization arising from the adjoint equation presents numerical challenges that can cause `bvp4c` to fail to obtain solutions when no-flux boundary conditions that contain the non-local term are prescribed. We decide to rewrite the final-time adjoint equations as initial-time problems, so as to re-use the forward problem solver to solve the adjoint equation as well. Transforming the adjoint equation also eliminates the negative Laplacian and the numerical challenges that come with it.

4.2.3 Rewriting the Adjoint Equation as an Initial-Time PDE

We transform the adjoint equation by re-parameterizing time t as $\tau = T - t$, where T is the final time. For example, the adjoint equation:

$$\begin{aligned} -\partial_t q - \nabla^2 q - \bar{\mathbf{w}}\cdot\nabla q + \nabla V_{\text{ext}}\cdot\nabla q &= \bar{\rho} - \widehat{\rho} \quad \text{in } Q,\\ q &= 0 \quad \text{at } t = T,\\ \frac{\partial q}{\partial n} &= 0 \quad \text{on } \partial Q, \end{aligned}$$

becomes

$$\begin{aligned} \partial_\tau q - \nabla^2 q - \bar{\mathbf{w}}\cdot\nabla q + \nabla V_{\text{ext}}\cdot\nabla q &= \bar{\rho} - \widehat{\rho} \quad \text{in } Q,\\ q &= 0 \quad \text{at } \tau = 0,\\ \frac{\partial q}{\partial n} &= 0 \quad \text{on } \partial Q, \end{aligned}$$

where $q = q(\mathbf{x}, \tau)$, $\rho = \rho(\mathbf{x}, \tau)$ and $\mathbf{w} = \mathbf{w}(\mathbf{x}, \tau)$. Since we have a straightforward and fast forward PDE solver, it is advantageous to rewrite our adjoint problem also as a forward PDE. However, it introduces the new challenge of needing information on ρ and $\mathbf{w}$ at later times τ that are not readily available to solve for q. If we can supply these later time values of ρ, the optimality system essentially decouples, since successive estimates are provided for the iterative approaches. One approach is to use interpolation to find the later values given the initial time condition, ρ_0, and final time condition, q_T. In order to reduce approximation errors during the interpolation, we can employ the multiple shooting technique to split the time interval into smaller pieces, provide good guesses for ρ and q at the start and end of each interval, interpolate on the smaller time intervals, and impose matching conditions to find the solution ρ and q. Another approach is to use a variation of the fixed-point algorithm that decouples the optimality system by requiring an initial guess for the control variable instead. The guess of the control variable is then used to compute for the state variable first, then the adjoint variable, and the procedure is repeated until solutions satisfying some tolerance condition are obtained. Another possibility is to employ the Newton–Krylov method that considers the full space–time discretization of the forward–backward system and cast it as a large-scale set of nonlinear equations, which can be solved via a Newton method. We now present the details of all three approaches.

4.3 A Multiple Shooting Solver

After rewriting the adjoint equations as an initial-time PDE, we are able to solve the system simultaneously as an initial value system, and after discretizing in space, we obtain a system of non-linear ordinary differential equations (ODEs). Extensive work on using direct multiple shooting as a fast solver for ODE-constrained optimal control problems by exploiting the structure of the problem has been done by Bock and his co-authors. For example, in [38], they developed a multiple shooting algorithm for the numerical solution of parameterized optimal control problems in connection with a recursive quadratic programming technique. The authors introduced a condensing algorithm for the solution of the approximating linearly constrained quadratic subproblems, and high rank update procedures, which are especially suited for optimal control problems and lead to significant improvements of the convergence behaviour and reductions of computing time and storage requirements. The algorithm is completely derivative-free due to internal numerical differentiation schemes, and it can be conveniently combined with indirect multiple shooting. Also in [76], the authors show the effectiveness of the direct multiple shooting algorithm to solve a non-linear ODE-constrained optimization problem from a robot model generator. Hence, we are motivated to explore using a multiple shooting algorithm to solve the PDE-constrained optimization problems we are interested in. We follow the multiple shooting method [175], derived from the popular shooting method [91, 134, 265] to solve boundary value ODEs.

A boundary value problem may be stated as the ODE:

$$y'(t) = g(y, t), \quad \text{on } (0, T), \quad y(T) = c, \tag{4.1}$$

where y is a variable of interest dependent on time, $(0, T)$ is a time interval, with T as final time, and c is some prescribed value y at final time. For simple boundary value problems that have an analytic solution, the solution is obtained by integrating both sides of (4.1) over the time domain $(0, T)$ to get an expression for y with an integration constant. One can then substitute the boundary condition $y(T) = c$ into the expression to evaluate the integration constant. For more complex problems that cannot be solved with analytical techniques, numerical algorithms are employed to obtain solutions, for example, finite difference or shooting methods. In the shooting method, a guess for the initial time value of y, $y(0) = y_0$ is given. The ODE is then solved multiple times until the final time value of an iterate coincides with the final time condition $y(T) = c$.

The fast convergence of a shooting method clearly depends on the accuracy of the initial time guess, which can be non-trivial to find. The multiple shooting method can be described

as a more robust way to apply the shooting method. The first step of multiple shooting is to split the time interval into subintervals, for example, $n+1$ subintervals of the same size (t_i, t_{i+1}), $i = 0, 1, \ldots n$ and $t_{i+1} - t_i = h$, for all i. An initial guess $y(t_i)$ is then provided at the start of each subinterval. The ODE is then solved independently on each subinterval, and a solution is obtained when the final time value of y on each subinterval coincide with the initial time value of y on the consecutive subinterval. This matching of endpoints of the subintervals constitute the bulk of the numerical challenge in multiple shooting. Since we already have an accurate initial value problem solver that can apply arbitrary boundary conditions, we only have to tackle the matching conditions to obtain the optimal solutions we seek.

4.3.1 Setting Up Matching Conditions for Multiple Shooting Method

Let the time interval be discretized into $n+1$ points as $t = t_0, t_1, \ldots, t_n$. Then let the guesses for ρ and q at these time points be $\rho_0, \rho_1, \ldots, \rho_n$ and $q_0, q_1, \ldots, q_n$, respectively. Now let the numerical solutions from our forward problem solver at the time point t_i, $i = 0, 1, \ldots, n$ be $\tilde{\rho}_i$ and $\tilde{q}_i$. Then the matching conditions for the numerical solution to be continuous on the whole time interval is

$$\begin{pmatrix} \rho_0 \\ \rho_1 \\ \vdots \\ \rho_n \end{pmatrix} = \begin{pmatrix} \tilde{\rho}_0 \\ \tilde{\rho}_1 \\ \vdots \\ \tilde{\rho}_n \end{pmatrix} \quad \text{and} \quad \begin{pmatrix} q_0 \\ q_1 \\ \vdots \\ q_n \end{pmatrix} = \begin{pmatrix} \tilde{q}_0 \\ \tilde{q}_1 \\ \vdots \\ \tilde{q}_n \end{pmatrix}.$$

We can now write these matching conditions as a root problem and use any of MATLAB's root solvers, preferably `fsolve`, to find a solution as follows:

$$\begin{pmatrix} \rho_0 & q_0 \\ \rho_1 & q_1 \\ \vdots & \vdots \\ \rho_n & q_n \end{pmatrix} - \begin{pmatrix} \tilde{\rho}_0 & \tilde{q}_0 \\ \tilde{\rho}_1 & \tilde{q}_1 \\ \vdots & \vdots \\ \tilde{\rho}_n & \tilde{q}_n \end{pmatrix} = \begin{pmatrix} 0 & 0 \\ 0 & 0 \\ \vdots & \vdots \\ 0 & 0 \end{pmatrix}.$$

Since we know the values of ρ_1 and q_n from the problem, we only have to solve for values of ρ and q at the other time points. The algorithm is detailed as follows:

Algorithm 3 Multiple Shooting

```
Set up spatial domain Ω using Chebyshev or Fourier points
Divide time interval, t = (0, T), into n + 1 points
Assign initial guesses to ρ and q at each time point
while error > tolerance do
    for i = 1 to n steps do
        Solve ODE on (t_i, t_{i+1})
        Find error between initial guesses and ODE solution at matching time points
    end for
end while
```

Although the multiple shooting Algorithm 3 makes it possible to solve the initial value system, it can be computationally expensive to use for problems in two dimensions (demonstrated in Section 5.4), and the convergence of the root solver largely depends on good initial guesses which are not trivial to find. It is therefore necessary to explore more computationally efficient algorithms. In the next section, we discuss a fixed-point algorithm which is often observed to be faster for our problems compared to the multiple shooting approach.

4.4 A Fixed-Point–Armijo–Wolfe-type Solver

4.4.1 The Fixed–Point Algorithm

We consider the fixed-point problem (see [123]):

$$\text{Find } x_* \in \text{ Fix}(T) := \{x_* \in \Omega \text{ such that } T(x_*) = x_*\}, \tag{4.2}$$

where Ω is a real Hilbert space with inner product $\langle \cdot, \cdot \rangle$ and its induced norm $\| \cdot \|$. T is a nonexpansive mapping from Ω onto itself, and one assumes that $\text{Fix}(T) \neq \emptyset$. Problem (4.2) includes constrained convex optimization problems and one useful algorithm for solving it is the Krasnosel'skiĭ–Mann algorithm [23, 34, 63, 145] defined as follows: given the current iterate $x_i \in \Omega$ and step size $\lambda_i \in (0, 1)$ the next iterate x_{i+1} of the algorithm is

$$\begin{aligned} x_{i+1} &= (1 - \lambda_i)x_i + \lambda_i T(x_i) \\ &\text{or} \\ x_{i+1} &= x_i + \lambda_i (T(x_i) - x_i). \end{aligned} \tag{4.3}$$

Assuming that $(\lambda_i)_{i \in \mathcal{N}}$ satisfies the condition

$$\sum_{i=0}^{\infty} \lambda_i (1 - \lambda_i) = \infty, \tag{4.4}$$

the sequence $(x_i)_{i \in \mathcal{N}}$ generated by (4.3) weakly converges to a fixed point of T [23]. This result indicates that an iterative algorithm using (4.3) with constant step sizes (e.g., $\lambda_i := \lambda \in (0, 1) \in \mathcal{N}$) or diminishing step sizes (e.g., $\lambda_i := 1/(i + 1) \in \mathcal{N}$) can solve (4.2).

Now, [5] and [44] follow the guidelines of a semi-Lagrangian scheme developed in [48] to solve mean field optimal control problems. We extend their algorithms here, combining their approach with guidelines for using the Krasnosel'skiĭ–Mann algorithm to solve constrained smooth convex optimization in [123]. The aim is to find the control variable, for example $w \in (0, T) \times \Omega$, that is a fixed point of the optimality system. The iterative step will be:

$$\begin{aligned} w_{i+1} &= (1 - \lambda_i)w_i + \lambda_i w_i^g \\ &\text{or} \\ w_{i+1} &= w_i + \lambda_i (w_i^g - w_i), \end{aligned} \tag{4.5}$$

assuming that $(\lambda_i)_{i \in \mathbb{N}}$ satisfies the condition

$$\sum_{i=0}^{\infty} \lambda_i (1 - \lambda_i) = \infty. \tag{4.6}$$

Here, w_i^g corresponds to $T(w_i)$ which we defined as w obtained by solving the first-order optimality system from the PDE-constrained optimization problem. The steps in the fixed–point algorithm would proceed as follows:

1. Provide initial data for the control variable, w_0.
2. Solve the state equation using initial data for the control variable to obtain data for the state variable.
3. Solve for the adjoint variable by substituting current estimates for the state and control variables into the adjoint equation.
4. Obtain new data for the control variable, w_i^g, by substituting the data for the state and adjoint variables into the gradient equation.
5. Update the iterate w_{i+1} using the rule (4.5).
6. Repeats steps (2) to (5) until the stopping criteria is satisfied.

The stopping criteria for the Krasnosel'skiĭ–Mann algorithm is

$$\|x_{i+1} - x_i\| = 0,$$

but for practical reasons, it is sufficient to specify ϵ, a small number (for example 10^{-6}) so that

$$\|x_{i+1} - x_i\| \leq \epsilon.$$

The solution w_* to the fixed-point algorithm will then also be a solution to the optimality system, and equally the state and adjoint solutions used to obtain w_* will be solutions of the forward and adjoint equations. The fixed-point algorithm is as follows:

Algorithm 4 Fixed–Point Algorithm

1: Input $w_0, \lambda, TOL, \epsilon$
2: **while** $\epsilon > TOL$ **do**
3: Solve state equation for ρ_i using w_i
4: Solve adjoint equation for q_i using ρ_i and w_i
5: Solve gradient equation for w_i^g using ρ_i and q_i
6: $\epsilon = \|w_i - w_i^g\|_2$
7: Test for convergence
8: $w_{i+1} = (1 - \lambda)w_i + \lambda w_i^g$
9: $i = i + 1$
10: **end while**

Propositions 10 and 11 in [62] show that the Krasnosel'skiĭ–Mann iterations (4.3) with the condition (4.6) has the rate of convergence:

$$\|x_i - T(x_i)\| = \mathcal{O}\left(\left\{\sum_{k=0}^{i} \lambda_k(1 - \lambda_k)\right\}^{\frac{1}{2}}\right).$$

This fact indicates that, even if (4.6) is satisfied, Algorithm 4 does not always converge quickly. This has motivated modifications and variants for the fixed-point algorithm by either adaptively selecting the step size using line search methods or by changing the direction term $(w_i^g - w_i)$ using different rules. We keep the direction term the same, and following work in [123], adapt an Armijo–Wolfe-like rule to adaptively select the step size λ_i in order to accelerate convergence of the fixed-point scheme.

4.4.2 The Armijo–Wolfe Rule

One approach to achieve faster convergence for the fixed-point algorithm is to use line search methods that can find a more adequate step size λ_i at each iteration so that $\|w_{i+1} - w_i^g\|$ decreases dramatically.

The classical Armijo–Wolfe rule was developed for gradient-descent type algorithms utilized to solve optimization problems [121,163]. Here, we use an Armijo–Wolfe-type rule to adaptively choose step sizes in a fixed-point method, following work in [123] showing its effectiveness combined with a fixed-point algorithm for smooth convex optimization problems. The work in [163] proposed an adaptive line search framework that determined a step size to satisfy an Armijo–Wolfe-type condition while also converging to a fixed-point of the system using a potential function. The potential function P_i is defined by (4.7), (4.8), and (4.9):

$$w_i(\lambda) := w_i + \lambda d_i, \tag{4.7}$$
$$Q_i(\lambda) := w_i(\lambda) - w_i^g(\lambda), \tag{4.8}$$
$$P_i(\lambda) := \|Q_i(\lambda)\|^2 \quad \forall \lambda \in (0, 1), \tag{4.9}$$

where

$$d_i := -(w_i - w_i^g), \tag{4.10}$$

We note that $w_i(\lambda_i)$ in (4.7) coincides with w_{i+1} in (4.5). We then consider the minimization problem of P_i over $(0,1)$:

$$\text{Find } \lambda_i \in (0,1) \text{ such that } \quad P_i(\lambda_i) = \min_{\lambda \in (0,1)} P_i(\lambda). \tag{4.11}$$

When the solution λ_i to (4.11) can be obtained at each iteration then $P_i(\lambda_i) \leq P_i(0)$ holds for all $i \in \mathbb{N}$. Also if $w_{i+1} := w_i(\lambda_i)$ then $\|w_{i+1} - w_{i+1}^g\| \leq \|w_i - w_i^g\|$, i.e. $\|w_i - w_i^g\|$ is monotonically decreasing. Since the solution to the minimization problem (4.11) cannot be found easily, λ_i can be chosen to yield an approximate minimum for (4.11) at each iteration, specifically, to satisfy the following Armijo–Wolfe conditions [263,264]: given $w_i, d_i \in (0,T) \times \Omega$ and $\delta, \sigma \in (0,1)$ with $\delta < \sigma$,

$$P_i(\lambda_i) - P_i(0) \quad < \quad \delta \lambda_i \langle Q_i(0), d_i \rangle, \tag{4.12}$$

$$\langle Q_i(\lambda_i), d_i \rangle \quad > \quad \sigma \langle Q_i(0), d_i \rangle. \tag{4.13}$$

Condition (4.12) is the Armijo-type condition for P_i. Under the conditions $d_i := -(w_i - w_i^g)$ and $w_{i+1} = w_i(\lambda_i)$, $i \in \mathbb{N}$, Algorithm (4) with (4.12) satisfies

$$\|w_{i+1} - w_{i+1}^g\|^2 \leq (1 - \delta\lambda_i)\|w_i - w_i^g\|^2, \quad i \in \mathbb{N}$$

which implies for all $i \in \mathbb{N}$

$$\|w_i - w_i^g\| = \mathcal{O}\left(\left\{ \sum_{k=0}^{i} \lambda_k \right\}^{-\frac{1}{2}} \right). \tag{4.14}$$

Hence the step size conditions (4.6), (4.12), and (4.13) affect the efficiency of Algorithm 4. From investigation in [181], there is a possibility that Algorithm 4 with only the Armijo-type condition (4.12) does not make reasonable progress because it allows very short step sizes that can slow down convergence. Hence, condition (4.13) based on the curvature condition discussed in [181] is used to ensure that λ_i is not too small and unacceptable short steps are ruled out. Further, [163] shows that when λ_i satisfying only the Armijo rule is not small enough, Algorithm 4 with Wolfe-type conditions (4.12) and (4.13) will have a better convergence rate than Algorithm 4 with only the Armijo-type condition. Another main concern is how to update d_i to accelerate the search for a fixed point of system. However, work in [163] indicates the definition for d_i in (4.10) has considerable success in finding the step size, hence we do not explore variations of d_i. We now write the algorithm to compute the step sizes satisfying (4.12) and (4.13) with appropriately chosen δ and σ from [151], i.e. $\delta = 0.3$ and $\sigma = 0.5$. The Wolfe-type conditions are written as:

$$\begin{aligned} A_i(\lambda) \quad &: \quad \|w_i(\lambda) - w_i^g(\lambda)\|^2 - \|w_i - w_i^g\|^2 < \delta\lambda \langle w_i - w_i^g, d_i \rangle, \\ W_i(\lambda) \quad &: \quad \langle w_i(\lambda) - w_i^g(\lambda), d_i \rangle > \sigma \langle w_i - w_i^g, d_i \rangle, \end{aligned} \tag{4.15}$$

where for this problem, $w_i(\lambda) = w_{i+1}$ and $w_i^g(\lambda) = w_{i+1}^g$, $d_i = -(w_i - w_i^g)$.

Algorithm 5 Armijo-Wolfe-type Algorithm

Require $A_i(\cdot), W_i(\cdot)$
Ensure $A_i(\lambda), W_i(\lambda)$, $\lambda = 0, \beta = \infty, t = \lambda_0 \in (0, 1)$
loop
  if $\sim A_i(t)$ **then**
    $\beta = t$
  else if $\sim W_i(t)$ **then**
    $\lambda = t$
  else
    λ is found
  end if
  if $\beta < \infty$ **then**
    $t = \dfrac{1}{2}(\lambda + \beta)$
  else
    $t = 2\lambda$
  end if
end loop

We will usually set λ_0 to 1 for rapid convergence, but for some more sensitive problems it may be less than 1. The norms and inner products in (4.15) are defined as:

$$\|w_i - w_i^g\| = \sqrt{(w_i - w_i^g) \cdot (w_i - w_i^g)}$$

Likewise,

$$\langle w_i - w_i^g, d_i \rangle = (w_i - w_i^g) \cdot d_i,$$

Here, $w_i(\lambda) = w_{i+1}$ and $w_i^g(\lambda) = w_{i+1}^g$ with λ as the step size. Hence when $\lambda = 0$, $w_i(\lambda) = w_i$ which implies that $A_i(0) = 0 < \delta\langle w_i - w_i^g, d_i\rangle$ and $W_i(0) : \langle w_i - w_i^g, d_i\rangle > \sigma\langle w_i - w_i^g, d_i\rangle$ are always true since the right hand side of $A_i(0)$ is always positive and $0 < \sigma < 1$ respectively.

We compare the performance of the fixed-point algorithm with and without the Armijo–Wolfe-type rule in Chapter 5.

4.5 A Newton–Krylov Solver

With the goal of achieving satisfactory convergence in a significantly smaller number of iterations than the fixed-point algorithm, we also explore a higher-order Newton-type method. The typical drawback of such a strategy is that one usually needs to solve very large linear systems of equations, unless we design a highly efficient discretization procedure. Furthermore, given the non-local integral particle interaction terms in the PDEs, the linear systems are unquestionably dense for the particle dynamics problems under consideration.

To evade this primary difficulty, and exploit the faster convergence achieved by higher-order optimization methods, we employ a recently devised Newton–Krylov method for PDE-constrained optimization problems [112] (see also [133, 138] for more general descriptions of such methods), and adapt this to the problem at hand by efficiently describing the PDEs and the associated Jacobian on the discrete level, as well as solving the Newton system efficiently. We highlight that such a method has recently been applied to PDE-constrained optimization problems which involve integral terms (see [2]), which is new for advection-diffusion problems, and problems with non-local interaction terms. Using the flow control problem (5.1), and source control problem (5.4) in Chapter 5 as examples, we describe the Newton–Krylov algorithm. The state and adjoint equations may be described in the following general form (see [112]), by separating the spatial and temporal derivatives in each case:

$$\begin{aligned} \mathbf{u}'(t) &= \mathbf{F}(t, \mathbf{u}, \mathbf{v}), \qquad & \mathbf{u}(0) &= \mathbf{u}_0 \in \mathbb{R}^N, \\ \mathbf{v}'(t) &= \mathbf{G}(t, \mathbf{u}, \mathbf{v}), \qquad & \mathbf{v}(T) &= \mathbf{0} \in \mathbb{R}^N, \end{aligned}$$

where $\mathbf{u}, \mathbf{v} : [0, T] \mapsto \mathbb{R}^N$ denote the state and adjoint variables ρ and q evaluated at each point in the time variable, and $\mathbf{u}_0$ corresponding to the initial condition $\rho_0(\mathbf{x})$. The vector functions $\mathbf{F}$ and $\mathbf{G}$ arise from a method of lines discretization of the state and adjoint PDEs at each time-step.

Following the working in [112], we may then consider approximations $\widetilde{\mathbf{u}}_k$, $\widetilde{\mathbf{v}}_k$ to $\mathbf{u}$, $\mathbf{v}$ at the kth time-step t_k, $k \in \{0, 1, ..., n\}$, and define Chebyshev interpolants $\widetilde{\mathbf{u}}(t)$, $\widetilde{\mathbf{v}}(t)$ based on these approximations. The residual functions:

$$\mathbf{r}_u(t) := \int_0^t \mathbf{F}(\tau, \widetilde{\mathbf{u}}(\tau), \widetilde{\mathbf{v}}(\tau)) \, \mathrm{d}\tau - \widetilde{\mathbf{u}}(t) + \widetilde{\mathbf{u}}(0), \quad \mathbf{r}_v(t) := \int_0^t \mathbf{G}(\tau, \widetilde{\mathbf{u}}(\tau), \widetilde{\mathbf{v}}(\tau)) \, \mathrm{d}\tau - \widetilde{\mathbf{v}}(t) + \widetilde{\mathbf{v}}(0),$$

can then be approximated at each time-step, along with the exact imposition of initial/final-time conditions, to obtain the expressions:

$$\begin{aligned}(\mathbf{r}_{u,0}, \mathbf{r}_{u,1}, \ldots, \mathbf{r}_{u,n}) &= (\mathbf{F}_0, \mathbf{F}_1, \ldots, \mathbf{F}_n)Q + (\widetilde{\mathbf{u}}_0 - \widetilde{\mathbf{u}}_0, \widetilde{\mathbf{u}}_0 - \widetilde{\mathbf{u}}_1, \ldots, \widetilde{\mathbf{u}}_0 - \widetilde{\mathbf{u}}_n), \\ (\mathbf{r}_{v,0}, \mathbf{r}_{v,1}, \ldots, \mathbf{r}_{v,n}) &= (\mathbf{G}_0, \mathbf{G}_1, \ldots, \mathbf{G}_n)Q + (\widetilde{\mathbf{v}}_0 - \widetilde{\mathbf{v}}_0, \widetilde{\mathbf{v}}_0 - \widetilde{\mathbf{v}}_1, \ldots, \widetilde{\mathbf{v}}_0 - \widetilde{\mathbf{v}}_n).\end{aligned}$$

Here, $\mathbf{r}_{u,k}$ and $\mathbf{r}_{v,k}$ approximate $\mathbf{r}_u(t_k)$ and $\mathbf{r}_v(t_k)$, $\mathbf{F}_k$ and $\mathbf{G}_k$ denote the functions $\mathbf{F}$ and $\mathbf{G}$ evaluated at time t_k, and $Q = [q_{i,j}]_{i,j=0,1,\ldots,n}$ is a $(n+1) \times (n+1)$ collocation matrix arising from cumulative integration. Based on this, we then wish to (approximately) solve $\mathbf{R} = \mathbf{0}$, where the global residual function $\mathbf{R} : \mathbb{R}^{2N(n+1)} \to \mathbb{R}^{2N(n+1)}$ is given by

$$\mathbf{R} : \begin{pmatrix} \widetilde{\mathbf{u}}_0 \\ \widetilde{\mathbf{v}}_0 \\ \widetilde{\mathbf{u}}_1 \\ \widetilde{\mathbf{v}}_1 \\ \widetilde{\mathbf{u}}_2 \\ \widetilde{\mathbf{v}}_2 \\ \vdots \\ \widetilde{\mathbf{u}}_n \\ \widetilde{\mathbf{v}}_n \end{pmatrix} \mapsto \begin{pmatrix} \mathbf{0} \\ \mathbf{0} \\ \sum_{k=0}^n q_{k,1}\mathbf{F}_k \\ \sum_{k=0}^n q_{k,1}\mathbf{G}_k \\ \sum_{k=0}^n q_{k,2}\mathbf{F}_k \\ \sum_{k=0}^n q_{k,2}\mathbf{G}_k \\ \vdots \\ \sum_{k=0}^n q_{k,n}\mathbf{F}_k \\ \sum_{k=0}^n q_{k,n}\mathbf{G}_k \end{pmatrix} + \begin{pmatrix} \widetilde{\mathbf{u}}_0 - \mathbf{u}_0 \\ \widetilde{\mathbf{v}}_n \\ \widetilde{\mathbf{u}}_0 - \widetilde{\mathbf{u}}_1 \\ \widetilde{\mathbf{v}}_0 - \widetilde{\mathbf{v}}_1 \\ \widetilde{\mathbf{u}}_0 - \widetilde{\mathbf{u}}_2 \\ \widetilde{\mathbf{v}}_0 - \widetilde{\mathbf{v}}_2 \\ \vdots \\ \widetilde{\mathbf{u}}_0 - \widetilde{\mathbf{u}}_n \\ \widetilde{\mathbf{v}}_0 - \widetilde{\mathbf{v}}_n \end{pmatrix}. \tag{4.16}$$

Applying Newton iteration for this problem leads to an iterative procedure of the form

$$\mathbf{x}^{(k+1)} = \mathbf{x}^{(k)} - [\mathbf{J}(\mathbf{x}^{(k)})]^{-1}\mathbf{R}(\mathbf{x}^{(k)})$$

with $\mathbf{J}$ denoting the Jacobian matrix of the residual function $\mathbf{R}$. Although Jacobian-free Newton–Krylov methods have been studied [138], we choose to form the blocks of the Jacobian matrix explicitly due to the availability of this information for the PDE systems under consideration, in order to achieve rapid convergence of the Newton scheme. This requires us to accurately form the functions $\mathbf{F}$ and $\mathbf{G}$, as well as the derivatives of these functions in the directions $\mathbf{u}$ and $\mathbf{v}$. Having formed the appropriate terms of the Newton system at each iteration, these are solved inexactly using an inner Krylov method, specifically the Generalized Minimal Residual (GMRES) algorithm [218]. We describe a suitable preconditioner for solving our PDE systems with GMRES in Section 7.1

We conclude that the combination of 2DChebClass [1] and a fixed-point or Newton–Krylov solver, can enforce essentially arbitrary boundary conditions, such as non-local Robin type, with no additional cost to the user. We are therefore in a position to demonstrate the performance of our numerical framework on a number of applications from multiscale particle dynamics in the coming chapters.

Chapter 5

A Fixed-Point Algorithm for Non-Local Advection-Diffusion Interacting Optimization Problems

In this chapter, we present an *optimize-then-discretize* approach to solve optimization problems constrained by DDFT PDEs featuring source or potential flow terms, and a non-local integral term. We find first-order continuous optimality conditions using the Lagrangian method and employ our novel combination of the pseudospectral discretization scheme, and a first-order fixed-point method, modified to include a mixing rate to find numerical solutions.

The chapter is structured as follows. In Section 5.1, we present the PDE-constrained optimization problems we are interested in solving, and derive their first-order optimality conditions in Section 5.2. In Section 5.3, we introduce our numerical notations and then provide validation tests for the fixed-point method with or without the Armijo–Wolfe-like rule, benchmarked against the multiple shooting method in Section 5.4. Finally in Section 5.5, we present numerical solutions to some examples of the flow control and source control PDE-constrained optimization problems and conclude with remarks of the effectiveness of the fixed-point method.

All numerical computations are carried out on an HP Pavillion laptop running Windows 11, Intel Core i5-8250U 1.80GHz, 8 GB RAM.

5.1 PDE-Constrained Optimization Problems Constrained by a Class of Dynamic Density Functional Theory Models

Many complex systems, ranging from large-scale robotic systems [269] to opinion formation in social systems [52], can be described as multiscale dynamical systems comprising many interacting agents. Here, we use *multiscale* to refer to to microscopic interactions causing macroscopic behaviours. In many such systems, the mutual goal of agents is to perform a desired behaviour, for example, translating as a group (schooling), maintaining the center of mass of the group (flocking), or clustering at single points (concensus) [11, 47, 49]. These studies have successfully shown that the behaviour of large networks of interacting agents can be described and controlled by density functions represented by, for example, the advection-diffusion equation. Naturally, the question arises as to how to optimize agent density functions such that their mutual goals are optimized. Distributed optimal control was introduced in [88], as a coarse-grained optimal control approach that enables the optimization of a cost functional that captures the macroscopic performance of a multiscale dynamical system. The agents' density functions, and/or their moments and controls are driven to reach a desired behaviour.

Motivated by distributed optimal control problems with constraints described by PDEs from multiscale particle dynamics, and their numerous applications in physical and industrial sys-

tems, we provide in this thesis a comprehensive approach for solving distributed optimal control problems, constrained by a class of non-linear and non-local DDFT models. These primarily consist of advection-diffusion equations with additional integral terms that describe systems with interacting agents. These problems are well suited for applications that involve group behaviour such as schooling, flocking, swarming, and aggregating. We provide a framework that covers systems prescribed with arbitrary boundary conditions including Dirichlet, Neumann, no-flux, periodic or a mixture of these boundary conditions.

We introduce the two main PDE-constrained optimization problem structures that we initially consider within a multiscale particle dynamics setting. A significant complication compared to standard PDE-constrained optimization problems is the addition of an integral, interaction term. In the following, the terms 'flow control' and 'source control' refer to the application of the control variable either non-linearly, as a vector field within an advection operator, or linearly, as a scalar source term in the PDE. In nature, transport in fluids occurs through a combination of advection and diffusion. Hence, more realistic problems can be modelled as *optimal flow control problems*. Potential future work may include extending the framework to cover DDFT PDEs that describe both agent density function and their moments, for example inertia, or Fundamental Measure Theory models for hard particles.

Non-Local Optimal Flow Control Problem

We start with the following problem involving minimizing a cost functional containing a sum of L^2-norm terms within the entire space–time interval $Q = \Omega \times (0, T)$, constrained by a non-linear time-dependent advection-diffusion equation with additional non-local integral term, i.e, a DDFT model. The control is applied non-linearly in the form of a vector 'flow' term:

$$\begin{aligned} \min_{\rho,\mathbf{w}} \quad & \mathcal{J}(\rho,\mathbf{w}) \coloneqq \frac{1}{2}\int_0^T\int_\Omega (\rho-\widehat{\rho})^2\,dxdt + \frac{\beta}{2}\int_0^T\int_\Omega \|\mathbf{w}\|^2\,dxdt \\ \text{s.t.} \quad & \mathcal{D}(\rho,\mathbf{w}) - \nabla_{\mathbf{r}}\cdot\mathcal{I}(\rho) = f \qquad \text{in } Q, \\ & \rho = \rho_0(\mathbf{x}) \quad \text{at } t=0, \end{aligned} \tag{5.1}$$

where

$$\mathcal{D}(\rho,\mathbf{w}) = \partial_t\rho - \nabla^2\rho + \nabla\cdot(\rho\mathbf{w}) - \nabla\cdot(\rho\nabla V_{\text{ext}}), \quad \mathcal{I}(\rho) = \kappa\int_\Omega \rho(\mathbf{r})\rho(\mathbf{r}')\mathbf{K}(\mathbf{r},\mathbf{r}')\,dr'.$$

Here, Q consists of some given spatial domain, $\Omega \subset \mathbb{R}^d$, $d \in \{1,2,3\}$, with boundary $\partial\Omega$, and a time interval $(0,T)$, with T a prescribed 'final time' up to which the process is modelled. The scalar function ρ and the vector-valued function $\mathbf{w}$ are the *state* and *control variables*, respectively, $\beta > 0$ is a given *regularization parameter*, and $\widehat{\rho}(\mathbf{x},t)$, $V_{\text{ext}}(\mathbf{x},t)$, $f(\mathbf{x},t)$, $\rho_0(\mathbf{x})$ are prescribed functions corresponding to the *desired state*, *external potential*, PDE source term, and initial condition respectively. We highlight that frequently $f(\mathbf{x},t) = 0$, which results in conservation of mass (one reason we allow the case $f(\mathbf{x},t) \neq 0$ is to enable us to more readily construct analytic test problems for (5.1)). The operator $\nabla_{\mathbf{r}}$ with the subscript $\mathbf{r}$ serves to emphasize which variable we are applying the operator with respect to. The control vector, $\mathbf{w}$, arises from the potential flows discussed in Chapter 2. Additionally, the non-local integral term, $\mathcal{I}(\rho)$ models interactions between individual particles or agents, where $\mathbf{K}$ denotes some vector function. We are particularly interested in the case where $\mathbf{K}$ is odd, i.e., $\mathbf{K}(\mathbf{r},\mathbf{r}') = -\mathbf{K}(\mathbf{r}',\mathbf{r})$; and is the gradient of an even potential, $\mathbf{K}(\mathbf{r},\mathbf{r}') = \nabla_{\mathbf{r}}V_2(\mathbf{r}-\mathbf{r}')$, with $V_2(\mathbf{x}) = V_2(\|\mathbf{x}\|)$. However, we present the approach for a general $\mathbf{K}$. The parameter κ models the particle interaction strength and, for a decreasing $V_2(\|\mathbf{x}\|)$ as $\|\mathbf{x}\| \to \infty$, the integral term $\mathcal{I}(\rho)$ models repulsive interactions when κ is positive and attractive interactions when κ is negative. Of course, much more general choices of V_2 are possible, and setting κ to zero reduces the model to a standard non-linear advection-diffusion equation control problem.

We consider two possibilities for the boundary conditions imposed on ρ, specifically the Dirichlet boundary condition:

$$\rho = c \quad \text{on } \partial Q, \tag{5.2}$$

for a given constant $c \in \mathbb{R}$, and the 'no-flux type' boundary condition:

$$\mathcal{N}(\rho, \mathbf{w}) + \mathcal{I}(\rho) \cdot \mathbf{n} = 0 \quad \text{on } \partial Q, \tag{5.3}$$

where

$$\mathcal{N}(\rho, \mathbf{w}) = \frac{\partial \rho}{\partial n} - \rho \mathbf{w} \cdot \mathbf{n} + \rho \frac{\partial V_{\text{ext}}}{\partial n},$$

with $\frac{\partial}{\partial n}$ denoting the derivative with respect to the normal $\mathbf{n}$.

Non-Local Optimal Source Control Problem

We also consider the following problem, with an analogous cost functional to the flow control problem, but now with a scalar function for the control variable, which is applied linearly in the form of a PDE source term. This is again minimized subject to a non-linear time-dependent advection-diffusion equation with an additional integral term:

$$\begin{aligned} \min_{\rho, w} \quad & \mathcal{J}(\rho, w) = \frac{1}{2} \int_0^T \int_\Omega (\rho - \widehat{\rho})^2 \, dxdt + \frac{\beta}{2} \int_0^T \int_\Omega w^2 \, dxdt \\ \text{s.t.} \quad & \mathcal{D}_l(\rho, w) - \nabla_r \cdot \mathcal{I}(\rho) = f \qquad \text{in } Q, \\ & \rho = \rho_0(\mathbf{x}) \quad \text{at } t = 0, \end{aligned} \tag{5.4}$$

where

$$\mathcal{D}_l(\rho, w) = \partial_t \rho - \nabla^2 \rho - \nabla \cdot (\rho \nabla V_{\text{ext}}) - w.$$

This is posed along with the Dirichlet boundary condition (5.2), or the 'no-flux type' boundary condition:

$$\mathcal{N}_l(\rho) + \mathcal{I}(\rho) \cdot \mathbf{n} = 0 \quad \text{on } \partial Q, \tag{5.5}$$

where

$$\mathcal{N}_l(\rho) = \frac{\partial \rho}{\partial n} + \rho \frac{\partial V_{\text{ext}}}{\partial n}.$$

Both (5.1) and (5.4) constitute an optimization problem constrained by forward PDEs which need to be solved, which is numerically challenging. For the flow control problem we optimize the particle behaviour through a (vector) flow function; for the source control problem we have control of the particle behaviour only through a (scalar) source function.

5.2 First-Order Optimality Conditions

Following the *optimize-then-discretize* approach to solve PDE-constrained optimization problems, we first derive the continuous Lagrangian first-order optimality conditions. We refer to [5] for a rigorous as well as formal derivation of optimality conditions for a problem with a number of similar structures to our systems. A key assumption which we make below is the existence of a control-to-state mapping, allowing the expression of a reduced cost function in terms of the control variable. The optimality system for our problems consist of a *state equation* which is the forward PDE in the optimization problem, and *adjoint equation* and *gradient equation* of the form

$$\begin{aligned} \mathcal{D}^*(\bar{\rho}, \bar{\mathbf{w}}) + \mathcal{I}^*(\bar{\rho}, q) &= \bar{\rho} - \hat{\rho} \quad \text{in } Q, \\ q &= \mathbf{0} \quad \text{at } t = T, \\ \beta \bar{\mathbf{w}} + \bar{\rho} \nabla q &= \mathbf{0} \quad \text{on } Q, \end{aligned} \tag{5.6}$$

and

$$\begin{aligned} \mathcal{D}_l^*(\bar{\rho}, \bar{w}) + \mathcal{I}^*(\bar{\rho}, q) &= \bar{\rho} - \hat{\rho} \quad \text{in } Q, \\ q &= 0 \quad \text{at } t = T, \\ \beta \bar{w} + q &= 0 \quad \text{on } Q. \end{aligned} \tag{5.7}$$

Here, (5.6) arises for the flow control problem (5.1), while (5.7) arises for the source control problem (5.4) with appropriate space boundary conditions, where

$$\mathcal{I}^*(\bar{\rho}, q) = \kappa \left(\int_\Omega \bar{\rho}(\mathbf{r}') \mathbf{K}(\mathbf{r}, \mathbf{r}') dr' \right) \cdot \nabla_{\mathbf{r}} q_1(\mathbf{r}) + \kappa \int_\Omega \left(\bar{\rho}(\mathbf{r}') \mathbf{K}(\mathbf{r}', \mathbf{r}) \cdot \nabla_{\mathbf{r}'} q_1(\mathbf{r}') \right) dr'. \tag{5.8}$$

As an example, we perform the working for the optimal source control (5.4) with no-flux boundary condition (5.5), and later discuss the working for periodic boundary conditions in Chapter 6.

5.2.1 Optimal Source Control Problem with No-Flux Boundary Conditions

We now consider the optimization problem in (5.4) initially with $\kappa = 0$, supplemented with a no-flux type boundary condition:

$$\begin{aligned} \min_{\rho, w} \quad & \mathcal{J}(\rho, w) \coloneqq \frac{1}{2} \int_0^T \int_\Omega (\rho - \widehat{\rho})^2 \, dxdt + \frac{\beta}{2} \int_0^T \int_\Omega w^2 \, dxdt \\ \text{s.t.} \quad & \mathcal{D}_l(\rho, w) = f \qquad \text{in } Q, \\ & \rho = \rho_0(\mathbf{x}) \quad \text{at } t = 0, \\ & (\nabla \rho + \rho \nabla V_{\text{ext}}) \cdot \mathbf{n} = 0 \quad \text{on } \partial Q. \end{aligned} \tag{5.9}$$

We obtain the optimality system by the method of Lagrange multipliers. We introduce the two Lagrange multipliers q_1 and q_2, and consider the Lagrangian:

$$\begin{aligned} \mathcal{L}(\rho, w, q_1, q_2) = & \frac{1}{2} \int_0^T \int_\Omega (\rho - \widehat{\rho})^2 \, dxdt + \frac{\beta}{2} \int_0^T \int_\Omega w^2 \, dxdt \\ & - \int_0^T \int_\Omega \left(\partial_t \rho - \nabla^2 \rho - \nabla \cdot (\rho \nabla V_{\text{ext}}) - w - f \right) q_1 \, dxdt \\ & - \int_0^T \int_{\partial\Omega} \left(\frac{\partial \rho}{\partial n} + \rho \nabla V_{\text{ext}} \cdot \mathbf{n} \right) q_2 \, dsdt. \end{aligned} \tag{5.10}$$

Applying the KKT conditions $D_{q_i} \mathcal{L}(\bar{\rho}, \bar{w}, q_1, q_2) h = 0$, $i = 1, 2$, to the Fréchet derivatives with respect to q_1 and q_2, respectively, produces the forward PDE:

$$\begin{aligned} \partial_t \bar{\rho} - \nabla^2 \bar{\rho} - \nabla \cdot (\bar{\rho} \nabla V_{\text{ext}}) - \bar{w} = f \quad & \text{in } Q \\ \bar{\rho} = \rho_0(\mathbf{x}) \quad & \text{at } t = 0, \\ (\nabla \bar{\rho} + \bar{\rho} \nabla V_{\text{ext}}) \cdot \mathbf{n} = 0 \quad & \text{on } \partial Q. \end{aligned}$$

The Fréchet derivative with respect to ρ in the direction h of (5.10)is

$$\begin{aligned} D_\rho \mathcal{L}(\rho, w, q_1, q_2) h = & \int_0^T \int_\Omega (\rho - \widehat{\rho}) h \, dxdt - \int_0^T \int_\Omega \left(\partial_t h - \nabla^2 h - \nabla \cdot (h \nabla V_{\text{ext}}) \right) q_1 \, dxdt \\ & - \int_0^T \int_{\partial\Omega} q_2 \left(\frac{\partial h}{\partial n} + h \nabla V_{\text{ext}} \cdot \mathbf{n} \right) dsdt \\ = & \int_0^T \int_\Omega (\rho - \widehat{\rho}) h \, dxdt + \int_0^T \int_\Omega \left(h \partial_t q_1 + h \nabla^2 q_1 - h \nabla V_{\text{ext}} \cdot \nabla q_1 \right) dxdt \\ & - \int_\Omega q_1(\mathbf{x}, T) h(\mathbf{x}, T) - q_1(\mathbf{x}, 0) h(\mathbf{x}, 0) \, dx \\ & + \int_0^T \int_{\partial\Omega} \left(q_1 \frac{\partial h}{\partial n} - h \frac{\partial q_1}{\partial n} + h q_1 \nabla V_{\text{ext}} \cdot \mathbf{n} \right) dsdt \\ & - \int_0^T \int_{\partial\Omega} q_2 \left(\frac{\partial h}{\partial n} + h \nabla V_{\text{ext}} \cdot \mathbf{n} \right) dsdt, \end{aligned}$$

and with respect to w is:

$$D_w\mathcal{L}(\rho, w, q_1, q_2)h = \int_0^T \int_\Omega (\beta wh + hq_1)\, dxdt.$$

For a stationary point, the optimal state and control $\bar{\rho}$ and $\bar{w}$ must satisfy

$$D_\rho\mathcal{L}(\bar{\rho}, \bar{w}, q_1, q_2)h = 0 \quad \forall h \in L^2(0, T; H^1(\Omega)) \tag{5.11}$$

and

$$D_w\mathcal{L}(\bar{\rho}, \bar{w}, q_1, q_2)h = 0 \quad \forall h \in L^2(0, T; \Omega). \tag{5.12}$$

If we consider all $h \in C_0^\infty(Q)$, such that $h|_{\partial\Omega} = 0 = \dfrac{\partial h}{\partial n}|_{\partial\Omega}$, and $h = 0$ at $t = 0$ and $t = T$, then by the Fundamental Lemma of Calculus of Variations, equations (5.11) and (5.12) become

$$\begin{aligned} -\partial_t q_1 - \nabla^2 q_1 + \nabla V_{\text{ext}} \cdot \nabla q_1 &= \bar{\rho} - \widehat{\rho}, \\ \beta\bar{w} + q_1 &= 0. \end{aligned}$$

Dropping the condition $h = 0$ on at $t = T$ then gives the equation:

$$\int_\Omega q_1(\mathbf{x}, T)h(\mathbf{x}, T)\, dx = 0,$$

which implies the final time condition for q_1,

$$q_1(\mathbf{x}, T) = 0.$$

Also dropping the condition $\dfrac{\partial h}{\partial n} = 0$ gives

$$\int_0^T \int_{\partial\Omega} (q_1 - q_2)\frac{\partial h}{\partial n}\, dsdt = 0$$

which implies that $q_1 = q_2$ on $\partial\Omega$. Considering all remaining h gives the boundary condition:

$$\frac{\partial q_1}{\partial n} = 0 \quad \text{on } \partial Q.$$

After relabelling q_1 as q, the adjoint equation becomes:

$$\begin{aligned} -\partial_t q - \nabla^2 q + \nabla V_{\text{ext}} \cdot \nabla q &= \bar{\rho} - \widehat{\rho} \quad \text{in } Q, \\ q &= 0 \quad \text{at } t = T, \\ \frac{\partial q}{\partial n} &= 0 \quad \text{on } \partial Q, \end{aligned}$$

and almost everywhere:

$$\beta\bar{w} + q = 0.$$

We note that the optimality system for optimal source control problem with Dirichlet boundary condition is almost identical except for the boundary conditions of the state and adjoint equations. This observation arises in a range of optimal control problems, where optimality systems of optimization problems that differ only in the boundary conditions, are identical except on the boundary conditions. We obtain the following optimality system for problem (5.9):

$$\begin{aligned} \partial_t\bar{\rho} - \nabla^2\bar{\rho} - \nabla \cdot (\bar{\rho}\nabla V_{\text{ext}}) - \bar{w} &= f \quad \text{in } Q, \\ \bar{\rho} &= \rho_0(\mathbf{x}) \quad \text{at } t = 0, \\ (\nabla\bar{\rho} + \bar{\rho}\nabla V_{\text{ext}}) \cdot \mathbf{n} &= 0 \quad \text{on } \partial Q, \end{aligned} \tag{5.13}$$

$$
\begin{aligned}
-\partial_t q - \nabla^2 q + \nabla V_{\text{ext}} \cdot \nabla q &= \bar{\rho} - \widehat{\rho} \quad \text{in } Q, \\
q &= 0 \quad \text{at } t = T, \\
\frac{\partial q}{\partial n} &= 0 \quad \text{on } \partial Q,
\end{aligned}
$$

$$
\beta \bar{w} + q = 0 \quad \text{in } Q.
$$

5.2.2 Adding a Non-local Interacting Term

We now derive the optimality system when $\kappa \neq 0$ for the optimal source control problem with no-flux boundary condition . We focus on the non-local term in the Lagrangian as all other terms have been accounted for in the preceding section. Since the non-local term does not contain the control variable w, the gradient equation remains the same. The working for an example where the control variable appears in the non-local integral term is discussed in Chapter 6. We also note that this working is the same for the optimal flow control problem with no-flux boundary condition (5.1) as it contains the same non-local term.

If we again let q_1 and q_2 be the Lagrangian multipliers corresponding to the interior and boundary of the domain respectively, then the Lagrangian is given by

$$
\begin{aligned}
\mathcal{L}(\rho, w, q_1, q_2) = \frac{1}{2} \int_0^T \int_\Omega (\rho - \widehat{\rho})^2 \, dxdt + \frac{\beta}{2} \int_0^T \int_\Omega w^2 \, dxdt \\
- \int_0^T \int_\Omega \left(\partial_t \rho - \nabla^2 \rho - \nabla \cdot (\rho \nabla V_{\text{ext}}) - w - f \right) q_1 \, dxdt \\
- \int_0^T \int_{\partial\Omega} \left(\frac{\partial \rho}{\partial n} + \rho \nabla V_{\text{ext}} \cdot \mathbf{n} \right) q_2 \, dsdt \\
- \mathcal{M}(\rho, q_1, q_2),
\end{aligned}
$$

and the additional term of interest is $\mathcal{M}(\rho, w, q_1, q_2)$, where

$$
\begin{aligned}
\mathcal{M}(\rho, q_1, q_2) = \kappa \int_0^T \int_\Omega q_1(\mathbf{r}) \nabla_{\mathbf{r}} \cdot \left(\int_\Omega \rho(\mathbf{r}) \rho(\mathbf{r}') \mathbf{K}(\mathbf{r}, \mathbf{r}') dr' \right) drdt \\
- \kappa \int_0^T \int_{\partial\Omega} q_2 \left(\int_\Omega \rho(\mathbf{r}) \rho(\mathbf{r}') \mathbf{K}(\mathbf{r}, \mathbf{r}') dr' \right) \cdot \mathbf{n} \, dsdt.
\end{aligned} \tag{5.14}
$$

The Fréchet derivative of the product $\rho(\mathbf{r})\rho(\mathbf{r}')$ in the direction h is

$$
\lim_{\epsilon \to 0} \frac{(\rho(\mathbf{r}) + \epsilon h(\mathbf{r}))(\rho(\mathbf{r}') + \epsilon h(\mathbf{r}')) - \rho(\mathbf{r})\rho(\mathbf{r}')}{\epsilon} = \rho(\mathbf{r}) h(\mathbf{r}') + \rho(\mathbf{r}') h(\mathbf{r}).
$$

Hence the Fréchet derivative of the Lagrangian (5.14) with respect to ρ in the direction h becomes

$$
\begin{aligned}
D_\rho \mathcal{M}(\rho, q_1, q_2) h = \kappa \int_0^T \int_\Omega q_1(\mathbf{r}) \nabla_{\mathbf{r}} \cdot \left(\int_\Omega (\rho(\mathbf{r}) h(\mathbf{r}') + h(\mathbf{r}) \rho(\mathbf{r}')) \mathbf{K}(\mathbf{r}, \mathbf{r}') dr' \right) drdt \\
- \kappa \int_0^T \int_{\partial\Omega} q_2 \left(\int_\Omega (\rho(\mathbf{r}) h(\mathbf{r}') + h(\mathbf{r}) \rho(\mathbf{r}')) \mathbf{K}(\mathbf{r}, \mathbf{r}') dr' \right) \cdot \mathbf{n} dsdt.
\end{aligned}
$$

After applying the vector calculus identity (3.6) and the Divergence Theorem, we obtain,

$$
\begin{aligned}
D_\rho \mathcal{M}(\rho, w, q_1, q_2) h = -\kappa \int_0^T \int_\Omega \left(\int_\Omega (\rho(\mathbf{r}) h(\mathbf{r}') + h(\mathbf{r}) \rho(\mathbf{r}')) \mathbf{K}(\mathbf{r}, \mathbf{r}') dr' \right) \cdot \nabla_{\mathbf{r}} q_1(\mathbf{r}) drdt \\
+ \kappa \int_0^T \int_{\partial\Omega} q_1 \left(\int_\Omega (\rho(\mathbf{r}) h(\mathbf{r}') + h(\mathbf{r}) \rho(\mathbf{r}')) \mathbf{K}(\mathbf{r}, \mathbf{r}') dr' \right) \cdot \mathbf{n} dsdt \\
- \kappa \int_0^T \int_{\partial\Omega} q_2 \left(\int_\Omega (\rho(\mathbf{r}) h(\mathbf{r}') + h(\mathbf{r}) \rho(\mathbf{r}')) \mathbf{K}(\mathbf{r}, \mathbf{r}') dr' \right) \cdot \mathbf{n} dsdt.
\end{aligned}
$$

It is clear that the boundary terms cancel each other out in this no-flux boundary condition case, since we know $q_1 = q_2$ on ∂Q from the case $\kappa = 0$. In the Dirichlet boundary condition case, we reach the same conclusion that $q_1 = 0$ on ∂Q when we consider $h \in C_0^\infty(Q)$ such that $h = 0$ on $\partial\Omega$. Hence, moving forward, we can omit the boundary terms from our derivative. To make h the subject, we swap the order of integration and perform a change of variable $\mathbf{r}' = \mathbf{r}$ to obtain:

$$\begin{aligned} D_\rho \mathcal{M}(\rho, w, q_1, q_2)h &= -\kappa \int_0^T \int_\Omega h(\mathbf{r}) \left(\int_\Omega \rho(\mathbf{r}')\mathbf{K}(\mathbf{r}, \mathbf{r}')dr' \right) \cdot \nabla_{\mathbf{r}} q_1(\mathbf{r}) dr dt \\ &\quad - \kappa \int_0^T \int_\Omega h(\mathbf{r}') \left(\int_\Omega \rho(\mathbf{r})\mathbf{K}(\mathbf{r}, \mathbf{r}') \cdot \nabla_{\mathbf{r}} q_1(\mathbf{r}) dr \right) dr' dt \\ &= -\kappa \int_0^T \int_\Omega h(\mathbf{r}) \left(\int_\Omega \rho(\mathbf{r}')\mathbf{K}(\mathbf{r}, \mathbf{r}')dr' \right) \cdot \nabla_{\mathbf{r}} q_1(\mathbf{r}) dr dt \\ &\quad - \kappa \int_0^T \int_\Omega h(\mathbf{r}) \left(\int_\Omega \rho(\mathbf{r}')\mathbf{K}(\mathbf{r}', \mathbf{r}) \cdot \nabla_{r'} q_1(\mathbf{r}') dr' \right) dr dt. \end{aligned}$$

Hence the optimality system for the source control problem (5.9) with $\kappa \neq 0$ after making appropriate choices for h as above, is:

$$\begin{aligned} \mathcal{D}_l(\bar{\rho}, \bar{w}) - \nabla_r \cdot \mathcal{I}(\bar{\rho}) &= f \quad \text{in } Q, \\ \bar{\rho} &= \rho_0(\mathbf{x}) \quad \text{at } t = 0, \\ \mathcal{N}_l(\bar{\rho}) + \mathcal{I}(\bar{\rho}) \cdot \mathbf{n} &= 0 \quad \text{on } \partial Q, \end{aligned} \tag{5.15}$$

$$\begin{aligned} \mathcal{D}_l^*(\bar{\rho}) + \mathcal{I}^*(\bar{\rho}, q) &= \bar{\rho} - \widehat{\rho} \quad \text{in } Q, \\ q &= 0 \quad \text{at } t = T \\ \frac{\partial q}{\partial n} &= 0 \quad \text{on } \partial Q, \end{aligned}$$

$$\beta \bar{w} + q = 0 \quad \text{in } Q,$$

where

$$\mathcal{D}_l^*(\bar{\rho}) = -\partial_t q - \nabla^2 q + \nabla V_{\text{ext}} \cdot \nabla q,$$

and

$$\mathcal{I}^*(\bar{\rho}, q) = \kappa \left(\int_\Omega \bar{\rho}(\mathbf{r}')\mathbf{K}(\mathbf{r}, \mathbf{r}')dr' \right) \cdot \nabla_{\mathbf{r}} q_1(\mathbf{r}) + \kappa \int_\Omega \left(\bar{\rho}(\mathbf{r}')\mathbf{K}(\mathbf{r}', \mathbf{r}) \cdot \nabla_{\mathbf{r}'} q_1(\mathbf{r}') \right) dr'.$$

5.3 Overview of Numerical Algorithm

After obtaining continuous first-order optimality conditions in Section 5.2, we move on to the *discretize* step. We utilize the pseudospectral discretization as described in Section 4.1, and denote the discretized versions of the variables ρ, q, and $\mathbf{w}$ by P, Q, and W, respectively. The matrices P, Q, and W are of the form $A = [\boldsymbol{a_0}, \boldsymbol{a_1}, ..., \boldsymbol{a_n}]$, where the vectors $\boldsymbol{a_k}$ represent the solutions at the discretized times $k \in \{0, 1, ..., n\}$, where n is the number of time steps. In particular, the first column of P, denoted by $\boldsymbol{\rho_0}$, corresponds to the initial condition $\rho(\mathbf{x}, 0)$. If the spatial domain is one-dimensional, P, Q, and W are of size $N \times (n+1)$, where N is the number of spatial points. In the two-dimensional case, P and Q are of size $(N_1 N_2) \times (n+1)$, where N_j is the number of spatial points in the direction of x_j. The discretized control W for linear (source) control problems is also a scalar and $(N_1 N_2) \times (n+1)$ dimensional, while it is $(2N_1 N_2) \times (n+1)$ dimensional for non-linear (flow) control problems as the control is a vector. Now we employ the fixed-point algorithm as described in Section 4.4 to obtain numerical solutions.

5.4 Validation of Fixed-Point Solvers

We now provide the results of a number of tests validating the fixed-point optimization solver with and without the Armijo–Wolfe rule. We first measure the error generated using these methods against known exact solutions for problems with no interaction terms ($\kappa = 0$), for a number of test problems. We then investigate the robustness of our algorithms using an initial guess for the control given by various perturbations of an exact solution. For uniformity, the scalar control variable w or $\mathbf{w}$ is also denoted as $\mathbf{w}$ in the tables throughout this section.

5.4.1 Measures of Accuracy

All errors presented henceforth in this chapter are calculated as a measure of the difference between a variable of interest, y, and a reference value y_R, e.g., a previous iterate of $W^{(i)}$ for w, or an analytic solution to a test problem. The error measure $\mathcal{E}$ is composed of an L^2 error in space and an L^∞ error in time. We define absolute and relative L^2 spatial errors as

$$\mathcal{E}_{Abs}(t) = \|y(\mathbf{x},t) - y_R(\mathbf{x},t)\|_{L^2(\Omega)}\,, \qquad \mathcal{E}_{Rel}(t) = \frac{\|y(\mathbf{x},t) - y_R(\mathbf{x},t)\|_{L^2(\Omega)}}{\|y_R(\mathbf{x},t)\|_{L^2(\Omega)} + 10^{-10}}\,,$$

respectively, where the small additional term in the denominator prevents division by zero. Then, $\mathcal{E}_{Abs}$ and $\mathcal{E}_{Rel}$ are used in the full error measure:

$$\mathcal{E} = \max_{t\in[0,T]} \left[\min\left(\mathcal{E}_{Rel}(t), \mathcal{E}_{Abs}(t)\right)\right]. \tag{5.16}$$

The minimum between absolute and relative spatial error is taken to avoid choosing an erroneously large relative error, caused by division of one numerically very small term by another.

5.4.2 Test Problems with Analytic Solutions

We present test problems, posed on a spatial domain $\Omega = (-1,1)^d$, where d is the spatial dimension of the problem. Test Problem 1, as defined below, solves the 2D flow control problem (5.1), imposed with no-flux boundary conditions, while Test Problem 2 solves the 2D source control problem (5.4), also with no-flux boundary conditions. The performance of the numerical method is measured by providing it with analytical solutions of w or $\mathbf{w}$, and input variables: $\widehat{\rho}$, f, V_{ext}, ρ_0. The expectation is that each iterative solver converges within one iteration to the exact numerical solution triplet (P, W, Q) when provided with the exact solutions as initial guesses. Furthermore, the vectors P and Q should differ from the exact analytic solution only by an order of the specified `ode15s` tolerance, which is 10^{-8} for the experiments here. Since W is updated using P and Q, the control error may possibly be larger. The error $\mathcal{E}_\rho$ between the exact solution for the state variable, evaluated at the discretized time points $k \in \{0, 1, ..., n\}$, and the numerical solution obtained for the state, ρ, is measured using the norm in (5.16). The errors $\mathcal{E}_q$ and $\mathcal{E}_{\mathbf{w}}$ are derived equivalently. Here, we fix the mixing rate of the fixed-point solver to be $\lambda = 0.1$, a value we obtained from experimentation.

Test Problem 1: Two-Dimensional Flow Control Problem with No-Flux Boundary Conditions

The following triplet $(\rho, \mathbf{w}, q)$ solves the flow control problem (5.1) with no-flux boundary condition (5.3), $d = 2$, and $\kappa = 0$:

$$\begin{aligned}
\rho &= \beta^{1/2} e^t \cos(\pi x_1)\cos(\pi x_2),\\
\mathbf{w} &= \pi e^t (e^T - e^t)\left[\sin(\pi x_1)\cos(\pi x_1)\cos^2(\pi x_2),\ \cos^2(\pi x_1)\sin(\pi x_2)\cos(\pi x_2)\right]^T,\\
q &= \beta^{1/2}(e^T - e^t)\cos(\pi x_1)\cos(\pi x_2),
\end{aligned}$$

where

$$\widehat{\rho} = -2\pi^2\beta^{1/2}(e^T - e^t)\cos(\pi x_1)\cos(\pi x_2)$$

		$\beta = 10^{-3}$	$\beta = 10^{-1}$	$\beta = 10^{1}$	$\beta = 10^{3}$
$N = 20$, $n = 10$	$\mathcal{E}_\rho$	5.7297×10^{-8}	5.2765×10^{-7}	9.7571×10^{-7}	9.7641×10^{-7}
	$\mathcal{E}_q$	5.9512×10^{-9}	3.8980×10^{-8}	1.8645×10^{-7}	2.6429×10^{-7}
	$\mathcal{E}_\mathbf{w}$	1.2436×10^{-6}	1.0805×10^{-6}	1.0817×10^{-6}	1.0818×10^{-6}
$N = 30$, $n = 20$	$\mathcal{E}_\rho$	8.8098×10^{-9}	7.9219×10^{-9}	7.2815×10^{-9}	7.2815×10^{-9}
	$\mathcal{E}_q$	1.7637×10^{-8}	8.6029×10^{-9}	1.5988×10^{-8}	5.4360×10^{-9}
	$\mathcal{E}_\mathbf{w}$	2.8968×10^{-6}	5.8504×10^{-8}	2.6148×10^{-8}	8.4382×10^{-9}
$N = 42$, $n = 30$	$\mathcal{E}_\rho$	1.0100×10^{-8}	8.1475×10^{-9}	6.8638×10^{-9}	6.8638×10^{-9}
	$\mathcal{E}_q$	1.7337×10^{-8}	8.2434×10^{-9}	1.7543×10^{-8}	5.3626×10^{-9}
	$\mathcal{E}_\mathbf{w}$	2.8582×10^{-6}	5.3157×10^{-8}	2.8860×10^{-8}	9.1237×10^{-9}

Table 5.1: Test Problem 1: Error measures for state ρ, adjoint q, and control $\mathbf{w}$, for a range of N, n, and β using the fixed-point solver.

		$\beta = 10^{-3}$	$\beta = 10^{-1}$	$\beta = 10^{1}$	$\beta = 10^{3}$
$N = 20$, $n = 10$	$\mathcal{E}_\rho$	5.7297×10^{-8}	5.2765×10^{-7}	9.7571×10^{-7}	9.7641×10^{-7}
	$\mathcal{E}_q$	5.9512×10^{-9}	3.8980×10^{-8}	1.8645×10^{-7}	2.6429×10^{-7}
	$\mathcal{E}_\mathbf{w}$	1.2436×10^{-6}	1.0805×10^{-6}	1.0817×10^{-6}	1.0818×10^{-6}
$N = 30$, $n = 20$	$\mathcal{E}_\rho$	8.8098×10^{-9}	7.9219×10^{-9}	7.2815×10^{-9}	7.2815×10^{-9}
	$\mathcal{E}_q$	1.7637×10^{-8}	8.6029×10^{-9}	1.5988×10^{-8}	5.4360×10^{-9}
	$\mathcal{E}_\mathbf{w}$	2.8968×10^{-6}	5.8504×10^{-8}	2.6148×10^{-8}	8.4382×10^{-9}
$N = 42$, $n = 30$	$\mathcal{E}_\rho$	1.0100×10^{-8}	8.1475×10^{-9}	6.8638×10^{-9}	6.8638×10^{-9}
	$\mathcal{E}_q$	1.7337×10^{-8}	8.2434×10^{-9}	1.7543×10^{-8}	5.3626×10^{-9}
	$\mathcal{E}_\mathbf{w}$	2.8582×10^{-6}	5.3157×10^{-8}	2.8860×10^{-8}	9.1237×10^{-9}

Table 5.2: Test Problem 1: Error measures for state ρ, adjoint q, and control $\mathbf{w}$, for a range of N, n, and β using the fixed-point Armijo–Wolfe-type solver.

$$
\begin{aligned}
&\quad - \pi^2\beta^{1/2}e^t(e^T - e^t)^2\left[\sin^2(\pi x_1)\cos(\pi x_1)\cos^3(\pi x_2) + \cos^3(\pi x_1)\sin^2(\pi x_2)\cos(\pi x_2)\right],\\
V_{\text{ext}} &= 0,\\
f &= (1+2\pi^2)\beta^{1/2}e^t\cos(\pi x_1)\cos(\pi x_2) + 2\pi^2\beta^{1/2}e^{2t}(e^T - e^T)\cos^3(\pi x_1)\cos^3(\pi x_2)\\
&\quad - 2\pi^2\beta^{1/2}e^{2t}(e^T - e^T)\sin^2(\pi x_1)\cos(\pi x_1)\cos^3(\pi x_2)\\
&\quad - 2\pi^2\beta^{1/2}e^{2t}(e^T - e^T)\cos^3(\pi x_1)\sin^2(\pi x_2)\cos(\pi x_2),\\
\rho_0 &= \beta^{1/2}\cos(\pi x_1)\cos(\pi x_2).
\end{aligned}
$$

Tables 5.1 and 5.2 display the error in the numerical solution for different choices of spatial and time points as well as for different values of β. For ρ and q, it is shown that the choice of 10 points in space is not sufficient to reach the accuracy of the ODE solver of 10^{-8} for both fixed point and fixed-point with Armijo–Wolfe solvers, while 20 to 30 points are sufficient. The error for $\mathbf{w}$ with small β is also bigger than 10^{-8}. This is due to the updating method used within the optimization solver, see Section 4.4. All configurations for this test converged within one iteration of the optimization algorithm for both fixed-point and fixed-point with Armijo–Wolfe solvers as expected.

Test Problem 2 : Two-Dimensional Source Control Problem with No-Flux Boundary Conditions

The following triplet (ρ, w, q) solves the source control problem (5.4) with the zero Dirichlet boundary condition (5.2), with $c = \kappa = 0$:

$$
\begin{aligned}
\rho &= 2e^t\prod_{i=1}^{d}\cos(\pi x_i),\\
w &= -\frac{1}{\beta}(e^T - e^t)\prod_{i=1}^{d}\cos(\pi x_i) \quad [q = -\beta w],
\end{aligned}
$$

		$\beta = 10^{-3}$	$\beta = 10^{-1}$	$\beta = 10^{1}$	$\beta = 10^{3}$
$N = 20$, $n = 10$	$\mathcal{E}_\rho$	9.1788×10^{-9}	9.1680×10^{-9}	9.1679×10^{-9}	9.1678×10^{-9}
	$\mathcal{E}_q$	1.6866×10^{-8}	1.6865×10^{-8}	1.6865×10^{-8}	1.6865×10^{-8}
	$\mathcal{E}_\mathbf{w}$	2.3997×10^{-8}	2.2360×10^{-8}	1.8131×10^{-9}	1.8131×10^{-11}
$N = 30$, $n = 20$	$\mathcal{E}_\rho$	8.5863×10^{-9}	8.5862×10^{-9}	8.5863×10^{-9}	8.5862×10^{-9}
	$\mathcal{E}_q$	8.6407×10^{-9}	8.6407×10^{-9}	8.6407×10^{-9}	8.6407×10^{-9}
	$\mathcal{E}_\mathbf{w}$	4.4505×10^{-8}	1.5050×10^{-8}	8.6407×10^{-10}	8.6407×10^{-12}
$N = 42$, $n = 30$	$\mathcal{E}_\rho$	9.1152×10^{-9}	9.1153×10^{-9}	9.1152×10^{-9}	9.1152×10^{-9}
	$\mathcal{E}_q$	1.7020×10^{-8}	1.7020×10^{-8}	1.7020×10^{-8}	1.7020×10^{-8}
	$\mathcal{E}_\mathbf{w}$	2.4169×10^{-8}	2.4169×10^{-8}	1.7434×10^{-9}	1.7434×10^{-11}

Table 5.3: Test Problem 2: Error measures for state ρ, adjoint q, and control $\mathbf{w}$, for a range of N, n and β using the fixed-point solver.

		$\beta = 10^{-3}$	$\beta = 10^{-1}$	$\beta = 10^{1}$	$\beta = 10^{3}$
$N = 20$, $n = 10$	$\mathcal{E}_\rho$	9.1788×10^{-9}	9.1680×10^{-9}	9.1679×10^{-9}	9.1678×10^{-9}
	$\mathcal{E}_q$	1.6866×10^{-8}	1.6865×10^{-8}	1.6865×10^{-8}	1.6865×10^{-8}
	$\mathcal{E}_\mathbf{w}$	2.3997×10^{-8}	2.2360×10^{-8}	1.8131×10^{-9}	1.8131×10^{-11}
$N = 30$, $n = 20$	$\mathcal{E}_\rho$	8.5863×10^{-9}	8.5862×10^{-9}	8.5863×10^{-9}	8.5862×10^{-9}
	$\mathcal{E}_q$	8.6407×10^{-9}	8.6407×10^{-9}	8.6407×10^{-9}	8.6407×10^{-9}
	$\mathcal{E}_\mathbf{w}$	4.4505×10^{-8}	1.5050×10^{-8}	8.6407×10^{-10}	8.6407×10^{-12}
$N = 42$, $n = 30$	$\mathcal{E}_\rho$	9.1152×10^{-9}	9.1153×10^{-9}	9.1152×10^{-9}	9.1152×10^{-9}
	$\mathcal{E}_q$	1.7020×10^{-8}	1.7020×10^{-8}	1.7020×10^{-8}	1.7020×10^{-8}
	$\mathcal{E}_\mathbf{w}$	2.4169×10^{-8}	2.4169×10^{-8}	1.7434×10^{-9}	1.7434×10^{-11}

Table 5.4: Test Problem 2: Error measures for state ρ, adjoint q, and control $\mathbf{w}$, for a range of N, n and β using the fixed-point Armijo–Wolfe-type solver.

where $\mathbf{x} = [x_1, ..., x_d]^T$, and

$$
\begin{aligned}
\widehat{\rho} = & \left[-d\pi^2 e^T + \left(1 + d\pi^2\right) e^t\right] \prod_{i=1}^{d} \cos\left(\pi x_i\right) \\
& - \pi^2 (e^T - e^t) \sum_{i=1}^{d} \sin^2\left(\pi x_i\right) \prod_{j=1, j\neq i}^{d} \cos^2\left(\pi x_j\right), \\
V_{\text{ext}} = & \prod_{i=1}^{d} \cos\left(\pi x_i\right), \\
f = & \left[\frac{1}{\beta} e^T + \left(2 + 2d\pi^2 - \frac{1}{\beta}\right) e^t\right] \prod_{i=1}^{d} \cos\left(\pi x_i\right) + 2d\pi^2 e^t \prod_{i=1}^{d} \cos^2\left(\pi x_i\right) \\
& - 2\pi^2 e^t \sum_{i=1}^{d} \sin^2\left(\pi x_i\right) \prod_{j=1, j\neq i}^{d} \cos^2\left(\pi x_j\right), \\
\rho_0 = & \, 2 \prod_{i=1}^{d} \cos\left(\pi x_i\right).
\end{aligned}
$$

Tables 5.3 and 5.4 displays the results for this problem for $d = 2$. As expected, all errors for the numerical solution of the three variables are of the order of the specified ODE tolerance of 10^{-8}. This could be an indication that the source control problem is easier to solve numerically than the flow control problem that need more space points to reach the same tolerance.

5.4.3 Perturbation of Test Problems with Analytic Solutions

It is necessary to provide an initial guess for the control variable to commence the optimization routine using the fixed-point algorithm. Therefore, one way to validate the numerical method is to perturb the exact solution for the control, taken from a test problem with an analytic solution, and use this as an initial guess within the optimization solver. In the first iteration, the solutions for ρ and q differ from the exact solution. The optimization method then converges to the exact, known analytical optimal solution.

Firstly, we use a perturbation in time only. We define $f(t)$ as::

$$f(t) = \frac{e^{-a/t}}{e^{-a/t} + e^{-a/(1-t)}},$$

for a given constant a. We then define $g(t)$ as:

$$\begin{aligned} g(t) &= \frac{1}{2} f(a, t - t_0) \times f(-a, t - t_0) \\ &= \frac{1}{2} \frac{e^{-a/(t-t_0)}}{e^{-a/(t-t_0)} + e^{-a/(1-t-t_0)}} \times \frac{e^{a/(t-t_0)}}{e^{a/(t-t_0)} + e^{a/(1-t-t_0)}}, \end{aligned}$$

for given constant t_0, and normalize it by

$$\tilde{g}(t) = \frac{g(t)}{\max |g(t)|}.$$

A similar perturbation can be made in the spatial variable for given constants a and x_0, taking into account the difference in length of spatial and time domains:

$$\begin{aligned} j(\mathbf{x}) &= \prod_{i=1}^{d} \frac{e^{-2a/x_i}}{e^{-2a/x_i} + e^{-2a/(1-x_i)}}, \\ h(\mathbf{x}) &= \frac{1}{2} \prod_{i=1}^{d} j(x_i - x_0) \times j(x_i - x_0) \\ &= \frac{1}{2} \prod_{i=1}^{d} \frac{e^{-2a/(x_i-x_0)}}{e^{-2a/(x_i-x_0)} + e^{-2a/(1-x_i-x_0)}} \times \frac{e^{2a/(x_i-x_0)}}{e^{2a/(x_i-x_0)} + e^{2a/(1-x_i-x_0)}}. \end{aligned}$$

Again, this is then normalized by

$$\tilde{h}(\mathbf{x}) = \frac{h(\mathbf{x})}{\max |h(\mathbf{x})|}.$$

These perturbation functions are chosen such that the perturbation is smooth and respects the initial condition for ρ and final time condition for q, by preserving the initial guess at the first or final time point. The perturbations are applied to the exact solution for the control, $\mathbf{w}_{ex}$, as follows:

$$\begin{aligned} \mathbf{w}_{p,1} &= \mathbf{w}_{ex}(1 + \epsilon \tilde{g}(t)), \\ \mathbf{w}_{p,2} &= \mathbf{w}_{ex}(1 + \epsilon \tilde{g}(t)\tilde{h}(x)). \end{aligned}$$

For our test problems, we take $a = 0.7$, $x_0 = t_0 = -0.01$, and the perturbation strength is taken to be either $\epsilon = 0.1$ or $\epsilon = 0.5$. The chosen numbers of points in space and time are $N = 30$ and $n = 20$, the ODE tolerances are again 10^{-8}, and the tolerance for the fixed-point solvers is 10^{-4}.

Test Problem 1 : Two-Dimensional Flow Control Problem with No-Flux Boundary Conditions

We perturb the analytic solution $\mathbf{w}$ for Test Problem 1 defined in Section 5.4.2, and run the fixed-point algorithms. Results are presented in Table 5.5 for the fixed-point solver and in Table

		$\beta = 10^{-3}$	$\beta = 10^{-1}$	$\beta = 10^{1}$	$\beta = 10^{3}$
$0.1\tilde{g}(t)$	$\mathcal{E}_\rho$	9.5057×10^{-7}	9.5357×10^{-6}	1.6175×10^{-5}	1.6173×10^{-5}
	$\mathcal{E}_q$	6.8795×10^{-7}	6.8704×10^{-6}	1.8446×10^{-5}	1.8445×10^{-5}
	$\mathcal{E}_\mathbf{w}$	2.4318×10^{-5}	2.4549×10^{-5}	2.4568×10^{-5}	2.4564×10^{-5}
	Time	1308.6781	1449.4828	1646.4077	2612.1153
$0.5\tilde{g}(t)$	$\mathcal{E}_\rho$	8.7878×10^{-7}	8.7963×10^{-6}	1.4924×10^{-5}	1.4924×10^{-5}
	$\mathcal{E}_q$	6.5321×10^{-7}	6.5344×10^{-6}	1.7717×10^{-5}	1.7717×10^{-5}
	$\mathcal{E}_\mathbf{w}$	2.2541×10^{-5}	2.2827×10^{-5}	2.2835×10^{-5}	2.2834×10^{-5}
	Time	1667.2647	1871.3040	2178.5330	3205.2786
$0.1\tilde{g}(t)\tilde{h}(x)$	$\mathcal{E}_\rho$	1.2353×10^{-6}	1.2348×10^{-5}	2.5891×10^{-5}	2.5891×10^{-5}
	$\mathcal{E}_q$	1.1160×10^{-6}	1.1121×10^{-5}	2.6792×10^{-5}	2.6794×10^{-5}
	$\mathcal{E}_\mathbf{w}$	5.1346×10^{-5}	5.1264×10^{-5}	5.1243×10^{-5}	5.1244×10^{-5}
	Time	2964.0040	3458.0557	4327.1525	6014.9723
$0.5\tilde{g}(t)\tilde{h}(x)$	$\mathcal{E}_\rho$	2.4217×10^{-6}	2.4183×10^{-5}	5.0076×10^{-5}	5.0075×10^{-5}
	$\mathcal{E}_q$	2.8667×10^{-6}	2.8569×10^{-5}	6.7440×10^{-5}	6.7438×10^{-5}
	$\mathcal{E}_\mathbf{w}$	1.0696×10^{-4}	1.0674×10^{-4}	1.0672×10^{-4}	1.0672×10^{-4}
	Time	3286.5995	3791.5241	4877.0730	6818.7013

Table 5.5: Test Problem 1, Error measures for $\mathbf{w}_c, \rho$, and q, for four perturbation strategies for $\mathbf{w}$, and a range of β, using the fixed-point solver.

5.6 for the fixed-point Armijo–Wolfe-type solver. The mixing rate for the fixed-point method is fixed at 0.01, smaller compared to 0.1 used for the analytic tests, as the solver did not converge for $\lambda = 0.1$. There could be a higher rate than 0.01 for which the solver could converge, but this highlights the disadvantage of having to fix the rate, as it becomes time-consuming to continuously experiment to find a value that works. The fixed-point Armijo–Wolfe-type scheme addresses this issue by adaptively choosing the mixing rate for each iteration of the fixed-point algorithm. We see clearly that the fixed-point Armijo–Wolfe solver gives more accurate solutions in the most perturbed case $0.5\tilde{g}(t)\tilde{h}(x)$, and in considerably faster times.

Test Problem 3: Two-Dimensional Flow Control Problem with Dirichlet Boundary Conditions

The following triplet $(\rho, \mathbf{w}, q)$ forms a solution to the first-order continuous optimality conditions derived for the advection–diffusion flow control problem (5.1) with the zero Dirichlet boundary conditions (5.2) (with $c = 0$), where $d = 2$ and $\kappa = 0$:

$$\begin{aligned}
\rho &= 2\beta^{1/2} e^t \cos\left(\frac{\pi x_1}{2}\right) \cos\left(\frac{\pi x_2}{2}\right), \\
\mathbf{w} &= \frac{\pi}{2} e^t (e^T - e^t) \left[\sin(\pi x_1)\cos^2\left(\frac{\pi x_2}{2}\right),\ \cos^2\left(\frac{\pi x_1}{2}\right)\sin(\pi x_2)\right]^T, \\
q &= \beta^{1/2}(e^T - e^t)\cos\left(\frac{\pi x_1}{2}\right)\cos\left(\frac{\pi x_2}{2}\right),
\end{aligned}$$

and

$$\begin{aligned}
\widehat{\rho} = {} & \beta^{1/2} e^t \cos\left(\frac{\pi x_1}{2}\right)\cos\left(\frac{\pi x_1}{2}\right) - \beta^{1/2}\frac{\pi^2}{2}(e^T - e^t)\cos\left(\frac{\pi x_1}{2}\right)\cos\left(\frac{\pi x_1}{2}\right) \\
& - \frac{\pi^2}{2}\beta^{1/2} e^t (e^T - e^t)^2 \left(\cos\left(\frac{\pi x_1}{2}\right)\cos\left(\frac{\pi x_2}{2}\right)\right) \\
& \left[\sin^2\left(\frac{\pi x_1}{2}\right)\cos^2\left(\frac{\pi x_2}{2}\right) + \cos^2\left(\frac{\pi x_1}{2}\right)\sin^2\left(\frac{\pi x_2}{2}\right)\right], \\
V_{\text{ext}} = {} & 0, \\
f = {} & \left(2 + \pi^2\right)\beta^{1/2} e^t \cos\left(\frac{\pi x_1}{2}\right)\cos\left(\frac{\pi x_1}{2}\right) \\
& + 2\pi^2 \beta^{1/2} e^{2t}(e^T - e^t)
\end{aligned}$$

		$\beta = 10^{-3}$	$\beta = 10^{-1}$	$\beta = 10^{1}$	$\beta = 10^{3}$
$0.1\tilde{g}(t)$	$\mathcal{E}_\rho$	5.1437×10^{-7}	5.1747×10^{-6}	8.1260×10^{-6}	8.1274×10^{-6}
	$\mathcal{E}_q$	3.6801×10^{-7}	3.6824×10^{-6}	1.0568×10^{-5}	1.0567×10^{-5}
	$\mathcal{E}_{\mathbf{w}}$	1.2544×10^{-5}	1.2513×10^{-5}	1.2539×10^{-5}	1.2536×10^{-5}
	Time	50.5399	57.9044	64.6229	88.1553
$0.5\tilde{g}(t)$	$\mathcal{E}_\rho$	4.2095×10^{-7}	4.2313×10^{-6}	8.0370×10^{-6}	8.0369×10^{-6}
	$\mathcal{E}_q$	3.3455×10^{-7}	3.3701×10^{-6}	8.7902×10^{-6}	8.7901×10^{-6}
	$\mathcal{E}_{\mathbf{w}}$	1.3007×10^{-5}	1.3040×10^{-5}	1.3044×10^{-5}	1.3044×10^{-5}
	Time	68.7226	80.1268	83.7763	118.8148
$0.1\tilde{g}(t)\tilde{h}(x)$	$\mathcal{E}_\rho$	1.2034×10^{-6}	1.2025×10^{-5}	2.5103×10^{-5}	2.5103×10^{-5}
	$\mathcal{E}_q$	1.3161×10^{-6}	1.3112×10^{-5}	3.1237×10^{-5}	3.1236×10^{-5}
	$\mathcal{E}_{\mathbf{w}}$	5.2368×10^{-5}	5.2263×10^{-5}	5.2244×10^{-5}	5.2243×10^{-5}
	Time	136.2212	157.4796	181.3432	248.2429
$0.5\tilde{g}(t)\tilde{h}(x)$	$\mathcal{E}_\rho$	2.4829×10^{-6}	2.4796×10^{-5}	5.2493×10^{-5}	5.2492×10^{-5}
	$\mathcal{E}_q$	3.0505×10^{-6}	3.0378×10^{-5}	7.0328×10^{-5}	7.0327×10^{-5}
	$\mathcal{E}_{\mathbf{w}}$	1.1177×10^{-4}	1.1152×10^{-4}	1.1150×10^{-4}	1.1150×10^{-4}
	Time	153.5402	174.9906	206.2008	278.8848

Table 5.6: Test Problem 1, Error measures for $\mathbf{w}_c, \rho$ and q, for four perturbation strategies for $\mathbf{w}$, and a range of β, using the fixed-point Armijo–Wolfe-type solver

		$\beta = 10^{-3}$	$\beta = 10^{-1}$	$\beta = 10^{1}$	$\beta = 10^{3}$
$0.1\tilde{g}(t)$	$\mathcal{E}_\rho$	1.8763×10^{-6}	1.8426×10^{-5}	2.3699×10^{-5}	2.3706×10^{-5}
	$\mathcal{E}_q$	1.1663×10^{-6}	1.1789×10^{-5}	2.7252×10^{-5}	2.7256×10^{-5}
	$\mathcal{E}_{\mathbf{w}}$	2.7222×10^{-5}	2.7376×10^{-5}	2.7399×10^{-5}	2.7395×10^{-5}
	Time	1192.4954	1397.2214	1513.6407	2131.2100
$0.5\tilde{g}(t)$	$\mathcal{E}_\rho$	2.0781×10^{-6}	2.0985×10^{-5}	2.6663×10^{-5}	2.6655×10^{-5}
	$\mathcal{E}_q$	1.0119×10^{-6}	1.0120×10^{-5}	2.3057×10^{-5}	2.3052×10^{-5}
	$\mathcal{E}_{\mathbf{w}}$	3.0588×10^{-5}	3.0922×10^{-5}	3.0671×10^{-5}	3.0671×10^{-5}
	Time	1502.3516	2179.7623	2007.6461	2789.2350
$0.1\tilde{g}(t)\tilde{h}(x)$	$\mathcal{E}_\rho$	4.0223×10^{-6}	4.0205×10^{-5}	4.8308×10^{-5}	4.8309×10^{-5}
	$\mathcal{E}_q$	8.6170×10^{-7}	8.6359×10^{-6}	1.8223×10^{-5}	1.8224×10^{-5}
	$\mathcal{E}_{\mathbf{w}}$	8.2796×10^{-5}	8.2813×10^{-5}	8.2809×10^{-5}	8.2812×10^{-5}
	Time	3363.3732	4009.3855	4524.1034	6612.7847
$0.5\tilde{g}(t)\tilde{h}(x)$	$\mathcal{E}_\rho$	4.1149×10^{-6}	4.1105×10^{-5}	4.8184×10^{-5}	4.8185×10^{-5}
	$\mathcal{E}_q$	8.3413×10^{-7}	8.3325×10^{-6}	1.7995×10^{-5}	1.7996×10^{-5}
	$\mathcal{E}_{\mathbf{w}}$	8.1443×10^{-5}	8.1336×10^{-5}	8.1332×10^{-5}	8.1332×10^{-5}
	Time	3398.9344	3961.2500	4596.8063	6213.6490

Table 5.7: Test Problem 3, Error measures for $\mathbf{w}_c, \rho$, and q, for four perturbation strategies for $\mathbf{w}$, and a range of β, using the fixed-point solver.

		$\beta = 10^{-3}$	$\beta = 10^{-1}$	$\beta = 10^{1}$	$\beta = 10^{3}$
$0.1\tilde{g}(t)$	$\mathcal{E}_\rho$	2.1266×10^{-6}	2.1280×10^{-5}	2.6991×10^{-5}	2.6990×10^{-5}
	$\mathcal{E}_q$	1.0965×10^{-6}	1.0843×10^{-5}	2.0691×10^{-5}	2.0691×10^{-5}
	$\mathcal{E}_{\mathbf{w}}$	3.0020×10^{-5}	3.0049×10^{-5}	3.0066×10^{-5}	3.0065×10^{-5}
	Time	44.8588	48.1979	56.3187	82.0822
$0.5\tilde{g}(t)$	$\mathcal{E}_\rho$	2.1777×10^{-6}	2.1784×10^{-5}	2.2691×10^{-5}	2.2690×10^{-5}
	$\mathcal{E}_q$	7.7499×10^{-7}	7.8584×10^{-6}	1.5434×10^{-5}	1.5435×10^{-5}
	$\mathcal{E}_{\mathbf{w}}$	3.5884×10^{-5}	3.5914×10^{-5}	3.5916×10^{-5}	3.5915×10^{-5}
	Time	60.2759	69.6970	79.6313	107.9467
$0.1\tilde{g}(t)\tilde{h}(x)$	$\mathcal{E}_\rho$	3.1750×10^{-6}	3.1722×10^{-5}	3.8426×10^{-5}	3.8427×10^{-5}
	$\mathcal{E}_q$	6.8170×10^{-7}	6.8338×10^{-6}	1.4486×10^{-5}	1.4487×10^{-5}
	$\mathcal{E}_{\mathbf{w}}$	6.5854×10^{-5}	6.5862×10^{-5}	6.5857×10^{-5}	6.5860×10^{-5}
	Time	148.7203	166.6562	198.9496	269.7107
$0.5\tilde{g}(t)\tilde{h}(x)$	$\mathcal{E}_\rho$	3.5576×10^{-6}	3.5522×10^{-5}	4.1639×10^{-5}	4.1639×10^{-5}
	$\mathcal{E}_q$	7.2899×10^{-7}	7.2799×10^{-6}	1.5723×10^{-5}	1.5724×10^{-5}
	$\mathcal{E}_{\mathbf{w}}$	7.1174×10^{-5}	7.1136×10^{-5}	7.1134×10^{-5}	7.1137×10^{-5}
	Time	150.6307	169.3740	200.7258	272.7978

Table 5.8: Test Problem 3, Error measures for $\mathbf{w}_c, \rho$ and q, for four perturbation strategies for $\mathbf{w}$, and a range of β, using the fixed-point Armijo–Wolfe-type solver

$$\begin{aligned}
&\left[\cos^3\left(\frac{\pi x_1}{2}\right)\cos^3\left(\frac{\pi x_2}{2}\right) - \cos^3\left(\frac{\pi x_1}{2}\right)\sin^2\left(\frac{\pi x_2}{2}\right)\cos\left(\frac{\pi x_2}{2}\right)\right.\\
&\left.-\cos^3\left(\frac{\pi x_2}{2}\right)\sin^2\left(\frac{\pi x_1}{2}\right)\cos\left(\frac{\pi x_1}{2}\right)\right],\\
\rho_0 = 2\beta^{1/2}&\cos\left(\frac{\pi x_1}{2}\right)\cos\left(\frac{\pi x_2}{2}\right).
\end{aligned}$$

Tables 5.7 and 5.8 show the results for the fixed-point and fixed-point Armijo–Wolfe solvers, respectively. Both solvers are able to converge to the known exact solutions with the set tolerance 10^{-4}. It is clear that for this problem, the fixed-point Armijo–Wolfe-type scheme is the faster of the two solvers.

5.4.4 Computational Time and Efficiency of Solvers

In this section, we consider a test problem with interaction terms turned on, $\kappa = -1$, or 1, and compare the computational time taken for convergence by the fixed-point algorithm with or without Armijo–Wolfe-type conditions. We also include the multiple shooting method that uses the inbuilt MATLAB function `fsolve` to show how much slower it is compared to the fixed-point methods.

Test Problem 4: One-Dimensional Flow Control Problem with No-Flux Boundary Conditions

In this example, we consider the flow control problem (5.1) with no-flux boundary conditions (5.3), with $d = 1$ and $\kappa = 0$, and provide the following inputs for the optimization problem:

$$\begin{aligned}
\rho &= 0.5,\\
\mathbf{w} &= \mathbf{0},\\
q &= \beta(e^T - e^t))\cos(\pi x),\\
\widehat{\rho} &= \frac{1-t}{2} + \frac{t}{2}\left(\sin(\frac{\pi(x-2)}{2} + \frac{1}{2})\right),\\
V_{\text{ext}} &= 0.
\end{aligned}$$

We first solve the forward problem using the initial condition ρ_0 and control $\mathbf{w} = \mathbf{0}$ and record the cost functional $\mathcal{J}_{uc} = \frac{1}{2}\int_0^1\int_{-1}^1(\widehat{\rho}-\rho)^2\,dxdt$ for the forward problem. We then solve optimization

		F-P A–W	F-P	MS
$\kappa = -1$	$\mathcal{J}_{uc}$	4.3751×10^{-2}	4.3751×10^{-2}	4.3751×10^{-2}
	$\mathcal{J}_c$	1.0897×10^{-3}	1.0897×10^{-3}	1.0897×10^{-3}
	`Iter` (func eval)	223(1406)	667(667)	39(35380)
	Time (s)	$1.5494 \times 10^{+0}$	$1.5765 \times 10^{+2}$	$3.2995 \times 10^{+4}$
$\kappa = 1$	$\mathcal{J}_{uc}$	4.3365×10^{-2}	4.3365×10^{-2}	4.3365×10^{-2}
	$\mathcal{J}_c$	2.0370×10^{-3}	2.0370×10^{-3}	2.0374×10^{-3}
	`Iter` (func eval)	80(404)	656(656)	40(38801)
	Time (s)	8.0414×10^{-01}	$1.0487 \times 10^{+2}$	$3.4389 \times 10^{+4}$

Table 5.9: Cost functionals of the forward, and optimization problem, with the time taken, number of iterations, and number of function evaluations required for the fixed-point method, fixed-point Armijo–Wolfe-type, and multiple shooting solvers to converge.

		F-P A–W vs F-P	F-P A–W vs MS	F-P vs MS
$\kappa = -1$	$\mathcal{E}_\rho$	4.1349×10^{-8}	3.3688×10^{-4}	3.3688×10^{-4}
	$\mathcal{E}_q$	8.2676×10^{-9}	2.6075×10^{-5}	2.6073×10^{-5}
	$\mathcal{E}_{\mathbf{w}}$	5.8185×10^{-6}	2.4332×10^{-2}	2.4333×10^{-2}
$\kappa = 1$	$\mathcal{E}_\rho$	2.8742×10^{-7}	5.0626×10^{-4}	5.0626×10^{-4}
	$\mathcal{E}_q$	2.6805×10^{-8}	3.0059×10^{-5}	3.0064×10^{-5}
	$\mathcal{E}_{\mathbf{w}}$	1.2020×10^{-5}	1.8267×10^{-2}	1.8267×10^{-2}

Table 5.10: The difference in the solutions of the fixed-point, fixed-point Armijo–Wolfe-type, and multiple shooting solvers.

problem and evaluate its cost functional, $\mathcal{J}_c = \frac{1}{2}\int_0^1\int_{-1}^1(\widehat{\rho}-\bar{\rho})^2\,dxdt + \frac{\beta}{2}\int_0^1\int_{-1}^1\|\mathbf{w}\|^2\,dxdt$.

Note that the comparison is slightly impacted by the fact that convergence is measured differently by these numerical methods. Though both multiple shooting and fixed-point methods employ the same `ode15s` solver with the same tolerance, multiple shooting compares values of ρ and q at chosen start and end points in time for its convergence criteria, while the fixed-point methods use values of $\mathbf{w}$ for all times, in deciding convergence. However, a general comparison can be made regarding the relative efficiency of the three approaches. We also highlight that the cost of a single PDE solve in 2D is significantly higher than the 1D example studied here, so any corresponding performance gains will be amplified in higher dimensions. We choose $N = 30$, $n = 20$, the ODE solver tolerance is again set to be 10^{-8}, the optimality tolerance is 10^{-4}, and $\beta = 10^{-3}$.

As can be seen in Table 5.9, the running time of the fixed-point Armijo–Wolfe algorithm is the smallest and that for multiple shooting is the biggest. The cost functional for the optimized problem $\mathcal{J}_c$ is always lower than in the uncontrolled forward problem, $\mathcal{J}_{uc}$. The superior computational performance of the fixed-point Armijo–Wolfe solver can be confirmed by comparing the number of function evaluations for each method, which is an important measure when dealing with large systems, such as the two-dimensional problems, since each iteration is costly for large problems.

As seen in Table 5.10, the differences in ρ and q, denoted $\mathcal{E}_\rho$ and $\mathcal{E}_q$, between the three methods, are broadly in line with the optimality tolerance set, 10^{-4}. However, the difference in the computed controls, $\mathcal{E}_{\mathbf{w}}$, differs to a greater extent because $\mathbf{w}$ is updated using both the optimal values of ρ and q, with errors being compounded.

As further validated in this section, the fixed-point Armijo–Wolfe solver proves to be more efficient and hence we adopt it for most of the numerical experiments performed in the next section. However, in the case of a numerically challenging example that requires a small mixing rate at each iteration (note that this cannot be pre-determined and only is noticeable when the algorithm is running), it then becomes more advantageous to skip the Armijo–Wolfe step and fix a small mixing rate. This is because the extra function evaluations performed in the Armijo–Wolfe step will add to the computational time required for convergence, but not significantly decrease the number of fixed-point iterations. This leads to worse convergence times compared to fixing a small mixing rate, and avoiding the extra function evaluations.

5.5 Numerical Experiments for Optimization Problems Constrained by Non-Local Advection-Diffusion Equations

The optimal control problems (5.1) and (5.4) require inputs in terms of the desired state $\widehat{\rho}$, the PDE source term f, and the external potential V_{ext}, alongside initial and final time conditions for ρ and q, respectively. These are stated for the individual examples below. We also require an interaction kernel, which here we fix as

$$\mathbf{K}(\mathbf{r}, \mathbf{r}') = \nabla V_2(\mathbf{r} - \mathbf{r}'), \qquad V_2(\mathbf{x}) = \kappa e^{-\|\mathbf{x}\|^2}.$$

Interest lies in how the solution to the optimization problems changes upon varying the interaction strength, κ. Here we consider three representative values: $\kappa = 0$ (no interaction), $\kappa = -1$ (attraction), and $\kappa = 1$ (repulsion). The value $\kappa = 0$ is chosen as a baseline, since in this case the PDE constraint reduces to an advection-diffusion equation. The attraction and repulsion strengths are chosen to showcase interesting differences between the solutions. If $|\kappa|$ is too small, diffusion dominates the solution, and no significant differences can be observed from the non-interacting case. Furthermore, if $|\kappa|$ is too large, steep gradients form, which are difficult to resolve numerically.

As a baseline, we solve the forward PDE using $\mathbf{w} = \mathbf{0}$. We evaluate the associated cost functional $\mathcal{J}$, the value of which is denoted by $\mathcal{J}_{uc}$. We then expect that applying the optimization method lowers the value of the cost functional, which we then aim to minimize by optimizing $\mathbf{w}$, resulting in a cost $\mathcal{J}_c$. This cost depends on the value of the regularization parameter β and it is expected that the optimal amount of control applied will increase with decreasing β. For the initial guess for the control in the optimization algorithm, we take $\mathbf{w} = \mathbf{0}$, corresponding to the reference system.

In the following examples, the domain considered is $\Omega \times (0, T) = (-1, 1)^d \times (0, 1)$. The number of spatial points is $N = 40$ for one-dimensional examples, $N_1 = N_2 = 30$ for two-dimensional examples, and the number of time points is $n = 30$, unless stated otherwise. The tolerances in the ODE and iterative solvers are set to 10^{-8} and 10^{-4}, respectively.

5.5.1 One-Dimensional Problems

We present four examples involving the flow control problem (5.1) and source control problem (5.4) with additional non-local integral term, equipped with no-flux type boundary conditions (5.3) and (5.5), respectively, and Dirichlet boundary conditions (5.2). We keep the target variable $\widehat{\rho}$ the same for all the examples to explore the interesting dynamics that different boundary conditions and control variables present.

1D Example 1: Flow Control with No-Flux Type Boundary Conditions

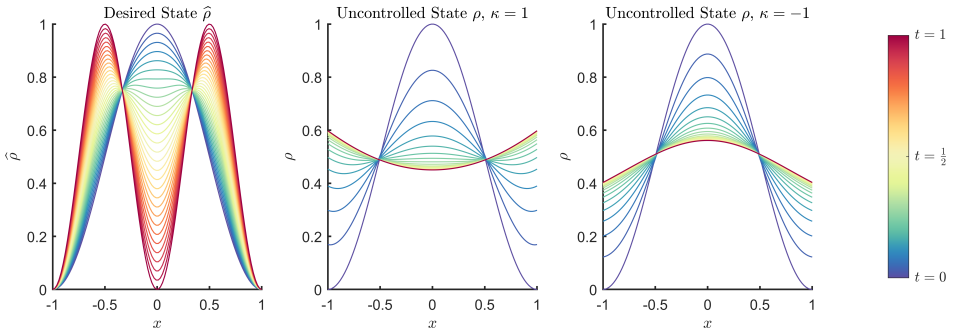

Figure 5.1: 1D Example 1: Desired state $\widehat{\rho}$ and uncontrolled state ρ for $\kappa = 1$ and $\kappa = -1$. Colours denote different times.

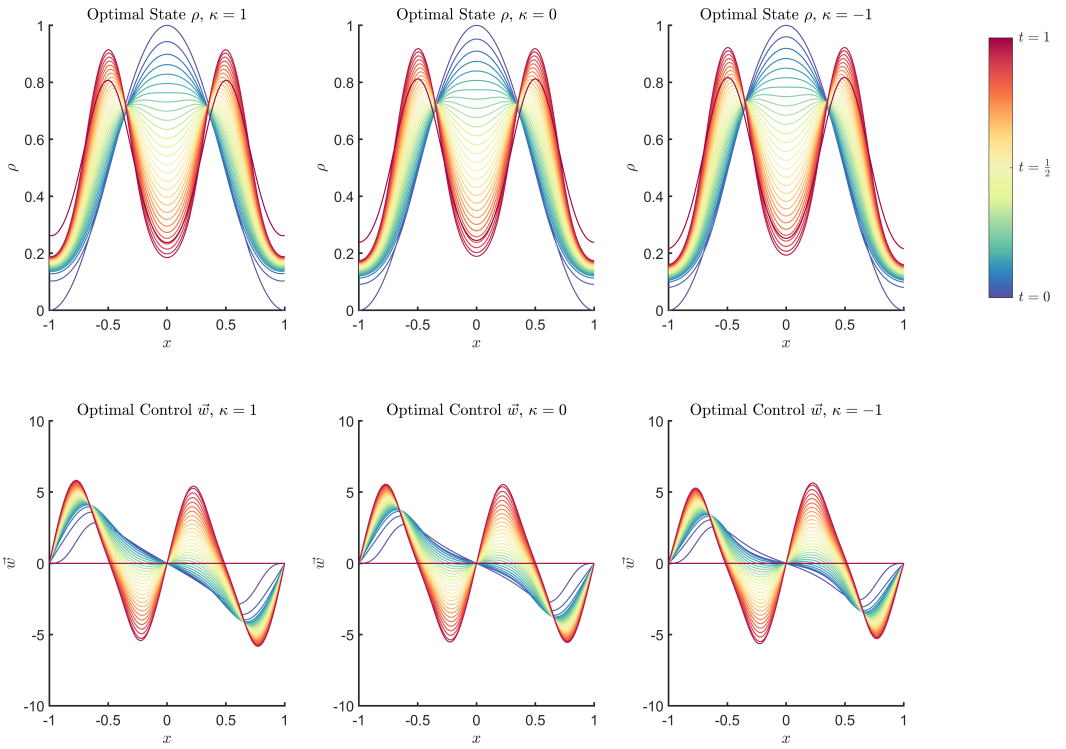

Figure 5.2: 1D Example 1: Optimal state ρ and corresponding optimal control $\mathbf{w}$ for $\kappa = 1, 0, -1$, $\beta = 10^{-3}$.

The chosen inputs are:

$$\widehat{\rho} = \frac{1-t}{2}\left(\cos(\pi x) + 1\right) + \frac{t}{2}\left(-\cos(2\pi x) + 1\right), \quad \rho_0 = \frac{1}{2}\cos(\pi x) + \frac{1}{2}, \quad f = 0, \quad V_{\text{ext}} = 0,$$

and the corresponding results are shown in Table 5.11. In Table 5.11, the value of the cost functional for the initial configuration ($\mathcal{J}_{uc}$), where $\mathbf{w} = \mathbf{0}$, is compared with the optimized case ($\mathcal{J}_c$) for different values of β and for each of the interaction strengths. As expected, in all cases $\mathcal{J}_c \leq \mathcal{J}_{uc}$, even when they are the same to the number of digits presented, and the lowest values of $\mathcal{J}_c$ occur for the smallest β values. For large values of β, applying control is heavily penalized and the optimal control approaches zero, which coincides with the uncontrolled case. This is reflected in the number of iterations `Iter`, which is small when β is large (and hence when $\mathbf{w} = \mathbf{0}$ is a good initial guess), and vice versa. We note that we show results up to the very large value $\beta = 10^3$, purely to demonstrate that the number of iterations required is very

		$\beta = 10^{-3}$	$\beta = 10^{-1}$	$\beta = 10^{1}$	$\beta = 10^{3}$
$\kappa = -1$	$\mathcal{J}_{uc}$	0.0536	0.0536	0.0536	0.0536
	$\mathcal{J}_c$	0.0097	0.0493	0.0535	0.0536
	`Iter`	131	9	2	1
$\kappa = 0$	$\mathcal{J}_{uc}$	0.0669	0.0669	0.0669	0.0669
	$\mathcal{J}_c$	0.0109	0.0603	0.0668	0.0669
	`Iter`	173	8	2	1
$\kappa = 1$	$\mathcal{J}_{uc}$	0.0839	0.0839	0.0839	0.0839
	$\mathcal{J}_c$	0.0125	0.0749	0.0838	0.0839
	`Iter`	143	8	2	1

Table 5.11: 1D Example 1: Cost $\mathcal{J}_{uc}$ of applying no control (i.e., $\mathbf{w} = \mathbf{0}$), optimal control cost $\mathcal{J}_c$, and number of iterations `Iter` required, for a range of values of the interaction strength κ and regularization parameter β.

		$\beta = 10^{-3}$	$\beta = 10^{-1}$	$\beta = 10^{1}$	$\beta = 10^{3}$
$\kappa = -1$	$\mathcal{J}_{uc}$	0.1417	0.1417	0.1417	0.1417
	$\mathcal{J}_c$	0.0356	0.1327	0.1416	0.1417
$\kappa = 0$	$\mathcal{J}_{uc}$	0.1545	0.1545	0.1545	0.1545
	$\mathcal{J}_c$	0.0380	0.1455	0.1544	0.1545
$\kappa = 1$	$\mathcal{J}_{uc}$	0.1661	0.1661	0.1661	0.1661
	$\mathcal{J}_c$	0.0411	0.1575	0.1660	0.1661

Table 5.12: 1D Example 2: Cost when $\mathbf{w} = \mathbf{0}$, optimal control cost, and iterations required, for a range of κ, β.

low due to the model allowing the imposition of almost no control.

The desired state $\widehat{\rho}$ and uncontrolled states ρ, for $\kappa = 1$ and $\kappa = -1$, are shown in Figure 5.1. Note that they are independent of β, which is not used in the forward problem. The uncontrolled ρ depends strongly on the interaction strength κ, accumulating mass in the centre of the domain for attractive interactions and at the boundary for repulsive interactions, suggesting that different optimal controls will be required. The optimal states ρ for $\kappa = 1, 0, -1$ and corresponding optimal controls, with $\beta = 10^{-3}$, are shown in Figure 5.2. For this (relatively small) value of β, the optimal state ρ is very similar to $\widehat{\rho}$, regardless of the choice of interaction. However, the corresponding control plots reveal the effects of interactions on the optimal controls. The control is focussed on transporting the mass from the middle of the domain onto two piles centred at $x = -0.5$ and $x = 0.5$. We note in particular the complexity of the optimal control. We believe this is a consequence of the steep optimal control and state, which requires a more accurate numerical resolution. We next study the effects of the boundary condition on the dynamics and control; Figure 5.4 also shows the results for the corresponding Dirichlet case, described below.

1D Example 2: Flow Control with Dirichlet Boundary Conditions

Here we use the same inputs as in 1D Example 1, but replace the no-flux boundary conditions with Dirichlet conditions. Table 5.12 again shows the results for a range of β values and different interaction strengths. The results for $\kappa = 1$ and $\beta = 10^{-3}$ are shown in Figure 5.3. The observations are in line with those in 1D Example 1. However, both the optimal state ρ and the optimal control are qualitatively different when considering Dirichlet boundary conditions rather than no-flux conditions. This indicates that the Dirichlet boundary conditions are harder to apply in this problem, due to the steep shape of the desired state. This steepness is somewhat less impactful in 1D Example 1, where the desired state is not closely matched by the optimal state at the boundaries. In this example, while the optimal state matches the desired state perfectly at the boundary, the peaks of the desired state are matched less closely. In Figure 5.4, this can be confirmed by considering the control plots. The optimal control for 1D Example 2 is larger than for 1D Example 1, specifically between the boundaries of the domain and the peaks of the desired state, indicating numerical challenges in this region.

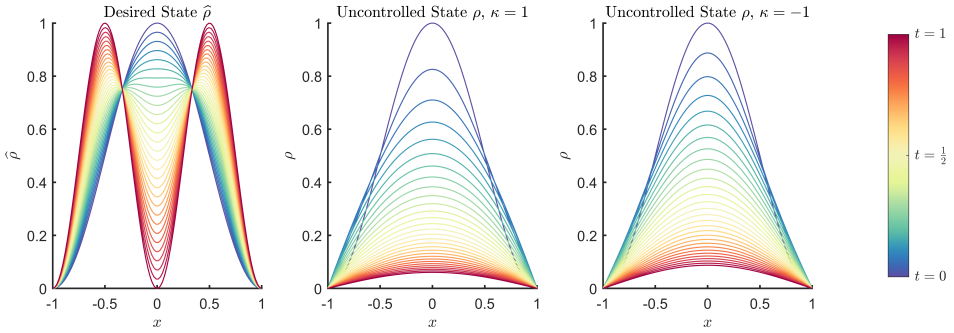

Figure 5.3: 1D Example 2: Desired state $\widehat{\rho}$ and uncontrolled state ρ for $\kappa = 1$ and $\kappa = -1$. Colours denote different times.

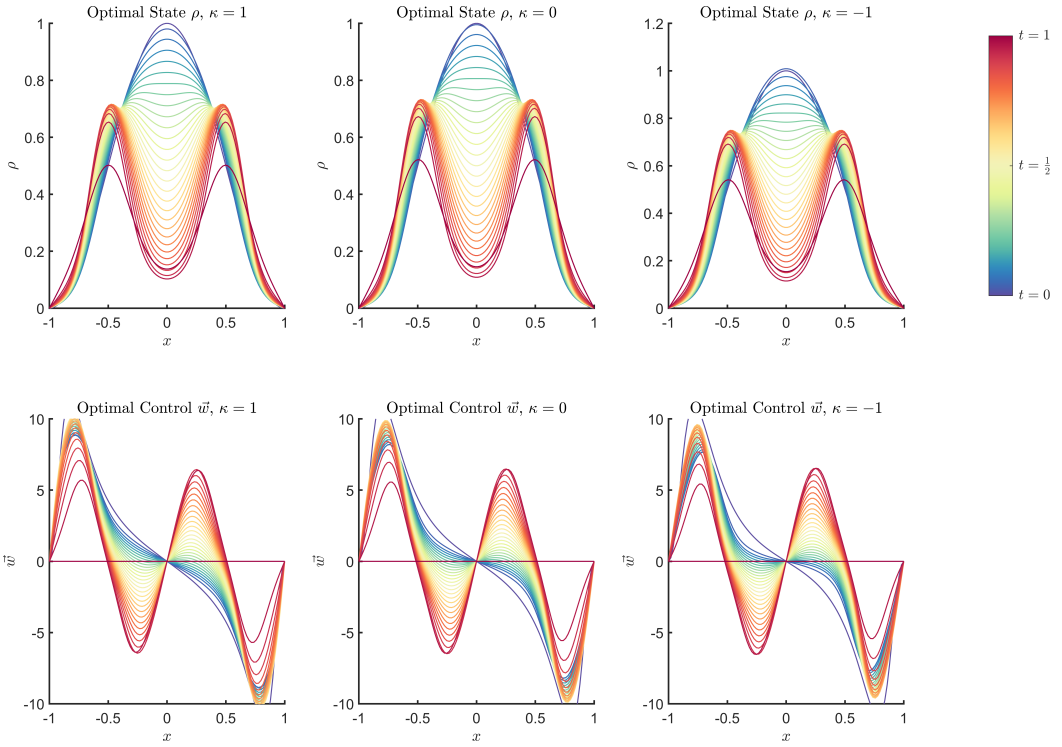

Figure 5.4: 1D Example 2: Optimal state ρ and corresponding optimal control $\mathbf{w}$ for $\kappa = 1, 0, -1$, $\beta = 10^{-3}$.

1D Example 3: Source Control with Dirichlet Boundary Conditions

The inputs for this problem are:

$$\widehat{\rho} = \frac{1-t}{2}\left(\cos(\pi x) + 1\right) + \frac{t}{2}\left(-\cos(\pi x) + 1\right), \quad \rho_0 = \frac{1}{2}\cos(\pi x) + \frac{1}{2}, \quad f = 0,$$
$$V_{\text{ext}} = -\frac{1}{2}\left((x+0.3)^2 - 0.2\right)\left((x-0.4)^2 - 0.3\right).$$

Note that, since V_{ext} is non-zero, the fixed-point optimization computations become more challenging and require a smaller mixing rate for most iterations, hence it is more efficient to omit the Armijo–Wolfe step and fix the mixing rate at $\lambda = 0.001$.

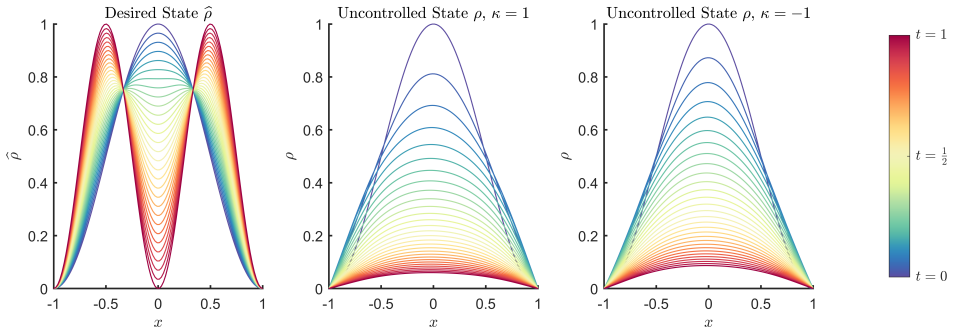

Figure 5.5: 1D Example 3: Desired state $\widehat{\rho}$ and uncontrolled state ρ for $\kappa = 1$ and $\kappa = -1$. Colours denote different times.

We have the same desired state from 1D Examples 1 and 2, and similar uncontrolled states as 1D Example 2. There is however a huge difference in the profile of the optimized source control here compared to the optimized flow control in 1D Example 2. The optimized control mimics the desired state and explicitly displaces the particles to conform to the desired state.

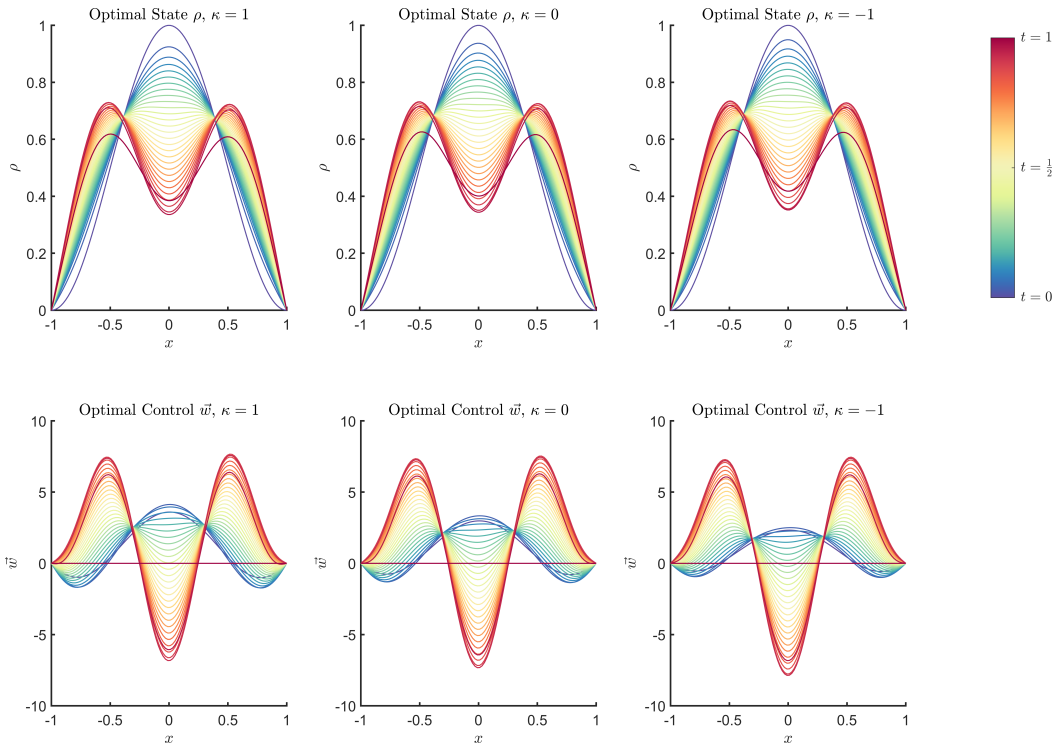

Figure 5.6: 1D Example 3: Optimal state ρ and corresponding optimal control w for $\kappa = 1, 0, -1$, $\beta = 10^{-3}$.

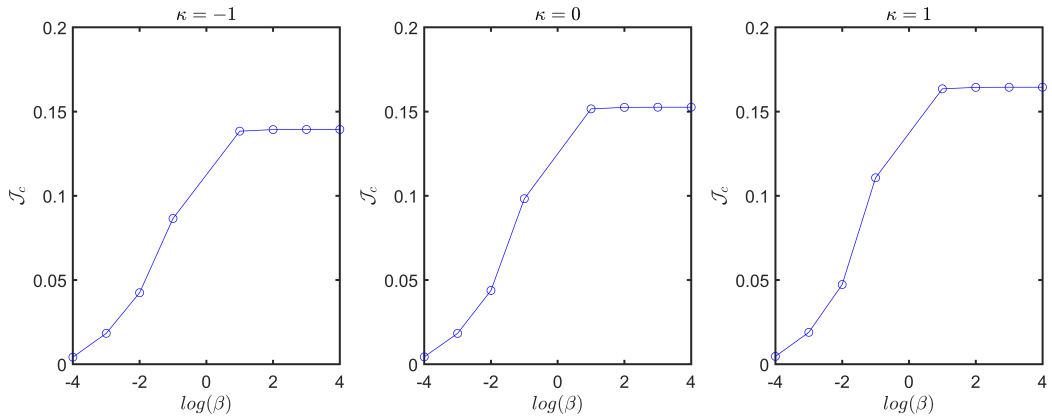

Figure 5.7: Relationship between β and the optimized cost functional $\mathcal{J}_c$ for different κ.

The non-zero external potential V_{ext} appears to be an advantage in achieving an optimal set-up, as we see the values of $\mathcal{J}_c$ in Table 5.13 show our optimized state is closer to the desired state than in 1D Example 2, and we are applying less control here. We also see, in Figure 5.7, the trend of increasing β with increased optimization cost that has been observed in all the examples in this section. In particular, the case $\kappa = -1$ gives the best optimization results for this problem. This suggests that attractive interactions are a better suited choice to achieve the desired state. Also, after some value of β, in this instance $\beta = 10^2$, the cost functional barely increases, showing that the cost is only significantly reduced when $\beta < 10^2$.

1D Example 4: Source Control with No-Flux Boundary Conditions

The inputs for this problem are:

$$\widehat{\rho} = \frac{1-t}{2} + \frac{t}{2}\left(-\cos(\pi x) + 1\right), \quad \rho_0 = \frac{1}{2}, \quad f = 0, \quad V_{\text{ext}} = 0.$$

		$\beta = 10^{-3}$	$\beta = 10^{-1}$	$\beta = 10^{1}$	$\beta = 10^{3}$
$\kappa = -1$	$\mathcal{J}_{uc}$	0.1394	0.1394	0.1394	0.1394
	$\mathcal{J}_c$	0.0184	0.0865	0.1384	0.1394
$\kappa = 0$	$\mathcal{J}_{uc}$	0.1526	0.1526	0.1526	0.1526
	$\mathcal{J}_c$	0.0183	0.0983	0.1516	0.1526
$\kappa = 1$	$\mathcal{J}_{uc}$	0.1645	0.1645	0.1645	0.1645
	$\mathcal{J}_c$	0.0190	0.1107	0.1635	0.1645

Table 5.13: 1D Example 3: Cost when $w = 0$, optimal control cost, and iterations required, for a range of κ, β.

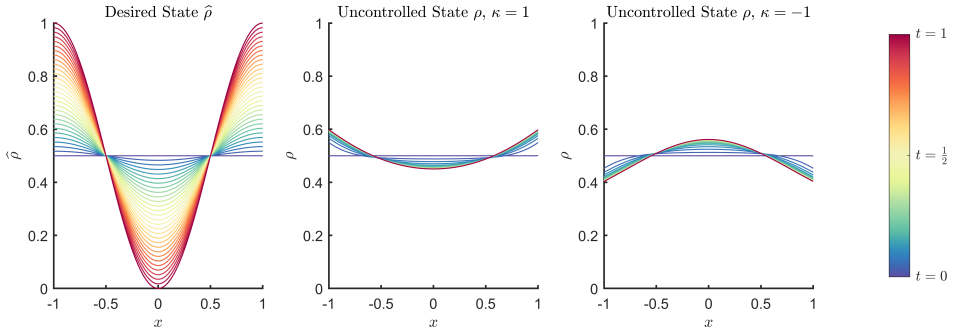

Figure 5.8: Example 4: Desired state $\widehat{\rho}$ and uncontrolled state ρ for $\kappa = 1$ and $\kappa = -1$. Colours denote different times.

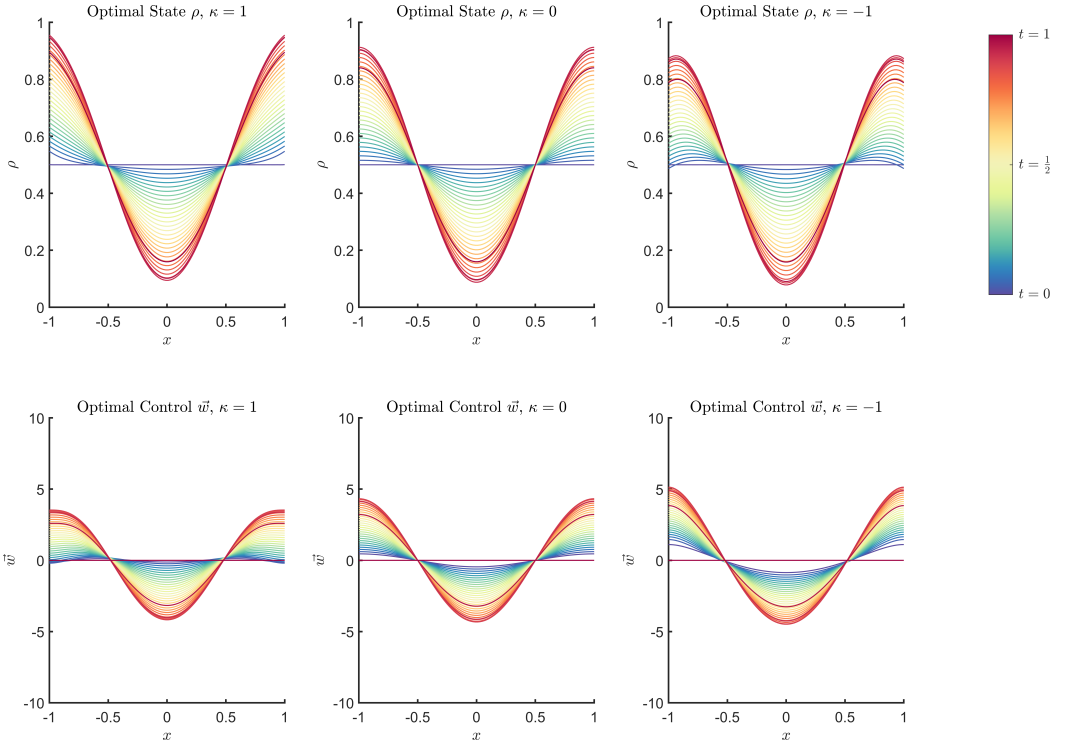

Figure 5.9: 1D Example 4: Optimal state ρ and corresponding optimal control w for $\kappa = 1, 0, -1$, $\beta = 10^{-3}$.

We use the fixed-point algorithm for this example, as a small mixing rate is required for each iteration. The mixing parameter λ is set to 0.001. The corresponding values of the cost functional are shown in Table 5.14. Once again the optimization costs are smaller that the cost of the uncontrolled problem, and we observe same trend of the optimization cost increasing

		$\beta = 10^{-3}$	$\beta = 10^{-1}$	$\beta = 10^{1}$	$\beta = 10^{3}$
$\kappa = -1$	$\mathcal{J}_{uc}$	0.0606	0.0606	0.0606	0.0606
	$\mathcal{J}_c$	0.0060	0.0554	0.0606	0.0606
$\kappa = 0$	$\mathcal{J}_{uc}$	0.0417	0.0417	0.0417	0.0417
	$\mathcal{J}_c$	0.0045	0.0383	0.0416	0.0417
$\kappa = 1$	$\mathcal{J}_{uc}$	0.0286	0.0286	0.0286	0.0286
	$\mathcal{J}_c$	0.0036	0.0265	0.0285	0.0286

Table 5.14: 1D Example 4: Cost when $w = 0$, optimal control cost, and iterations required, for a range of κ, β.

		$\beta = 10^{-3}$	$\beta = 10^{-1}$	$\beta = 10^{1}$	$\beta = 10^{3}$
$\kappa = -1$	$\mathcal{J}_{uc}$	0.0113	0.0113	0.0113	0.0113
	$\mathcal{J}_c$	0.0013	0.0104	0.0113	0.0113
	`Iter`	676	700	290	1
$\kappa = 0$	$\mathcal{J}_{uc}$	0.0104	0.0104	0.0104	0.0104
	$\mathcal{J}_c$	0.0013	0.0096	0.0104	0.0104
	`Iter`	676	688	289	1
$\kappa = 1$	$\mathcal{J}_{uc}$	0.0111	0.0111	0.0111	0.0111
	$\mathcal{J}_c$	0.0016	0.0102	0.0111	0.0111
	`Iter`	679	683	290	1

Table 5.15: 2D Example 1: Cost when $\mathbf{w} = \mathbf{0}$, optimal control cost, and iterations required, for a range of κ, β.

with increasing β. Figure 5.8 shows the desired state that starts as a uniform distribution, and over time separates into three regions: two mirror distributions at the boundaries and a flipped distribution in the centre. The uncontrolled state for $\kappa = 1$ mimics the target's behaviour the best, as it pushes the particles towards the boundaries, while the case $\kappa = -1$ pulls the particles towards the centre of the spatial domain. This suggests that repulsive particle interactions are a more appropriate choice to achieve the desired state. This is evident in Figure 5.9 which shows the profiles for the optimal states and control over time. We observe that the optimal state when $\kappa = 1$ is the closest to the desired state. Though the optimal controls portray similar behaviour, a closer look shows that more control is exerted on the boundaries when $\kappa = -1$.

5.5.2 Two-Dimensional Problems

In this section, we demonstrate the modular and flexible nature of our approach by applying it to problems in two spatial dimensions. The main difference is that the PDE discretization requires an increased number of points from N to $N_1 N_2$, where N_j are typically of the same order of magnitude as N, resulting in increased computational cost. This is a key motivation for the development of fast optimization solvers, such as the fixed-point method. Note that here the non-linear flow control becomes a true (2D) vector field, rather than a scalar field as it is in the 1D case.

2D Example 1: Flow Control with No-Flux Boundary Conditions

For this example we have the following set up:

$$\widehat{\rho} = \frac{1-t}{4} + \frac{t}{4}\left(\sin\left(\frac{\pi(x_1-2)}{2}\right)\sin\left(\frac{\pi(x_2-2)}{2}\right)+1\right), \quad \rho_0 = \frac{1}{4}, \quad f = 0, \quad V_{\text{ext}} = 0,$$

where $\mathbf{x} = (x_1,\ x_2)^T$. The results for this example are displayed in Table 5.15. Figure 5.10 shows the uncontrolled state and the desired state with $\kappa = 1$ and $\beta = 10^{-3}$. We observe in the uncontrolled state, that an initial uniform condition with no control introduced remains relatively uniform inside the domain with slightly more particles at the corners of the domain. This behaviour is far from the specified desired state, where we have two relatively large bumps

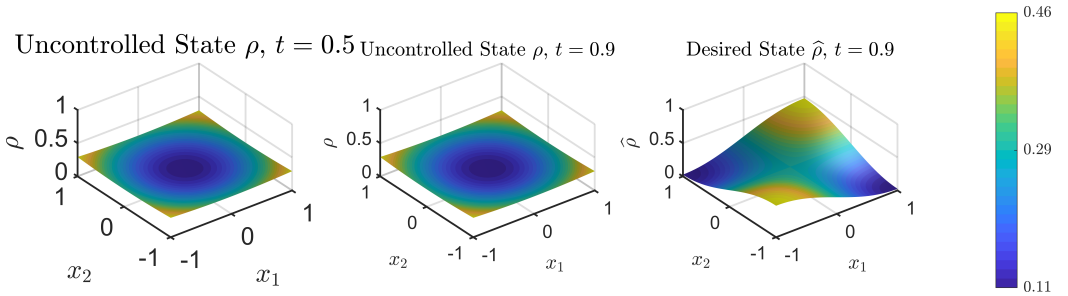

Figure 5.10: 2D Example 1: Uncontrolled ρ and desired state $\widehat{\rho}$, with $\beta = 10^{-3}$ and $\kappa = -1$.

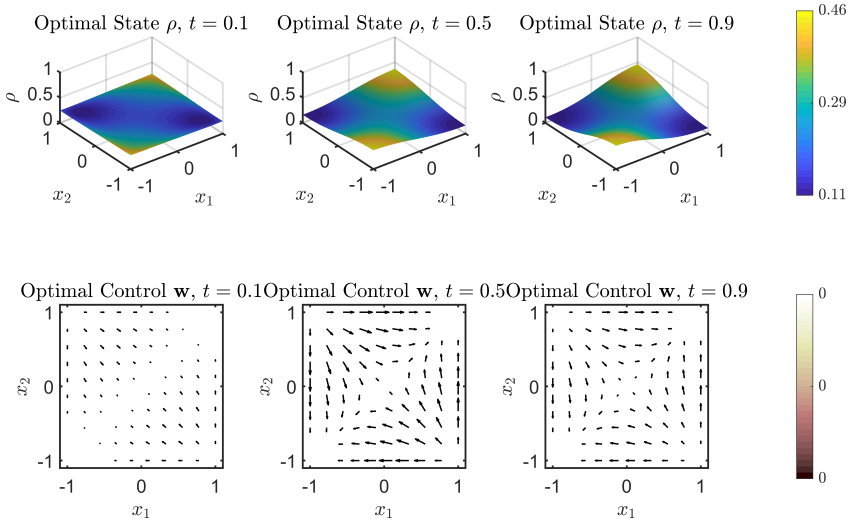

Figure 5.11: 2D Example 1: Controlled ρ and optimal control $\mathbf{w}$, with $\beta = 10^{-3}$ and $\kappa = -1$.

of particles towards two corners of the domain: $(-1, -1)$, and $(1, 1)$. Figure 5.11 shows the state and control when optimization is applied to the forward problem. The optimal state over time distributes more particles towards the corners $(-1, -1)$, and $(1, 1)$. This behaviour of the optimal state can clearly be attributed to the optimal control, which acts towards the two corners where the particles are concentrated. It acts particularly strongly on the emerging slopes of the two bumps, since steep mass accumulation is hard to achieve under the influence of diffusion and interaction forces. Table 5.15 shows the cost of optimization against the cost of applying no control and clearly illustrate that the optimized system has lower cost associated with it.

2D Example 2: Flow Control with No-Flux Boundary Conditions

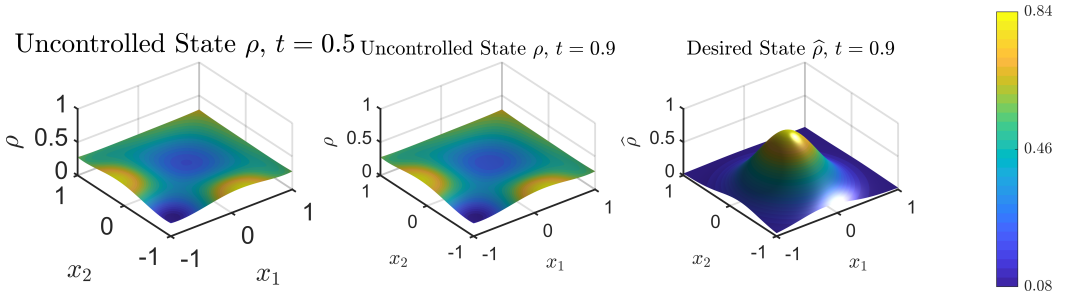

Figure 5.12: 2D Example 2: Uncontrolled ρ and desired state $\widehat{\rho}$, with $\beta = 10^{-3}$ and $\kappa = -1$.

We consider another example for the flow control problem with no-flux type boundary

		$\beta = 10^{-3}$	$\beta = 10^{-1}$	$\beta = 10^{1}$	$\beta = 10^{3}$
$\kappa = -1$	$\mathcal{J}_{uc}$	0.0400	0.0400	0.0400	0.0400
	$\mathcal{J}_c$	0.0046	0.0370	0.0400	0.0400
	`Iter`	717	778	347	1
$\kappa = 0$	$\mathcal{J}_{uc}$	0.0478	0.0478	0.0478	0.0478
	$\mathcal{J}_c$	0.0064	0.0450	0.0478	0.0478
	`Iter`	718	784	343	1
$\kappa = 1$	$\mathcal{J}_{uc}$	0.0556	0.0556	0.0556	0.0556
	$\mathcal{J}_c$	0.0085	0.0530	0.0556	0.0556
	`Iter`	720	787	339	1

Table 5.16: 2D Example 2: Cost when $\mathbf{w} = \mathbf{0}$, optimal control cost, and iterations required, for a range of κ, β.

conditions:

$$\widehat{\rho} = \frac{1-t}{4} + \frac{t}{Z} e^{-3\left((x_1+0.2)^2+(x_2+0.2)^2\right)}, \quad \rho_0 = \frac{1}{4}, \quad f = 0,$$
$$V_{\text{ext}} = \left((x_1+0.3)^2 - 1\right)\left((x_1-0.4)^2 - 0.5\right)\left((x_2+0.3)^2 - 1\right)\left((x_2-0.4)^2 - 0.5\right),$$

with $Z \approx 0.9921$ a normalization constant. In this example, we also have a uniform initial condition for the state, as in 2D Example 1, but we include a non-zero external potential and specify a different desired state. In Figure 5.12, the results for the uncontrolled problem and desired state are illustrated for $\beta = 10^{-3}$ and $\kappa = -1$. Figure 5.12 demonstrates the effect of V_{ext} on the state. The particles accumulate in regions with potential wells and the areas where the potential is steep are avoided. The desired state in this example portrays attractive interactions and an accumulation of particles towards the centre of the domain.

Results for the optimization problem for $\beta = 10^{-3}$ and various interaction strengths, κ, are shown in Figures 5.13 and 5.14. It is noticeable in Figure 5.14, which shows the actions of the optimal controls and external potential, that the control acts to drive the particle distribution towards the desired state. However, the control does not act uniformly around the peak of the desired state, but also acts strongly in the area between the location of the desired peak and the point $(-1,-1)$. This is due to the external potential being steep in this area and more control is needed to reach the desired state than in other parts of the domain. Since the desired state requires the particles to accumulate in one part of the domain, more control has to be applied to the repulsive particles, which oppose the desired clustering. This is evident in Figure 5.14, when comparing the magnitude of the control, symbolised by differently sized arrows, for $\kappa = 1$ (repulsion) with the other two cases. In the attractive configuration, the effect of the attraction supports the control action, so less control is needed to reach the desired state. The numerical solution takes between 1 and 750 iterations for the fixed-point solver to converge, over an average time of 60 minutes depending on the problem considered (fewer iterations when β is large and more when β is small).

2D Example 3: Source Control Problem with No-Flux Boundary Conditions

The chosen inputs for this example are

$$\rho_0 = \frac{1}{4}, \quad V_{\text{ext}} = \cos\left(\frac{\pi x_1}{5} - \frac{\pi}{5}\right)\sin\left(\frac{\pi x_2}{5}\right),$$
$$\widehat{\rho} = \frac{1}{4}(1-t) + t\left(\frac{1}{4}\sin\left(\frac{\pi\,(x_1-2)}{2}\right)\sin\left(\frac{\pi(x_2-2)}{2}\right) + \frac{1}{4}\right).$$

We once again prescribe a uniform initial condition for the state and the same desired state as in 2D Example 1. However, we specify a non-zero external potential to study the interesting dynamics it introduces into the optimality system. Figure 5.15 shows the desired state which concentrates the density at two opposite corners of the domain: $(-1,1)$, and $(1,1)$. The uncontrolled state, shown in Figure 5.15 as well, moves the density towards $(1,-1)$ where the external potential exerts the least strength.

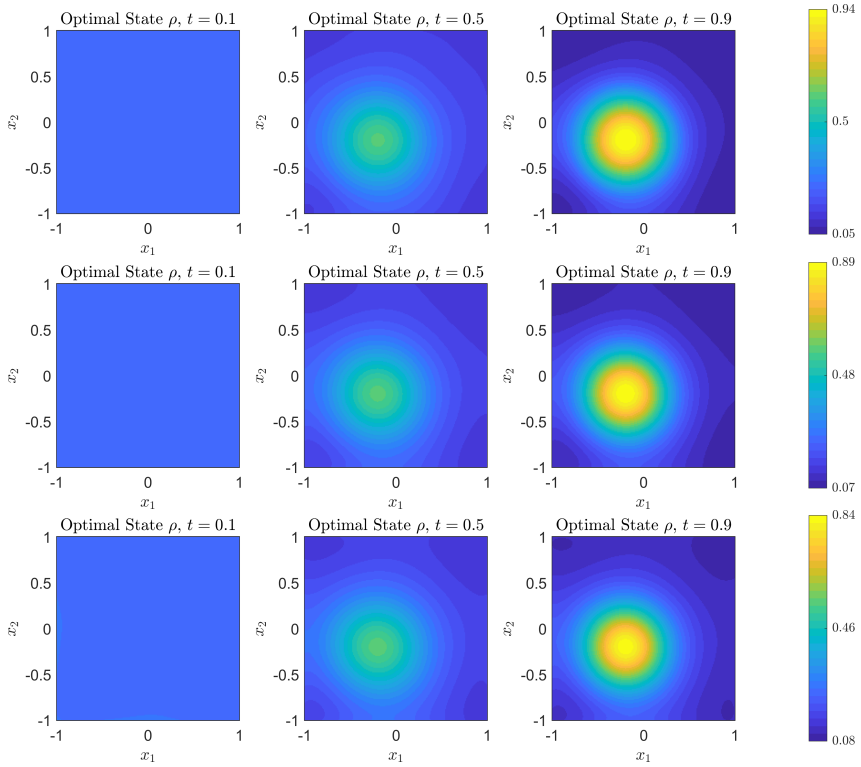

Figure 5.13: 2D Example 2: Snapshots of the optimal ρ for different interaction strengths, $\kappa = -1$, $\kappa = 0$, and $\kappa = 1$ (top to bottom), with $\beta = 10^{-3}$.

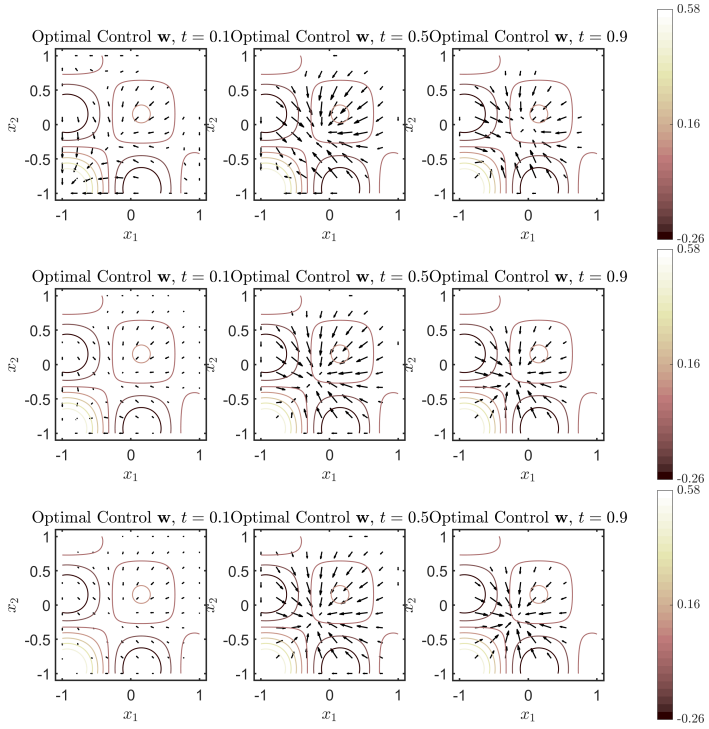

Figure 5.14: 2D Example 2: Snapshots of the optimal control for different interaction strengths, $\kappa = -1$, $\kappa = 0$ and $\kappa = 1$ (top to bottom), with $\beta = 10^{-3}$. The lengths of the arrows are proportional to $\|\mathbf{w}\|$. A contour plot of the external potential V_{ext} is superimposed for reference, with a corresponding colorbar on the right-hand side.

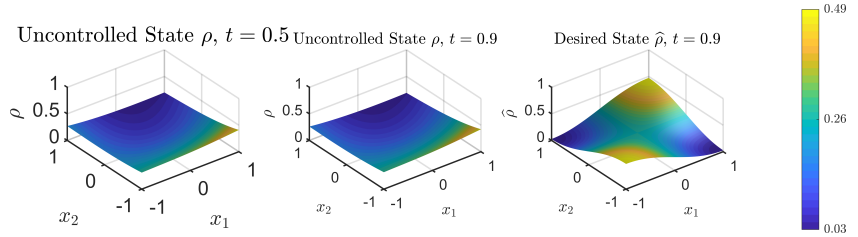

Figure 5.15: 2D Example 3: Uncontrolled ρ and desired state $\widehat{\rho}$, with $\beta = 10^{-3}$ and $\kappa = -1$.

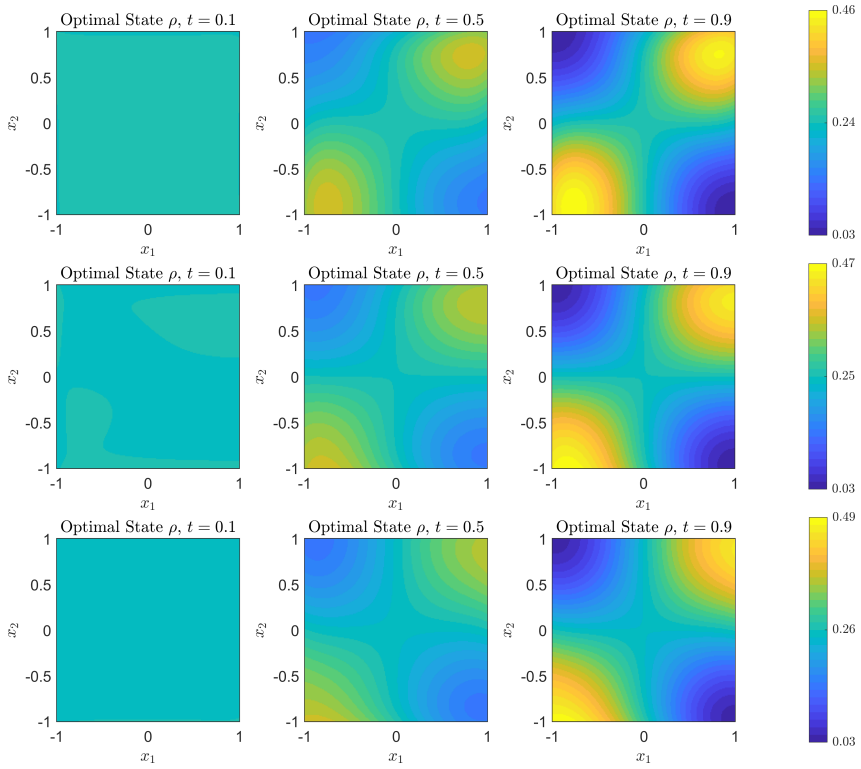

Figure 5.16: 2D Example 3: Snapshots of the optimal ρ for $\kappa = -1$, $\kappa = 0$, and $\kappa = 1$ (top to bottom), for $\beta = 10^{-3}$.

In Figure 5.16 we show (for $\beta = 10^{-3}$) the optimal states for different interaction strengths, with the corresponding optimal controls in Figure 5.17. Since β is small, the optimal state is very close to the desired state. We can observe clear effects of the external potential V_{ext} on the optimal state and the control. Since V_{ext} is large around $x_2 = 1$, more control has to be applied in this area to force the density towards $\widehat{\rho}$. It can also be seen that the state is slightly asymmetric because of this effect, despite $\widehat{\rho}$ being symmetric.

The effect of the different interaction strengths on the state can be observed in Figure 5.16, by inspecting the shape of the particle distribution. The desired state prescribes higher density near the two corners $(-1, -1)$ and $(1, 1)$. Without control or an external potential, repulsive particles accumulate on the boundary of the domain, whilst attractive particles favour the centre of the domain. Hence in this example, where the target density is higher near the boundary, less control needs to be applied for repulsive particles. For attractive particles, the accumulated particles are arranged in a rounder shape, while the repulsive particles are more spread out, as would be expected from their interactions.

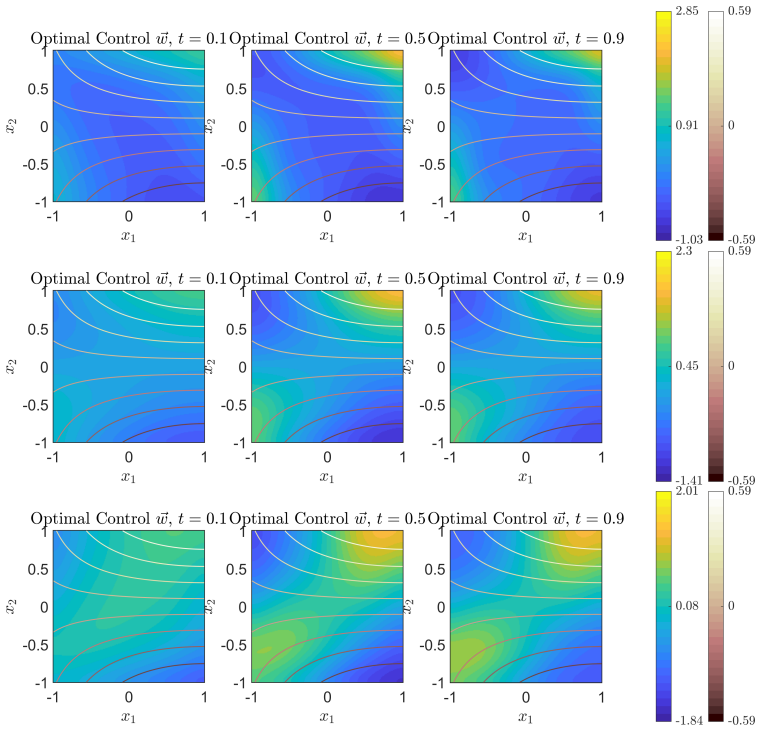

Figure 5.17: 2D Example 3: Snapshots of the optimal control for $\kappa = -1$, $\kappa = 0$ and $\kappa = 1$ (top to bottom), for $\beta = 10^{-3}$. A contour plot of the external potential V_{ext} is superimposed on the control plots for reference, with a corresponding colorbar on the right-hand side.

5.6 Remarks

We see that the fixed-point method converges for a number of 1D and 2D test problems involving non-local particle interactions. Convergence can take a couple of minutes for 1D problems and hours for 2D problems. However it is reliable, which is a significant motivation of this methodology for these very tough problems. The Armijo–Wolfe rule can accelerate convergence in a range of settings by reducing the required number of iterations, and function evaluations. Utilizing fixed smaller mixing rates for the fixed-point methods can lead to longer convergence times, however applying the Armijo–Wolfe rule in such cases can lead to even slower convergence times. We also observe that $w = 0$ or $\mathbf{w} = \mathbf{0}$ becomes a worse initial guess for smaller values of β, leading to more iterations being required for convergence. This is specific to the problems considered in this chapter due to the choice of $\widehat{\rho}$ corresponding to $w = 0$.

One advantage of the fixed-point method is that it is generalizable to problems with box constraints, which we consider in Chapter 6. However, the number of iterations required for convergence suggests that a higher-order method could be valuable. We implement the higher-order Newton–Krylov method for examples in Chapter 7 to highlight this.

The successful optimization of the non-local interacting problems discussed here opens up avenues to solve optimization problems in real-life applications that involve non-local interactions. In the next chapter, we shift our focus to the field of opinion dynamics where opinions of agents are modelled with particle dynamics equations.

Chapter 6

An Active Set–Fixed-Point Method for PDE-Constrained Problems from Opinion Dynamics

6.1 Background

Opinion dynamics is the study of the evolution of people's opinions in a social system. It is part of the larger field of mathematical modelling in the social sciences [52, 248, 249]. When a common decision has to be taken, we usually see a single position emerging known as *consensus*, or a state of co-existence of different opinions known as *clusters*. The framework of interacting particles naturally models this opinion evolution and hence we are able to utilize ideas from statistical physics and nonlinear science to model opinion dynamics systems.

Opinion dynamics models fall under a class of models describing the motion of a collection of individual entities at the microscopic scale interacting through simple rules that appear in biology, mathematics, physics, and engineering. These types of models have been proposed to describe the flocking of birds [46, 49, 160, 185], the schooling of fish [11, 20, 118], and swarms of bacteria [139], among others. Other versions of these models appear in the Keller–Segel model [132] for slime mold, the Vicsek model of phase transitions [253], the Cucker–Smale model for flocking [65, 66, 176], and robotics [43, 47, 154], as well as similar models [174, 244].

Opinion dynamics models are governed by interaction rules dictated by the model. Interesting models that have been proposed based on different interaction rules include: the DeGroot model [29, 72], voter model [26, 122, 198], Sznajd model [229, 237], majority rule model [92, 144, 242], bounded-confidence model [71, 116, 256], and continuous opinions and discrete actions (CODA) [168, 169] models. The DeGroot model is generally considered the classical model in opinion dynamics where weights assigned to each agent's continuous opinion in the system do not change over time. DeGroot [72] proved that the consensus opinion is a linear combination of the initial opinions of all agents, and Berger [29] presented a sufficient and necessary condition to reach a consensus in the DeGroot model. The voter model describes the social dynamics of public choices on social issues. In the voter model, all agents are placed on a regular lattice, their opinion (or choice) is denoted as a binary variable, and an agent updates his/her opinion based on that of a randomly selected neighbor. The Sznajd and majority rule models are extensions of the voter model based on different perspectives on networks. The majority rule model considers heterogeneous networks and hypergraphs, while the Sznajd models has been applied on the Erdos–Rényi (ER) random graph [84], the small-world (SW) network [180], and the scale-free (SF) network [19]. The interaction rule of the bounded confidence model is becoming a popular tool in model opinion dynamics due to its consideration of psychological factors. It has a natural PDE formulation and as a result is the model of choice in this thesis as we seek to solve PDE-constrained optimization problems. In the bounded confidence model, an agent's opinion will only be influenced by agents whose

opinions differ from his/her own by no more than a certain confidence level. The CODA model presented in [168] is a hybrid approach where each individual notices only the choices of other individuals and is not aware of their internal opinions.

Opinion dynamics has been applied in different fields, in particular public opinion management, political elections, and markets. In public opinion management, Ding *et al.* [77] focussed on the control of public opinions, which is a key problem in practical opinion dynamics and proposed an opinion control rule with minimum adjustments to support consensus reaching in the bounded confidence model. They also investigated the effects of adjustment thresholds and bounded confidences on the opinion control rule. The influence of mass media in the dynamics of the two-dimensional Sznajd model was considered in [64]. Kurz, in [148], studied the optimal control problem of minimizing the convergence (freezing) time in the discrete Hegselmann–Krause model of opinion dynamics. Pineda and Buendía in [193] focused on the effects of an external mass media on continuous opinion dynamics with heterogeneous bounds of confidence. They discovered that in the absence of mass media, diversity of bounds of confidence can improve the capacity of the systems to reach consensus. They also showed the existence, for certain parameter values, of a counter-intuitive effect in which the persuasion capacity of the mass media decreases if the mass media intensity is too large.

In the sector of political elections, Boundin *et al.* used a kinetic opinion dynamics model to investigate the influence of mass media on the Scottish independence referendum of 2014 [40]. The Sznajd rule was used in [35] to study the Brazilian election results. Bravomarquez *et al.* in [42] conducted an empirical study of opinion time series created from Twitter data on the 2008 U.S. elections with the focus of establishing whether a time series is appropriate or not for generating a reliable predictive model. Gonzalez *et al.* in [102] studied a model for elections based on the Sznajd model, and the exponent they obtained for the distribution of votes during the transient regime agreed with those obtained for real elections in Brazil and India.

In markets, Oster and Feigel [184] proposed an opinion dynamics model to describe stock and option price formation and showed a good fit of option prices to real data. Varma *et al.* [252] analyzed competition between two firms, where each firm attempts to sway the public opinion to its own side by spending money on advertising or providing discounts for specific consumers, thus capturing a larger market share. A recommender system was presented in [53] based on opinion dynamics to help users select the right products or services in information overload scenarios. Finally, Quattrociocchi *et al.* [202] investigated how mainstream media signed interaction might shape the opinion space, focusing on how different numbers of media and interaction patterns of the information system affect collective debates and opinion distribution.

In this chapter, we detail the evolution of the bounded confidence interval model for opinion dynamics, and construct PDE-constrained optimization problems for opinion dynamics including additional bound constraints. Next, we present a novel combination of an active set fixed-point numerical algorithm and pseudospectral or finite difference discretization to solve these optimization problems. We conclude with numerical experiments solving optimization problems constrained by the one-dimensional bounded confidence interval opinion dynamics model.

6.1.1 The Evolution of the Bounded Confidence Interval Model for Opinion Dynamics

The bounded confidence interval models were originally proposed as deterministic, discrete time processes [71, 116, 256] and have been extended to include noise or randomness [194–196, 236], modelling uncertainty in observations or external influences. Related models include continuous time ODEs [47], SDEs, and PDEs [141, 255]. We refer to [52, 199, 200] for comprehensive reviews.

The discrete time bounded confidence models were independently designed by Deffuant *et al.* (DW) and Hegselmann *et al.* (HK) in [71] and [116], respectively. Both models received significant attention as they reflected more accurately the real-world situations where one is more likely to be influenced by others with similar opinions. The main difference between the DW and HK models is: in the DW model, two randomly chosen individuals meet and pairwise averaging is implemented, and hence, this model is suitable for where individuals meet in small groups and exchange information face-to-face, while the HK model captures communication in

large groups (which is practical in the era of social media), and individuals move to the average opinion of all other individuals which lie in the area of confidence. It is shown for both models (see [71,116]) that for large numbers of individuals there is always a final state which is a perfect consensus or set of opinion clusters. For the rest of this thesis, we do not discuss the DW model any further, but focus on the HK model.

The Classical Hegselmann–Krause (HK) Model

Take a system with N fixed number of agents/individuals. Now, $x_i(t)$ is the location/position of agent i at time t on the real line. The position of an agent represents its opinion. At each time step, the opinion x_i of the agent i, $i = 1, 2, \ldots, N$, moves to the average opinion of other agents that are within a fixed distance R of itself, i.e. ,

$$x_i(t+1) = \frac{\sum_{j:|x_i(t)-x_j(t)|\leq R} x_j(t)}{|I_i(\mathbf{x}, t)|}. \tag{6.1}$$

where $I_i(\mathbf{x}, t) := \{j : |x_i(t) - x_j(t)| \leq R\}$. The underlying assumption is that people are immune to the influence of others whose opinions differ greatly from theirs. Hence, if two groups of agents are initially separated by a distance greater than R, then they will form decoupled dynamical systems (clusters) with no interaction between them.

The model in (6.1) is rewritten in [47] as

$$x_i(t+1) = x_i(t) + \sum_{j=1}^{N} a_{ij}(x_j(t) - x_i(t)),$$

where

$$a_{ij} = \begin{cases} |I_i(\mathbf{x}, t)|^{-1} & j \in I_i(\mathbf{x}, t) \\ 0 & \text{otherwise.} \end{cases}$$

Now, instead of jumping to the average opinion, if we move towards it continuously in time, then we have the equivalent continuous time ODE expressed in [177] as

$$\frac{d}{dt}x_i = \sum_{j=1}^{N} a_{ij}(x_j - x_i), \tag{6.2}$$

where

$$a_{ij} = \frac{\phi_{ij}}{\sum_k \phi_{ik}}, \quad \phi_{ij} = \phi(|x_j - x_i|).$$

and $i = 1, 2, \ldots, N$. Here, $0 \leq \phi \leq 1$ is the scaled influence function which acts on the 'difference of opinions' $|x_i - x_j|$. We note that a_{ij} in the model (6.2) is not symmetric, and in [177], a symmetric version,

$$a_{ij} = \frac{\phi(|x_j - x_i|)}{N} \tag{6.3}$$

is proposed which still captures the original HK rules. The assumption is that agents react to their differences relative to other agents and not the position of others. Since a_{ij} depends on the relative difference $|x_i - x_j|$, we have a non-linear model. Motsch *et al.* in [177] also studied the mean-field limit of (6.2), specifically with the symmetric sub-stochastic matrix A defined by the entries in (6.3).

The Noisy Hegselmann–Krause Model

In the classic bounded confidence models, final states are always a consensus or clusters. However in real social systems, public opinions do not reach such ideal states, and there is always uncertainty involved. Hence to make the models more realistic, Pineda *et al.* in [194–196] introduced noise into the models in the following ways. With a given probability, an individual at each time step can

- take a random jump inside the given opinion space,
- take a random jump in a small interval centered around its current opinion,

or follow the classical HK rule. This noise can be interpreted as 'free-will' or 'self-thinking' where individuals change their opinions in a random way, the death and birth of individuals or the replacement of individuals in a system whose total size is not fixed. The aim was to analyse which aspects of the original dynamics are robust with respect to noise and study which additional complex collective phenomena can emerge. They successfully implemented this noise in the DW model in [194] and [196] first, then in the HK model in [195] through master equations. They discovered that the noise induces phase transitions or order–disorder transitions. There are now studies (see [80, 96, 221, 255]) around approximating the critical conditions (extent of noise) for systems to move from order (consensus or clusters) to disorder (uniform) and vice versa using linear stability analysis, and the agreement is that diffusion induces an order–disorder transition. In the disordered state, the distribution of opinions tends to be uniform while for ordered, a set of defined clusters are formed, although some opinion may spread between them.

In 2015, Garnier *et al.* [93] introduced the stochastic continuous space and time opinion dynamics model with exogenous randomness, which was a build up of the model in (6.2) with independent Brownian motions accounting for the noise in each agent's opinion.

$$dx_i = -\frac{1}{N}\sum_{j:|x_i-x_j|\leq R}(x_i - x_j)dt + \sigma dW_t^{(i)}, \tag{6.4}$$

where $x_i(t)$ is agent i's opinion modelled as a real valued process, and $i = 1, 2, \ldots, N$. Here, $W_t^{(i)}$ represents an independent Wiener process and σ is a non-negative constant that controls the magnitude of noise. The case $\sigma = 0$ implies there is no randomness (i.e. , the deterministic case) and $\sigma \neq 0$ means the system is stochastic. The summation represents the attracting force that pulls agents together while diffusion keeps them active under Brownian motion.

The corresponding mean-field limit non-linear Fokker–Planck equation that models the agents' density profile is obtained as:

$$\partial_t \rho(x,t) = \nabla_x \cdot \left(\rho(x,t)\int (x-y)\rho(y,t)\mathbf{1}_{|x-y|\leq R}\,dy\right) + \frac{\sigma^2}{2}\nabla_x^2\rho(x,t), \tag{6.5}$$

where ρ is the limiting density of the N-body distribution $\rho^N(x,t) := \frac{1}{N}\sum \delta_{x_j}(t)(dx)$ as $N \to \infty$, the term with ∇_x^2 represents the diffusion process that flattens ρ, and the integral term is the advection of the density caused by the attraction, where

$$\mathbf{1}_{|x-y|\leq R} = \begin{cases} 1 & |x-y| \leq R, \\ 0 & \text{otherwise.} \end{cases}$$

Periodic boundary conditions were imposed for technical convenience, but to solve (6.4) and (6.5) on a finite interval, Neumann type boundary conditions are recommended [96]. This is because agents near the edges of the population have, on average, more agents inside than outside, and hence feel a net force inwards. So, if one starts with a uniform distribution, the agents will end up clustering. This happens in the PDE experiments where Neumann type boundary conditions are imposed. In the periodic case, the uniform state remains uniform.

At this point, we see clearly the similarities between the opinion dynamics Fokker–Planck equation (6.5) and the DDFT Fokker–Planck equations used in the optimization problems (5.1) and (5.4) in Chapter 5. In fact, one can write (6.5) as a DDFT model (see [96]). The similarity arises through the non-local and non-linear 2-body integral term. This motivates the study of opinion dynamics optimization problems done in this chapter, and the application of the same numerical algorithms utilized in Chapter 5 for the DDFT problems to these opinion dynamics problems.

Garnier *et al.* in [93], used linear stability analysis of the associated Fokker–Planck equation (6.5) to estimate the number of clusters, the time to cluster formation, and the critical strength of randomness to have cluster formation. They extensively discuss the cluster dynamics after

their formation and long-term behaviour of the clusters, confirming any analytical findings with numerical simulations.

Well-posedness (existence, uniqueness, and non-negativity) of the solution to (6.5) together with regularity issues were established in [50, 58]. In [255], Wang *et al* introduced an order parameter for analysing the order and disorder of the opinion system, and described a pseudospectral method for simulating the system in (6.5) efficiently with sufficient accuracy, but only for periodic boundary conditions. They also derived a theoretical explanation for the $2R$ conjecture that states that, for a random initial distribution in a fixed interval, the final configuration consists of clusters separated by a distance of roughly $2R$.

Introduction of Radicals and Effects of Boundary Conditions

The persistent disagreement and clustering exhibited in some real-world systems be captured by introducing agents with persistent behaviour. One such approach is named radical opinions and can be attributed to 'stubborn individuals' or a position shared by a group of close-minded opinion leaders with the expectation that, they increase the attractive forces in their neighbourhood.

Models with radical opinions are studied in [117] and [270], where their numerical results demonstrate high sensitivity of clusters to radicals' opinions positioned at a single point in the domain, and reveal counter-intuitive effects such as an increase in number of radicals sometimes reducing their number of followers. In [141], the authors consider the stochastic bounded confidence model in (6.4) with additional radical opinions which are distributed over a fixed interval $[0, 1]$. The radical opinions serve as an infinite-dimensional control input into the Fokker–Planck equation in (6.5), and they incorporate even 2-periodic boundary conditions to distinguish the two extreme opinions at 0 and 1 (which periodic boundary conditions fail to do). They show well-posedness of the new model in a certain class of initial conditions and provide existence result and a global estimate for the corresponding stationary equation and find a lower bound on the noise level that guarantees exponential convergence of the dynamics to stationary state. However, Goddard *et al.* show in [96] that even 2-periodic boundary conditions create a mirror system which can strongly influence the dynamics and produce potentially undesirable effects. They instead introduce no-flux or Robin boundary conditions which most faithfully reproduce the underlying mechanisms in the deterministic model in (6.2), and conserve mass without conflating the extreme opinions. They also point out differences to be mindful of in the SDE model (6.4) and PDE model (6.5), such as how large N should be (usually 10^{23} in statistical mechanics compared to hundreds or thousands in social systems for these models to demonstrate agreement). They implement robust pseudospectral methods which effectively implements both periodic and no-flux boundary conditions (see Chapter 4).

For the SDE model with radicals, the indexing of 'normal' individuals as $1, 2, \ldots, N$ is retained, and radicals are added in and indexed by $N + 1, N + 2, \ldots, N + N_r$. We then have the equation

$$dx_i = -\frac{1}{N} \sum_{j:|x_i - x_j| \leq R} (x_i - x_j)dt + \sigma dW_t^{(i)}, \quad i = 1, 2, \ldots, N, \tag{6.6}$$

$$dx_i = 0, \quad i = N + 1, N + 2, \ldots, N + N_r. \tag{6.7}$$

We note that the sum is over $j = 1, 2, \ldots, N + N_r$. The corresponding Fokker–Planck PDE is:

$$\partial_t \rho(x, t) = \nabla_x \cdot \left(\rho(x, t) \int (x - y)(\rho(y, t) + M\rho_r(y, t))\mathbf{1}_{|x-y| \leq R}\, dy \right) + \frac{\sigma^2}{2} \nabla_x^2 \rho(x, t), \tag{6.8}$$

where ρ_r determines the (fixed) distribution of radicals, and is normalized to have size 1, and M is a parameter used to scale the mass of the radicals. For physical reasons, ρ_r should be non-negative(which will motivate work in Section 6.3.2). However, a negative ρ_r can be attributed to negative advertising in some applications.

6.1.2 Motivation for Opinion Dynamics PDE-Constrained Optimization Problems

While there are several studies on the phase transitions caused by noise in opinion dynamics models, the introduction of radicals give rise to several questions about their influence on phase transitions. Recent studies in [96] present interesting numerical results on the effects of fixed radical opinions and of boundary conditions on the phase transitions. Other authors have considered control of the discrete HK model [77] and optimal control of convergence time for consensus [148]. Optimal control of radicals therefore follows naturally as an extension of these works. With the success of our numerical algorithms (as shown in Chapter 5) on optimization problems constrained by similar DDFT equations with non-local integral terms, we are motivated to apply related numerical methods to solve optimization problems constrained by the opinion dynamics Fokker–Planck PDE (6.8) with respect to the opinions ρ as the state variable and ρ_r as the control variable. One advantage of obtaining optimized radical distributions by solving a PDE-constrained optimization problem is that we can specify a desired distribution for the opinion state to reach at all times. We are also able to investigate the following questions:

1. How does the choice of boundary conditions affect the optimal distribution of radicals?
2. How does the optimal distribution of radicals behave?
3. Does the finite difference discretization outperform the pseudospectral method when non-smooth constraints are applied?
4. Does an Active-Set strategy (see Sections 3.5 and 6.3.2) suitably converge for an optimal control problem with non-local and nonlinear parabolic PDEs as constraints? Note that they have historically been applied to elliptic problems.

In the next section, we formulate a PDE-constrained optimization problem for opinion dynamics and derive the first-order optimality system using the continuous Lagrange method.

6.2 Opinion Dynamics PDE-Constrained Optimization Problems

We are interested in minimizing some cost functional subject to the opinion dynamics PDE in (6.8) so as to study optimized radical distributions ρ_r that can drive our agent density ρ to a target distribution $\widehat{\rho}$. We adopt the cost functional presented in Chapter 5 which minimizes the 'distance' (L^2-norm of the difference in variables) between the state and target variables and the norm of the control multiplied by a regularization parameter. We present the following problem written over the space–time domain $Q = \Omega \times (0, T)$ in more than one spatial variable,

$$\begin{aligned} \min_{\rho,\rho_r} \quad & \mathcal{J}(\rho,\rho_r) \coloneqq \frac{1}{2}\int_0^T \int_\Omega (\rho-\widehat{\rho})^2 \, dxdt + \frac{\beta}{2}\int_0^T \int_\Omega \rho_r^2 \, dxdt \\ \text{s.t} \quad & \partial_t \rho - \frac{\sigma^2}{2}\nabla^2\rho - \nabla_{\mathbf{x}} \cdot \mathcal{I}(\rho,\rho_r) = 0 \quad \text{in } Q, \\ & \rho = \rho_0(\mathbf{x}) \quad \text{at } t = 0, \end{aligned} \tag{6.9}$$

where

$$\mathcal{I}(\rho,\rho_r) = \rho(\mathbf{x},t)\int_\Omega (\mathbf{1}_{\|\mathbf{x}-\mathbf{y}\|\leq R})(\mathbf{x}-\mathbf{y})(\rho(\mathbf{y},t)+\rho_r(\mathbf{y},t))\, dy.$$

Here, $\Omega \subset \mathbb{R}^d$, with boundary $\partial\Omega$, and T prescribes a final time up to which the process is modelled. The scalar functions $\rho(\mathbf{x},t)$ and $\rho_r(\mathbf{x},t)$ are the *state* ('normal' opinions) and *control* (radical opinions) variables respectively, and $\widehat{\rho}(\mathbf{x},t)$ is the desired state. Also, $\beta > 0$ remains the regularization parameter. The vector term $\mathbf{x}-\mathbf{y}$ in the non-local integral term corresponds to the kernel $\mathbf{K}(\mathbf{x},\mathbf{y})$ seen in previous examples in Chapter 5.

We consider two boundary conditions imposed on ρ, the 'no-flux type' boundary condition:

$$\left(\frac{\sigma^2}{2}\nabla\rho + \mathcal{I}(\rho,\rho_r)\right)\cdot\mathbf{n} = 0 \quad \text{on } \partial Q, \tag{6.10}$$

and the case of periodic boundary conditions in one-dimension on $\Omega = [a, b]$:

$$\rho(a,t) = \rho(b,t), \tag{6.11}$$

$$\left(\frac{\sigma^2}{2}\nabla\rho + \mathcal{I}(\rho,\rho_r)\right)\cdot n\Big|_{x=a} = -\left(\frac{\sigma^2}{2}\nabla\rho + \mathcal{I}(\rho,\rho_r)\right)\cdot n\Big|_{x=b}, \tag{6.12}$$

where $n \to \mathbf{n}$ is the normal vector at the boundary, and the vectors $\mathbf{x}, \mathbf{y}$ are replaced with the scalars x, y respectively for the 1D case. Both periodic conditions (6.11) and (6.12) are trivial consequences of the imposition of periodicity on ρ and ρ_r, and the flux condition (6.12) is necessary to enforce periodicity numerically.

We obtain continuous first optimality conditions using the *optimize-then-discretize* approach. The workings are similar to the examples in Chapter 5, but we pay particular attention to the non-local term here as it is over a bounded subdomain and not the whole domain.

In [50], existence of solutions, and non-uniqueness of steady states are discussed, as well as the existence of phase transitions for a more general forward McKean–Vlasov equation including the noisy Hegselmann–Krausse model for opinion dynamics on a torus. In [5], the authors show the existence of mean field optimal controls for a similar optimization problem to (6.9), but with the Wasserstein norm, both in the stochastic and deterministic settings, and with no-flux boundary conditions. Hence, the opinion dynamics optimization problem (and others like it) have very rich dynamics, and questions such as existence and uniqueness of solutions are important and interesting. These topics are beyond the scope of the thesis, but would form valuable avenues for future research.

6.2.1 First-Order Optimality Conditions for Periodic Boundary Conditions

We consider the optimization problem (6.9) with 1D periodic boundary conditions (6.11). We introduce three Lagrange multipliers q_1, q_2 and q_3 corresponding to the interior of the domain, first, and second boundary conditions respectively. We note that q_2 and q_3 enforce the periodic boundary conditions prescribed, and hence only depend on time. We may then write our Lagrangian operator as:

$$\begin{aligned}
\mathcal{L}(\rho,\rho_r,q_1,q_2,q_3) = {} & \frac{1}{2}\int_0^T\int_\Omega (\rho-\widehat{\rho})^2\,dxdt + \frac{\beta}{2}\int_0^T\int_\Omega \rho_r^2\,dxdt \\
& - \int_0^T\int_\Omega \left(\partial_t\rho - \frac{\sigma^2}{2}\nabla^2\rho - \nabla_x\cdot\left[\rho(x,t)\int_\Omega (\mathbf{1}_{|x-y|\le R})(x-y)\rho_r(y,t)\,dy\right]\right) q_1 \\
& \quad - \nabla_x\cdot\left[\rho(x,t)\int_\Omega (\mathbf{1}_{|x-y|\le R})(x-y)\rho(y,t)\,dy\right] q_1\,dxdt \\
& - \int_0^T (\rho(b,t)-\rho(a,t))q_2\,dt \\
& - \int_0^T q_3\left(\frac{\sigma^2}{2}\nabla\rho + \rho(x,t)\int_\Omega (\mathbf{1}_{|x-y|\le R})(x-y)(\rho(y,t)+\rho_r(y,t))\,dy\right)\cdot n\Big|_{x=b} \\
& \quad + q_3\left(\frac{\sigma^2}{2}\nabla\rho + \rho(x,t)\int_\Omega (\mathbf{1}_{|x-y|\le R})(x-y)(\rho(y,t)+\rho_r(y,t))\,dy\right)\cdot n\Big|_{x=a}\,dt.
\end{aligned}$$

Here also, the optimal pair $(\bar{\rho},\bar{\rho_r})$ should satisfy the KKT conditions:

$$\begin{aligned}
D_\rho\mathcal{L}(\bar{\rho},\bar{\rho_r},q_1,q_2,q_3)h = 0 \quad & \forall h \in L^2(0,T;H^1(\Omega)), \\
D_{q_1,q_2,q_3}\mathcal{L}(\bar{\rho},\bar{\rho_r},q_1,q_2,q_3)h = 0 \quad & \forall h \in L^2(0,T;H^1(\Omega)), \\
D_{\rho_r}\mathcal{L}(\bar{\rho},\bar{\rho_r},q_1,q_2,q_3)h = 0 \quad & \forall h \in L^2(0,T;\Omega).
\end{aligned}$$

The KKT condition with respect to (q_1, q_2, q_3) in the direction h gives back the forward PDE, i.e.,

$$\begin{aligned} D_{q_1,q_2,q_3}\mathcal{L}(\bar{\rho}, \bar{\rho_r}, q_1, q_2, q_3)h = &- \int_0^T \int_\Omega \left(\partial_t \bar{\rho} - \frac{\sigma^2}{2}\nabla^2 \bar{\rho} - \nabla_x \cdot \mathcal{I}(\bar{\rho}, \bar{\rho}_r)\right) h \, dxdt \\ &- \int_0^T (\bar{\rho}(b,t) - \bar{\rho}(a,t))h \, dt \\ &- \int_0^T h\left(\frac{\sigma^2}{2}\nabla\bar{\rho} + \mathcal{I}(\bar{\rho}, \bar{\rho_r})\right) \cdot n\Big|_{x=b} \\ &+ h\left(\frac{\sigma^2}{2}\nabla\bar{\rho} + \mathcal{I}(\bar{\rho}, \bar{\rho_r})\right) \cdot n\Big|_{x=a} dt \\ = &\, 0. \end{aligned}$$

This implies that

$$\begin{aligned} \partial_t \bar{\rho} - \frac{\sigma^2}{2}\nabla^2\bar{\rho} - \nabla_x \cdot \mathcal{I}(\bar{\rho}, \bar{\rho_r}) = 0 \quad &\text{in } Q, \\ \bar{\rho} = \rho_0(x) \quad &\text{at } t = 0, \\ \bar{\rho}(a,t) = \bar{\rho}(b,t), \\ \left(\frac{\sigma^2}{2}\nabla\bar{\rho} + \mathcal{I}(\bar{\rho}, \bar{\rho_r})\right) \cdot n\Big|_{x=a} = -\left(\frac{\sigma^2}{2}\nabla\bar{\rho} + \mathcal{I}(\bar{\rho}, \bar{\rho_r})\right) \cdot n\Big|_{x=b}&. \end{aligned}$$

We now write the Fréchet derivate with respect to ρ in the direction h:

$$\begin{aligned} D_\rho\mathcal{L}(\rho, \rho_r, q_1, q_2, q_3)h = &\int_0^T \int_\Omega (\rho - \widehat{\rho})h \, dxdt \\ &- \int_0^T \int_\Omega \left(\partial_t h - \frac{\sigma^2}{2}\nabla^2 h - \nabla_x \cdot \left[h(x,t)\int_\Omega (\mathbf{1}_{|x-y|\le R})(x-y)\rho_r(y,t)\,dy\right]\right) q_1 \\ &\quad - \left(\nabla_x \cdot \left[\int_\Omega (\mathbf{1}_{|x-y|\le R})(x-y)(\rho(x,t)h(y,t) + h(x,t)\rho(y,t))\,dy\right]\right) q_1 \, dxdt \\ &- \int_0^T (h(b,t) - h(a,t))q_2 \, dt \\ &- \int_0^T q_3 \left(\frac{\sigma^2}{2}\nabla h + h\int_\Omega (\mathbf{1}_{|x-y|\le R})(x-y)\rho_r(y)\,dy\right) \cdot n\Big|_{x=b} \\ &\quad + q_3 \left(\int_\Omega (\mathbf{1}_{|x-y|\le R})(x-y)(\rho(x,t)h(y,t) + h(x,t)\rho(y,t))\,dy\right) \cdot n\Big|_{x=b} \\ &\quad + q_3 \left(\frac{\sigma^2}{2}\nabla h + h\int_\Omega (\mathbf{1}_{|x-y|\le R})(x-y)\rho_r(y,t)\,dy\right) \cdot n\Big|_{x=a} \\ &\quad + q_3 \left(\int_\Omega (\mathbf{1}_{|x-y|\le R})(x-y)(\rho(x,t)h(y,t) + h(x,t)\rho(y,t))\,dy\right) \cdot n\Big|_{x=a} dt \end{aligned}$$

After applying the vector calculus identity (3.6) and the Divergence Theorem, we obtain

$$\begin{aligned} D_\rho\mathcal{L}(\rho, \rho_r, q_1, q_2, q_3) = &\int_0^T \int_\Omega (\rho - \widehat{\rho})h \, dxdt \\ &- \int_0^T \int_\Omega \left(-\partial_t q_1 - \frac{\sigma^2}{2}\nabla^2 q_1 + \left[\int_\Omega (\mathbf{1}_{|x-y|\le R})(x-y)\rho_r(y,t)\,dy\right] \cdot \nabla q_1\right) h \\ &\quad + \left(\int_\Omega (\mathbf{1}_{|x-y|\le R})(x-y)(\rho(x,t)h(y,t) + h(x,t)\rho(y,t))\,dy\right) \cdot \nabla_x q_1(x,t) \, dxdt \\ &- \int_\Omega (q_1(x,T)h(x,T) - q_1(x,0)h(x,0)) \, dx \end{aligned}$$

$$
\begin{aligned}
&- \int_0^T \left(\frac{\sigma^2}{2} h \nabla q_1 - \frac{\sigma^2}{2} q_1 \nabla h - h q_1 \int_\Omega (\mathbf{1}_{|x-y|\leq R})(x-y)\rho_r(y,t)\,dy \right) \cdot n \Big|_{x=b} \\
&\quad + \left(q_1 \int_\Omega (\mathbf{1}_{|x-y|\leq R})(x-y)(\rho(x,t)h(y,t) + h(x,t), \rho(y,t))\,dy \right) \cdot n \Big|_{x=b} \\
&\quad + \left(\frac{\sigma^2}{2} h \nabla q_1 - \frac{\sigma^2}{2} q_1 \nabla h - h q_1 \int_\Omega (\mathbf{1}_{|x-y|\leq R})(x-y)\rho_r(y,t)\,dy \right) \cdot n \Big|_{x=a} \\
&\quad + \left(q_1 \int_\Omega (\mathbf{1}_{|x-y|\leq R})(x-y)(\rho(x,t)h(y,t) + h(x,t), \rho(y,t))\,dy \right) \cdot n \Big|_{x=a} dt \\
&- \int_0^T (h(b,t) - h(a,t)) q_2 \, dt \\
&- \int_0^T q_3 \left(\frac{\sigma^2}{2} \nabla h + h \int_\Omega (\mathbf{1}_{|x-y|\leq R})(x-y)\rho_r(y)\,dy \right) \cdot n \Big|_{x=b} \\
&\quad + q_3 \left(\int_\Omega (\mathbf{1}_{|x-y|\leq R})(x-y)(\rho(x,t)h(y,t) + h(x,t)\rho(y,t))\,dy \right) \cdot n \Big|_{x=b} \\
&\quad + q_3 \left(\frac{\sigma^2}{2} \nabla h + h \int_\Omega (\mathbf{1}_{|x-y|\leq R})(x-y)\rho_r(y,t)\,dy \right) \cdot n \Big|_{x=a} \\
&\quad + q_3 \left(\int_\Omega (\mathbf{1}_{|x-y|\leq R})(x-y)(\rho(x,t)h(y,t) + h(x,t)\rho(y,t))\,dy \right) \cdot n \Big|_{x=a} dt.
\end{aligned}
$$

We then follow the same workings as for the optimal flow control problem (5.1) in Chapter 5 to make h the subject in the non-local integral term. We swap the order of integrals with respect to x and y and perform a change of variables $y = x$. We do not make h the subject in the boundary terms as we anticipate from previous workings in Chapter 5, that those terms evaluate to zero for the choices of h made. We then get that

$$
\begin{aligned}
D_\rho \mathcal{L}(\rho, \rho_r, q_1, q_2, q_3) = &\int_0^T \int_\Omega (\rho - \widehat{\rho}) h \, dx dt \\
&- \int_0^T \int_\Omega \left(-\partial_t q_1 - \frac{\sigma^2}{2} \nabla^2 q_1 + \left[\int_\Omega (\mathbf{1}_{|x-y|\leq R})(x-y)\rho_r(y,t)\,dy \right] \cdot \nabla q_1 \right) h \\
&\quad - h \left(\int_\Omega (\mathbf{1}_{|x-y|\leq R})(x-y)\rho(y,t) \cdot \nabla_y q_1(y,t)\,dy \right) \\
&\quad + h \left(\int_\Omega (\mathbf{1}_{|x-y|\leq R})(x-y)\rho(y,t)\,dy \right) \cdot \nabla_x q_1(x,t)\,dx dt \\
&- \int_\Omega (q_1(x,T)h(x,T) - q_1(x,0)h(x,0))\ dx \\
&- \int_0^T \left(\frac{\sigma^2}{2} h \nabla q_1 - \frac{\sigma^2}{2} q_1 \nabla h - h q_1 \int_\Omega (\mathbf{1}_{|x-y|\leq R})(x-y)\rho_r(y,t)\,dy \right) \cdot n \Big|_{x=b} \\
&\quad + \left(q_1 \int_\Omega (\mathbf{1}_{|x-y|\leq R})(x-y)(\rho(x,t)h(y,t) + h(x,t)\rho(y,t))\,dy \right) \cdot n \Big|_{x=b} \\
&\quad + \left(\frac{\sigma^2}{2} h \nabla q_1 - \frac{\sigma^2}{2} q_1 \nabla h - h q_1 \int_\Omega (\mathbf{1}_{|x-y|\leq R})(x-y)\rho_r(y,t)\,dy \right) \cdot n \Big|_{x=a} \\
&\quad + \left(q_1 \int_\Omega (\mathbf{1}_{|x-y|\leq R})(x-y)(\rho(x,t)h(y,t) + h(x,t)\rho(y,t))\,dy \right) \cdot n \Big|_{x=a} dt \\
&- \int_0^T (h(b,t) - h(a,t)) q_2 \, dt \\
&- \int_0^T q_3 \left(\frac{\sigma^2}{2} \nabla h + h \int_\Omega (\mathbf{1}_{|x-y|\leq R})(x-y)\rho_r(y)\,dy \right) \cdot n \Big|_{x=b} \\
&\quad + q_3 \left(\int_\Omega (\mathbf{1}_{|x-y|\leq R})(x-y)(\rho(x,t)h(y,t) + h(x,t)\rho(y,t))\,dy \right) \cdot n \Big|_{x=b}
\end{aligned}
$$

$$+ q_3 \left(\frac{\sigma^2}{2} \nabla h + h \int_\Omega (\mathbf{1}_{|x-y|\leq R})(x-y)\rho_r(y,t)\,dy \right) \cdot n \Big|_{x=a}$$
$$+ q_3 \left(\int_\Omega (\mathbf{1}_{|x-y|\leq R})(x-y)(\rho(x,t)h(y,t) + h(x,t)\rho(y,t))\,dy \right) \cdot n \Big|_{x=a} dt.$$

We similarly write the Fréchet derivate with respect to ρ_r in the direction h as

$$\begin{aligned} D_{\rho_r}\mathcal{L}(\rho,\rho_r,q_1,q_2,q_3)h = &\int_0^T \int_\Omega \beta\rho_r h\,dxdt \\ &+ \int_0^T \int_\Omega \nabla_x \cdot \left[\rho \int_\Omega (\mathbf{1}_{|x-y|\leq R})(x-y)h(y,t)\,dy \right] q_1\,dxdt \\ &- \int_0^T q_3 \left(\rho(x,t) \int_\Omega (\mathbf{1}_{|x-y|\leq R})(x-y)h(y,t)\,dy \right) \cdot n \Big|_{x=b} \\ &\quad + q_3 \left(\rho(x,t) \int_\Omega (\mathbf{1}_{|x-y|\leq R})(x-y)h(y,t)\,dy \right) \cdot n \Big|_{x=a} dt, \end{aligned}$$

and make h the subject in the second term to obtain

$$\begin{aligned} D_{\rho_r}\mathcal{L}(\rho,\rho_r,q_1,q_2,q_3) = &\int_0^T \int_\Omega \beta\rho_r h\,dxdt \\ &- \int_0^T \int_\Omega h(x,t) \left[\int_\Omega -\rho(y,t)(\mathbf{1}_{|x-y|\leq R})(x-y)\cdot\nabla_y q_1(y,t)\,dy \right] dxdt \\ &+ \int_0^T \int_{\partial\Omega} q_1(x,t) \left[\rho \int_\Omega (\mathbf{1}_{|x-y|\leq R})(x-y)h(y,t)\,dy \right] \cdot n\,dsdt \\ &- \int_0^T q_3 \left(\rho(x,t) \int_\Omega (\mathbf{1}_{|x-y|\leq R})(x-y)h(y,t)\,dy \right) \cdot n \Big|_{x=b} \\ &\quad + q_3 \left(\rho(x,t) \int_\Omega (\mathbf{1}_{|x-y|\leq R})(x-y)h(y,t)\,dy \right) \cdot n \Big|_{x=a} dt. \end{aligned}$$

As stated earlier, the optimal solution should satisfy

$$\begin{aligned} D_\rho \mathcal{L}(\bar\rho,\bar\rho_r,q_1,q_2,q_3)h = 0 \quad \forall h \in L^2(0,T;H^1(\Omega)), \\ D_{\rho_r} \mathcal{L}(\bar\rho,\bar\rho_r,q_1,q_2,q_3)h = 0 \quad \forall h \in L^2(0,T;\Omega). \end{aligned}$$

In particular, if we choose $h \in C_0^\infty(Q)$ such that $h = \dfrac{\partial h}{\partial n} = 0$ on ∂Q and $h(x,0) = h(x,T) = 0$, then the KKT conditions by the Fundamental Lemma of Calculus of Variations reduce to

$$\partial_t q_1 + \frac{\sigma^2}{2}\nabla^2 q_1 - \nabla q_1 \cdot \left(\int_\Omega (\mathbf{1}_{|x-y|\leq R})(x-y)\bar\rho_r(y,t)\,dy \right) + \int_\Omega (\mathbf{1}_{|x-y|\leq R})(x-y)\bar\rho(y,t)\cdot\nabla_y q_1(y,t)\,dy$$
$$- \nabla q_1 \cdot \left(\int_\Omega (\mathbf{1}_{|x-y|\leq R})\bar\rho(y,t)\,dy \right) + \bar\rho - \widehat{\rho} = 0,$$

which describes the *adjoint* PDE on the interior of the domain and

$$\beta\bar\rho_r + \int_\Omega (\mathbf{1}_{|x-y|\leq R})(x-y)\bar\rho(y,t)\cdot\nabla_y q_1(y,t)\,dy = 0,$$

which is the *gradient* equation.

Now, to obtain the final time condition for the adjoint variable we drop the condition $h(x,T) = 0$ to obtain

$$\int_\Omega q_1(x,T)h(x,T)\,dx = 0$$

which by the Fundamental Lemma of Calculus of Variations implies

$$q_1(x,T) = 0.$$

If we now drop the condition $\frac{\partial h}{\partial n} = 0$ on the boundary and choose $\frac{\partial h}{\partial n}\big|_{x=b} = 0$, $\frac{\partial h}{\partial n}\big|_{x=a} = 0$ in turn, we obtain that $q_3(b,t) = q_1(b,t)$ and $q_3(a,t) = q_1(a,t)$ which must hold also for periodicity reasons. We also note that

$$q_1(a,t) = q_1(b,t)$$

follows from the periodicity of ρ, and ρ_r. We now drop the condition $h = 0$ on the boundary and choose h such that $h(a,t) = h(b,t)$ and $\left(\int_\Omega (\mathbf{1}_{|x-y|\le R})(x-y)h(y,t)\,dy\right)\cdot n\Big|_{x=b} = -\left(\int_\Omega (\mathbf{1}_{|x-y|\le R})(x-y)h(y,t)\,dy\right)\cdot n\Big|_{x=a}$ to obtain:

$$\int_0^T h(a,t)\left[\frac{\partial q_1}{\partial n}(a,t) + \frac{\partial q_1}{\partial n}(b,t)\right]\,dt = 0,$$

which implies

$$\frac{\partial q_1}{\partial n}(a,t) = -\frac{\partial q_1}{\partial n}(b,t).$$

The remaining variations of h give the relationships between q_1, q_2, and q_3. We then rename q_1 as q and have the optimality system for problem (6.9) with periodic boundary conditions (6.11) as:

$$\begin{aligned}
&\partial_t\bar\rho - \frac{\sigma^2}{2}\nabla^2\bar\rho - \nabla_x\cdot\mathcal{I}(\bar\rho,\bar\rho_r) = 0 \quad \text{in } Q,\\
&\bar\rho = \rho_0(x) \quad \text{at } t=0,\\
&\bar\rho(a,t) = \bar\rho(b,t),\\
&\left(\frac{\sigma^2}{2}\nabla\bar\rho + \mathcal{I}(\bar\rho,\bar\rho_r)\right)\cdot n\Big|_{x=a} = -\left(\frac{\sigma^2}{2}\nabla\bar\rho + \mathcal{I}(\bar\rho,\bar\rho_r)\right)\cdot n\Big|_{x=b},
\end{aligned}$$

$$\begin{aligned}
&\partial_t q_1 + \frac{\sigma^2}{2}\nabla^2 q_1 - \nabla q_1\cdot\left(\int_\Omega (\mathbf{1}_{|x-y|\le R})(x-y)\bar\rho_r(y,t)\,dy\right) + \bar\rho - \widehat\rho\\
&+ \int_\Omega (\mathbf{1}_{|x-y|\le R})(x-y)\bar\rho(y,t)\cdot\nabla_y q_1(y,t)\,dy\\
&- \nabla q_1\cdot\left(\int_\Omega (\mathbf{1}_{|x-y|\le R})\bar\rho(y,t)\,dy\right) = 0 \quad \text{in } Q,\\
&q = 0 \quad \text{at } t = T,\\
&q(a,t) = q(b,t),\\
&\frac{\partial q}{\partial n}(a,t) = -\frac{\partial q}{\partial n}(b,t),
\end{aligned}$$

$$\beta\bar\rho_r + \int_\Omega (\mathbf{1}_{|x-y|\le R})(x-y)\bar\rho(y,t)\cdot\nabla_y q_1(y,t)\,dy = 0.$$

Having derived the optimality system for the opinion dynamics PDE-Constrained optimization problem with periodic boundary conditions, we tackle no-flux boundary conditions next.

6.2.2 First-Order Optimality Conditions for No-Flux Boundary Conditions

We also consider the problem (6.9) but with no-flux boundary conditions (6.10) in a general dimension d. The optimization problem is written as:

$$\begin{aligned}
\min_{\rho,\rho_r} \quad & \frac{1}{2}\int_0^T \int_\Omega (\rho - \widehat{\rho})^2 \, dxdt + \frac{\beta}{2}\int_0^T \int_\Omega \rho_r^2 \, dxdt \qquad (6.13)\\
\text{s.t} \quad & \partial_t \rho = \frac{\sigma^2}{2}\nabla^2 \rho + \nabla_{\mathbf{x}} \cdot I(\rho, \rho_r) \quad \text{in } Q,\\
& \rho = \rho_0(\mathbf{x}) \quad \text{at } t = 0,\\
& \left(\frac{\sigma^2}{2}\nabla\rho + \rho \int_\Omega (\mathbf{1}_{\|\mathbf{x}-\mathbf{y}\|\le R})(\mathbf{x}-\mathbf{y})(\rho(\mathbf{y},t) + \rho_r(\mathbf{y},t))\, dy\right)\cdot \mathbf{n} = 0 \quad \text{on } \partial Q.
\end{aligned}$$

Following the same workings described in Chapter 5 for flow control problem with no flux boundary conditions and the treatment of the non-local terms from the opinion dynamics PDE-Constrained optimization problem with periodic boundary conditions above, we obtain the optimality system:

$$\begin{aligned}
& \partial_t \bar{\rho} - \frac{\sigma^2}{2}\nabla^2 \bar{\rho} - \nabla_{\mathbf{x}} \cdot I(\bar{\rho}, \bar{\rho}_r) = 0 \quad \text{in } \partial Q,\\
& \bar{\rho} = \rho_0(\mathbf{x}) \quad \text{at } t = 0,\\
& \left(\frac{\sigma^2}{2}\nabla\bar{\rho} + I(\bar{\rho}, \bar{\rho}_r)\right)\cdot \mathbf{n} = 0 \quad \text{on } \partial Q,
\end{aligned}$$

$$\begin{aligned}
& \partial_t q + \frac{\sigma^2}{2}\nabla^2 q - \nabla q \cdot \left(\int_\Omega (\mathbf{1}_{\|\mathbf{x}-\mathbf{y}\|\le R})(\mathbf{x}-\mathbf{y})\bar{\rho}_r(\mathbf{y},t)\, dy\right) + \bar{\rho} - \widehat{\rho}\\
& + \int_\Omega (\mathbf{1}_{\|\mathbf{x}-\mathbf{y}\|\le R})(\mathbf{x}-\mathbf{y})\bar{\rho}(\mathbf{y},t)\cdot \nabla_{\mathbf{y}} q(\mathbf{y},t)\, dy\\
& - \nabla_{\mathbf{x}} q \cdot \left(\int_\Omega (\mathbf{1}_{\|\mathbf{x}-\mathbf{y}\|\le R})(\mathbf{x}-\mathbf{y})\bar{\rho}(\mathbf{y},t)\, dy\right) = 0 \quad \text{in } Q,\\
& q = 0 \quad \text{at } t = T,\\
& \nabla q \cdot \mathbf{n} = 0 \quad \text{on} \quad \partial Q,
\end{aligned}$$

$$\beta\bar{\rho}_r + \int_\Omega (\mathbf{1}_{\|\mathbf{x}-\mathbf{y}\|\le R})(\mathbf{x}-\mathbf{y})\bar{\rho}(\mathbf{y},t)\cdot \nabla_{\mathbf{y}} q(\mathbf{y},t)\, dy = 0.$$

We have now derived the optimality systems for the opinion dynamics optimization problems we are interested. In the following section we will discuss the introduction of box constraints into the optimization problem.

6.3 An Active Set-Fixed-Point Algorithm for Problems with Additional Control Constraints

In opinion dynamics, one typically is interested in the interactions of a population of humans. As such, there is an underlying assumption that the density of opinions should remain non-negative. For this assumption to be satisfied, we are required to impose non-negativity constraints on the optimized radical distribution. The inclusion of bound constraints on the control poses a significant additional challenge for optimization methods. Ideally, continuous control constraints should be applied, but the lack of literature to tackle such cases make it a good candidate for future work. Instead, we impose pointwise constraints that are equally capable of achieving the non-negativity condition if computations are done on a very fine grid or good interpolation techniques are implemented. It is important to note that the non-smoothness arising from pointwise

constraints is a disadvantage for the pseudospectral discretization. Hence, we alternatively use the finite difference discretization that does not assume smoothness of solutions.

6.3.1 First Order Optimality Conditions for Opinion Dynamics Optimization Problem with Additional Bound Constraints

We consider the problem (6.9) with no-flux boundary conditions (6.10) imposed and additional bound constraints on the control:

$$\begin{aligned}
\min_{\rho,\rho_r} \quad & \mathcal{J}(\rho,\rho_r) := \frac{1}{2}\int_0^T\int_\Omega (\rho-\widehat{\rho})^2\,dxdt + \frac{\beta}{2}\int_0^T\int_\Omega \rho_r^2\,dxdt \qquad (6.14)\\
\text{s.t} \quad & \partial_t\rho - \frac{\sigma^2}{2}\nabla^2\rho - \nabla_{\mathbf{x}}\cdot\mathcal{I}(\rho,\rho_r) = 0 \quad \text{in } Q,\\
& \rho = \rho_0(\mathbf{x}) \quad \text{at } t=0,\\
& \left(\frac{\sigma^2}{2}\nabla\rho + I(\rho,\rho_r)\right)\cdot\mathbf{n} = 0 \quad \text{on } \partial Q,\\
& \rho_a \le \rho_r \le \rho_b \quad a.e. \text{ in } \Omega \quad \text{(bound constraints)}\ .
\end{aligned}$$

We define $\rho_{ad} := \{\rho_r : \rho_a \le \rho_r \le \rho_b \quad a.e. \text{ in } \Omega\},\ \rho_a, \rho_b \in \mathbb{R}$ as the set of all admissible functions. Following the working on the Poisson control problem in Section 3.5, the first order optimality system is obtained as

$$\begin{aligned}
&\partial_t\bar{\rho} - \frac{\sigma^2}{2}\nabla^2\bar{\rho} - \nabla_{\mathbf{x}}\cdot I(\bar{\rho},\bar{\rho_r}) = 0 \quad \text{in } \partial Q,\\
&\bar{\rho} = \rho_0(\mathbf{x}) \quad \text{at } t=0,\\
&\left(\frac{\sigma^2}{2}\nabla\bar{\rho} + I(\bar{\rho},\bar{\rho_r})\right)\cdot\mathbf{n} = 0 \quad \text{on } \partial Q,
\end{aligned}$$

$$\begin{aligned}
&\partial_t q + \frac{\sigma^2}{2}\nabla^2 q - \nabla q\cdot\left(\int_\Omega (\mathbf{1}_{\|\mathbf{x}-\mathbf{y}\|\le R})(\mathbf{x}-\mathbf{y})\bar{\rho}_r(\mathbf{y},t)\,dy\right) + \bar{\rho} - \widehat{\rho}\\
&+ \int_\Omega (\mathbf{1}_{\|\mathbf{x}-\mathbf{y}\|\le R})(\mathbf{x}-\mathbf{y})\bar{\rho}(\mathbf{y},t)\cdot\nabla_{\mathbf{y}} q(\mathbf{y},t)\,dy\\
&- \nabla_{\mathbf{x}} q\cdot\left(\int_\Omega (\mathbf{1}_{\|\mathbf{x}-\mathbf{y}\|\le R})(\mathbf{x}-\mathbf{y})\bar{\rho}(\mathbf{y},t)\,dy\right) = 0 \quad \text{in } Q,\\
&q = 0 \quad \text{at } t=T,\\
&\nabla q\cdot\mathbf{n} = 0 \quad \text{on} \quad \partial Q
\end{aligned}$$

$$(\rho_r - \bar{\rho_r})\left(\beta\bar{\rho_r} + \int_\Omega (\mathbf{1}_{\|\mathbf{x}-\mathbf{y}\|\le R})(\mathbf{x}-\mathbf{y})\bar{\rho}(\mathbf{y},t)\cdot\nabla_{\mathbf{y}} q(\mathbf{y},t)\,dy\right) \ge 0$$

where the final inequality follows from the variational inequality

$$F'(\bar{\rho_r})(\rho_r - \bar{\rho_r}) \ge 0 \quad \forall \rho_r \in \rho_{ad},$$

discussed in Section 3.5.

6.3.2 The Primal-Dual Active Set Strategy

We present an Active-Set strategy to tackle (6.14) in 1D, following work done in [70,126,147].We introduce a Lagrange multiplier associated with the box constraints following the the Poisson control example illustrated in Section 3.5 :

$$\mu := \beta\bar{\rho_r} + \int_\Omega (\mathbf{1}_{\|\mathbf{x}-\mathbf{y}\|\le R})(\mathbf{x}-\mathbf{y})\bar{\rho}(\mathbf{y},t)\cdot\nabla_{\mathbf{y}} q(\mathbf{y},t)\,dy. \qquad (6.15)$$

The optimal control is then expressed as:

$$\bar{\rho_r} = \begin{cases} = \rho_b & \mu < 0 \\ \in \rho_{ad} & \mu = 0 \\ = \rho_a & \mu > 0 \end{cases}$$

The quantity $\rho_r - \mu$ is an indicator of whether a constraint is active or not and forms the basis of constructing active sets. The active sets are defined for example, on the discretized 1D spatial grid $\{x_1, x_2, \ldots, x_N\}$ as

$$A_+ = \{i \in \{1, 2, \ldots, N\} : (\rho_r - \mu)_i > (\rho_b)_i\}, \tag{6.16}$$
$$A_- = \{i \in \{1, 2, \ldots, N\} : (\rho_r - \mu)_i < (\rho_a)_i\}, \tag{6.17}$$
$$A_I = \{i \in \{1, 2, \ldots, N\}\} \setminus (A_+ \cup A_-), \tag{6.18}$$

where N, is the number of spatial points and $(\rho_r - \mu)_i$, $(\rho_b)_i$ and $(\rho_a)_i$ are the value of $(\rho_r - \mu)_i$, (ρ) and (ρ_a) at the point x_i, respectively.

The control $\rho_r^{(k)}$ is introduced as the approximation to the solution $\bar{\rho_r}$ at step k of the active set algorithm. This notation is also used for the state and adjoint variables. The sets $A_+^{(k)}, A_-^{(k)}, A_I^{(k)}$ are defined using $\rho_r^{(k-1)}$ and $\mu^{(k-1)}$ in the definitions 6.16, 6.17, and 6.18. The following conditions [32] have to hold in each step of the iterative procedure:

$$\partial_t \rho^{(k)} = \frac{\sigma^2}{2}\nabla^2 \rho^{(k)} + \nabla_{\mathbf{x}} \cdot \left[\rho^{(k)} \int_\Omega (\mathbf{1}_{\|\mathbf{x}-\mathbf{y}\| \le R})(\mathbf{x}-\mathbf{y})(\rho^{(k)}(\mathbf{y},t) + \rho_r^{(k)}(\mathbf{y},t))\, dy\right] \quad \text{in } Q, \tag{6.19}$$
$$\rho^{(k)} = \rho_0(\mathbf{x}) \quad \text{at } t = 0,$$
$$\left(\frac{\sigma^2}{2}\nabla \rho^{(k)} + \rho^{(k)} \int_\Omega (\mathbf{1}_{\|\mathbf{x}-\mathbf{y}\| \le R})(\mathbf{x}-\mathbf{y})(\rho^{(k)}(\mathbf{y},t) + \rho_r^{(k)}(\mathbf{y},t))\, dy\right) \cdot \mathbf{n} = 0 \quad \text{on } \partial Q,$$

$$\partial_t q^{(k)} = -\frac{\sigma^2}{2}\nabla^2 q^{(k)} + \nabla q^{(k)} \cdot \left(\int_\Omega (\mathbf{1}_{\|\mathbf{x}-\mathbf{y}\| \le R})(\mathbf{x}-\mathbf{y})\rho_r^{(k)}(\mathbf{y},t)\, dy\right) \tag{6.20}$$
$$- \int_\Omega (\mathbf{1}_{\|\mathbf{x}-\mathbf{y}\| \le R})(\mathbf{x}-\mathbf{y})\rho^{(k)}(\mathbf{y},t) \cdot \nabla_{\mathbf{y}} q^{(k)}(\mathbf{y},t)\, dy,$$
$$+ \nabla_{\mathbf{x}} q^{(k)} \cdot \left(\int_\Omega (\mathbf{1}_{\|\mathbf{x}-\mathbf{y}\| \le R})(\mathbf{x}-\mathbf{y})\rho^{(k)}(\mathbf{y},t)\, dy\right) - \rho^{(k)} + \widehat{\rho} \quad \text{in } Q, \tag{6.21}$$
$$q^{(k)} = 0 \quad \text{at } t = T,$$
$$\nabla q^{(k)} \cdot \mathbf{n} = 0 \quad \text{on} \quad \partial Q,$$

$$\left(\beta \rho_r^{(k)} + \int_\Omega (\mathbf{1}_{\|\mathbf{x}-\mathbf{y}\| \le R})(\mathbf{x}-\mathbf{y})\rho^{(k)}(\mathbf{y},t) \cdot \nabla_{\mathbf{y}} q^{(k)}(\mathbf{y},t)\, dy\right) - \mu = 0, \tag{6.22}$$
$$\mu^{(k)} = 0 \text{ on } A_I^{(k)},$$
$$\rho_r^{(k)} = \rho_a \text{ on } A_-^{(k)},$$
$$\rho_r^{(k)} = \rho_b \text{ on } A_+^{(k)}.$$

For convergence properties of the primal–dual active set strategy, we refer to [32]. The authors give sufficient conditions for convergence in finitely many iterations for discretized problems. They show that the algorithm behaves extremely efficiently and typically converges in fewer than five iterations for some examples of elliptic optimal control problems. Most existing analysis is done for (linear) elliptic problems, as in this case the analysis is not affected by the necessary linearization of the PDE in addition to the box constraints, and we base our discussion on [32].

The active-set–fixed-point algorithm for solving (6.14) is then written as:

Algorithm 6 Active set algorithm, opinion dynamics optimization

1: Define initial values for $\rho_r^{(0)}$, $\rho^{(0)}$, $q^{(0)}$, and $\mu^{(0)}$
2: Set the sets $A_+^{(0)}$, $A_-^{(0)}$, and $A_I^{(0)}$ using $\rho_r^{(0)}$, and $\mu^{(0)}$ via (6.16), (6.17), and (6.18)
3: **for** $k = 1, 2, \ldots$ **do**
4: Solve (6.19), (6.21), (6.22) on the free variables from previous iteration via the fixed-point method (Algorithm 4) with or without the Armijo–Wolfe steps (Algorithm 5) on $A_I^{(k-1)}$
5: Update μ^k via (6.15)
6: Find active sets $A_-^{(k)}, A_+^{(k)}, A_I^{(k)}$ using $\rho_r^{(k)}$, and $\mu^{(k)}$
7: **if** $A_-^{(k)} = A_-^{(k-1)}$, $A_+^{(k)} = A_+^{(k-1)}$, and $A_I^k = A_I^{(k-1)}$ **then**
8: Stop, algorithm converged
9: **end if**
10: **end for**

6.3.3 Validation of the Active-Set Algorithm

The finite difference method is adopted as the choice of discretization for problems with additional bound constraints, as it less sensitive to non-smoothness of solutions compared to the pseudospectral method. We provide validation for the active-set strategy by solving the optimization problem constrained by the 1D Poisson equation written as

$$\begin{aligned} \min_{\rho,w} \quad & \frac{1}{2}\int_\Omega (\rho - \widehat{\rho})^2\, dx + \frac{\beta}{2}\int_\Omega w^2\, dx \\ \text{s.t} \quad & -\nabla\cdot(\nabla\rho) - w = f \quad \text{in } Q, \\ & \rho = 0 \quad \text{on } \partial Q, \\ & w_a \le w \le w_b \quad a.e. \text{ in } Q. \end{aligned}$$

where $Q = [-1, 1]$. The following conditions have to hold at each step of the iterative procedure:

$$\begin{aligned} -\nabla\cdot(\nabla\bar{\rho}^{(k)}) - \bar{w}^{(k)} &= f^{(k)} \quad \text{in } Q, \\ \bar{\rho}^{(k)} &= 0 \quad \text{on } \partial Q, \\ -\nabla\cdot(\nabla q^{(k)}) &= \bar{\rho}^{(k)} - \widehat{\rho} \quad \text{in } Q, \\ q^{(k)} &= 0 \quad \text{on } \partial Q, \\ \beta\bar{w}^{(k)} + q^{(k)} - \mu^{(k)} &= 0 \quad \text{in } Q, \\ \bar{w}^{(k)} &= w_a \text{ on } A_-^{(k)}, \\ \bar{w}^{(k)} &= w_b \text{ on } A_+^{(k)}, \\ \mu^{(k)} &= 0 \text{ on } A_I^{(k)}. \end{aligned}$$

The following triplet (ρ, w, q) solves the 1D Poisson control problem with Dirichlet boundary conditions

$$\begin{aligned} \rho &= \frac{1}{\pi^2}\sin(\pi x), \\ q &= -\beta\sin(\pi x), \\ w &= \operatorname*{proj}_{-\alpha,\alpha}(\sin(\pi x)), \quad 0 < \alpha \le 1, \end{aligned}$$

where

$$\begin{aligned} \widehat{\rho} &= \left(\beta\pi^2 + \frac{1}{\pi^2}\right)\sin(\pi x), \\ f &= \sin(\pi x) - \operatorname*{proj}_{-\alpha,\alpha}(\sin(\pi x)), \quad 0 < \alpha \le 1, \end{aligned}$$

and

$$\underset{-\alpha,\alpha}{\text{proj}}\left(\sin(\pi x)\right) = \begin{cases} -\alpha & \sin(\pi x) < -\alpha \\ \sin(\pi x) & -\alpha < \sin(\pi x) < \alpha \\ \alpha & \sin(\pi x) > \alpha \end{cases} .$$

We note that step 4 in the active set Algorithm 6 is not done via the fixed-point algorithm, but rather via solving the matrix equation

$$\begin{pmatrix} C & 0 & D^2 \\ 0 & \beta I & B \\ D^2 & C & 0 \end{pmatrix} \begin{pmatrix} \rho \\ w \\ q \end{pmatrix} = \begin{pmatrix} \widehat{\rho} \\ \beta A_+ - \beta A_- \\ -d \end{pmatrix},$$

where all terms in the left most matrix are in $\mathbb{R}^{N\times N}$. The term D^2 is the discretized Laplacian operator with $D^2(1,1) = D^2(N,N) = 1$ and zero in the positions $D^2(1, 2:N)$ and $D^2(N, 2:N)$ to prevent the operator from acting on the boundaries. Here, I is the identity matrix and $C = I$, with $C(1,1) = C(N,N) = 0$ to similarly not act on the boundary, and B is a diagonal matrix with the active set A_I on the diagonal. The active sets A_+, A_- and A_I are as defined earlier. Finally, d is an $N \times 1$ vector that represents the values of ρ on the boundary, $d(1) = d(N) = 0$ and values of f in the interior. We provide the initial guess $w^{(0)} = 1-x^2$ to the active set method and compare the performance of the finite difference discretization against the pseudospectral method. We use spatial points $N = 20$, 30 and 50 for the pseudospectral method, and $N = 100$, 500 and 1000 for the finite difference method. Note that the finite difference implementations used here require more points than used with pseudospectral methods to achieve comparable accuracy. Tables 6.1 and 6.2 shows the error in the numerical solution, and number of iterations required for the active-set strategy to converge, for different choices of spatial points as well as for different values of β. Here, we fix $\alpha = 0.7$, but the results are robust under varying this. The values in Table 6.1 show that the finite difference discretization achieves an accuracy of between 10^{-2} and 10^{-6}, depending on the number of spatial points used and β. Table 6.2 show that the pseudospectral method attains accuracy of on average 10^{-13} which is understandable due to its exponential convergence properties. Figure 6.1 shows the optimal control w for both discretizations. Here, we notice undesirable "smoothing" actions on the optimal control produced by the pseudospectral method at the points close to the bounds -0.7 and 0.7, while the finite difference scheme produces a true cut-off of the control at the bounds. This constitutes the primary reason for preferring finite difference methods when bound constraints are applied.

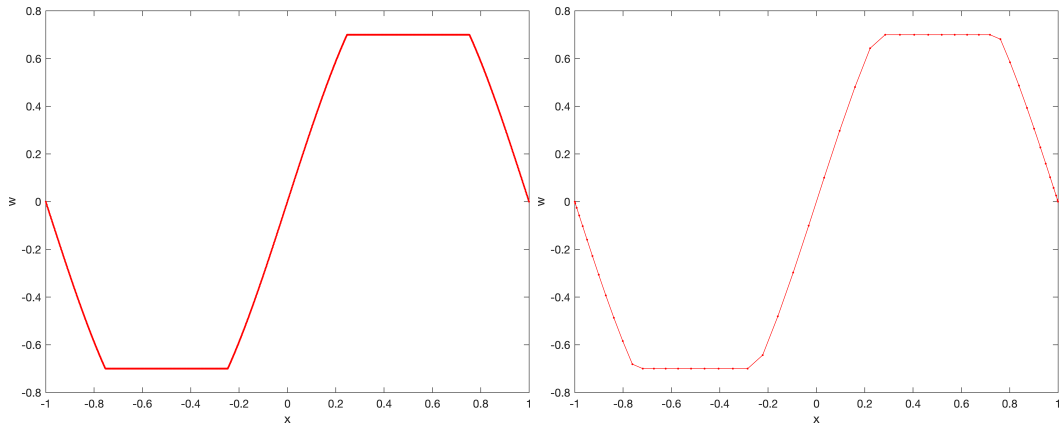

Figure 6.1: The optimal control w for a Poisson optimization problem with bound constraints $-0.7 \leq w \leq 0.7$ solved using an active-set strategy and finite difference (left) and pseudospectral (right) schemes.

		$\beta = 10^{-5}$	$\beta = 10^{-3}$	$\beta = 10^{-1}$
$N = 100$	$\mathcal{E}_\rho$	5.0202×10^{-5}	1.5013×10^{-4}	3.8812×10^{-4}
	$\mathcal{E}_q$	1.2412×10^{-2}	1.1569×10^{-3}	2.9589×10^{-4}
	$\mathcal{E}_w$	1.3240×10^{-3}	5.5299×10^{-4}	1.5163×10^{-4}
	`Iter`	7	6	4
$N = 500$	$\mathcal{E}_\rho$	1.9560×10^{-6}	5.9039×10^{-6}	1.5274×10^{-5}
	$\mathcal{E}_q$	4.8238×10^{-4}	4.5486×10^{-5}	1.1645×10^{-5}
	$\mathcal{E}_w$	5.2230×10^{-5}	2.1768×10^{-5}	5.9689×10^{-6}
	`Iter`	8	6	4
$N = 1000$	$\mathcal{E}_\rho$	4.9071×10^{-7}	1.4786×10^{-6}	3.8067×10^{-6}
	$\mathcal{E}_q$	1.2144×10^{-4}	1.1408×10^{-5}	2.9058×10^{-6}
	$\mathcal{E}_w$	1.3073×10^{-5}	5.4370×10^{-6}	1.4833×10^{-6}
	`Iter`	8	6	4

Table 6.1: Error measures for state ρ, adjoint q, and control w, for a range of N and β using the finite difference discretization, and Active Set iterations required for convergence.

		$\beta = 10^{-5}$	$\beta = 10^{-3}$	$\beta = 10^{-1}$
$N = 20$	$\mathcal{E}_\rho$	5.2056×10^{-15}	6.5925×10^{-15}	8.5403×10^{-15}
	$\mathcal{E}_q$	2.6029×10^{-13}	3.1072×10^{-14}	6.6285×10^{-15}
	$\mathcal{E}_w$	3.7512×10^{-14}	6.3092×10^{-14}	7.1192×10^{-15}
	`Iter`	5	4	4
$N = 30$	$\mathcal{E}_\rho$	1.3762×10^{-14}	1.7135×10^{-14}	5.0200×10^{-14}
	$\mathcal{E}_q$	6.6606×10^{-13}	9.6382×10^{-14}	1.8576×10^{-14}
	$\mathcal{E}_w$	8.4760×10^{-14}	2.1444×10^{-13}	1.5636×10^{-14}
	`Iter`	6	5	3
$N = 50$	$\mathcal{E}_\rho$	1.4671×10^{-14}	4.0141×10^{-14}	5.3721×10^{-14}
	$\mathcal{E}_q$	1.2166×10^{-12}	3.2017×10^{-13}	2.0031×10^{-14}
	$\mathcal{E}_w$	2.3731×10^{-13}	4.3826×10^{-13}	1.9500×10^{-14}
	`Iter`	6	5	3

Table 6.2: Error measures for state ρ, adjoint q, and control w, for a range of N and β using the pseudospectral discretization, and Active Set iterations required for convergence.

6.4 Numerical Experiments

For all examples, we fix the number of space and time points N and n to be 200 and 50 respectively, the pair (σ, R) to $(0.1, 0.2)$, and $\beta = 0.1$. Combinations of the pair (σ, R) produces different final states and in some cases causes phase transitions (see [96]). Our choice of (σ, R) is informed by observing the dynamics captured in [96] for different initial conditions ρ_0 and boundary conditions. The constants $m_\rho, m_{\rho_r}, m_{\widehat{\rho}}$ used in the examples represent the normalized mass of the state, radical and desired variables respectively, and we fix $m_\rho = m_{\widehat{\rho}} = 1$, and $m_{\rho_r} = 0.2$. The numerical experiments start with solving a forward problem given an initial condition ρ_0 and a distribution of radicals we call forward radicals, ρ_r. We then solve an optimization problem with the solution to the forward problem as the desired state $\widehat{\rho}$ and the initial guess for ρ_r to be zero at all times. The aim is to compare the optimal and forward radicals. To emphasize the effects of boundary conditions on the dynamics, we place majority of the mass of the system close to the boundaries. We also observe the values of β that give the lowest optimization cost for the examples.

6.4.1 Target Example 1: Uniform Initial Condition with Gaussian Radicals

We have the following initial condition and forward radical distribution:

$$\begin{aligned} \rho_0 &= 1, \\ \rho_r &= m_{\rho_r} Z^{-1} \left[\exp\left(-cd(x - x_0)^2 \right) \right], \end{aligned}$$

where $d(x - x_0)$ is the periodic Euclidean distance. Here, ρ_r is constructed as a Gaussian distribution normalized to have mass 1 (same as ρ, so mass is conserved) using the constant $Z = \int_\Omega \rho_r dx$. The constant $x_0 = 0.8$ is the centre of a Gaussian distribution and c determines the sharpness of the peak of the distribution. In this example we set $c = 1000$ to create a steep density of radicals in the domain. We solve the optimization problem with no bound constraints first, then with non-negativity constraint: $\rho_r \geq 0$. Figure 6.2 shows the results of the forward

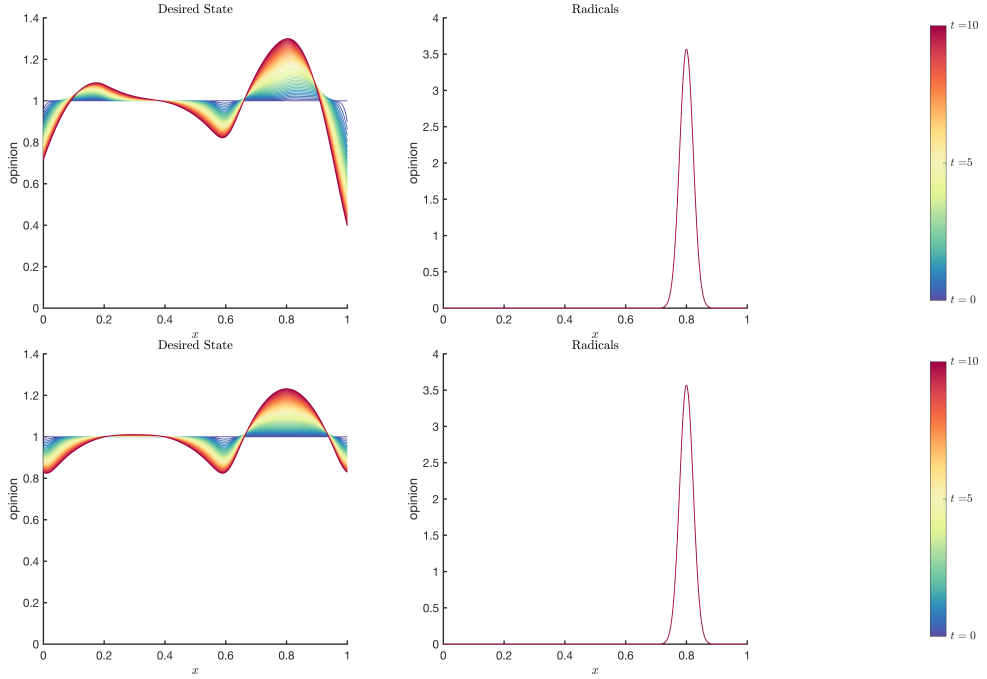

Figure 6.2: Target Example 1: The desired state from the forward problem together with the forward radicals for no-flux (top) and periodic (bottom) boundary conditions, with $\beta = 1$ and a colorbar for time on the right-hand side.

problem and the forward radicals. We see in Figure 6.2 that the introduction of radicals breaks

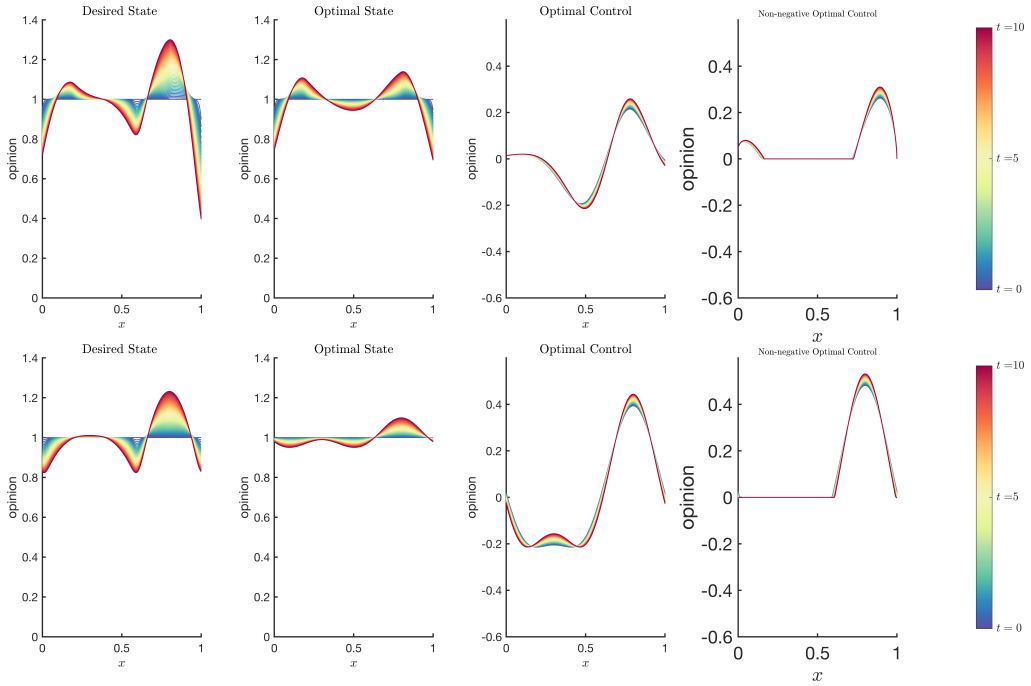

Figure 6.3: Target Example 1: The optimal state and control (with and without bounds) together with the desired state for no-flux (top) and periodic (bottom) boundary conditions, with $\beta = 1$ and a colorbar for time on the right-hand side.

the uniform distribution into what looks like two clusters. The state when periodic boundary conditions are prescribed also shows periodic behaviour, exhibiting more roundedness of its clusters compared to the no-flux boundary conditions case. Figure 6.3 shows the optimal state and control when the results of the forward problem are chosen as the desired state. We observe the optimal states for both no-flux and periodic boundary conditions exhibit similar behaviour to their desired state, likely due to the moderately small value of β. The optimal control, when no-flux boundary conditions are imposed, are clearly non-periodic compared to the periodic case, driving most of the mass of the optimized radicals towards where the bigger cluster of the desired state is. For the periodic case, the masses at the boundaries flow into each other, hence the optimized radicals are also distributed to the smaller cluster of the desired state. We see in the right-most plots in Figure 6.3, that the active-set strategy successfully bounds the optimized control to be non-negative. We notice that the non-negative parts of the optimal control remain similar to the non-bounded case and only grow to compensate for the cut off of the rest of the control. We observe the following values for case of no-flux boundary conditions. The cost functional for the forward problem is $\mathcal{J}_f = 1.1232$ while the optimization cost is $J_c = 0.4761$. The fixed-point algorithm converged in 37 iterations and took 34 seconds. The optimization cost of including non-negative bound constraints is $J_{bc} = 0.5141$. The active set-fixed-point algorithm converged in 6467 seconds and required 3 iterations of the active set strategy to converge. In the case of periodic boundary conditions, we observe a similar trend that the cost of optimization is lower than the cost of the forward problem. Experimentation with lower values of β such as 10^{-1}, and $10^{-}2$ result in optimization costs that are greater than the cost of the forward problem, suggesting that allowing a larger mass of optimized radicals is not advantageous in the example we consider. We consider next another example that applies bound constraints.

6.4.2 Target Example 2: Uniform Initial Condition with Double Gaussian Radicals

In this example we use the inputs:

$$\rho_0 = 1,$$
$$\rho_r = m_{\rho_r} Z^{-1} \left[\lambda \exp\left(-cd(x-x_1)^2\right) + (1-\lambda)\exp\left(-cd(x-x_2)^2\right)\right],$$

where $d(x-x_i)$ is the periodic Euclidean distance. Here, ρ_r is a double Gaussian distribution with centres $x_1 = 0.2$ and $x_2 = 0.8$, $c = 1000$ and $\lambda = 0.5$, and Z is a normalization constant that is equal to the mass of ρ_r. This example is inspired by a bi-partisan country holding

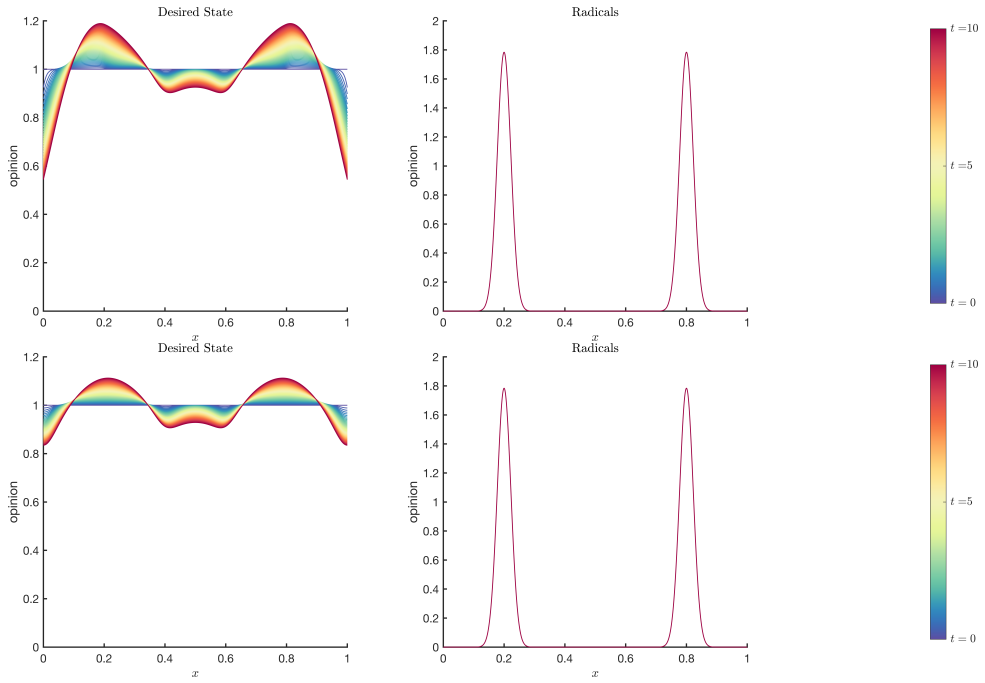

Figure 6.4: Target Example 2: The desired state which is the forward solution and the radical distribution for no-flux (top) and periodic (bottom) boundary conditions, with $\beta = 1$ and a colorbar for time on the right-hand side.

general elections, or the recent United Kingdom poll on whether or not to leave the European union. In these scenarios, there are only two choices available to the population. And in most cases, each both parties runs campaigns to garner support in order to win the vote. We start the initialize the system as a uniform distribution where voters have uniformly spread opinion and no party has the winning hand. We introduce two Gaussian radicals centred close to the extreme ends of the domain to mimick campaign leaders representing their respective parties. We set $\lambda = 0.5$ in ρ_r to keep both sides the same in terms of the strength of their influence. We see in Figure 6.4 the results of the forward problem. As expected the populations' opinion start to split into two clusters, rallying around the radicals. However, we notice a smaller third cluster which may be interpreted as neutral opinions in the middle of the two extreme clusters. In the no-flux boundary condition case, the clusters at the boundaries have steeper slopes close to the boundary, as by the original HK model, those on the boundary can only be pulled inwards. Whereas, in the periodic case, the opinions at the two extremes drift into each other. It may be argued that the periodic case portrays a more realistic view of society, where someone on the extreme left of an opinion is more likely to switch instantly to be on the extreme right, rather than first become neutral, and then switch. This may also not be realistic as people with extreme opinions are unlikely to change their position. Figure 6.5 shows the optimal states and control for when bound constraints are applied and not applied. Interestingly, despite the different behaviour of the desired state for periodic and no-flux boundary conditions, the optimal radical distributions behave very similarly except for the slight increase of control on

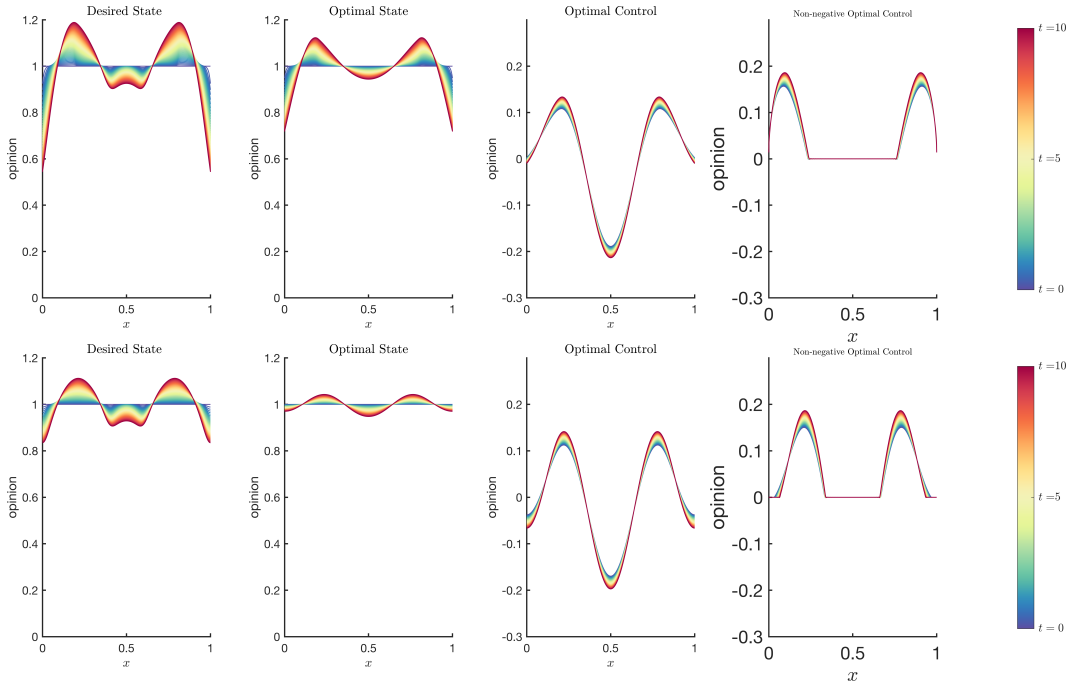

Figure 6.5: Target Example 2: The optimal state and control (with and without bounds) together with the desired state for no-flux (top) and periodic (bottom) boundary conditions, with $\beta = 1$ and a colorbar for time on the right-hand side.

the boundary for the no-flux case. They both concentrate the density of the radicals where the clusters are formed in the desired state. We also notice the absence of the middle cluster in the optimal state, suggesting that the value of β used can be reduced for closer results to the desired state. Once, again we achieve the non-negative bound constraint imposed on the control when applying the active set strategy. We observe the following values for case of no-flux boundary conditions. The cost functional for the forward problem is $\mathcal{J}_f = 0.7942$ while the optimization cost is $J_c = 0.3608$. The fixed-point algorithm converged in 30 iterations and took 27 seconds. The optimization cost of including non-negative bound constraints is $J_{bc} = 0.4084$. The active set-fixed-point algorithm converged in 5585 seconds and required 3 iterations of the active set strategy to converge. Since the optimal states and control with and without bound constraints are very similar, we do not show them henceforth.

6.4.3 Target Example 3: Gaussian Initial Condition and Uniform Target

For this example, we specify a target distribution that is not a result of the forward problem. We use the following inputs:

$$\rho_0 = m_\rho Z \left[\exp\left(-cd(x - x_0)^2\right)\right]$$
$$\widehat{\rho} = 1,$$

where Z is a normalisation constant, $x_0 = 0.2$ is the centre of the Gaussian distribution ρ_0 and $c_{\widehat{\rho}} = 50$ determines the steepness of the distribution, and $d(x-x_0)$ is the periodic Euclidean distance. This example seeks to investigate the dynamics of driving a system initially at consensus into chaos (uniform state). Figure 6.6 show the results of a forward problem which starts at the consensus, ρ_0, with no radicals applied. We see from the uncontrolled state in figure 6.6, that the consensus continues to grow for both periodic and non-flux boundary conditions behaving in some sense in the opposite direction of our goal of a uniform state. We can already deduce from the forward problem, that this scenario will require more control to achieve the desired state compared to the examples we have seen so far. This deduction is evident in the plots of

the optimal states and controls presented in Figure 6.7. For the first time, we observe optimal states that are barely close to the desired state. Granted, the dynamics show the optimal state for both boundary conditions spreading the opinions over the domain instead of growing the cluster, as in the forward problem, and suggesting that when run for the longer times and a smaller value of β, the states may eventually become uniform over the domain. However, running this example for longer times and a smaller value of β using the fix-point method require possibly days of computational time, as one requires more points in space and time, and a very small mixing rate. hence, we trade-off driving the state closer to the desired for faster convergence (approximately 7 hours). Here, we notice an impactful influence of the choice of boundary conditions on the optimal distribution of radicals. The case of periodic boundary conditions exhibit four regions with peaks in the domain, three positive peaks, and a negative peak. Technically, the peak on the left most of the domain can be thought of as part of the peak on the rightmost part of the periodic domain. The positive peaks act to increase the mass of opinions in the centre and right extreme of the domain, while the negative peak reduces the mass of opinions in the consensus on the left side of the domain. The presence of the four peaks clearly drive the initial consensus much more lower towards a uniform state, compared to the no-flux case. In comparison, the no-flux optimal control only exerts force on three regions in the domain, concentrating a negative force where the consensus is and a positive force in the middle of the domain.

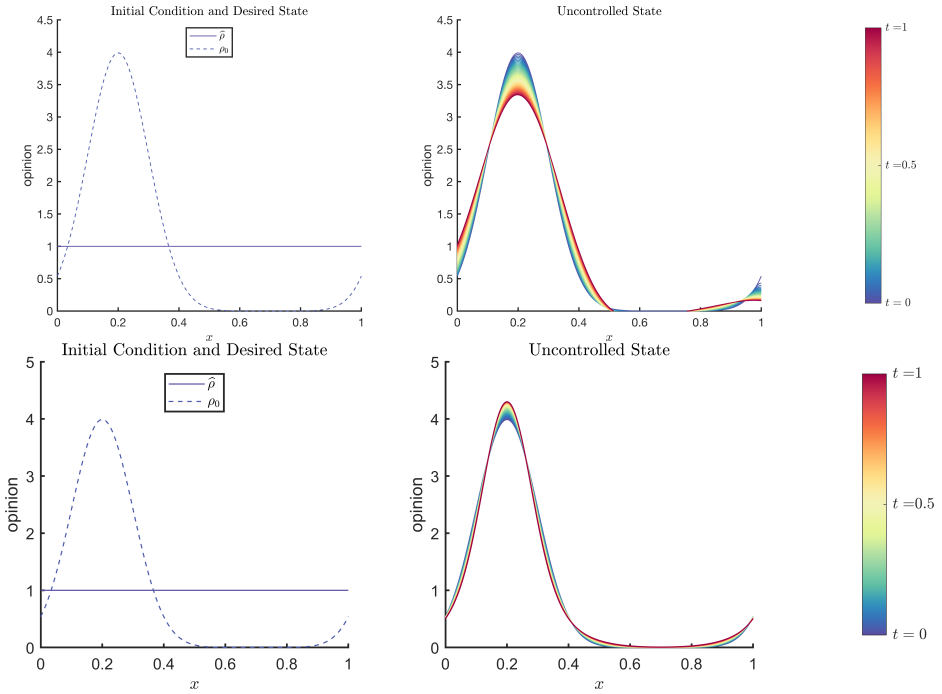

Figure 6.6: Target Example 3: The desired state which is the forward solution, and the radical distribution for no-flux (top) and periodic (bottom) boundary conditions, with $\beta = 10^{-1}$ and a colorbar for time on the right-hand side.

6.4.4 Target Example 4: Double Gaussian Initial Condition and Target

In this example, we start with an initial condition that combines two Gaussian distributions of which have the same mass. We then introduce a smaller mass of radicals centred on the right Gaussian. The inputs are:

$$\rho_0 = m_\rho Z_\rho \left[\lambda \exp\left(-cd(x-x_0)^2\right) + (1-\lambda)\exp\left(-cd(x-x_1)^2\right)\right],$$
$$\rho_r = m_{\rho_r} Z_{\rho_r} \exp\left(-c_{\rho_r} d(x-x_2)^2\right),$$

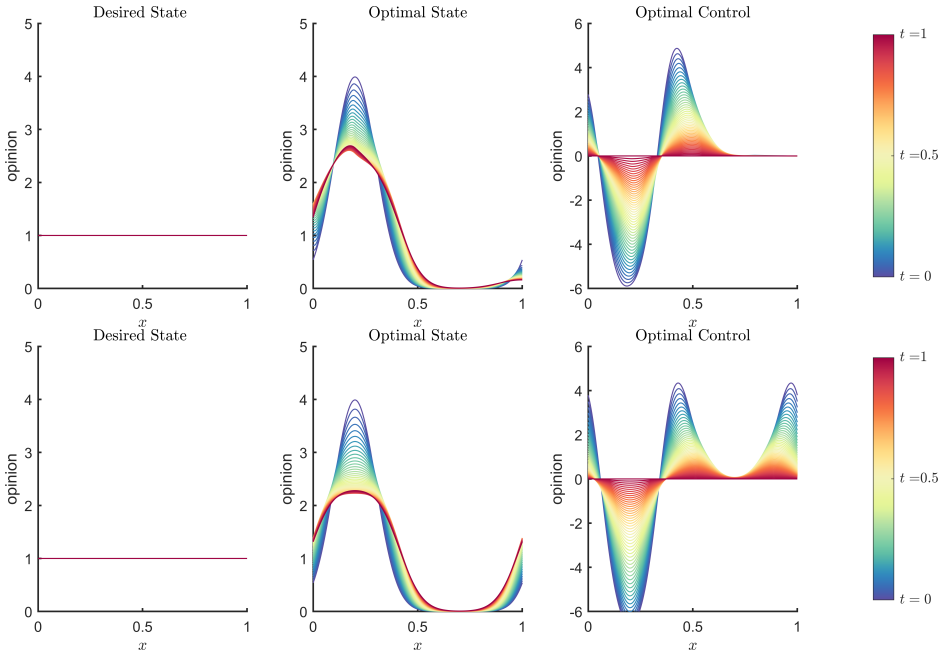

Figure 6.7: Target Example 3: The initial optimal state and, control together with the desired state for no-flux (top) and periodic (bottom) boundary conditions, with $\beta = 10^{-1}$ and a colorbar for time on the right-hand side.

where $x_0 = 0.2, x_1 = x_2 = 0.8$ and $c = 50, c_{\rho_r} = 1000$. Here also, Z_ρ, and Z_{ρ_r} are normalization constants for ρ, and ρ_r, respectively. We present the dynamics for a scenario which begins with

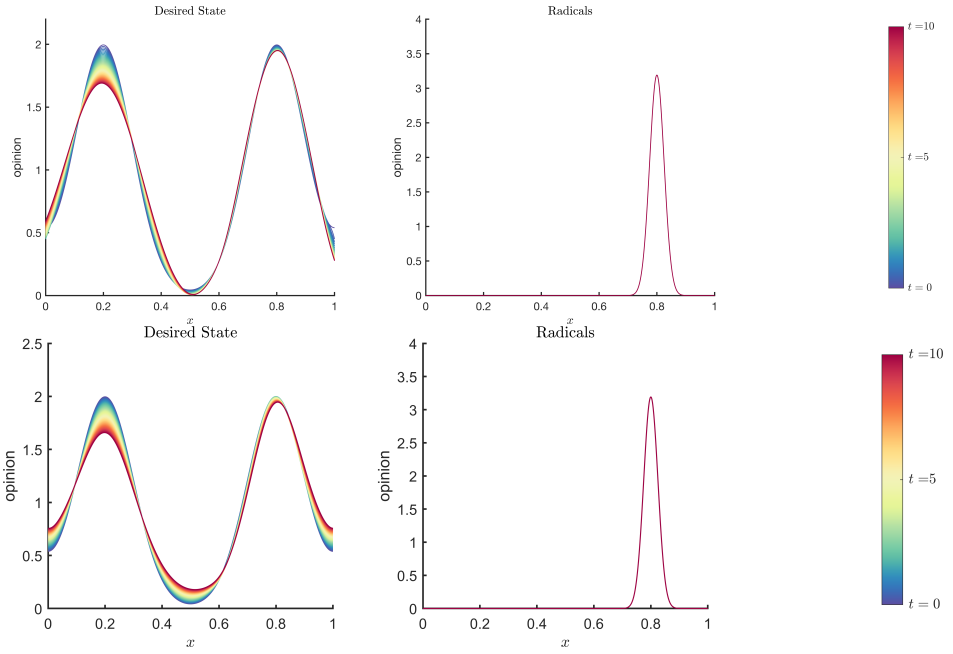

Figure 6.8: Target Example 4: The desired state together with the forward radicals for no-flux (top) and periodic (bottom) boundary conditions, with $\beta = 10^{-1}$ and a colorbar for time on the right-hand side.

two equal clusters, and a radical distributed centred on the right cluster. This example can be interpreted as a case of two competitor businesses that own the equal share of the market. One business with the hope of beating their competitor to become the largest market share holder initiates a series of advertising campaigns to promotes its products (in this scenerio, negative

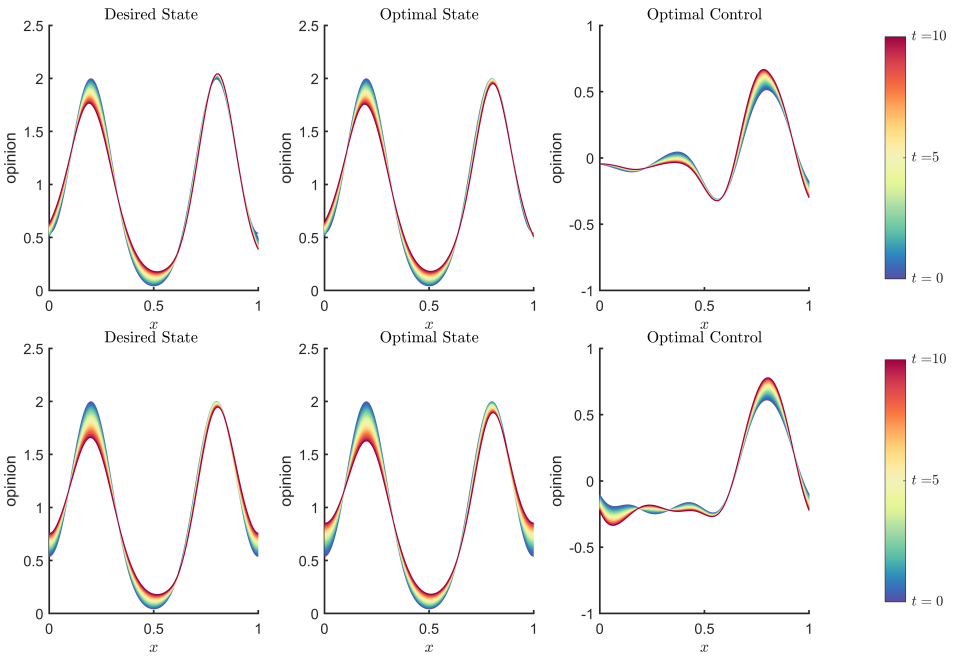

Figure 6.9: Target Example 4: The initial optimal state and control together with the desired state for no-flux (top) and periodic (bottom) boundary conditions, with $\beta = 10^{-1}$ and a colorbar for time on the right-hand side.

control can be explained as negative advertisement towards their competitor). In the case where the other business refuses to spend money on advertising campaigns, will they lose their market share? The results of the forward problem shown in Figure 6.8 suggest that the outcome will be in favour of the business that spent money on campaigns. The introduction of a radical population on the right side of the domain causes the right cluster to grow at the expense of the left cluster. In the optimized state and control plots in Figure 6.9, we see that the same desired state can be attained by applying both positive and negative control (advertisement) compared to the non-negative forward control. Once again, the optimal control behaves differently for the two boundary conditions. The no-flux case applies more negative control around the middle of the domain while the periodic boundary condition apply more negative control towards the left boundary fo the domain. This can be explained in our scenario as, in the case where extreme customers of both business are more likely to instantly switch sides (periodic case), one may infer that, it is more beneficial to target negative advertisements at the most loyal customers of your competitor. Also, in the case where the most loyal customers are definitely less likely to change their minds, it is more advantageous to target negative advertisement at the neutral customers who have no loyalty to either business.

6.5 Remarks

The fixed-point method once again, converges for problems with non-local and non-linear interacting terms arising from opinion dynamics, encouraging further studies on theoretical questions about the existence and uniqueness of optimal controls of opinion dynamics optimization problems. However, it is computationally demanding, taking about 3 hours to converge for the examples in this chapter, making it necessary to develop a faster higher-order method for the two-dimensional examples explored in Chapter 7. The active-set strategy performs well for the non-linear parabolic PDEs presented in this chapter, and demonstrates the need for further theoretical work on the convergence of the strategy for non-linear and non-local parabolic PDEs. We also observe from the examples presented in this chapter, that different boundary conditions influence optimal controls differently, and boundary conditions should be chosen to more accurately reflect the system being modelled for reliable results.

In the next chapter, we consider two-dimensional opinion dynamics problems and a robots

swarming optimization problem, and use a higher order Newton–Krylov algorithm for faster convergence.

Chapter 7

A Newton–Krylov Method for Higher Dimensional Opinion Dynamics and Robot Swarming Optimization Problems

In this chapter, we focus on more real-world applications of PDE-constrained optimization problems. We consider the growing research area of higher-dimensional opinion dynamics, where opinions about more than one aspect are measured, and a crop pollination system using robots from the field of swarm modelling. In order to get faster convergence for the more numerically challenging higher dimensional problems, we employ the higher-order Newton–Krylov algorithm discussed in Section 4.5.

This chapter is structured as follows. In Section 7.1, we describe how we perform preconditioning in the Newton–Krylov algorithm, and in Section 7.2, we consider the two-dimensional opinion dynamics optimization problem and detail the Newton–Krylov method for the problem. We then show results of numerical experiments. We detail the robot swarming model and its optimization problem in Section 7.3, deriving the continuous optimality conditions. We then provide explicit expressions for the equations in the Newton–Krylov method and finally present numerical results. We conclude by giving remarks on the efficiency of the Newton–Krylov algorithm for these example problems.

7.1 Preconditioning for Newton–Krylov Algorithm

To tackle the problems outlined in this chapter, we apply the Newton–Krylov algorithm defined in Section 4.5. For this to be an efficient algorithm, we require a preconditioner for the GMRES algorithm, specifically tailored to the PDE-constrained optimization problems at hand. We follow the working of [2, 112]. Computing the Jacobian of the residual $\mathbf{R}$ defined at the end of Section 4.5 (4.16), we obtain:

$$J = \left(\begin{array}{cc|c} I & 0 & B \\ 0 & 0 & \\ \hline & \widetilde{C} & D \end{array}\right)$$

$$= \left(\begin{array}{cc|ccccc} I & 0 & \cdots & \cdots & \cdots & 0 & 0 \\ 0 & 0 & \cdots & \cdots & \cdots & 0 & I \\ \hline q_{01}D^f_{u,0} + M & q_{01}D^f_{v,0} & q_{11}D^f_{u,1} - M & q_{11}D^f_{v,1} & \cdots & q_{n1}D^f_{u,n} & q_{n1}D^f_{v,n} \\ q_{01}D^g_{u,0} & q_{01}D^g_{v,0} + M & q_{11}D^g_{u,1} & q_{11}D^g_{v,1} - M & \cdots & q_{n1}D^g_{u,n} & q_{n1}D^g_{v,n} \\ \vdots & \vdots & \vdots & \vdots & \ddots & \vdots & \vdots \\ q_{0n}D^f_{u,0} + M & q_{0n}D^f_{v,0} & q_{1n}D^f_{u,1} & q_{1n}D^f_{v,1} & \cdots & q_{nn}D^f_{u,n} - M & q_{nn}D^f_{v,n} \\ q_{0n}D^g_{u,0} & q_{0n}D^g_{v,0} + M & q_{1n}D^g_{u,1} & q_{1n}D^g_{v,1} & \cdots & q_{nn}D^g_{u,n} & q_{nn}D^g_{v,n} - M \end{array}\right)$$

where M discretizes the time derivative, n is the number of time-steps, q_{ij} denote entries of

Q as defined in Section 4.5, $D^f_{u,i}$ denotes the Jacobian of $f(t, \mathbf{u}, \mathbf{v})$ with respect to u at point i, and similarly for $D^g_{u,i}$, $D^f_{v,i}$, and $D^g_{v,i}$.

We need to solve systems of this form. After post-multiplying the system by

$$\begin{pmatrix} 1 & & & & \\ 1 & 1 & & & \\ 1 & 1 & 1 & & \\ \vdots & & & \ddots & \\ 1 & & & & 1 \end{pmatrix} \otimes \begin{pmatrix} I & 0 \\ 0 & I \end{pmatrix},$$

to obtain an invertible $(1,1)$-block, we have to solve a system involving the matrix

$$\left(\begin{array}{cc|c} I & 0 & B \\ 0 & I & \\ \hline & C & D \end{array}\right),$$

where C is a transformation of matrix $\widetilde{C}$. This may be reduced to a Schur complement system involving

$$S = D - CB.$$

We precondition S by :

$$P = \widehat{D} - \widehat{C}B, \quad \widehat{D} = Q^T_{1:n,1:n} \otimes G, \quad \widehat{C} = \begin{pmatrix} \sum_{i=0}^n q_{i,0} \\ \sum_{i=0}^n q_{i,1} \\ \vdots \\ \sum_{i=0}^n q_{i,n} \end{pmatrix} \otimes G,$$

where $\otimes$ denotes the Kronecker product, and

$$G = \begin{pmatrix} D^f_{u,k} - M & D^f_{v,k} \\ D^g_{u,k} & D^g_{v,k} - M \end{pmatrix}$$

with k a suitably-chosen time point (e.g. corresponding to $t = \frac{T}{2}$).

Then, by Woodbury identity:

$$P^{-1} = \widehat{D}^{-1} + \widehat{D}^{-1}\widehat{C}\left(\begin{pmatrix} I & 0 \\ 0 & I \end{pmatrix} - B\widehat{D}^{-1}\widehat{C}\right)^{-1} B\widehat{D}^{-1}.$$

By simple algebra, we have that

$$P^{-1} = F\widehat{D}^{-1} = \left(\begin{array}{cc|cc|c|cc} I & & & & & 0 & 0 \\ & I & & & & 0 & c_1 I \\ \hline & & I & & & 0 & 0 \\ & & & I & & 0 & c_2 I \\ \hline & & & & \ddots & \vdots & \vdots \\ \hline & & & & & I & 0 \\ & & & & & 0 & c_n I \end{array}\right) \widehat{D}^{-1}$$

for easily-computable constants c_i. This preconditioner is readily applied to a vector. The main computational costs are computing an LU factorization of Q one time in the entire algorithm, and computing an LU factorization of G (small, compared to the entire system) once per Newton iteration. We apply a fixed number of 500 GMRES iterations per Newton step, as the remainder of the algorithm is computationally cheap in comparison to these factorization costs.

7.2 Two-Dimensional Opinion Dynamics Optimization Problem

In Chapter 6, we introduced the Fokker–Planck opinion dynamics model with radicals (6.8) where individuals' opinions are described by one-dimensional values, representing an opinion or single topic. However, in reality, people have opinions on many different subjects, ranging from sports and entertainment to spiritual beliefs and moral principles, interactions among which can be represented by vectors of opinions to generate more practical results. Multidimensional opinion dynamics is a novel area of research with recent works in [108, 186, 224] focussing on social networks and the voter model. The large-scale nature of higher-dimensional problems (more discretization points) make them computational demanding and we therefore require a faster algorithm to obtain results in minutes compared to days. The success of the recently developed higher-order Newton–Krylov algorithm to solve 2D and 3D optimization problems from multiscale particle dynamics in [2], makes solving higher dimensional opinion dynamics problems with the Newton–Krylov algorithm a natural extension of the work in this thesis.

In this section, we consider the opinion dynamics optimization problem (6.9) in 2D with periodic boundary conditions on $Q = \Omega \times (0,T)$, $\Omega \subset \mathbb{R}^2$ written as:

$$\begin{aligned} \min_{\rho,\rho_r} \quad & \mathcal{J}(\rho,\rho_r) \coloneqq \frac{1}{2}\int_0^T \int_\Omega (\rho - \widehat{\rho})^2 \, dxdt + \frac{\beta}{2}\int_0^T \int_\Omega \rho_r^2 \, dxdt \\ \text{s.t} \quad & \partial_t \rho - \frac{\sigma^2}{2}\nabla^2 \rho - \nabla_{\mathbf{x}} \cdot \mathcal{I}(\rho,\rho_r) = 0 \quad \text{in } Q, \\ & \rho = \rho_0(\mathbf{x}) \quad \text{at } t = 0, \end{aligned}$$

where $Q = \Omega \times (0,T)$,,

$$\mathcal{I}(\rho,\rho_r) = \rho(\mathbf{x},t)\int_\Omega (\mathbf{1}_{\|\mathbf{x}-\mathbf{y}\|\leq R})(\mathbf{x}-\mathbf{y})(\rho(\mathbf{y},t)+\rho_r(\mathbf{y},t))\,dy,$$

and periodicity is enforced via

$$\begin{aligned} \rho(\mathbf{x},t)\Big|_{\Omega_l} &= \rho(\mathbf{x},t)\Big|_{\Omega_r}, \\ \rho(\mathbf{x},t)\Big|_{\Omega_t} &= \rho(\mathbf{x},t)\Big|_{\Omega_b}, \\ \left(\frac{\sigma^2}{2}\nabla\rho + \mathcal{I}(\rho,\rho_r)\right)\cdot\mathbf{n}\Big|_{\Omega_l} &= -\left(\frac{\sigma^2}{2}\nabla\rho + \mathcal{I}(\rho,\rho_r)\right)\cdot\mathbf{n}\Big|_{\Omega_r}, \\ \left(\frac{\sigma^2}{2}\nabla\rho + \mathcal{I}(\rho,\rho_r)\right)\cdot\mathbf{n}\Big|_{\Omega_t} &= -\left(\frac{\sigma^2}{2}\nabla\rho + \mathcal{I}(\rho,\rho_r)\right)\cdot\mathbf{n}\Big|_{\Omega_b} \quad \text{on } \partial Q. \end{aligned}$$

Here Ω_l represents the left boundary of the spatial domain, Ω_r, the right side, Ω_t the top and Ω_b, the bottom. Similarly to the reasoning of the previous chapter, periodic conditions on the density and flux are trivial consequences of the imposition of periodicity on ρ and ρ_r, and the flux condition is necessary to enforce periodicity numerically.

Though no-flux type boundary conditions are also natural candidates for the bounded confidence model [96], we impose periodic boundary conditions here for ease of numerical implementation. Following similar working as for the 1D problem with periodic boundary conditions in Section 6.2, we obtain the optimality system for the 2D problem as

$$\begin{aligned} \partial_t \bar{\rho} - \frac{\sigma^2}{2}\nabla^2\bar{\rho} - \nabla_{\mathbf{x}}\cdot\mathcal{I}(\bar{\rho},\bar{\rho}_r) &= 0 \\ \bar{\rho} &= \rho_0(\mathbf{x}) \quad \text{at } t = 0, \\ \bar{\rho}(\mathbf{x},t)\Big|_{\Omega_l} &= \bar{\rho}(\mathbf{x},t)\Big|_{\Omega_r}, \\ \bar{\rho}(\mathbf{x},t)\Big|_{\Omega_t} &= \bar{\rho}(\mathbf{x},t)\Big|_{\Omega_b}, \end{aligned}$$

$$\left(\frac{\sigma^2}{2}\nabla\bar{\rho}+\mathcal{I}(\bar{\rho},\bar{\rho}_r)\right)\cdot\mathbf{n}\Big|_{\Omega_l} = -\left(\frac{\sigma^2}{2}\nabla\bar{\rho}+\mathcal{I}(\bar{\rho},\bar{\rho}_r)\right)\cdot\mathbf{n}\Big|_{\Omega_r},$$
$$\left(\frac{\sigma^2}{2}\nabla\bar{\rho}+\mathcal{I}(\bar{\rho},\bar{\rho}_r)\right)\cdot\mathbf{n}\Big|_{\Omega_t} = -\left(\frac{\sigma^2}{2}\nabla\bar{\rho}+\mathcal{I}(\bar{\rho},\bar{\rho}_r)\right)\cdot\mathbf{n}\Big|_{\Omega_b} \quad \text{on } \partial Q.$$

$$\begin{aligned}
\partial_t q + \frac{\sigma^2}{2}\nabla^2 q - \nabla_{\mathbf{x}} q\cdot\left(\int_\Omega (\mathbf{1}_{\|\mathbf{x}-\mathbf{y}\|\le R})(\mathbf{x}-\mathbf{y})\bar{\rho}_r(\mathbf{y},t)\,dy\right) + \int_\Omega (\mathbf{1}_{\|\mathbf{x}-\mathbf{y}\|\le R})(\mathbf{x}-\mathbf{y})\bar{\rho}(\mathbf{y},t)\cdot\nabla_{\mathbf{y}} q(\mathbf{y},t)\,dy \\
-\nabla_{\mathbf{x}}\cdot q\left(\int_\Omega (\mathbf{1}_{\|\mathbf{x}-\mathbf{y}\|\le R})(\mathbf{x}-\mathbf{y})\bar{\rho}(\mathbf{y},t)\,dy\right) = -\bar{\rho}+\widehat{\rho} \quad \text{in } Q \\
q = 0 \quad \text{at } t = T, \\
q(\mathbf{x},t)\Big|_{\Omega_l} = q(\mathbf{x},t)\Big|_{\Omega_r}, \\
q(\mathbf{x},t)\Big|_{\Omega_t} = q(\mathbf{x},t)\Big|_{\Omega_b}, \\
\frac{\sigma^2}{2}\nabla q\cdot\mathbf{n}\Big|_{\Omega_l} = -\frac{\sigma^2}{2}\nabla q\cdot\mathbf{n}\Big|_{\Omega_r}, \\
\frac{\sigma^2}{2}\nabla q\cdot\mathbf{n}\Big|_{\Omega_t} = -\frac{\sigma^2}{2}\nabla q\cdot\mathbf{n}\Big|_{\Omega_b} \quad \text{on } \partial Q.
\end{aligned}$$

$$\beta\bar{\rho}_r + \int_\Omega (\mathbf{1}_{\|\mathbf{x}-\mathbf{y}\|\le R})(\mathbf{x}-\mathbf{y})\bar{\rho}(\mathbf{y},t)\cdot\nabla_{\mathbf{y}} q(\mathbf{y},t)\,dy = 0.$$

We now briefly describe how the Newton–Krylov method may be applied to the opinion dynamics problem. The state and adjoint equations are described in the following general form by separating the spatial and temporal derivatives in each case:

$$\begin{aligned}
\mathbf{u}'(t) &= \mathbf{F}(t,\mathbf{u},\mathbf{v}), \qquad \mathbf{u}(0) = \mathbf{u}_0 \in \mathbb{R}^N, \\
\mathbf{v}'(t) &= \mathbf{G}(t,\mathbf{u},\mathbf{v}), \qquad \mathbf{v}(T) = \mathbf{0} \in \mathbb{R}^N,
\end{aligned}$$

where $\mathbf{u},\mathbf{v} : [0,T] \mapsto \mathbb{R}^N$ denote the state and adjoint variables ρ and q discretized in space and evaluated at each point in the time variable, and $\mathbf{u}_0$ corresponding to the initial condition $\rho_0(\mathbf{x})$. After the gradient equation is substituted into the state and adjoint equations, the vector functions $\mathbf{F}$ and $\mathbf{G}$ correspond to the following spatial terms:

$$\mathbf{F}(t,\mathbf{u},\mathbf{v}) \leftarrow \frac{\sigma^2}{2}\nabla^2\bar{\rho} + \nabla_{\mathbf{x}}\cdot\mathcal{I}\left(\bar{\rho}, -\frac{1}{\beta}\int_\Omega (\mathbf{1}_{\|\mathbf{z}-\mathbf{y}\|\le R})(\mathbf{z}-\mathbf{y})\bar{\rho}(\mathbf{y},t)\cdot\nabla_{\mathbf{y}} q(\mathbf{y},t)\,dy\right),$$

$$\begin{aligned}
\mathbf{G}(t,\mathbf{u},\mathbf{v}) \leftarrow -\frac{\sigma^2}{2}\nabla^2 q - \int_\Omega (\mathbf{1}_{\|\mathbf{x}-\mathbf{y}\|\le R})(\mathbf{x}-\mathbf{y})\bar{\rho}(\mathbf{y},t)\cdot\nabla_{\mathbf{y}} q(\mathbf{y},t)\,dy \\
- \nabla_{\mathbf{x}} q\cdot\left(\frac{1}{\beta}\int_\Omega (\mathbf{1}_{\|\mathbf{x}-\mathbf{y}\|\le R})(\mathbf{x}-\mathbf{y})\int_\Omega (\mathbf{1}_{\|\mathbf{z}-\mathbf{y}\|\le R})(\mathbf{z}-\mathbf{y})\bar{\rho}(\mathbf{y},t)\cdot\nabla_{\mathbf{y}} q(\mathbf{y},t)\,dy\,dz\right) \\
+ \nabla_{\mathbf{x}} q\cdot\left(\int_\Omega (\mathbf{1}_{\|\mathbf{x}-\mathbf{y}\|\le R})(\mathbf{x}-\mathbf{y})\bar{\rho}(\mathbf{y},t)\,dy\right) - \bar{\rho} + \widehat{\rho}.
\end{aligned}$$

As shown in Section 4.5, we obtain an iterative procedure of the form $\mathbf{x}^{(k+1)} = \mathbf{x}^{(k)} - [\mathbf{J}(\mathbf{x}^{(k)})]^{-1}\mathbf{R}(\mathbf{x}^{(k)})$, with $\mathbf{J}$ denoting the Jacobian matrix of the residual function, and we choose to explicitly state the Jacobian for our Newton–Krylov algorithm. In the code below, for the two-dimensional opinion dynamics problem with periodic boundary conditions, these quantities are denoted `JFu`, `JFv`, `JGu`, `JGv`, and our software [1] allows us to compute these quantities to spectral accuracy:

```
%% Construct F and G
function F_out = F(t,u,v)
F_out = K1(t,u,v)*u - K2(t,u,v)*v + f(t,u,v);
end
function G_out = G(t,u,v)
```

```
G_out = K3(t,u,v)*u - K4(t,u,v)*v + g(t,u,v);
end

function K1_out = K1(t,u,v)
temp1 = Conv1*( (Dx1*v).*u ) + Conv2*( (Dx2*v).*u );
temp2 = ConvVec*temp1;
K1_out = D0*L ...
            + dotVectorOperator(ConvVec*u,grad) ...
            + scalarOperator(div*(ConvVec*u))  ...
            -1/bet * ( dotVectorOperator(temp2,grad) ...
            + scalarOperator(div*temp2) );
end
function K2_out = K2(t,u,v)
K2_out = Z;
end
function K3_out = K3(t,u,v)
K3_out = -I ...
            - Conv1*scalarOperator(Dx1*v) ...
            - Conv2*scalarOperator(Dx2*v) ;
end
function K4_out = K4(t,u,v)
temp1 = Conv1*( (Dx1*v).*u ) + Conv2*( (Dx2*v).*u );
temp2 = ConvVec*temp1;
K4_out = D0*L ...
            - dotVectorOperator(ConvVec*u,grad) ...
            + 1/bet * dotVectorOperator(temp2,grad);
end

%% Specification of Jacobians
function J = JFu(t,u,v)
temp1 = Conv1*( (Dx1*v).*u ) + Conv2*( (Dx2*v).*u );
temp2 = ConvVec*temp1;
temp3 = Conv1*scalarOperator(Dx1*v) + Conv2*scalarOperator(Dx2*v);
temp4 = ConvVec*temp3;
J =  D0*L ...
        + dotVectorOperator(ConvVec*u,grad) + scalarOperator(div*(ConvVec*u)) ...
        + dotVectorOperator(grad*u,ConvVec) ...
        + scalarOperator(u) * div * ConvVec ...
        -1/bet * ( dotVectorOperator(temp2,grad) + scalarOperator(div*temp2) ...
        + dotVectorOperator(grad*u,temp4) + scalarOperator(u)*div*temp4 );
end
function J = JFv(t,u,v)
temp1 = Conv1*scalarOperator(u)*Dx1 + Conv2*scalarOperator(u)*Dx2;
temp2 = ConvVec*temp1;
J = -1/bet *  ( dotVectorOperator(grad*u,temp2) + scalarOperator(u)*div*temp2 );
end
function J = JGu(t,u,v)
temp1 = Conv1*scalarOperator(Dx1*v) + Conv2*scalarOperator(Dx2*v);
temp2 = ConvVec*temp1;
J = -I ...
        - Conv1*scalarOperator(Dx1*v) - Conv2*scalarOperator(Dx2*v) ...
        + dotVectorOperator(grad*v,ConvVec) ...
        - 1/bet * dotVectorOperator(grad*v,temp2);
end
function J = JGv(t,u,v)
temp1 = Conv1*scalarOperator(u)*(Dx1*v) + Conv2*scalarOperator(u)*(Dx2*v);
temp2 = ConvVec*temp1;
temp3 = Conv1*scalarOperator(u)*Dx1 + Conv2*scalarOperator(u)*Dx2;
temp4 = ConvVec*temp3;
J = -D0*L ...
        - ( Conv1 * scalarOperator(u) * Dx1 + Conv2 * scalarOperator(u) * Dx2 ...
            ) ...
        + dotVectorOperator(ConvVec*u,grad) ...
        -1/bet * ( dotVectorOperator(temp2,grad) ...
        + dotVectorOperator(grad*v,temp4));
end
```

All operators are spectral discretizations of relevant quantities and in more detail, `Dx1` and `Dx2` are matrices applying spatial derivatives in each direction, with `grad` corresponding to the gradient function, and `L` the Laplacian operator. The operators `Conv1` and `Conv2` apply a convolution integral in each direction, while `ConvVec` applies a convolution integral on both directions

at once. The function `scalarOperator` forms a scalar function, and `dotVectorOperator` takes an inner product of the first argument with the second argument applied to a subsequent term. Finally, `f` and `g` describe the source term of the state equation f and the desired state $\widehat{\rho}$ within the PDE operators.

For periodic boundary conditions, there is technically no boundary and the periodic property is implemented via the domain. We refer to the open-source software [1] for the structure of these boundary conditions, and [111] for a Newton–Krylov implementation. By devising routines to compute all derivatives and integration terms to spectral accuracy for particle dynamics systems, we are able to achieve rapid Newton convergence for a range of problems. We now present the numerical examples solved with the Newton–Krylov algorithm.

7.2.1 Numerical Experiments

Within our subsequent tests, we run a forward problem with no radicals to see the result of the uncontrolled state, and then run the optimization problem with a desired state. We fix $N = 20$ space points in each direction and use $n = 20$ time points, with a final time of $T = 10$. The pair (σ, R) is set at $(0.1, 0.4)$ which was determined experimentally to provide interesting dynamics. Here, we choose the norm $\|\cdot\|$ on $\mathbb{R}^2$ to be the Euclidean norm so that $\|\mathbf{x}-\mathbf{y}\| = \sqrt{(\mathbf{x}-\mathbf{y})\cdot(\mathbf{x}-\mathbf{y})}$. However, one can choose any norm, and comparison of results for different norms is an interesting extension of this work. For the following examples, we provide the initial condition for the state ρ_0, and the final condition for the adjoint q_T as the initial guess for ρ and q at all time points for the Newton–Krylov algorithm, noting that it is important to ensure the initial conditions and desired state are all periodic on the domain to preserve the periodic behaviour. We run the simulation for different values of the regularization parameter β.

2D Example 1: Uniform Initial Condition and Double Bump Target

For this example, we have the following inputs:

$$\begin{aligned}\rho_0(\mathbf{x}) &= 1,\\ q_T(\mathbf{x}) &= 0, \quad (T-t=0 \text{ at } t=T)\\ \widehat{\rho}(\mathbf{x},t) &= \sin(2\pi x_1)\sin(2\pi x_2)+2,\end{aligned}$$

where $\mathbf{x} = (x_1, x_2)$.We thus wish for a uniform distribution of opinions to develop into periodic set of clusters Figure 7.1 shows the fast convergence of the Newton–Krylov algorithm for this

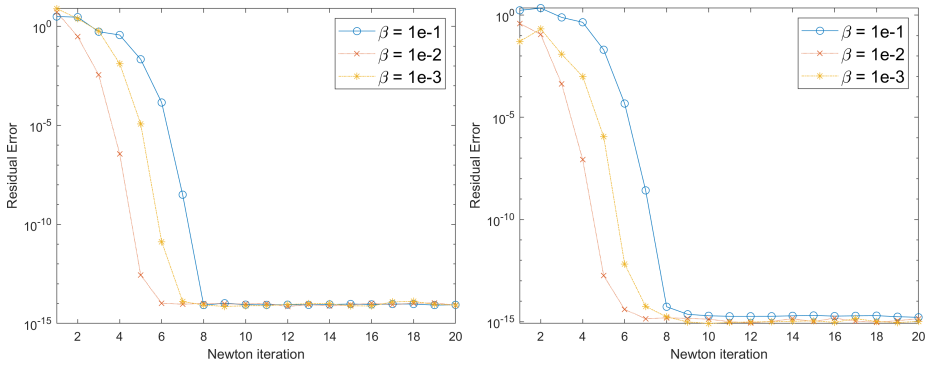

Figure 7.1: 2D Example 1: Convergence of the Newton–Krylov algorithm for an opinion dynamics problem for different values of β. Left: convergence in the state variable. Right: convergence in the adjoint variable. Convergence is measured using the residual error.

problem, for a range of β with the residual becoming $\approx 10^{-13}$ by the 10th Newton iteration. This indicates that the state and adjoint equations are satisfied accurately. We clearly see in Figure 7.2 that without a control the uniform distribution remains an approximately uniform distribution when periodic boundary conditions are imposed. During optimization, the optimal control is concentrated where the bumps in the desired state are present, and over time the control diminishes as the adjoint should be zero at time T . We also notice the periodic behaviour

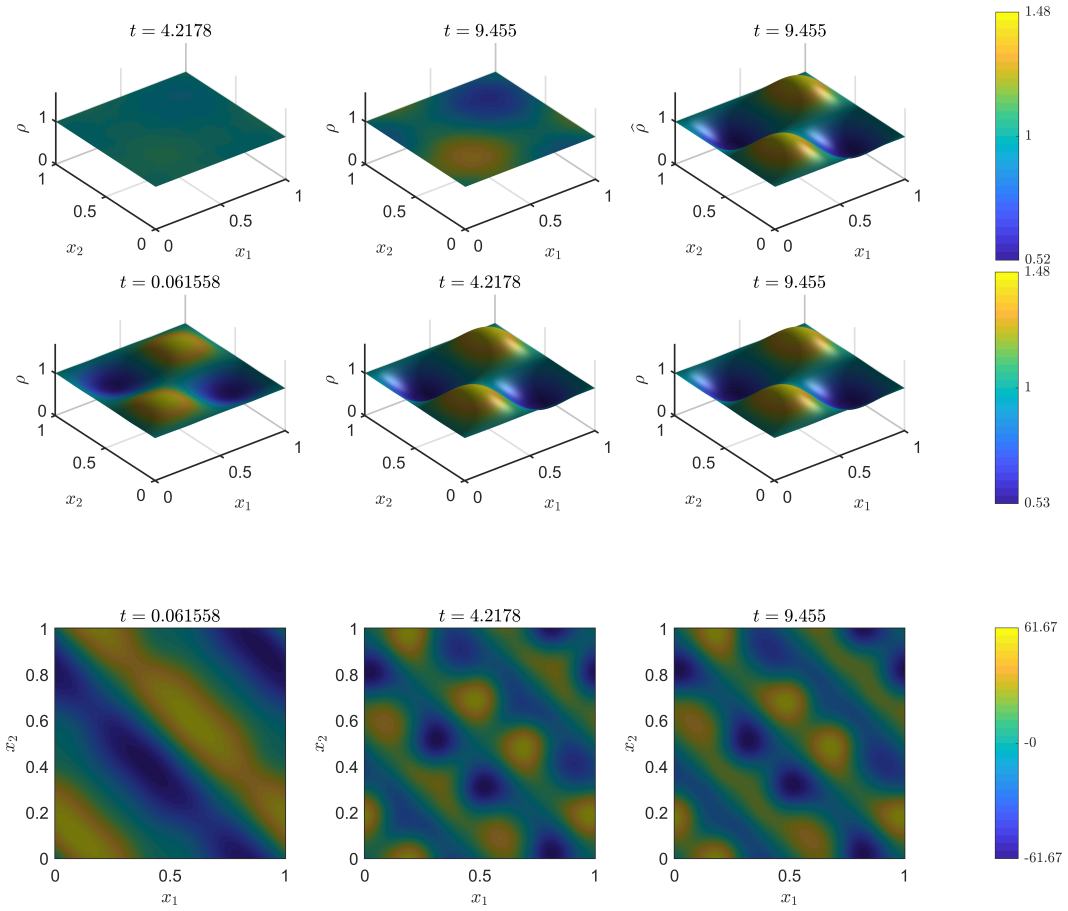

Figure 7.2: 2D Example 1: The uncontrolled forward state ρ together with the desired state $\widehat{\rho}$ (top), and the optimal state (middle) and optimal control (bottom) for periodic boundary conditions, with $\beta = 10^{-2}$.

of both the state and control. From Table 7.1, we observe that $\beta = 10^{-3}$ gives the least cost of optimization with the uncontrolled problem always costing more than the optimized problem.

2D Example 2: Double Bump Initial Condition and Uniform Target

For this example, we have the following inputs:

$$\begin{aligned} \rho_0(\mathbf{x}) &= \sin(2\pi x_1)\sin(2\pi x_2) + 2, \\ q_T(\mathbf{x}) &= 0, \\ \widehat{\rho}(\mathbf{x}, t) &= 1. \end{aligned}$$

This example is in some sense the reverse of Example 1, where we start with clusters and wish to move towards a uniform state. The residual errors for the Newton–Krylov algorithm similarly tend approximately to 10^{-13} by the 10th Newton iteration, reaching this point by

	$\beta = 10^{-1}$	$\beta = 10^{-2}$	$\beta = 10^{-3}$
$\mathcal{J}_c$	0.4608	0.1778	0.0635
`Iter`	8	5	7
`Time Taken`	729.2981	641.0903	609.5219

Table 7.1: 2D Example 1: Optimal control cost, number of iterations required, and time taken for Newton–Krylov algorithm to converge for a range of β.

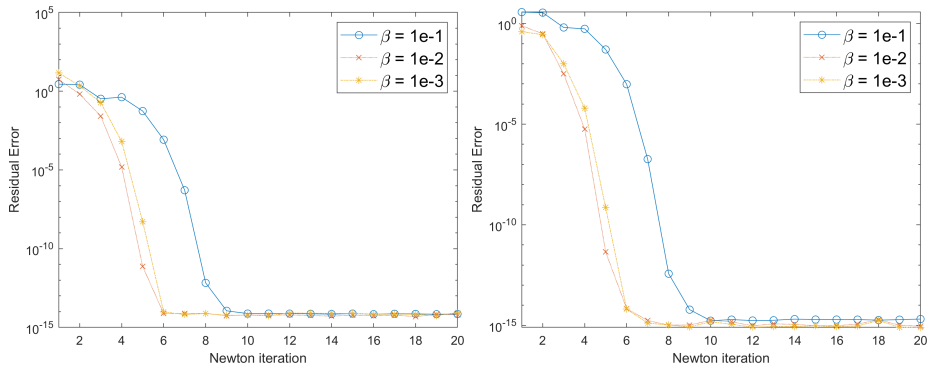

Figure 7.3: 2D Example 2: Convergence of the Newton–Krylov algorithm for an opinion dynamics problem for different values of β. Left: convergence in the state variable. Right: convergence in the adjoint variable. Convergence is measured using the residual error.

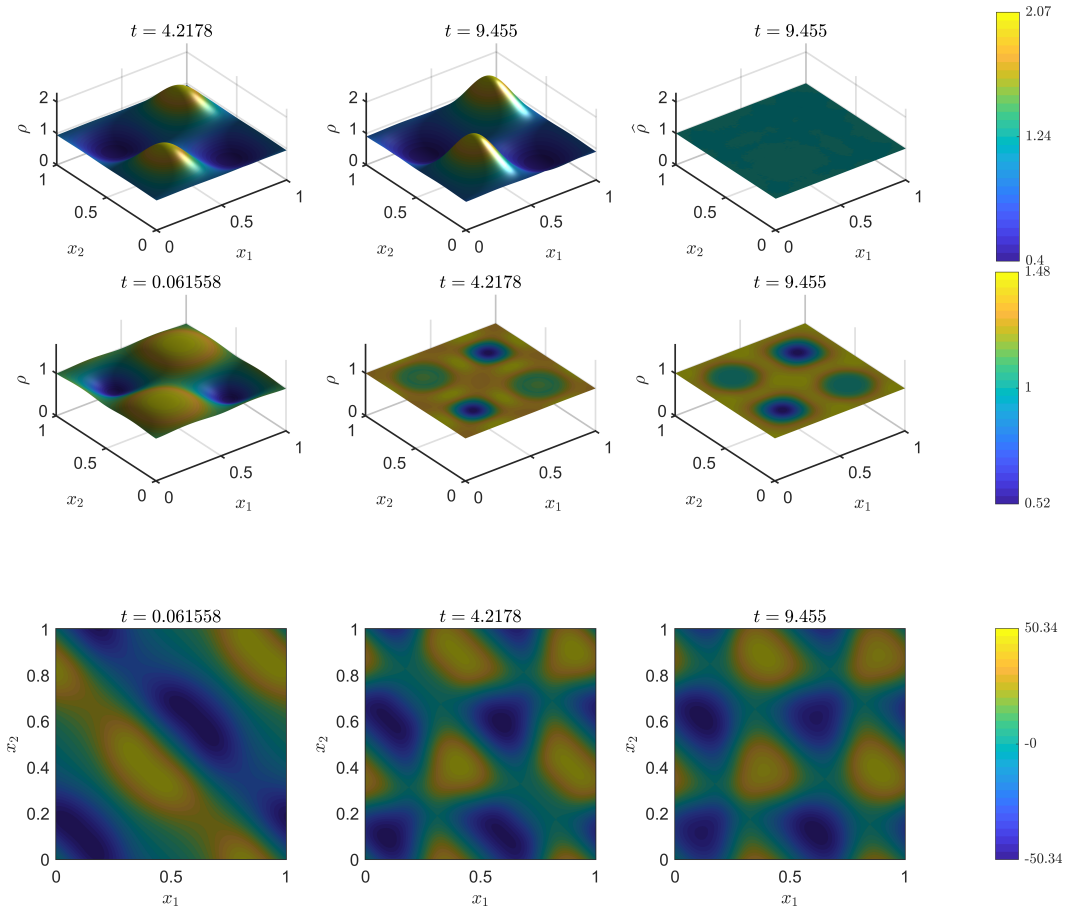

Figure 7.4: 2D Example 2: The uncontrolled forward state ρ together with the desired state $\widehat{\rho}$ (top), the optimal state (middle), and the optimal control (bottom) for a problem with periodic boundary conditions, with $\beta = 10^{-2}$.

the 6th iteration when β is 10^{-2} and 10^{-3}. Figure 7.4 shows very interesting behaviour of the optimal control for this problem where it is concentrated at the positions of the bumps

	$\beta = 10^{-1}$	$\beta = 10^{-2}$	$\beta = 10^{-3}$
$\mathcal{J}_c$	0.2818	0.1015	0.0401
`Iter`	9	6	6
`Time Taken`	509.3018	621.0285	438.3823

Table 7.2: 2D Example 2: Optimal control cost, number of iterations required, and time taken for Newton–Krylov algorithm to converge for a range of β.

for earlier times and afterwards acts in a 'grid-like' style, over the domain to achieve closeness to the uniform desired state. We also observe that the optimal state achieves dips where the bumps were positioned in its initial condition, suggesting that more control is applied where the bumps were. From the uncontrolled state, we see that the bumps grow larger with time when no control is imposed, hence significant control may be needed to reverse the natural growth. From Table 7.2, we see that the cost of optimization is the lowest when $\beta = 10^{-3}$ suggesting that smaller values of β will cause radicals that are perhaps bigger than the state distribution to be applied. The Newton–Krylov algorithm also proves to be fast, solving such a numerically challenging problem in between 150 and 300 seconds on an HP Pavillion laptop running Windows 11, Intel Core i5-8250U 1.80GHz, 8 GB RAM.

The numerical examples for our 2D opinion dynamics optimization problems indicate the effectiveness of the Newton–Krylov method for difficult problems, and the realistic dynamics of opinion behaviour in an optimal control setting. There are many interesting extensions to this work including theoretical questions on existence and uniqueness of optimal controls for this problem, solving 3D versions of the examples with the Newton–Krylov algorithm, adding bound constraints in the 2D and 3D problem (recent work in [188] explore an preconditioned inexact Active-Set method for non-linear optimal control problems that could be applied here), comparing results using different norms in evaluating the non-local term, and applying no-flux type boundary conditions. In the next section, we present a robot swarming optimization problem that is also solved using the Newton–Krylov algorithm.

7.3 Robot Swarming Optimization Problem

In the numerical examples to follow, we follow work presented in [269] on spatial coverage tasks by stochastic robotic swarms in which techniques are applied to optimize coverage performance. They consider a crop pollination scenario, where several rows of flowers are to be pollinated by a swarm of N microaerial vehicles and the objective which must be completed in time T is to achieve a target spatial pollination distribution $\widehat{\rho}(\mathbf{x})$, where $\mathbf{x} \in \Omega$. The swarm originates from a location in the field called the hive, and the robots are assumed to have sufficient power to undertake brief flights from the hive. They return to the hive to recharge after a complete flight. Each robot is equipped with a compass and thus can fly with a specified heading. However, the robots cannot communicate among themselves. A computer in the hive serves as a supervisory agent and calculates the parameters of the robots' motion and state transitions prior to their flight. The robots actions are modelled as an advection-diffusion PDE. It is straightforward to model the objective problem as a PDE-constrained optimization problem and use the rapidly converging Newton–Krylov method to solve the optimality system. Applying our numerical algorithms to this application also demonstrates the versatility of our numerical framework and the potential it possesses to be applied to other areas of multiscale particle dynamics.

The robot swarming model we consider is (see [269] for derivation):

$$\partial_t \rho_1 = -\boldsymbol{\nu} \cdot \nabla \rho_1 + D\nabla^2 \rho_1 - \sum_{j=1}^{n_f} k_j L_j \rho_1 + k_f \rho_2, \tag{7.1}$$

$$\partial_t \rho_2 = \sum_{j=1}^{n_f} k_j L_j \rho_1 - k_f \rho_2,$$

$$\partial_t \rho_3 = \sum_{j=1}^{n_f} k_j L_j \rho_1,$$

$$D\frac{\partial \rho_1}{\partial n} = \rho_1 \boldsymbol{\nu} \cdot \mathbf{n} \quad \text{on} \quad \partial Q, \tag{7.2}$$

$$\rho_1(\mathbf{x}, 0) = G_\delta(\mathbf{x} - X_0), \quad \rho_2(\mathbf{x}, 0) = 0, \quad \rho_3(\mathbf{x}, 0) = 0, \tag{7.3}$$

where $Q = \Omega \times (0, T)$ and $\Omega \subset \mathbb{R}^2$ represents a crop field. The robots' density is separated into ρ_1, the density of robots flying and ρ_2, the density of robots hovering (pollinating), while ρ_3 is the density of cumulative pollination.. The vector $\boldsymbol{\nu}(t) = (\nu_1(t), \nu_2(t))^T$ is the velocity of robots, $k_j(t), j = 1, 2, \ldots, n_f$ corresponds to the time dependent probability per unit time to pause at a crop of type j, n_f denotes the number of crop types, and k_f is the fixed probability per unit time to resume flying (determined by the time taken to pollinate). The parameter $L_j(\mathbf{x}), j = 1, 2, \ldots, n_f$, indicates if a robot is over region of crop type j, and D is the diffusion co-efficient, and $G_\delta(\mathbf{x} - X_0)$ is an initial distribution. The first equation in (7.1) therefore describes the time evolution of the density of flying robots affected by diffusion and advection terms, excluding the robots that have stopped over a crop, and including those that have resumed flying. The second equation describes the time evolution of the density of robots hovering over a crop which includes the robots that have stopped over a crop and excluding those that have resumed flying. The time evolution of the cumulative pollination is described by the third equation and takes into account the robots that hve stopped flying and are hovering over a crop to pollinate it. Equation (7.2) describes a no-flux type boundary condition on the density of flying robots and (7.3) provides the initial conditions for the three states.

7.3.1 Robot Swarming Optimization Problem and First Order Optimality Conditions

We consider the following optimization problem:

$$\min_{(\rho, \mathbf{u})} \mathcal{J}(\rho, \mathbf{u}) = \frac{1}{2}\|\rho_3 - \widehat{\rho}\|^2_{L^2([0,T]\times\mathbb{R}^2)} + \frac{\beta}{2}\|\mathbf{u}\|^2_{L^2(0,T)^\kappa}, \quad \kappa = n_f + 2,$$

subject to (7.1), (7.2), and (7.3).

The target pollination coverage denoted as $\widehat{\rho}(\mathbf{x}, t)$ is space and time-dependent compared to the space-dependent target $\rho_\Omega(\mathbf{x})$ considered in [269], and the control variable, $\mathbf{u} := (u_1, u_2, \ldots, u_{n_f+2})$, $u_1 = \nu_1$, $u_2 = \nu_2$, $u_{j+2} = k_j$, where $k_j \Delta t \leq 1$, $j = 1, 2, \ldots, n_f$, is only time-dependent. We introduce Lagrange multipliers q_1, q_2, q_3 which correspond to the state variables ρ_1, ρ_2, and ρ_3 respectively on the interior of the domain, and q_4 which corresponds to ρ_1 on the boundary, and write the Lagrangian formally as :

$$\begin{aligned}
\mathcal{L}(\rho_1, \rho_2, \rho_3, \mathbf{u}, q_1, q_2, q_3, q_4) = {} & \frac{1}{2}\int_0^T \int_\Omega (\rho_3 - \widehat{\rho})^2 \, dxdt + \frac{\beta}{2}\int_0^T \|\mathbf{u}\|^2 \, dt \\
& - \int_0^T \int_\Omega \left(\frac{\partial \rho_1}{\partial t} + \boldsymbol{\nu} \cdot \nabla \rho_1 - D\nabla^2 \rho_1 + \sum_{j=1}^{n_f} k_j L_j \rho_1 - k_f \rho_2 \right) q_1 \, dxdt \\
& - \int_0^T \int_\Omega \left(\frac{\partial \rho_2}{\partial t} - \sum_{j=1}^{n_f} k_j L_j \rho_1 + k_f \rho_2 \right) q_2 \, dxdt \\
& - \int_0^T \int_\Omega \left(\frac{\partial \rho_3}{\partial t} - \sum_{j=1}^{n_f} k_j L_j \rho_1 \right) q_3 \, dxdt \\
& - \int_0^T \int_{\partial\Omega} \left(D\frac{\partial \rho_1}{\partial n} - \rho_1 \boldsymbol{\nu} \cdot \mathbf{n} \right) q_4 \, dsdt.
\end{aligned}$$

Here again, the optimal states $\bar{\rho_1}, \bar{\rho_2}, \bar{\rho_3}$ and control $\bar{\mathbf{u}}$ should satisfy the first-order optimality conditions:

$$\begin{aligned}
&\mathcal{D}_q\mathcal{L}(\bar{\rho_1}, \bar{\rho_2}, \bar{\rho_3}, \bar{\mathbf{u}}, q_1, q_2, q_3, q_4)h = 0, \quad q = (q_1, q_2, q_3, q_4), \quad \forall h \in L^2(0, T; H^1(\Omega)),\\
&\mathcal{D}_{\rho_1}\mathcal{L}(\bar{\rho_1}, \bar{\rho_2}, \bar{\rho_3}, \bar{\mathbf{u}}, q_1, q_2, q_3, q_4)h = 0 \quad \forall h \in L^2(0, T; H^1(\Omega)),\\
&\mathcal{D}_{\rho_2}\mathcal{L}(\bar{\rho_1}, \bar{\rho_2}, \bar{\rho_3}, \bar{\mathbf{u}}, q_1, q_2, q_3, q_4)h = 0 \quad \forall h \in L^2(0, T; H^1(\Omega)),\\
&\mathcal{D}_{\rho_3}\mathcal{L}(\bar{\rho_1}, \bar{\rho_2}, \bar{\rho_3}, \bar{\mathbf{u}}, q_1, q_2, q_3, q_4)h = 0 \quad \forall h \in L^2(0, T; H^1(\Omega)),\\
&\mathcal{D}_{\mathbf{u}}\mathcal{L}(\bar{\rho_1}, \bar{\rho_2}, \bar{\rho_3}, \bar{\mathbf{u}}, q_1, q_2, q_3, q_4)\mathbf{h} = 0 \quad \forall \mathbf{h} \in L^2(0, T)^d.
\end{aligned}$$

The optimality conditions with respect to the adjoint variables recover the state equations (7.1), (7.2), and (7.3):

$$\begin{aligned}
\partial_t\bar{\rho_1} &= -\boldsymbol{\nu}\cdot\nabla\bar{\rho_1} + D\nabla^2\bar{\rho_1} - \sum_{j=1}^{n_f} k_j L_j \bar{\rho_1} + k_f\bar{\rho_2},\\
\partial_t\bar{\rho_2} &= \sum_{j=1}^{n_f} k_j L_j \bar{\rho_1} - k_f\bar{\rho_2},\\
\partial_t\bar{\rho_3} &= \sum_{j=1}^{n_f} k_j L_j \bar{\rho_1} \quad \text{in } Q,\\
D\frac{\partial\bar{\rho_1}}{\partial n} &= \bar{\rho_1}\boldsymbol{\nu}\cdot\mathbf{n} \quad \text{on} \quad \partial Q,\\
\bar{\rho_1}(\mathbf{x}, 0) &= G_\delta(\mathbf{x} - X_0), \quad \bar{\rho_2}(\mathbf{x}, 0) = 0, \quad \bar{\rho_1}(\mathbf{x}, 0) = 0.
\end{aligned}$$

We now focus on the Fréchet derivative with respect to the state variables starting with ρ_1 and written as:

$$\begin{aligned}
\mathcal{D}_{\rho_1}\mathcal{L}(\rho_1, \rho_2, \rho_3, \mathbf{u}, q_1, q_2, q_3, q_4)h = &-\int_0^T\int_\Omega \left(\frac{\partial h}{\partial t} + \boldsymbol{\nu}\cdot\nabla h - D\nabla^2 h + \sum_{j=1}^{n_f} k_j L_j h\right) q_1\, dxdt\\
&-\int_0^T\int_\Omega \left(-\sum_{j=1}^{n_f} k_j L_j h\right) q_2\, dxdt\\
&-\int_0^T\int_\Omega \left(-\sum_{j=1}^{n_f} k_j L_j h\right) q_3\, dxdt\\
&-\int_0^T\int_{\partial\Omega} \left(D\frac{\partial h}{\partial n} - h\boldsymbol{\nu}\cdot\mathbf{n}\right) q_4\, dsdt.
\end{aligned}$$

We then make h the subject to obtain

$$\begin{aligned}
\mathcal{D}_{\rho_1}\mathcal{L}(\rho_1, \rho_2, \rho_3, \mathbf{u}, q_1, q_2, q_3, q_4)h = &-\int_0^T\int_\Omega \left(-\frac{\partial q_1}{\partial t} - \nabla\cdot(q_1\boldsymbol{\nu}) - D\nabla^2 q_1 + \sum_{j=1}^{n_f} k_j L_j q_1\right) h\, dxdt\\
&-\int_\Omega q_1(\mathbf{x}, T)h(\mathbf{x}, T) - q_1(\mathbf{x}, 0)h(\mathbf{x}, 0)\, dx\\
&+\int_0^T\int_{\partial\Omega} -Dh\frac{\partial q_1}{\partial n} + Dq_1\frac{\partial h}{\partial n} - hq_1\nu\cdot n\, dsdt\\
&-\int_0^T\int_\Omega \left(-\sum_{j=1}^{n_f} k_j L_j q_2\right) h\, dxdt
\end{aligned}$$

$$-\int_0^T\int_\Omega\left(-\sum_{j=1}^{n_f}k_jL_jq_3\right)h\,dxdt$$
$$-\int_0^T\int_{\partial\Omega}\left(D\frac{\partial h}{\partial n}-h\boldsymbol{\nu}\cdot\mathbf{n}\right)q_4\,dsdt.$$

For a stationary point, the optimal state $(\bar{\rho_1},\bar{\rho_2},\bar{\rho_3})$ and control $\bar{\mathbf{u}}$ must satisfy

$$\mathcal{D}_{\rho_1}\mathcal{L}(\bar{\rho_1},\bar{\rho_2},\bar{\rho_3},\bar{\mathbf{u}},q_1,q_2,q_3,q_4)h=0\quad\forall h\in L^2(0,T;H^1(\Omega)).$$

In particular, if we choose $h(\mathbf{x},t)\in C_0^\infty(Q)$ such that $h|_{\partial Q}=0=\dfrac{\partial h}{\partial n}|_{\partial Q}$ and $h(\mathbf{x},0)=h(\mathbf{x},T)=0$, we have that

$$-\int_0^T\int_\Omega\left(-\frac{\partial q_1}{\partial t}-\nabla\cdot(q_1\boldsymbol{\nu})-D\nabla^2q_1+\sum_{j=1}^{n_f}k_jL_jq_1\right)h\,dxdt$$
$$-\int_0^T\int_\Omega\left(-\sum_{j=1}^{n_f}k_jL_jq_2\right)h\,dxdt-\int_0^T\int_\Omega\left(-\sum_{j=1}^{n_f}k_jL_jq_3\right)h\,dxdt=0$$

and by the Fundamental Lemma of the Calculus of Variations, we obtain the first adjoint equation:

$$\partial_tq_1=-\nabla\cdot(q_1\boldsymbol{\nu})-D\nabla^2q_1+\sum_{j=1}^{n_f}\bar{k}_jL_jq_1-\sum_{j=1}^{n_f}\bar{k}_jL_jq_2-\sum_{j=1}^{n_f}\bar{k}_jL_jq_3.$$

If we drop the condition $h=0$ at $t=T$ then we get the final time condition for q_1 as

$$q_1(\mathbf{x},T)=0.$$

Now, dropping the condition $\dfrac{\partial h}{\partial n}$ on the boundary of Q, together with the adjoint equation and final time condition, gives the relationship:

$$q_1=q_4,$$

and for all other h, we obtain the boundary condition:

$$D\frac{\partial q_1}{\partial n}=0\quad\text{on}\quad\partial Q.$$

We move on to the derivative with respect to q_2. We obtain that

$$\mathcal{D}_{\rho_2}\mathcal{L}(\rho_1,\rho_2,\rho_3,\mathbf{u},q_1,q_2,q_3,q_4)h=-\int_0^T\int_\Omega-k_fhq_1\,dxdt-\int_0^T\int_\Omega\left(\frac{\partial h}{\partial t}+k_fh\right)q_2\,dxdt$$

Making h the subject and using the same arguments as for q_1, we obtain the second adjoint equation with final time condition:

$$\partial_tq_2=k_f(-q_1+q_2),\quad q_2(\mathbf{x},T)=0.$$

Also, for the derivative with respect to q_3, we get that

$$\mathcal{D}_{\rho_3}\mathcal{L}(\rho_1,\rho_2,\rho_3,\mathbf{u},q_1,q_2,q_3,q_4)h=\int_0^T\int_\Omega(\rho_3-\widehat{\rho})h\,dxdt-\int_0^T\int_\Omega\frac{\partial h}{\partial t}q_3\,dxdt.$$

Making h the subject and applying the same arguments about the choices of h gives the third

adjoint equation with final time condition:

$$\partial_t q_3 = -\bar{\rho_3} + \widehat{\rho}, \quad q_3(\mathbf{x}, T) = 0.$$

Finally, we consider the derivative with respect to the control $\mathbf{u}$. We split the derivative into two components, one with respect to the velocity $\boldsymbol{\nu}$ and the other with respect to $(k_1, k_2, \ldots, k_{n_f})$. The derivative with respect to $\boldsymbol{\nu}$, neglecting data on $\partial\Omega$ gives:

$$\mathcal{D}_{\boldsymbol{\nu}}\mathcal{L}(\rho_1, \rho_2, \rho_3, \mathbf{u}, q_1, q_2, q_3, q_4)\mathbf{h} = \beta \int_0^T \mathbf{h} \cdot \boldsymbol{\nu}| \, dt - \int_0^T \int_\Omega q_1 \mathbf{h} \cdot \nabla \rho_1 \, dxdt.$$

The optimal state $\bar{\rho_1}$ and velocity $\bar{\boldsymbol{\nu}}$ should satisfy $\mathcal{D}_{\boldsymbol{\nu}}\mathcal{L}(\bar{\rho_1}, \bar{\rho_2}, \bar{\rho_3}, \bar{\mathbf{u}}, q_1, q_2, q_3, q_4)\mathbf{h} = \mathbf{0}$ for all $\mathbf{h}$ in $\left(L^2(0,T)\right)^2$, which by the Fundamental Lemma of Calculus implies that

$$\beta\bar{\boldsymbol{\nu}} - \int_\Omega q_1 \nabla \bar{\rho_1} = \mathbf{0}.$$

Now, we obtain the following for the derivative with respect to k_j:

$$\mathcal{D}_{k_j}\mathcal{L}(\rho_1, \rho_2, \rho_3, \mathbf{u}, q_1, q_2, q_3, q_4)h = \beta \int_0^T h_j k_j \, dt + \int_0^T \int_\Omega -h_j L_j \rho_1 q_1 + h_j L_j \rho_1 q_2 + h_j L_j \rho_1 q_3 \, dxdt,$$

for $j = 1, 2, \ldots, n_f$. The optimal variables then satisfy

$$\beta\bar{k}_j + \int_\Omega L_j \bar{\rho_1}(-q_1 + q_2 + q_3) \, dx = 0, \quad j = 1, 2, \ldots, n_f.$$

Altogether we obtain the optimality system:

$$\begin{aligned}
\partial_t \bar{\rho_1} &= -\bar{\boldsymbol{\nu}} \cdot \nabla \bar{\rho_1} + D\nabla^2 \bar{\rho_1} - \sum_{j=1}^{n_f} \bar{k}_j L_j \bar{\rho_1} + k_f \bar{\rho_2} \quad \text{in } Q, \\
\partial_t \bar{\rho_2} &= \sum_{j=1}^{n_f} \bar{k}_j L_j \bar{\rho_1} - k_f \bar{\rho_2} \quad \text{in } Q, \\
\partial_t \bar{\rho_3} &= \sum_{j=1}^{n_f} \bar{k}_j L_j \bar{\rho_1} \quad \text{in } Q, \\
D\frac{\partial \bar{\rho_1}}{\partial n} &= \bar{\rho_1}\bar{\boldsymbol{\nu}} \cdot \mathbf{n} \quad \text{on } \partial Q, \\
\bar{\rho_1}(x,0) &= G_\delta(x - X_0), \quad \bar{\rho_2}(x,0) = 0, \quad \bar{\rho_3}(x,0) = 0,
\end{aligned}$$

$$\begin{aligned}
\partial_t q_1 &= -\nabla \cdot (q_1 \bar{\boldsymbol{\nu}}) - D\nabla^2 q_1 + (q_1 - q_2 - q_3) \sum_{j=1}^{n_f} \bar{k}_j L_j \quad \text{in } Q, \\
\partial_t q_2 &= k_f(-q_1 + q_2) \quad \text{in } Q, \\
\partial_t q_3 &= -\bar{\rho_3} + \widehat{\rho}, \quad \text{in } Q, \\
D\frac{\partial q_1}{\partial n} &= 0 \quad \text{on } \partial Q, \\
q_1(x,T) &= 0, \quad q_2(x,T) = 0, \quad q_3(x,T) = 0,
\end{aligned}$$

$$\begin{aligned}
\beta\bar{\boldsymbol{\nu}} - \int_\Omega q_1 \nabla \bar{\rho_1} \, dx &= \mathbf{0} \quad \text{in } Q, \\
\beta\bar{k}_j + \int_\Omega L_j \bar{\rho_1}(-q_1 + q_2 + q_3) \, dx &= 0, \quad j = 1, 2, \ldots, n_f \quad \text{in } Q.
\end{aligned}$$

After obtaining the optimality system, we now solve it numerically using the Newton–Krylov

algorithm together with the pseudospectral discretization from our 2DChebClass PDECO software.

7.3.2 Newton–Krylov Equations

Here, we first substitute the gradient equations into the state and adjoint equations, noting that the optimal states $\bar{\rho_1}, \bar{\rho_2}$ and $\bar{\rho_3}$ satisfy the following:

$$\begin{aligned}
\partial_t \rho_1 &= -\frac{1}{\beta}\nabla\rho_1 \cdot \left(\int_\Omega q_1 \nabla\rho_1 \, dx\right) + D\nabla^2\rho_1 \\
&\quad + \frac{1}{\beta}\rho_1 \left(\sum_{j=1}^{n_f} L_j \int_\Omega L_j \rho_1(-q_1+q_2+q_3)\, d\mathbf{x}\right) + k_f\rho_2, \\
\partial_t \rho_2 &= -\frac{1}{\beta}\rho_1 \left(\sum_{j=1}^{n_f} L_j \int_\Omega L_j \rho_1(-q_1+q_2+q_3)\, dx\right) - k_f\rho_2, \\
\partial_t \rho_3 &= -\frac{1}{\beta}\rho_1 \left(\sum_{j=1}^{n_f} L_j \int_\Omega L_j \rho_1(-q_1+q_2+q_3)\, dx\right), \\
D\frac{\partial\rho_1}{\partial n} &= \frac{1}{\beta}\left(\rho_1 \int_\Omega q_1\nabla\rho_1 \, ds\right)\cdot\mathbf{n} \quad \text{on } \partial Q, \\
\rho_1(\mathbf{x},0) &= G_\delta(\mathbf{x}-X_0), \quad \rho_2(\mathbf{x},0)=0, \quad \rho_3(\mathbf{x},0)=0,
\end{aligned}$$

$$\begin{aligned}
\partial_t q_1 &= -\frac{1}{\beta}\nabla\cdot\left(q_1\int_\Omega q_1\nabla\rho_1\, dx\right) \\
&\quad - D\nabla^2 q_1 + \frac{1}{\beta}(-q_1+q_2+q_3)\left(\sum_{j=1}^{n_f} L_j \int_\Omega L_j\rho_1(-q_1+q_2+q_3)\, dx\right), \\
\partial_t q_2 &= k_f(-q_1+q_2), \\
\partial_t q_3 &= -\rho_3 + \widehat{\rho}, \quad \text{on } Q, \\
D\frac{\partial q_1}{\partial n} &= 0 \quad \text{on} \quad \partial Q \\
q_1(\mathbf{x},T) &= 0, \quad q_2(\mathbf{x},T)=0, \quad q_3(\mathbf{x},T)=0.
\end{aligned}$$

The residual functions are written as:

$$\begin{aligned}
\mathbf{F} &= (F_1,F_2,F_3) = K_1\mathbf{u} - K_2\mathbf{v} \\
\mathbf{G} &= (G_1,G_2,G_3) = K_3\mathbf{u} - K_4\mathbf{v} + \mathbf{g}
\end{aligned}$$

with $\mathbf{u} = (u_1,u_2,u_3)$ corresponding to the state variables ρ_1,ρ_2, and ρ_3 and $\mathbf{v} = (v_1,v_2,v_3)$ corresponding to the adjoint variables q_1, q_2, and q_3. Here, F_1, F_2, and F_3 represent the first, second, and third state equations respectively while G_1, G_2, and G_3 represent the first, second, and third adjoint equations respectively. The function g corresponds to the target variable $\widehat{\rho}$. The Jacobian with respect to the state variable in the direction $\mathbf{h} = (h_1,h_2,h_3)$ is written analytically as:

$$\begin{aligned}
JF_1(\mathbf{u})\mathbf{h} &= D\nabla^2 h_1 - \frac{1}{\beta}\nabla h_1 \cdot \left(\int_\Omega q_1\nabla\rho_1\, dx\right) - \frac{1}{\beta}\nabla\rho_1\cdot\left(\int_\Omega q_1\nabla h_1\, dx\right) \\
&\quad + \frac{1}{\beta}h_1\left(\sum_{j=1}^{n_f} L_j\int_\Omega L_j\rho_1(-q_1+q_2+q_3)\, dx\right) \\
&\quad + \frac{1}{\beta}\rho_1\left(\sum_{j=1}^{n_f} L_j\int_\Omega L_j h_1(-q_1+q_2+q_3)\, dx\right) + k_f h_2,
\end{aligned}$$

$$
\begin{aligned}
D\frac{\partial h_1}{\partial n} &= \frac{1}{\beta}\left(h_1\int_\Omega q_1\nabla\rho_1\,ds + \rho_1\int_\Omega q_1\nabla h_1\,ds\right)\cdot\mathbf{n} \quad \text{on } \partial Q,\\
JF_2(\mathbf{u})\mathbf{h} &= -\frac{1}{\beta}h_1\left(\sum_{j=1}^{n_f}L_j\int_\Omega L_j\rho_1(-q_1+q_2+q_3)\,dx\right)\\
&\quad -\frac{1}{\beta}\rho_1\left(\sum_{j=1}^{n_f}L_j\int_\Omega L_j h_1(-q_1+q_2+q_3)\,dx\right) - k_f\rho_2,\\
JF_3(\mathbf{u})\mathbf{h} &= -\frac{1}{\beta}h_1\left(\sum_{j=1}^{n_f}L_j\int_\Omega L_j\rho_1(-q_1+q_2+q_3)\,dx\right)\\
&\quad -\frac{1}{\beta}\rho_1\left(\sum_{j=1}^{n_f}L_j\int_\Omega L_j h_1(-q_1+q_2+q_3)\,dx\right).
\end{aligned}
$$

We implement these Jacobians in our code in a similar way as shown in the code snippet in Section 7.2. We now present numerical results for the 2D robotics optimization problem.

7.3.3 Numerical Experiments

We now apply the above methodology to a robot swarming example. We have a crop field with spatial domain $[0,1]\times[0,1]$ and a simulation up to final time, $T=1$. For simplicity, we choose only one type of flower for our numerical simulations, hence $n_f=1$. We choose the following initial condition for ρ_1:

$$G_\delta(x_1,x_2) = Z^{-1}\exp(1/\left((x_1-0.4)^2+(x_2-0.2)^2\right)),$$

where $\mathbf{x}=(x_1,x_2)$ and Z is a normalization constant such that $\int_\Omega G_\delta(x_1,x_2)d\mathbf{x}=1$. This initial condition is a smooth bump centred around the spatial point $(0.4,0.2)$. We then choose the desired state to be

$$\widehat{\rho} = 0.5\exp\left(-((x_1-0.75)^2+(x_2-0.75)^2)/2(0.2)^2\right),$$

another smooth bump centred on $(0.75,0.75)$. We use $n=21$ points in time and $N=10$ points in each spatial direction. We display the results for $\beta=10^{-2}$ for the diffusion constant $D=0.5$ and $D=1$. The problem becomes numerically challenging for smaller D as preventing the robots from diffusing freely over the domain restricts the extent to which they can pollinate the entire field and the problem becomes advection dominated.

2D Example 1: $D=1$

We see from the convergence plots in Figure 7.5 that the Newton–Krylov algorithm converges in 4,7, and 10 iterations for $\beta=1,10^{-1}$ and 10^{-2} respectively. This emphasizes the efficiency of the algorithm. We also see from Table 7.3 that the simulation takes at most 11 minutes to complete which is impressive for the scale of the problem as it is a system of altogether six state and adjoint equations. For the optimal states plots in Figure 7.6, we see the robots originating from one corner of the field $\mathbf{x}=(0,0)$ as shown in the plot for ρ_1, and hovering around another corner of the field $\mathbf{x}=(1,1)$, as seen in the plot for ρ_2, in order to attain the pollination density ρ_3 that is close to the desired state $\widehat{\rho}$. We see from the time probability graph of k_1 that with higher values of β, the probability of a robot to stop flying and hover over a flower in the field is high for earlier times, and decreases over time. Interestingly for $\beta=10^{-2}$, which has the lowest optimization cost as shown in Table 7.3, the probability is relatively high for all times, suggesting that increasing the number of times robots stop and pollinate positively affect achieving the desired state. The magnitude of the optimal velocity in Figure 7.7 starts off at $\|\boldsymbol{\nu}\|=0.12$ and sharply decreases to almost zero, also suggesting that it is only necessary for the robots to have more velocity at the start of the journey to reach the target the area they have to pollinate and rapidly slow down for the rest of the time left.

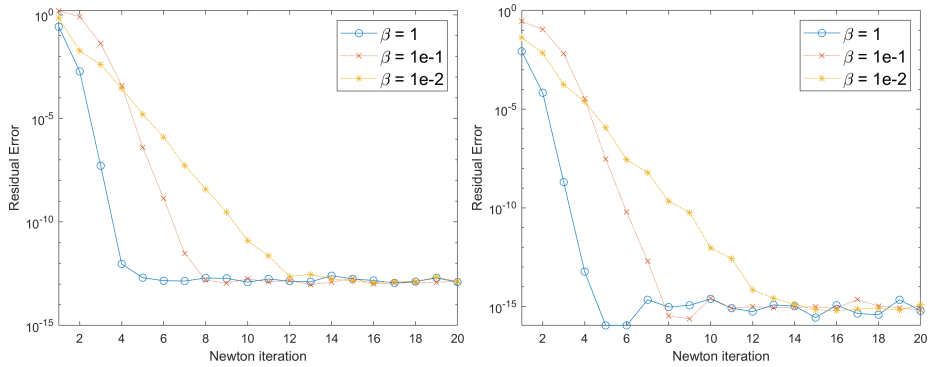

Figure 7.5: 2D Example 1: Convergence of the Newton–Krylov algorithm for a robots swarming problem with $D = 1$, and different values of β. Left: convergence in the state variable. Right: convergence in the adjoint variable. Convergence is measured using the residual error.

	$\beta = 1$	$\beta = 10^{-1}$	$\beta = 10^{-2}$
$\mathcal{J}_c$	0.0140	0.0110	0.0049
`Iter`	4	6	7
`Time Taken`	308.8120	428.7467	601.6953

Table 7.3: 2D Example 1: Optimal control cost, number of iterations required, and time taken for Newton–Krylov algorithm to converge for a range of β.

2D Example 2: $D = 0.5$

For $D = 0.5$, we see similar results to that of $D = 1$, except that for ρ_1, we observe that the robots do not spread as quickly over the domain. This is understandable as their diffusion properties are more restricted in this case. The optimal velocity also possesses similar behaviour, being its highest at the start of the journey and rapidly decreasing to a smaller value for the rest of the simulation. It also becomes clear that the case $D = 0.5$ is a more difficult problem to solve to $D = 1$. We see this in Table 7.4, where the optimization cost is slightly larger for all values of β compared to Table 7.3. Despite the increase in difficulty of solving the optimality system for $D = 0.5$, the Newton–Krylov method remains fast, converging in at most 12 minutes. algorithm converges.

7.4 Outlook

We observe that the Newton–Krylov algorithm is effective for difficult problems from opinion dynamics and robotics. Generally, we deduce that the higher-order Newton–Krylov method converges faster compared to the fixed-point algorithm, as the convergence times for similar 2D opinion dynamics problems are smaller in this chapter compared to that of the 1D opinion dynamics problems in Chapter 6. Questions that can be investigated following the work in this chapter include: existence and uniqueness of optimal controls for higher-order opinion dynamics and swarming optimization problems, introduction of bound constraints that can be tackled with a combination of an Active-Set strategy and the Newton–Krylov method, and alternative discretizations to the pseudospectral method that may perform better with non-

	$\beta = 1$	$\beta = 10^{-1}$	$\beta = 10^{-2}$
$\mathcal{J}_c$	0.0141	0.0112	0.0052
`Iter`	4	7	10
`Time Taken`	361.4393	510.2931	709.1298

Table 7.4: 2D Example 2: Optimal control cost, number of iterations required, and time taken for Newton–Krylov algorithm to converge for a range of β.

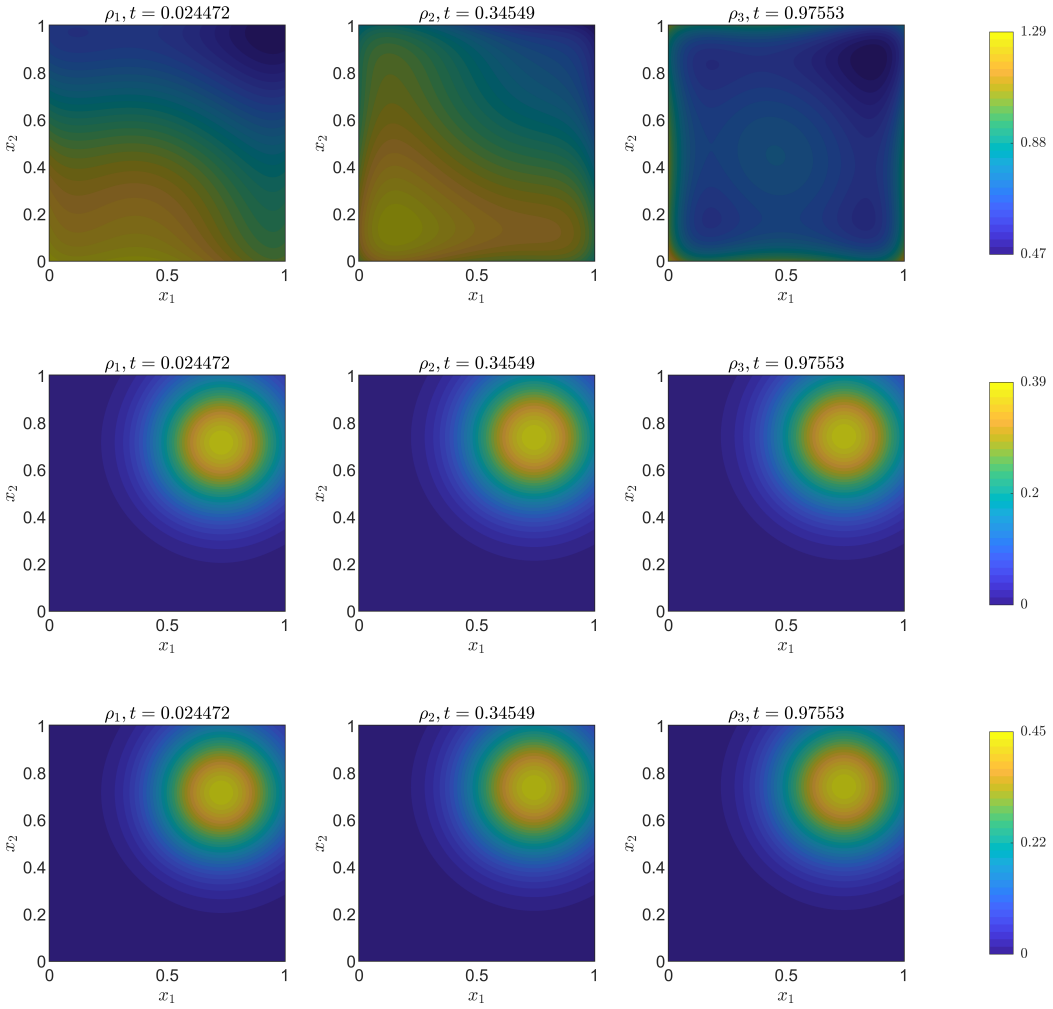

Figure 7.6: 2D Example 1: The optimal states ρ_1 (top), ρ_2 (middle), and ρ_3 (bottom) for $D = 1$ at different times.

smooth constraints. The robots swarming problem can also be extended to an example with more than one type of crop on the field so that $n_f > 1$, and this is really achievable using the methodology presented in this chapter.

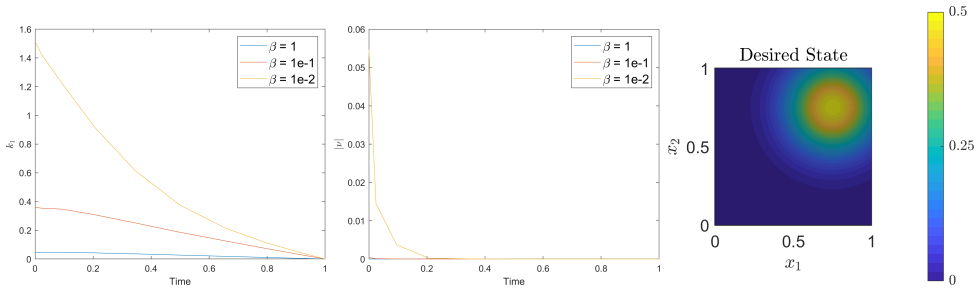

Figure 7.7: 2D Example 1: The optimal time probability k_1, the magnitude of the optimal velocity, and the desired state $\widehat{\rho}$.

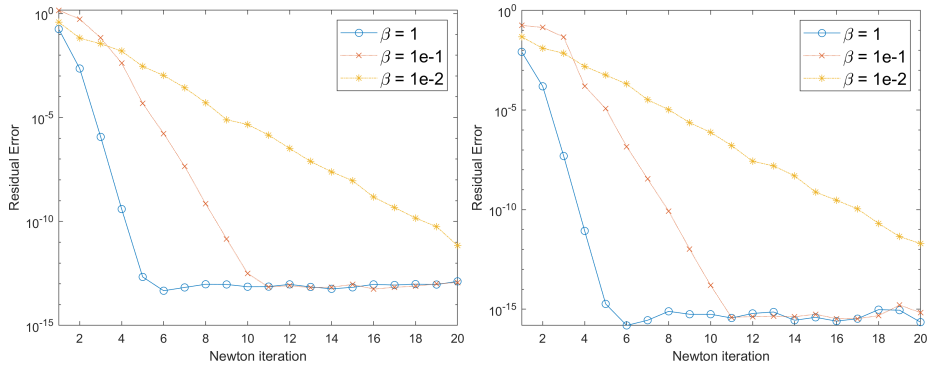

Figure 7.8: 2D Example 2: Convergence of the Newton–Krylov algorithm for a robots swarming problem with $D = 0.5$ and different values of β. Left: convergence in the state variable. Right: convergence in the adjoint variable. Convergence is measured using the residual error.

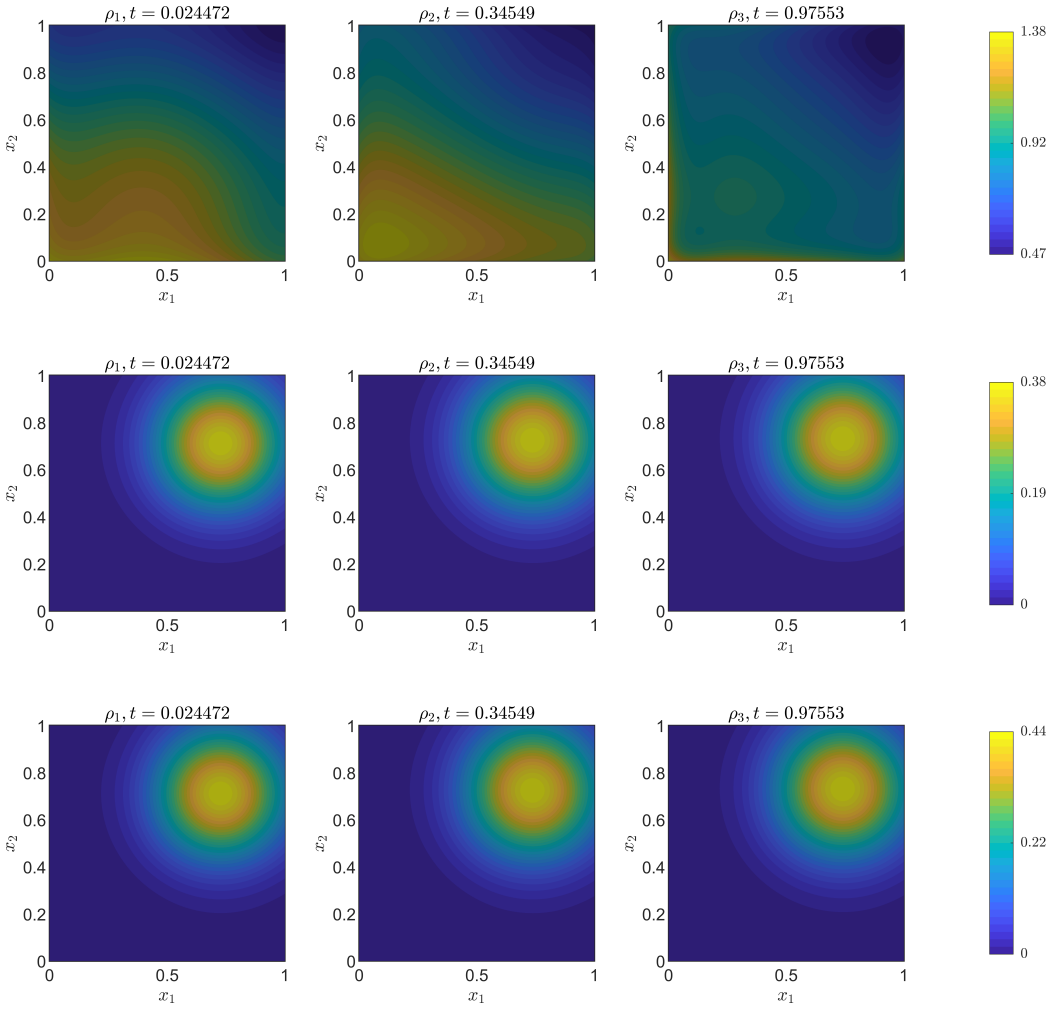

Figure 7.9: 2D Example 2: The optimal states ρ_1 (top), ρ_2 (middle), and ρ_3 (bottom) for $D = 1$ at different times.

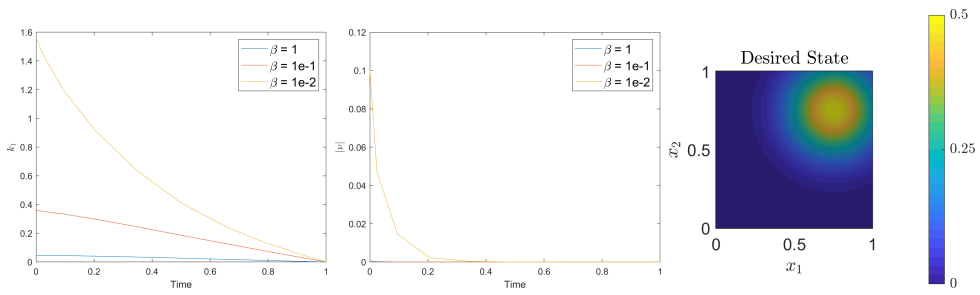

Figure 7.10: 2D Example 2: The optimal time probability k_1, the magnitude of the optimal velocity, and the desired state $\widehat{\rho}$

Chapter 8

Conclusion

8.1 Summary

In this thesis, we have aimed to develop a versatile numerical framework with accurate and efficient iterative methods to solve PDE-constrained problems from multiscale particle dynamics. The numerical framework we developed followed an *optimize-then discretize* approach, where we first found the continuous optimality conditions using a Lagrangian method, then solved the optimality system numerically using a combination of a discretization scheme and an iterative solver. We made our numerical framework modular, so one can have the flexibility to use both a discretization scheme and an iterative solver of one's choice. The discretization schemes we utilized were the pseudospectral method which was chosen for its fast convergence and suitability for systems with dense matrices that result from the non-local problems we considered, and the finite difference scheme which is simple to implement and not as sensitive to problems with non-smooth solutions compared to the pseudospectral method. The iterative solvers we employed included a fixed-point algorithm with and without an Armijo–Wolfe-type rule, which is reliable, robust, and generalizable to solve problems with bound constraints by incorporating a primal-dual active-set strategy, and a Newton–Krylov method which is robust and provides faster convergence compared to the fixed-point method.

We have considered a range of problems from multiscale particle dynamics and proposed iterative methods which converged robustly with respect to parameters involved in the problem set-up. The problems we tackled included the distributed source and flow control of the advection-diffusion equation with a non-linear, non-local interaction term, and the optimal control of radicals' distribution in a bounded confidence opinion dynamics model, also with a non-linear and non-local interaction term. Finally we presented results from the optimization of a robot swarming model involving a system of advection-diffusion equations with non-local terms.

We observed that the fixed-point method converges robustly for a number of 1D and 2D test problems involving non-local particle interactions. Convergence can take a couple of minutes for 1D problems in space or hours for 2D problems, however it is reliable. The Armijo–Wolfe rule can accelerate convergence in a range of settings by reducing the required number of iterations, and function evaluations. Utilizing smaller mixing rates for the fixed-point methods leads to longer convergence times. Hence, sometimes, one has to decide on a trade-off between reliable convergence and fast convergence. We also observed that a worse initial guess leads to more iterations being required for convergence, especially for smaller values of the regularization parameter, β.

The fixed-point method, once again, converged for problems with non-local and non-linear interacting terms arising from opinion dynamics. However, it was relatively slow, sometimes taking about 3 hours to converge for the examples in Chapter 6, making it necessary to use the higher-order Newton–Krylov method for the two-dimensional examples explored in Chapter 7. The active-set strategy performed very well for the non-linear parabolic PDEs presented in Chapter 6, and demonstrates the need for further theoretical work on the convergence of the strategy for non-linear and non-local parabolic PDEs. We also observed from the examples presented in Chapter 6, that different boundary conditions influence optimal controls differently,

and boundary conditions should be chosen to more accurately reflect the system being modelled in order to achieve reliable results.

In Chapter 7, we observed that the Newton–Krylov algorithm is effective for difficult problems from opinion dynamics and robotics. Generally, we deduce that the higher-order Newton–Krylov method converges faster compared to the fixed-point algorithm, as the convergence times for similar 2D opinion dynamics problems in Chapter 7 are sometimes smaller compared to that of the 1D opinion dynamics problems in Chapter 6.

8.2 Outlook

There are other variations on the problems considered in this thesis that could be investigated in the future, utilizing the same approach described in this thesis.

The DDFT examples and results presented in Chapter 5, can be generalized to include more physical effects like inertia and volume exclusion. The Newton–Krylov algorithm can also be extended to solve similar 3D examples arising from DDFT problems.

There are still many interesting dynamical processes to be uncovered in the 1D opinion dynamics optimization problems presented in Chapter 6. More features can be added to the forward problem which may affect the results of the optimization problem, for example, the confidence bound need not always be symmetric, since an agent might be more likely to move towards one direction than the other. Also, agents could have varying radii of confidence R, resulting in asymmetrical distributions which may produce interesting dynamics in the evolution of the optimal state and control. Phase transitions for certain combinations of (σ, R) are also yet to be explored in the optimal control setting.

Questions that can be investigated following the work in Chapter 7 include the existence and uniqueness of optimal controls for opinion dynamics problems and robots swarming problems, and convergence of the active set strategy for higher-order opinion dynamics and robot swarming problems. A numerical algorithm that combines the active-set strategy and Newton–Krylov method to tackle bound constraints for higher order problems can also studied. Another future work is the use of alternative discretizations to the pseudospectral method that may perform better with non-smooth constraints. The robot swarming problem can also be extended to examples with more than one type of crop on the field to simulate multi-crop farming scenarios.

Finally, the non-linear and non-local interacting PDEs that characterize the problems presented in this thesis are not unique to the applications discussed here. Other areas such as schooling of fish, fermentation of yeast, growth of cancer cells, interactions of photons, and chemical reactions present non-linear problems that our numerical framework could be extended to apply to. This may mean the use of different discretization schemes like the Hermite spectral method, which is a type of spectral scheme, or spectral-element methods which combine spectral methods with ideas from finite element approaches to achieve faster convergence on complex domains. It may also mean the adoption of state-of-the-art iterative solvers for dense linear systems.

Bibliography

[1] M. Aduamoah, B. D. Goddard, J. W. Pearson, and J. Roden. 2DChebClassPDECO [Software]. https://bitbucket.org/bdgoddard/2dchebclasspdecopublic/, 2020.

[2] M. Aduamoah, B. D. Goddard, J. W. Pearson, and J. C. Roden. Pseudospectral methods and iterative solvers for optimization problems from multiscale particle dynamics. *BIT Numerical Mathematics*, pages 1–41, 2022.

[3] V. Akcelik, G. Biros, and O. Ghattas. Parallel multiscale Gauss-Newton-Krylov methods for inverse wave propagation. In *SC'02: Proceedings of the 2002 ACM/IEEE Conference on Supercomputing*, page 41. IEEE, 2002.

[4] H. M. Al-Saedi, A. J. Archer, and J. Ward. Dynamical density-functional-theory-based modeling of tissue dynamics: application to tumor growth. *Physical Review E*, 98(2):022407, 2018.

[5] G. Albi, Y. P. Choi, M. Fornasier, and D. Kalise. Mean field control hierachy. *Applied Mathematics and Optimization*, 135:76–93, 2017.

[6] L. Almenar and M. Rauscher. Dynamics of colloids in confined geometries. *Journal of Physics: Condensed Matter*, 23(18):184115, 2011.

[7] P. Altevogt, O. A. Evers, J. G. E. M. Fraaije, N. M. Maurits, and B. A. C. van Vlimmeren. The MesoDyn project: software for mesoscale chemical engineering. *Journal of Molecular Structure: THEOCHEM*, 463(1-2):139–143, 1999.

[8] S. Angenent, S. Haker, and A. Tannenbaum. Minimizing flows for the Monge–Kantorovich problem. *SIAM Journal on Mathematical Analysis*, 35(1):61–97, 2003.

[9] H. Antil, T. S. Brown, and D. Verma. Moreau-Yosida regularization for optimal control of fractional elliptic problems with state and control constraints. *arXiv preprint arXiv:1912.05033*, 2019.

[10] S. S. Antman. The influence of elasticity on analysis: modern developments. *Bulletin of the American Mathematical Society*, 9(3):267–291, 1983.

[11] I. Aoki. A simulation study on the schooling mechanism in fish. *The Japanese Society of Fisheries Science*, 48(8):1081–1088, 1982.

[12] A. J. Archer. Dynamical density functional theory for dense atomic liquids. *Journal of Physics: Condensed Matter*, 18(24):5617, 2006.

[13] A. J. Archer and R. Evans. Binary Gaussian core model: Fluid-fluid phase separation and interfacial properties. *Physical Review E*, 64(4):041501, 2001.

[14] A. J. Archer and R. Evans. Dynamical density functional theory and its application to spinodal decomposition. *The Journal of Chemical Physics*, 121(9):4246–4254, 2004.

[15] A. J. Archer and M. Rauscher. Dynamical density functional theory for interacting Brownian particles: stochastic or deterministic? *Journal of Physics A: Mathematical and General*, 37(40):9325, 2004.

[16] S. R. Arridge. Optical tomography in medical imaging. *Inverse Problems*, 15(2):R41, 1999.

[17] M. Athans and P. L. Falb. *Optimal Control: an introduction to the theory and its applications*. Courier Corporation, 2013.

[18] S. Babel, M. Eikerling, and H. Löwen. Impedance resonance in narrow confinement. *The Journal of Physical Chemistry C*, 122(38):21724–21734, 2018.

[19] A. Barabási and R. Albert. Emergence of scaling in random networks. *Science*, 286(5439):509–512, 1999.

[20] A. B. Barbaro, K. Taylor, P. F. Trethewey, L. Youseff, and B. Birnir. Discrete and continuous models of the dynamics of pelagic fish: application to the capelin. *Mathematics and Computers in Simulation*, 79(12):3397–3414, 2009.

[21] R. C. Barnard, M. Frank, and M. Herty. Optimal treatment planning in radiotherapy based on boltzmann transport equations. *Trends in PDE Constrained Optimization*, pages 441–453, 2014.

[22] W. Barthel, C. John, and F. Tröltzsch. Optimal boundary control of a system of reaction diffusion equations. *Zeitschrift für Angewandte Mathematik und Mechanik*, 90(12):966–982, 2010.

[23] H. H. Bauschke, P. L. Combettes, et al. *Convex Analysis and Monotone Operator Theory in Hilbert Spaces*, volume 408. Springer, 2011.

[24] D. Behmardi and E. D. Nayeri. Introduction of Fréchet and Gâteaux derivative. *Applied Mathematical Sciences*, 2(20):975–980, 1985.

[25] M. Behrens, H. G. Bock, S. Engell, P. Khobkhun, and A. Potschka. Real-time PDE constrained optimal control of a periodic multicomponent separation process. *Trends in PDE Constrained Optimization*, pages 521–537, 2014.

[26] E. Ben-Naim, L. Frachebourg, and P. L. Krapivsky. Coarsening and persistence in the voter model. *Physical Review E*, 53(4):3078, 1996.

[27] J. D. Benamou and Y. Brenier. A computational fluid mechanics solution to the Monge-Kantorovich mass transfer problem. *Numerische Mathematik*, 84(3):375–393, 2000.

[28] M. Benzi, E. Haber, and L. Taralli. A preconditioning technique for a class of PDE-constrained optimization problems. *Advances in Computational Mathematics*, 35(2):149–173, 2011.

[29] R. L. Berger. A necessary and sufficient condition for reaching a consensus using degroot's method. *Journal of the American Statistical Association*, 76(374):415–418, 1981.

[30] M. Bergounioux. A Lagrangian method for optimal control problems with state constraints. *Journal of Optimization Theory and Applications*, 78(3):493–521, 1993.

[31] M. Bergounioux, M. Haddou, M. Hintermüller, and K. Kunisch. A comparison of a Moreau–Yosida-based active set strategy and interior point methods for constrained optimal control problems. *SIAM Journal on Optimization*, 11(2):495–521, 2000.

[32] M. Bergounioux, K. Ito, and K. Kunisch. Primal-dual strategy for constrained optimal control problems. *SIAM Journal on Control and Optimization*, 37(4):1176–1194, 1999.

[33] M. Bergounioux and K. Kunisch. Augemented Lagrangian techniques for elliptic state constrained optimal control problems. *SIAM Journal on Control and Optimization*, 35(5):1524–1543, 1997.

[34] V. Berinde and F. Takens. *Iterative Approximation of Fixed Points*, volume 1912. Springer, 2007.

[35] A. T. Bernardes, D. Stauffer, and J. Kertész. Election results and the Sznajd model on Barabasi network. *The European Physical Journal B- Condensed Matter and Complex Systems*, 25(1):123–127, 2002.

[36] D. P. Bertsekas. Projected Newton methods for optimization problems with simple constraints. *SIAM Journal on Control and Optimization*, 20(2):221–246, 1982.

[37] J. T. Betts. Survey of numerical methods for trajectory optimization. *Journal of Guidance, Control, and Dynamics*, 21(2):193–207, 1998.

[38] H. G. Bock and K. Plitt. A multiple shooting algorithm for direct solution of optimal control problems. *IFAC Proceedings Volumes*, 17(2):1603–1608, 1984.

[39] L. Boltzmann. Further studies on thermal equilibrium between gas molecules. *Wien Ber*, 66:275, 1872.

[40] L. Boudin and F. Salvarani. Opinion dynamics: Kinetic modelling with mass media, application to the Scottish independence referendum. *Physica A, Statistical Mechanics and its Applications*, 444:448–457, 2016.

[41] J. P. Boyd. *Chebyshev and Fourier Spectral Methods*. Courier Corporation, 2001.

[42] F. Bravo-Marquez, D. Gayo-Avello, M. Mendoza, and B. Poblete. Opinion dynamics of elections in Twitter. In *2012 Eighth Latin American Web Congress*, pages 32–39. IEEE, 2012.

[43] F. Bullo, J. Cortés, and S. Martinez. *Distributed Control of Robotic Networks: A Mathematical Approach to Motion Coordination Algorithms*. Princeton University Press, 2009.

[44] M. Burger, M. Francesco, P. A. Markowich, and M. T. Wolfram. Mean field games with nonlinear mobilities in pedestrian dynamics. *Discrete and Continuous Dynamics*, 19(5):1311–1333, 2014.

[45] M. Burger, R. Pinnau, M. Fouego, and S. Rau. Optimal control of self-consistent classical and quantum particle systems. *Trends in PDE Constrained Optimization*, pages 455–470, 2014.

[46] S. Camazine, J. L. Deneubourg, N. R. Franks, J. Sneyd, E. Bonabeau, and G. Theraula. *Self-organization in biological systems*. Princeton University Press, 2003.

[47] C. Canuto, F. Fagnani, and P. Tilli. An Eulerian aproach to the analysis of Krause's consensus models. *SIAM Journal on Control and Optimization*, 50(1):243–265, 2012.

[48] E. Carlini and F. J. Silva. A fully discrete semi-Lagrangian scheme for a first order mean field game problem. *SIAM Journal on Numerical Analysis*, 52(1):45–67, 2014.

[49] J. Carrillo, D. Kalise, F. Rossi, and E. Trélat. Controlling swarms towards flocks and mills. *arXiv preprint arXiv:2103.07304*, 2021.

[50] J. A. Carrillo, R. S. Gvalani, G. A. Pavliotis, and A. Schlichting. Long-time behaviour and phase transitions for the McKean–Vlasov equation on the torus. *Archive for Rational Mechanics and Analysis*, 235(1):635–690, 2020.

[51] R. Casanova, A. Silva, and A. R. Borges. A quantitative algorithm for parameter estimation in magnetic induction tomography. *Measurement Science and Technology*, 15(7):1412, 2004.

[52] C. Castellano, S. Fortunato, and V. Loreto. Statistical physics of social dynamics. *Reviews of Modern Physics*, 81(2):591, 2009.

[53] J. Castro, J. Lu, G. Zhang, Y. Dong, and L. Martínez. Opinion dynamics-based group recommender systems. *IEEE Transactions on Systems, Man, and Cybernetics: Systems*, 48(12):2394–2406, 2017.

[54] C. Chalmers, R. Smith, and A. J. Archer. Dynamical density functional theory for the evaporation of droplets of nanoparticle suspension. *Langmuir*, 33(50):14490–14501, 2017.

[55] S. Chandrasekhar. Stochastic problems in physics and astronomy. *Reviews of Modern Physics*, 15(1):1, 1943.

[56] A. Chauviere, H. Hatzikirou, I. G. Kevrekidis, J. S. Lowengrub, and V. Cristini. Dynamic density functional theory of solid tumor growth: preliminary models. *AIP Advances*, 2(1):011210, 2012.

[57] J. T. Chayes and L. Chayes. On the validity of the inverse conjecture in classical density functional theory. *Journal of Statistical Physics*, 36(3):471–488, 1984.

[58] B. Chazelle, Q. Jiu, Q. Li, and C. Wang. Well-posedness of the limiting equation of a noisy consensus model in opinion dynamics. *Journal of Differential Equations*, 263(1), 2015.

[59] M. Cheney, D. Isaacson, and J. C. Newell. Electrical impedance tomography. *SIAM Review*, 41(1):85–101, 1999.

[60] C. W. Clenshaw and A. R. Curtis. A method for numerical integration on an automatic computer. *Numerische Mathematik*, 2(1):197–205, 1960.

[61] S. S. Collis and M. Heinkenschloss. Analysis of the streamline upwind/Petrov Galerkin method applied to the solution of optimal control problems. *Technical Report, CAAM TR02-01*, 108, 2002.

[62] R. Cominetti, J. A. Soto, and J. Vaisman. On the rate of convergence of Krasnosel'skiĭ–Mann iterations and their connection with sums of bernoullis. *Israel Journal of Mathematics*, 199(2):757–772, 2014.

[63] R. Cominetti, J. A. Soto, and J. Vaisman. On the rate of convergence of Krasnosel'skiĭ-Mann iterations and their connection with sums of Bernoullis. *Israel Journal of Mathematics*, 199(2):757–772, 2014.

[64] N. Crokidakis. Effects of mass media on opinion spreading in the Sznajd sociophysics model. *Physica A, Statistical Mechanics and its Applications*, 391(4):1729–1734, 2012.

[65] F. Cucker and S. Smale. Emergent behavior in flocks. *IEEE Transactions on Automatic Control*, 52(5):852–862, 2007.

[66] F. Cucker and S. Smale. On the mathematics of emergence. *Japanese Journal of Mathematics*, 2(1):197–227, 2007.

[67] G. B. Dantzig and M. N. Thapa. *Linear Programming: Theory and Extensions*, volume 2. Springer, 2003.

[68] J. A. De La Torre, P. Español, and A. Donev. Finite element discretization of non-linear diffusion equations with thermal fluctuations. *The Journal of Chemical Physics*, 142(9):094115, 2015.

[69] D. de Las Heras, J. M. Brader, A. Fortini, and M. Schmidt. Particle conservation in dynamical density functional theory. *Journal of Physics: Condensed Matter*, 28(24):244024, 2016.

[70] J. C. De Los Reyes. Primal–dual active set method for control constrained optimal control of the Stokes equations. *Optimization Methods and Software*, 21(2):267–293, 2006.

[71] G. Deffuant, D. Neau, F. Amblard, and G. Weisbuch. Mixing beliefs among interacting agents. *Advances in Complex Systems*, (3):11, 2001.

[72] M. H. DeGroot. Reaching a consensus. *Journal of the American Statistical Association*, 69(345):118–121, 1974.

[73] J. K. G. Dhont. *An Introduction to Dynamics of Colloids*. Elsevier, 1996.

[74] A. Diaw and M. S. Murillo. A viscous quantum hydrodynamics model based on dynamic density functional theory. *Scientific Reports*, 7(1):1–9, 2017.

[75] M. Dick, M. Gugat, M. Herty, G. Leugering, S. Steffensen, and K. Wang. Stabilization of networked hyperbolic systems with boundary feedback. *Trends in PDE constrained optimization*, pages 487–504, 2014.

[76] M. Diehl, H. G. Bock, H. Diedam, and P.-B. Wieber. Fast direct multiple shooting algorithms for optimal robot control. *Fast motions in biomechanics and robotics: optimization and feedback control*, pages 65–93, 2006.

[77] Z. Ding, H. Liang, Y. Dong, F. Chiclana, E. Herrera-Viedma, and F. J. Cabrerizo. An opinion control rule with minimum adjustments to support the consensus reaching in bounded confidence model. *Procedia Computer Science*, 91:617–624, 2016.

[78] I. S. Duff, A. M. Erisman, and J. K. Reid. *Direct Methods for Sparse Matrices*. Oxford University Press, 2017.

[79] J. Dzubiella and C. N. Likos. Mean-field dynamical density functional theory. *Journal of Physics: Condensed Matter*, 15(6):L147, 2003.

[80] F. d'Amore, A. Clementi, and E. Natale. Phase transition of a non-linear opinion dynamics with noisy interactions. In *International Colloquium on Structural Information and Communication Complexity*, pages 255–272. Springer, 2020.

[81] H. Emmerich, H. Löwen, R. Wittkowski, T. Gruhn, G. I. Tóth, G. Tegze, and L. Gránásy. Phase-field-crystal models for condensed matter dynamics on atomic length and diffusive time scales: an overview. *Advances in Physics*, 61(6):665–743, 2012.

[82] H. Emmerich, P. Virnau, G. Wilde, and R. Spatschek. Heterogeneous nucleation and microstructure formation: Steps towards a system and scale bridging understanding. *The European Physical Journal Special Topics*, 223(3):337–346, 2014.

[83] M. Engel and M. Griebel. A multigrid method for constrained optimal control problems. *Journal of Computational and Applied Mathematics*, 235(15):4368–4388, 2011.

[84] P. Erdos, A. Rényi, et al. On the evolution of random graphs. *Institute of Mathematics, Hungarian Academy of Sciences*, 5(1):17–60, 1960.

[85] F. Fang, J. Satulovsky, and I. Szleifer. Kinetics of protein adsorption and desorption on surfaces with grafted polymers. *Biophysical Journal*, 89(3):1516–1533, 2005.

[86] S. Farokhirad, A. Ranganathan, J. Myerson, V. R. Muzykantov, P. S. Ayyaswamy, D. M. Eckmann, and R. Radhakrishnan. Stiffness can mediate balance between hydrodynamic forces and avidity to impact the targeting of flexible polymeric nanoparticles in flow. *Nanoscale*, 11(14):6916–6928, 2019.

[87] B. Fehrman and B. Gess. Well-posedness of nonlinear diffusion equations with nonlinear, conservative noise. *Archive for Rational Mechanics and Analysis*, 233(1):249–322, 2019.

[88] S. Ferrari, G. Foderaro, P. Zhu, and T. A. Wettergren. Distributed optimal control of multiscale dynamical systems: a tutorial. *IEEE Control Systems Magazine*, 36(2):102–116, 2016.

[89] A. Fortini, D. de Las Heras, J. M. Brader, and M. Schmidt. Superadiabatic forces in Brownian many-body dynamics. *Physical Review Letters*, 113(16):167801, 2014.

[90] L. J. D. Frink, A. G. Salinger, M. P. Sears, J. D. Weinhold, and A. L. Frischknecht. Numerical challenges in the application of density functional theory to biology and nanotechnology. *Journal of Physics: Condensed Matter*, 14(46):12167, 2002.

[91] L. Fu-hua and L. Ji-yao. Shooting method in singular perturbation problem of ordinary differential equations with boundary layers. *Applied Mathematics and Mechanics*, 9(7):659–665, 1988.

[92] S. Galam. Minority opinion spreading in random geometry. *The European Physical Journal B- Condensed Matter and Complex Systems*, 25(4):403–406, 2002.

[93] C. W. Gardiner. *Handbook of Stochastic Methods*, volume 3. Springer Berlin, 1985.

[94] R. Glowinski, Y. Song, and X. Yuan. An ADMM numerical approach to linear parabolic state constrained optimal control problems. *Numerische Mathematik*, 144(4):931–966, 2020.

[95] B. Goddard, A. Nold, and S. Kalliadasis. Multi-species dynamical density functional theory. *The Journal of Chemical Physics*, 138(14):144904, 2013.

[96] B. D. Goddard, B. Gooding, H. Short, and G. A. Pavliotis. Noisy bounded confidence models for opinion dynamics: the effect of boundary conditions on phase transitions. *IMA Journal of Applied Mathematics*, 87(1):80–110, 2022.

[97] B. D. Goddard, R. D. Mills-Williams, and G. Pavliotis. Well-posedness and equilibrium behaviour of overdamped dynamic density functional theory. *arXiv preprint arXiv:2002.11663*, 2020.

[98] B. D. Goddard, A. Nold, N. Savva, P. Yatsyshin, and S. Kalliadasis. Unification of dynamic density functional theory for colloidal fluids to include inertia and hydrodynamic interactions: derivation and numerical experiments. *Journal of Physics: Condensed Matter*, 25(3):035101, 2012.

[99] B. D. Goddard, G. A. Pavliotis, and S. Kalliadasis. The overdamped limit of dynamic density functional theory: rigorous results. *Multiscale Modeling & Simulation*, 10(2):633–663, 2012.

[100] S. N. Gomes, G. A. Pavliotis, and U. Vaes. Mean field limits for interacting diffusions with colored noise: phase transitions and spectral numerical methods. *Multiscale Modeling & Simulation*, 18(3):1343–1370, 2020.

[101] A. González, J. A. White, F. L. Román, S. Velasco, and R. Evans. Density functional theory for small systems: hard spheres in a closed spherical cavity. *Physical Review Letters*, 79(13):2466, 1997.

[102] M. C. Gonzalez, A. O. Sousa, and H. J. Herrmann. Opinion formation on a deterministic pseudo-fractal network. *International Journal of Modern Physics C*, 15(1):45–57, 2004.

[103] R. Griesse. Parametric sensitivity analysis in optimal control of a reaction-diffusion system–part ii: practical methods and examples. *Optimization Methods and Software*, 19(2):217–242, 2004.

[104] R. Griesse and S. Volkwein. A primal-dual active set strategy for optimal boundary control of a nonlinear reaction-diffusion system. *SIAM Journal on Control and Optimization*, 44(2):467–494, 2005.

[105] R. Griesse and S. Volkwein. Parametric sensitivity analysis for optimal boundary control of a 3D reaction-diffusion system. In *Large-Scale Nonlinear Optimization*, pages 127–149. Springer, 2006.

[106] M. Gröschel, W. Peukert, and G. Leugering. Modeling, analysis and optimization of particle growth, nucleation and ripening by the way of nonlinear hyperbolic integro-partial differential equations. *Trends in PDE Constrained Optimization*, pages 471–486, 2014.

[107] J. Gross. A density functional theory for vapor-liquid interfaces using the pcp-saft equation of state. *The Journal of Chemical physics*, 131(20):204705, 2009.

[108] D. A. Gubanov, I. V. Petrov, and A. G. Chkhartishvili. Multidimensional model of opinion dynamics in social networks: polarization indices. *Automation and Remote Control*, 82(10):1802–1811, 2021.

[109] M. D. Gunzburger. *Perspectives in Flow Control and Optimization*. SIAM, 2002.

[110] C. Gutsche, F. Kremer, M. Krüger, M. Rauscher, R. Weeber, and J. Harting. Colloids dragged through a polymer solution: Experiment, theory, and simulation. *The Journal of Chemical Physics*, 129(8):084902, 2008.

[111] S. Güttel and J. W. Pearson. PDEOptim [Software]. https://github.com/nla-group/pdeoptim/, 2020.

[112] S. Güttel and J. W. Pearson. A spectral-in-time Newton–Krylov method for nonlinear PDE-constrained optimization. *IMA Journal of Numerical Analysis*, 42(2):1478–1499, 2022.

[113] M. Haataja, L. Gránásy, and H. Löwen. Classical density functional theory methods in soft and hard matter. *Journal of Physics: Condensed Matter*, 22(36):360301, 2010.

[114] E. Haber. Quasi-Newton methods for large-scale electromagnetic inverse problems. *Inverse Problems*, 21(1):305, 2004.

[115] E. Haber. A parallel method for large scale time domain electromagnetic inverse problems. *Applied Numerical Mathematics*, 58(4):422–434, 2008.

[116] R. Hegselmann and U. Krause. Opinion dynamics and bounded confidence models, analysis, and simulation. *Journal of Artificial Societies and Social Simulation*, 5(3), 2002.

[117] R. Hegselmann and U. Krause. Opinion dynamics under the influence of radical groups, charismatic leaders, and other constant signals: A simple unifying model. *Networks and Heterogeneous Media*, 10(3):477–509, 2015.

[118] C. K. Hemelrijk and H. Hildenbrandt. Self-organized shape and frontal density of fish schools. *Ethology*, 114(3):245–254, 2008.

[119] M. Hintermüller, K. Ito, and K. Kunisch. The primal-dual active set strategy as a semismooth Newton method. *SIAM Journal on Optimization*, 13(3):865–888, 2002.

[120] M. Hinze and R. Pinnau. Second-order approach to optimal semiconductor design. *Journal of Optimization Theory and Applications*, 133(2):179–199, 2007.

[121] M. Hinze, R. Pinnau, M. Ulbrich, and S. Ulbrich. *Optimization with PDE Constraints*, volume 23. Springer International Publishing, 2009.

[122] R. A. Holley and T. M. Liggett. Ergodic theorems for weakly interacting infinite systems and the voter model. *The Annals of Probability*, pages 643–663, 1975.

[123] H. Iiduka. Line search fixed point algorithms based on nonlinear conjugate gradient directions: application to constrained smooth convex optimization. *Fixed Point Theory and Applications*, 2016(1):1–32, 2016.

[124] M. Inoue and A. Yoshimori. Effects of interactions between particles on dynamics in microrheology. *Journal of Molecular Liquids*, 200:81–84, 2014.

[125] M. Inoue and A. Yoshimori. Method for studying many-particle effects on nonequilibrium steady states. *Journal of the Physical Society of Japan*, 86(7):074604, 2017.

[126] K. Ito and K. Kunisch. Augmented Lagrangian methods for nonsmooth, convex optimization in Hilbert spaces. *Nonlinear Analysis: Theory, Methods & Applications*, 41(5-6):591–616, 2000.

[127] K. Ito and K. Kunisch. Semi-smooth Newton methods for state-constrained optimal control problems. *Systems & Control Letters*, 50(3):221–228, 2003.

[128] K. Ito and K. Kunisch. *Lagrange Multiplier Approach to Variational Problems and Applications*. SIAM, 2008.

[129] A. Joshi, W. Bangerth, and E. M. Sevick-Muraca. Non-contact fluorescence optical tomography with scanning patterned illumination. *Optics Express*, 14(14):6516–6534, 2006.

[130] J. Jost and X. Li-Jost. *Calculus of Variations*, volume 64. Cambridge University Press, 1998.

[131] G. Kahl and H. Löwen. Classical density functional theory: an ideal tool to study heterogeneous crystal nucleation. *Journal of Physics: Condensed Matter*, 21(46):464101, 2009.

[132] E. F. Keller and L. A. Segel. Initiation of slime mold aggregation viewed as an instability. *Journal of Theoretical Biology*, 26(3):399–415, 1970.

[133] C. T. Kelley. *Solving Nonlinear Equations With Newton's Method*. SIAM, 2003.

[134] A. Ü. Keskin. The shooting method for the solution of one-dimensional bvps. In *Boundary Value Problems for Engineers*, pages 167–258. Springer, 2019.

[135] M. V. Klibanov and T. R. Lucas. Numerical solution of a parabolic inverse problem in optical tomography using experimental data. *SIAM Journal on Applied Mathematics*, 59(5):1763–1789, 1999.

[136] M. G. Knepley, D. A. Karpeev, S. Davidovits, R. S. Eisenberg, and D. Gillespie. An efficient algorithm for classical density functional theory in three dimensions: Ionic solutions. *The Journal of Chemical Physics*, 132(12):124101, 2010.

[137] A. Knoll, K. S. Lyakhova, A. Horvat, G. Krausch, G. J. A. Sevink, A. V. Zvelindovsky, and R. Magerle. Direct imaging and mesoscale modelling of phase transitions in a nanostructured fluid. *Nature Materials*, 3(12):886–891, 2004.

[138] D. A. Knoll and D. E. Keyes. Jacobian-free Newton–Krylov methods: a survey of approaches and applications. *Journal of Computational Physics*, 193(2):357–397, 2004.

[139] A. L. Koch and D. White. The social lifestyle of myxobacteria. *Bioessays*, 20(12):1030–1038, 1998.

[140] M. Kohl, A. V. Ivlev, P. Brandt, G. E. Morfill, and H. Löwen. Microscopic theory for anisotropic pair correlations in driven binary mixtures. *Journal of Physics: Condensed Matter*, 24(46):464115, 2012.

[141] M. A. S. Kolarijani, A. V. Proskurnikov, and P. M. Esfahani. Macroscopic noisy bounded confidence models with distributed radical opinions. *IEEE Transactions on Automatic Control*, 66(3):1174–1189, 2020.

[142] V. Konarovskyi, T. Lehmann, and M. von Renesse. Dean-Kawasaki dynamics: ill-posedness vs. triviality. *Electronic Communications in Probability*, 24:1–9, 2019.

[143] H. A. Kramers. Brownian motion in a field of force and the diffusion model of chemical reactions. *Physica*, 7(4):284–304, 1940.

[144] P. L. Krapivsky and S. Redner. Dynamics of majority rule in two-state interacting spin systems. *Physical Review Letters*, 90(23):238701, 2003.

[145] M. A. Krasnosel'skii. Two comments on the method of successive approximations. *Uspekhi Matematicheskikh Nauk*, 10:123–127, 1955.

[146] M. Krüger and M. Rauscher. Colloid-colloid and colloid-wall interactions in driven suspensions. *The Journal of Chemical Physics*, 127(3):034905, 2007.

[147] K. Kunisch and A. Rösch. Primal-dual active set strategy for a general class of constrained optimal control problems. *SIAM Journal on Optimization*, 13(2):321–334, 2002.

[148] S. Kurz. Optimal control of the freezing time in the Hegselmann–Krause dynamics. *Journal of Difference Equations and Applications*, 21(8):633–648, 2015.

[149] G. Leugering, P. Benner, S. Engell, A. Griewank, H. Harbrecht, M. Hinze, R. Rannacher, and S. Ulbrich. Introduction. *Trends in PDE Constrained Optimization*, pages 1–5, 2014.

[150] R. J. Leveque. High-resolution conservative algorithms for advection in incompressible flow. *SIAM Journal on Numerical Analysis*, 33(2):627–665, 1996.

[151] A. S. Lewis and M. L. Overton. Nonsmooth optimization via quasi-Newton methods. *Mathematical Programming*, 141(1):135–163, 2013.

[152] B. Liebchen and H. Löwen. Modeling chemotaxis of microswimmers: From individual to collective behavior. In *Chemical Kinetics: Beyond the Textbook*, pages 493–516. World Scientific, 2020.

[153] Y. Liu and H. Liu. Development of reaction–diffusion DFT and its application to catalytic oxidation of no in porous materials. *AIChE Journal*, 66(2):e16824, 2020.

[154] J. Lorenz. Consensus strikes back in the Hegselmann-Krause model of continuous opinion dynamics under bounded confidence. *Journal of Artificial Societies and Social Simulation*, 9(1), 2006.

[155] J. Lorenz. Continuous opinion dynamics under bounded confidence: A survey. *International Journal of Modern Physics C*, 18(12):1819–1838, 2007.

[156] A. A. Louis, P. G. Bolhuis, and J. P. Hansen. Mean-field fluid behavior of the Gaussian core model. *Physical Review E*, 62(6):7961, 2000.

[157] H. Löwen. Density functional theory of inhomogeneous classical fluids: recent developments and new perspectives. *Journal of Physics: Condensed Matter*, 14(46):11897, 2002.

[158] H. Löwen and M. Heinen. Dynamical density functional theory for the diffusion of injected Brownian particles. *The European Physical Journal Special Topics*, 223(14):3113–3127, 2014.

[159] S. Ludwigs, A. Böker, A. Voronov, N. Rehse, R. Magerle, and G. Krausch. Self-assembly of functional nanostructures from abc triblock copolymers. *Nature Materials*, 2(11):744–747, 2003.

[160] R. Lukeman, Y. Li, and L. Edelstein-Keshet. Inferring individual rules from collective behavior. *Proceedings of the National Academy of Sciences*, 107(28):1257–12580, 2010.

[161] J. F. Lutsko. Mechanism for the stabilization of protein clusters above the solubility curve: the role of non-ideal chemical reactions. *Journal of Physics: Condensed Matter*, 28(24):244020, 2016.

[162] J. F. Lutsko and G. Nicolis. Mechanism for the stabilization of protein clusters above the solubility curve. *Soft Matter*, 12(1):93–98, 2016.

[163] T. L. Magnanti and G. Perakis. Solving variational inequality and fixed point problems by line searches and potential optimization. *Mathematical Programming*, 101(3):435–461, 2004.

[164] A. Malijevskỳ and A. J. Archer. Sedimentation of a two-dimensional colloidal mixture exhibiting liquid-liquid and gas-liquid phase separation: A dynamical density functional theory study. *The Journal of Chemical Physics*, 139(14):144901, 2013.

[165] F. Mannel and A. Rund. A hybrid semismooth quasi-Newton method for nonsmooth optimal control with PDEs. *Optimization and Engineering*, 22(4):2087–2125, 2021.

[166] U. M. B. Marconi and P. Tarazona. Dynamic density functional theory of fluids. *The Journal of Chemical Physics*, 110(16):8032–8044, 1999.

[167] U. M. B. Marconi and P. Tarazona. Nonequilibrium inertial dynamics of colloidal systems. *The Journal of Chemical Physics*, 124(16):164901, 2006.

[168] A. C. R. Martins. Continuous opinions and discrete actions in opinion dynamics problems. *International Journal of Modern Physics C*, 19(4):617–624, 2008.

[169] A. C. R. Martins. Discrete opinion models as a limit case of the CODA model. *Physica A: Statistical Mechanics and its Applications*, 395:352–357, 2014.

[170] T. P. Mathew, M. Sarkis, and C. E. Schaerer. Analysis of block matrix preconditioners for elliptic optimal control problems. *Numerical Linear Algebra with Applications*, 14(4):257–279, 2007.

[171] T. P. Mathew, M. Sarkis, and C. E. Schaerer. Analysis of block parareal preconditioners for parabolic optimal control problems. *SIAM Journal on Scientific Computing*, 32(3):1180–1200, 2010.

[172] N. D. Mermin. Thermal properties of the inhomogeneous electron gas. *Physical Review*, 137(5A):A1441, 1965.

[173] H. D. Mittelmann and H. Maurer. Solving elliptic control problems with interior point and SQP methods: control and state constraints. *Journal of Computational and Applied Mathematics*, 120(1-2):175–195, 2000.

[174] A. Mogilner and L. Edelstein-Keshet. A non-local model for a swarm. *Journal of Mathematical Biology*, 38(6):534–570, 1999.

[175] D. D. Morrison, J. D. Riley, and J. F. Zancanaro. Multiple shooting method for two-point boundary value problems. *Communications of the ACM*, 5(12):613–614, 1962.

[176] S. Motsch and E. Tadmor. A new model for self-organized dynamics and its flocking behavior. *Journal of Statistical Physics*, 144(5):923–947, 2011.

[177] S. Motsch and E. Tadmor. Heterophilious dynamics enhances consensus. *SIAM Review*, 56(4):577–621, 2014.

[178] I. Neitzel, U. Prüfert, and T. Slawig. Solving time-dependent optimal control problems in COMSOL multiphysics. In *Proceedings of the COMSOL Conference Hannover*, 2008.

[179] I. Neitzel, U. Prüfert, and T. Slawig. Strategies for time-dependent PDE control with inequality constraints using an integrated modeling and simulation environment. *Numerical Algorithms*, 50(3):241–269, 2009.

[180] M. E. J. Newman and D. J. Watts. Renormalization group analysis of the small-world network model. *Physics Letters A*, 263(4-6):341–346, 1999.

[181] J. Nocedal and S. J. Wright. *Numerical Optimization*, volume 2. Springer, 1999.

[182] A. Nold, B. Goddard, P. Yatsyshin, N. Savva, and S. Kalliadasis. Pseudospectral methods for density functional theory in bounded and unbounded domains. *Journal of Computational Physics*, 334:639–664, 2017.

[183] C. E. Orozco and O. N. Ghattas. Massively parallel aerodynamic shape optimization. *Computing Systems in Engineering*, 3(1-4):311–320, 1992.

[184] E. Oster and A. Feigel. Prices of options as opinion dynamics of the market players with limited social influence. *arXiv preprint arXiv:1503.08785*, 2015.

[185] J. K. Parrish and L. Edelstein-Keshet. Complexity, pattern, and evolutionary trade-offs in animal aggregation. *Science*, 284(5411):99–101, 1999.

[186] S. E. Parsegov, A. V. Proskurnikov, R. Tempo, and N. E. Friedkin. Novel multidimensional models of opinion dynamics in social networks. *IEEE Transactions on Automatic Control*, 62(5):2270–2285, 2016.

[187] A. T. Patera. A spectral element method for fluid dynamics: laminar flow in a channel expansion. *Journal of Computational Physics*, 54(3):468–488, 1984.

[188] J. W. Pearson and A. Potschka. A preconditioned inexact active-set method for large-scale nonlinear optimal control problems. *arXiv preprint arXiv:2112.05020*, 2021.

[189] J. W. Pearson and M. Stoll. Fast iterative solution of reaction-diffusion control problems arising from chemical processes. *SIAM Journal on Scientific Computing*, 35(5):B987–B1009, 2013.

[190] J. W. Pearson, M. Stoll, and A. J. Wathen. Preconditioners for state-constrained optimal control problems with Moreau–Yosida penalty function. *Numerical Linear Algebra with Applications*, 21(1):81–97, 2014.

[191] J. W. Pearson and A. J. Wathen. Fast iterative solvers for convection-diffusion control problems. 2011.

[192] W. F. Pfeffer. *The Divergence Theorem and Sets of Finite Perimeter*. Chapman and Hall/CRC, 2012.

[193] M. Pineda and G. M. Buendía. Mass media and heterogeneous bounds of confidence in continuous opinion dynamics. *Physica A: Statistical Mechanics and its Applications*, 420:73–84, 2015.

[194] M. Pineda, R. Toral, and E. Hernandez-Garcia. Noisy continuous-opinion dynamics. *Journal of Statistical Mechanics: Theory and Experiment*, 2009(08):P08001, 2009.

[195] M. Pineda, R. Toral, and E. Hernández-García. The noisy Hegselmann-Krause model for opinion dynamics. *European Physical Journal B86, 490*, 86(12):1–10, 2013.

[196] M. Pineda, R. Toral, and M. Hernández-García. Diffusing opinions in bounded confidence processes. *The European Physical Journal D*, 62:109–117, 2011.

[197] A. Poznyak. *Advanced Mathematical Tools for Control Engineers: Volume 1: Deterministic Systems*, volume 1. Elsevier, 2010.

[198] E. Presutti and H. Spohn. Hydrodynamics of the voter model. *The Annals of Probability*, 11(4):867–875, 1983.

[199] A. V. Proskurnikov and R. Tempo. A tutorial on modeling and analysis of dynamic social networks. Part i. *Annual Reviews in Control*, 43:65–79, 2017.

[200] A. V. Proskurnikov and R. Tempo. A tutorial on modeling and analysis of dynamic social networks. Part ii. *Annual Reviews in Control*, 45:166–190, 2018.

[201] A. Quarteroni and G. Rozza. Optimal control and shape optimization of aorto-coronaric bypass anastomoses. *Mathematical Models and Methods in Applied Sciences*, 13(12):1801–1823, 2003.

[202] W. Quattrociocchi, G. Caldarelli, and A. Scala. Opinion dynamics on interacting networks: media competition and social influence. *Scientific Reports*, 4(1):1–7, 2014.

[203] M. Rauscher, A. Domínguez, M. Krüger, and F. Penna. A dynamic density functional theory for particles in a flowing solvent. *The Journal of Chemical Physics*, 127(24):244906, 2007.

[204] T. Rees, H. S. Dollar, and A. J. Wathen. Optimal solvers for PDE-constrained optimization. *SIAM Journal on Scientific Computing*, 32(1):271–298, 2010.

[205] T. Rees and M. Stoll. Block-triangular preconditioners for PDE-constrained optimization. *Numerical Linear Algebra with Applications*, 17(6):977–996, 2010.

[206] T. Rees, M. Stoll, and A. Wathen. All-at-once preconditioning in PDE-constrained optimization. *Kybernetika*, 46(2):341–360, 2010.

[207] J. Reinhardt and J. M. Brader. Dynamics of localized particles from density functional theory. *Physical Review E*, 85(1):011404, 2012.

[208] J. Reinhardt, A. Scacchi, and J. M. Brader. Microrheology close to an equilibrium phase transition. *The Journal of Chemical Physics*, 140(14):144901, 2014.

[209] J. Reinhardt, F. Weysser, and J. M. Brader. Density functional approach to nonlinear rheology. *EPL (Europhysics Letters)*, 102(2):28011, 2013.

[210] M. Rex and H. Löwen. Dynamical density functional theory with hydrodynamic interactions and colloids in unstable traps. *Physical Review Letters*, 101(14):148302, 2008.

[211] M. Rex and H. Löwen. Dynamical density functional theory for colloidal dispersions including hydrodynamic interactions. *The European Physical Journal E*, 28(2):139–146, 2009.

[212] M. Rex, H. H. Wensink, and H. Löwen. Dynamical density functional theory for anisotropic colloidal particles. *Physical Review E*, 76(2):021403, 2007.

[213] R. D. Richtmyer and C. Burdorf. *Principles of Advanced Mathematical Physics*, volume 1. Springer, 1978.

[214] M. J. Robbins, A. J. Archer, and U. Thiele. Modelling the evaporation of thin films of colloidal suspensions using dynamical density functional theory. *Journal of Physics: Condensed Matter*, 23(41):415102, 2011.

[215] Y. Rosenfeld. Free-energy model for the inhomogeneous hard-sphere fluid mixture and density-functional theory of freezing. *Physical Review Letters*, 63(9):980, 1989.

[216] R. Roth. Fundamental measure theory for hard-sphere mixtures: a review. *Journal of Physics: Condensed Matter*, 22(6):063102, 2010.

[217] R. Roth, R. Evans, A. Lang, and G. Kahl. Fundamental measure theory for hard-sphere mixtures revisited: the white bear version. *Journal of Physics: Condensed Matter*, 14(46), 2002.

[218] Y. Saad and M. H. Schultz. GMRES: a generalized minimal residual algorithm for solving nonsymmetric linear systems. *SIAM Journal on Scientific Computing*, 7(3):856–869, 1986.

[219] H. E. Salzer. Lagrangian interpolation at the Chebyshev points xn, $\nu \equiv \cos(\nu\pi/n)$, $\nu = 0$ (1) n; some unnoted advantages. *The Computer Journal*, 15(2):156–159, 1972.

[220] A. Scacchi, M. Krüger, and J. M. Brader. Driven colloidal fluids: construction of dynamical density functional theories from exactly solvable limits. *Journal of Physics: Condensed Matter*, 28(24):244023, 2016.

[221] H. Schawe and L. Hernández. Higher order interactions destroy phase transitions in deffuant opinion dynamics model. *Communications Physics*, 5(1):1–9, 2022.

[222] M. Schmidt and J. M. Brader. Power functional theory for Brownian dynamics. *The Journal of Chemical Physics*, 138(21):214101, 2013.

[223] Z. Schuss. Singular perturbation methods in stochastic differential equations of mathematical physics. *SIAM Review*, 22(2):119–155, 1980.

[224] S. Schweighofer, D. Garcia, and F. Schweitzer. An agent-based model of multi-dimensional opinion dynamics and opinion alignment. *Chaos: An Interdisciplinary Journal of Nonlinear Science*, 30(9):093139, 2020.

[225] R. Shamey and X. Zhao. *Modelling, simulation and control of the dyeing process*. Elsevier, 2014.

[226] L. F. Shampine and M. W. Reichelt. The MATLAB ODE suite. *SIAM Journal on Scientific Computing*, 18(1):1–22, 1997.

[227] L. F. Shampine, M. W. Reichelt, and J. A. Kierzenka. Solving index-1 DAEs in MATLAB and Simulink. *SIAM Review*, 41(3):538–552, 1999.

[228] A. Shenoy, M. Heinkenschloss, and E. M. Cliff. Airfoil design by an all-at-once method. *International Journal of Computational Fluid Dynamics*, 11(1-2):3–25, 1998.

[229] F. Slanina and H. Lavicka. Analytical results for the Sznajd model of opinion formation. *The European Physical Journal B- Condensed Matter and Complex Systems*, 35(2):279–288, 2003.

[230] X.-L. Song and B. Yu. A two-phase strategy for control constrained elliptic optimal control problems. *Numerical Linear Algebra with Applications*, 25(4):e2138, 2018.

[231] R. F. Stengel. *Optimal Control and Estimation*. Courier Corporation, 1994.

[232] M. Stoll. One-shot solution of a time-dependent time-periodic PDE-constrained optimization problem. *IMA Journal of Numerical Analysis*, 34(4):1554–1577, 2014.

[233] M. Stoll, J. W. Pearson, and P. K. Maini. Fast solvers for optimal control problems from pattern formation. *Journal of Computational Physics*, 304:27–45, 2016.

[234] M. Stoll and A. Wathen. Preconditioning for partial differential equation constrained optimization with control constraints. *Numerical Linear Algebra with Applications*, 19(1):53–71, 2012.

[235] M. Stoll and A. J. Wathen. All-at-once solution if time-dependent PDE-constrained optimisation problems. *Oxford Center for Collaborative Applied Mathematics Technical Report*, 2010.

[236] W. Su, G. Chen, and Y. Hong. Noise leads to quasi-consensus of Hegselmann–Krause opinion dynamics. *Automatica*, 85:448–454, 2017.

[237] K. Sznajd-Weron and J. Sznajd. Opinion evolution in closed community. *International Journal of Modern Physics C*, 11(06):1157–1165, 2000.

[238] M. te Vrugt. The five problems of irreversibility. *arXiv preprint arXiv:2004.01276*, 2020.

[239] M. te Vrugt, J. Bickmann, and R. Wittkowski. Effects of social distancing and isolation on epidemic spreading modeled via dynamical density functional theory. *Nature Communications*, 11(1):1–11, 2020.

[240] M. te Vrugt, J. Bickmann, and R. Wittkowski. Containing a pandemic: nonpharmaceutical interventions and the 'second wave'. *Journal of Physics Communications*, 5(5):055008, 2021.

[241] M. te Vrugt, H. Löwen, and R. Wittkowski. Classical dynamical density functional theory: from fundamentals to applications. *Advances in Physics*, 69(2):121–247, 2020.

[242] C. J. Tessone, R. Toral, P. Amengual, H. S. Wio, and M. San Miguel. Neighborhood models of minority opinion spreading. *The European Physical Journal B- Condensed Matter and Complex Systems*, 39(4):535–544, 2004.

[243] U. M. Titulaer. Corrections to the Smoluchowski equation in the presence of hydrodynamic interactions. *Physica A: Statistical Mechanics and its Applications*, 100(2):251–265, 1980.

[244] C. M. Topaz, A. L. Bertozzi, and M. A. Lewis. A nonlocal continuum model for biological aggregation. *Bulletin of Mathematical Biology*, 68(7):1601, 2006.

[245] L. N. Trefethen. *Spectral Methods in MATLAB*. SIAM, 2000.

[246] F. Tröltzsch. *Optimal Control of Partial Differential Equations: Theory, Methods, and Applications*. American Mathematical Society, 2010.

[247] F. Tröltzsch and I. Yousept. PDE-constrained optimization of time-dependent 3D electromagnetic induction heating by alternating voltages. *ESAIM: Mathematical Modelling and Numerical Analysis*, 46(4):709–729, 2012.

[248] P. Turchin. Ages of discord. *Chaplin, CT: Beresta Books*, 2016.

[249] P. Turchin. *Historical dynamics*. Princeton University Press, 2018.

[250] M. Ulbrich and S. Ulbrich. Primal-dual interior-point methods for PDE-constrained optimization. *Mathematical Programming*, 117(1):435–485, 2009.

[251] S. van Teeffelen, R. Backofen, A. Voigt, and H. Löwen. Derivation of the phase-field-crystal model for colloidal solidification. *Physical Review E*, 79(5):051404, 2009.

[252] V. S. Varma, I. C. Morarescu, S. Lasaulce, and S. Martin. Opinion dynamics aware marketing strategies in duopolies. In *2017 IEEE 56th Annual Conference on Decision and Control (CDC)*, pages 3859–3864. IEEE, 2017.

[253] T. Vicsek, A. Czirók, E. Ben-Jacob, I. Cohen, and O. Shochet. Novel type of phase transition in a system of self-driven particles. *Physical Review Letters*, 75(6):1226, 1995.

[254] E. Vigmond and G. Plank. *Encyclopedia of Biomedical Engineering*. Elsevier, 2019.

[255] C. Wang, Q. Li, E. Weinan, and B. Chazelle. Noisy Hegselmann-Krause systems: phase transitions and the 2R-conjecture. *Journal of Statistical Physics*, 166:1209–1225, 2017.

[256] G. Weisbuch, G. Deffuant, F. Amblard, and J. P. Nadal. Meet, discuss, and segregate! *Complexity*, 7(3):55–63, 2002.

[257] H. H. Wensink and H. Löwen. Aggregation of self-propelled colloidal rods near confining walls. *Physical Review E*, 78(3):031409, 2008.

[258] B. L. Werkhoven, J. C. Everts, S. Samin, and R. Van Roij. Flow-induced surface charge heterogeneity in electrokinetics due to Stern-layer conductance coupled to reaction kinetics. *Physical Review Letters*, 120(26):264502, 2018.

[259] B. L. Werkhoven, S. Samin, and R. van Roij. Dynamic Stern layers in charge-regulating electrokinetic systems: three regimes from an analytical approach. *The European Physical Journal Special Topics*, 227(18):2539–2557, 2019.

[260] J. A. White, A. González, F. L. Román, and S. Velasco. Density-functional theory of inhomogeneous fluids in the canonical ensemble. *Physical Review Letters*, 84(6):1220, 2000.

[261] R. Wittkowski, H. Löwen, and H. R. Brand. Extended dynamical density functional theory for colloidal mixtures with temperature gradients. *The Journal of Chemical Physics*, 137(22):224904, 2012.

[262] R. Wittmann and J. M. Brader. Active Brownian particles at interfaces: An effective equilibrium approach. *EPL (Europhysics Letters)*, 114(6):68004, 2016.

[263] P. Wolfe. Convergence conditions for ascent methods. *SIAM Review*, 11(2):226–235, 1969.

[264] P. Wolfe. Convergence conditions for ascent methods. ii: Some corrections. *SIAM Review*, 13(2):185–188, 1971.

[265] W. Xie and H. Pang. The shooting method and integral boundary value problems of third-order differential equation. *Advances in Difference Equations*, 2016(1):1–10, 2016.

[266] P. Yatsyshin, N. Savva, and S. Kalliadasis. Spectral methods for the equations of classical density-functional theory: Relaxation dynamics of microscopic films. *The Journal of Chemical Physics*, 136(12):124113, 2012.

[267] Y. Ye, M. Ning, N.and Tian, L. Zhang, and J. Mi. Shear-induced microscopic structure damage in polymer nanocomposites: A dynamic density functional theoretical study. *The Journal of Physical Chemistry C*, 123(36):22529–22538, 2019.

[268] M. Zeneli, A. Nikolopoulos, S. Karellas, and N. Nikolopoulos. Numerical methods for solid-liquid phase-change problems. In *Ultra-High Temperature Thermal Energy Storage, Transfer and Conversion*, pages 165–199. Elsevier, 2021.

[269] F. Zhang, A. L. Bertozzi, K. Elamvazhuthi, and S. Berman. Performance bounds on spatial coverage tasks by stochastic robotic swarms. *IEEE Transactions on Automatic Control*, 63(6):1563–1578, 2017.

[270] Y. Zhao, L. Zhang, M. tang, and G. Kou. Bounded confidence opinion dynamics with opinion leaders and environmental noises. *Computers & Operations Research*, 74(3):205–213, 2016.